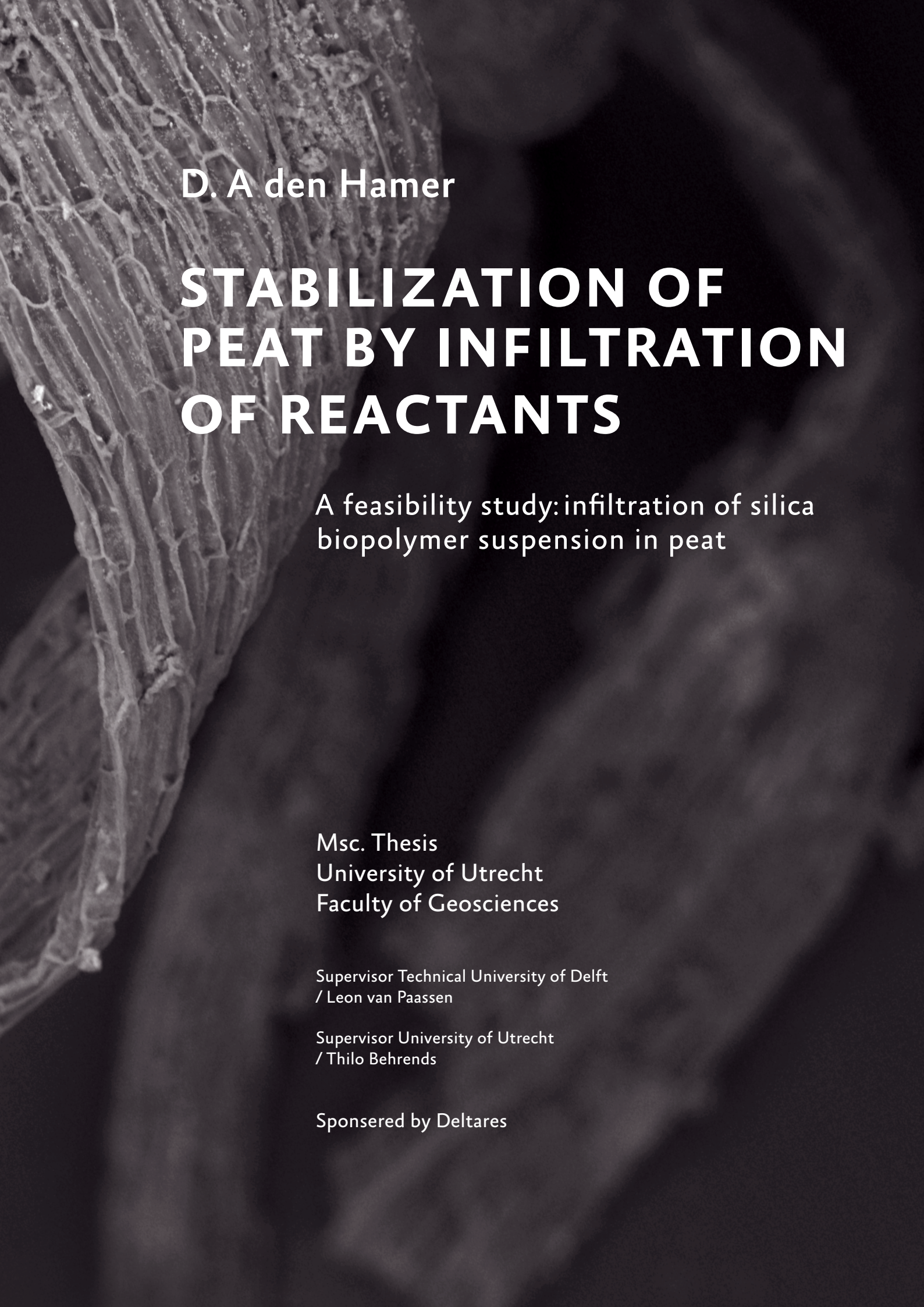

D. A den Hamer

STABILIZATION OF PEAT BY INFILTRATION OF REACTANTS

A feasibility study: infiltration of silica biopolymer suspension in peat

Msc. Thesis
University of Utrecht
Faculty of Geosciences

Supervisor Technical University of Delft
/ Leon van Paassen

Supervisor University of Utrecht
/ Thilo Behrends

Sponsered by Deltares

Date

February 2012

Number of pages

192

Table of contents

1	Introduction		9
2	Theoretic Background		12
	2.1	Peat in West Holland	12
	2.2	Conventional stabilization methods of soft soils	13
	2.3	Technical requirements	14
	2.4	Silica speciation and precipitation	14
	2.5	Solute and Colloidal Transport in Peat Soils	19
3	Retardation of Silica Particle Growth		25
	3.1	Experimental Procedure and Analytical Methods	27
	3.2	Results	32
	3.3	Discussion	55
	3.4	Conclusions with respect to research questions	59
4	Attachment to Peat Surface		63
	4.1	Experimental Procedure and Analytical Methods	64
	4.2	Results	69
	4.3	Discussion	84
	4.4	Conclusions	86
5	Infiltration Experiment		87
	5.1	Experimental procedure	88
	5.2	Tests performed	96
	5.3	Results	101
	5.4	Discussion	114
	5.5	Conclusions	117
6	Synergy and Future Research		118

Appendices

Appendix 1	Product Information Celquat L200
Appendix 2	Photon Correlation Spectroscopy
Appendix 3	Zeta Potential
Appendix 4	Electron Scanning Microscope
Appendix 5	Quantification Dissolved Silica
Appendix 6	Retardation Silica polymerization at Ci 100 ppm SiO2
Appendix 7	Retardation Silica Particle Growth in Absence of Biopolymer at Ci of 700 ppm SiO2
Appendix 8	Particle Size Distribution at 100 ppm SiO2 and biopolymer to silica wt. ratio of 0.1 and 0.5
Appendix 9	Derived Count Rate at Ci 300 ppm SiO2 and 30 or 150 ppm biopolymer
Appendix 10	Particle Size Distribution t2 at Ci 600 and 1250 ppm SiO2
Appendix 11	Particle Size Distribution at Ci 300 ppm SiO2 in presence and absence of peat pore water
Appendix 12	Zeta Potential Phase Diagrams
Appendix 13	Attachment Test Experimental Protocol
Appendix 14	Quantification Biopolymer L200
Appendix 15	Attachment Test Measurement Data
Appendix 16	Scavenging of DOC by Biopolymer L200
Appendix 17	Classification Peat Types
Appendix 18	Experimental Set-up Infiltration Test
Appendix 19	Analytical Methods Infiltration Test
Appendix 20	Column 4 and 2 after Experiment - Pictures
Appendix 21	SEM images and EDAX analyses

Summary

Construction on peat soils has proven to be a challenging task to civil engineers as this soil type is highly compressible. Especially in densely populated delta area's as the Rijn or the Maas delta in the western of the Netherlands infrastructure needs to be constructed on soft non-bearing soil layers. Construction on soft soils like peat is frequently accompanied by high geotechnical risks and costs. In conclusion, a peat layer is often unsuitable to use as a founding material. Conventional stabilization techniques have several disadvantages, among which is a strong reduction in the water storage capacity of the peat layer. A novel stabilization method was proposed, which takes infiltration and reactive transport as the starting point.

The goal was to strengthen the soil matrix *without a significant loss of porosity*. The aim was to create a silicate coating which encloses or at least connects the peat fibres, hereafter referred to as *fibre encapsulation*. It was proposed that encapsulation of the fibre alters the mechanical and chemical bulk properties of a peat layer. Stabilization should have been achieved by infiltration and transport of the reactive components (*in-situ* process). Transport distances well over 1 meter and low injection pressures increased the efficiency of the stabilization technique and thereby its applicability.

The starting point for this research project was the patent "Soil Strengthening Composition" (Zon, 2007). This patent introduces an *in-situ* treatment method to strengthen the solid matrix of a peat soil. However, several steps in the patented technique are not feasible when applied in the field. Hence, optimization of the patented treatment method and evaluation of its feasibility under continuous flow conditions was necessary. The most critical aspects of the patented method, which were the subjects of optimization, are enumerated below.

First of all, a highly concentrated source of silica was required that could function as injection fluid in a peat soil. A high silica load would reduce the number of flushes needed to stabilize a certain bulk volume. However, a distinctive characteristic of a peat soil is acidic to neutral pH conditions. The presence of silica in solution is restricted to concentrations less than 100 mg Si per liter in the pH range of 2 to 9.5 at soil temperature. To increase the efficiency of the treatment method the load of silica in the injection fluid had to be elevated well above the solubility product of amorphous silica. Therefore the phase transition of silica, from dissolved to solid form, needed to be inhibited or at least delayed. The biopolymer Celquat L200 was added to retard the polymerization process of silica and the subsequent growth of silica particles. Silica and the biopolymer were thereby the reactive components of the injection fluid. Secondly, a hardened layer of amorphous silica had to encapsulate the peat fibre. Mass transfer of silica from the pore fluid to fibre surface was therefore needed. Preservation of porosity was the aim. Hydraulic conductivity and water storage capacity of the layer had to be retained. Thirdly, infiltration was the method of choice to transport and place the reactive components. The horizontal hydraulic conductivity of a peat layer had to be 10^{-6} to 10^{-7} m/s or higher to obtain significant transport distances in one week. This was a crucial aspect to develop a promising in-situ stabilization technique.

Objective and research questions

The general objective was stabilization of peat through the formation of a silica based coating supplied by infiltration of the reactants. To reach the general objective, the critical aspects of the stabilization method as patented by Van der Zon (2007) were studied separately. The research parts concerned: (I) retardation of silica polymerization and silica particle growth, (II) attachment of silica to peat solids, and (III) infiltration of injection fluid trough peat. The related research questions are shortly described below.

Retardation of silica polymerization and silica particle growth

The injection fluid had to be a highly concentrated source of silicon at neutral to acid pH conditions. It was proposed that the concentration of dissolved and dispersed colloidal silica in the injection fluid could be elevated by the addition of the biopolymer Celquat L200.

The following questions were formulated:

- Does the biopolymer *retard the polymerization process silica* and *the growth of silica particles*? And what is the optimum composition of the injection fluid in terms of initial silica and biopolymer concentration?
- What is *the* impact *of dissolved and particulate organic matter on the efficiency of the biopolymer* to retard silica polymerization and to retard silica particle growth?
- What is the *impact of the biopolymer on the zeta potential*, as measure for the surface charge of a particle?

Attachment of silica to peat fibre surface

Attachment of silica to peat solids had to be obtained to improve the mechanical properties of the bulk material. However, repulsion between fibre surface and silica species in pore water was likely to oppose attachment of silica to fibre surface. In neutral to acid pH conditions, the surface charge of peat is negative. The surface charge of dissolved or colloidal silica is neutral to negative at pH values lower than 9.5. Equal charged surfaces result into repulsion. The proposed solution was again the use of cationic biopolymer Celquat L200 to initiate attachment between peat fibre and silica. The following research questions were formulated:

- Does the *biopolymer Celquat L200 initiate silica attachment* to peat solids? And what is the optimum initial concentration of silica in the injection fluid to maximize attachment?

Infiltration of injection fluid in peat

To achieve transport distances well over one meter of the reactive components through peat three conditions need to be met. The following research questions were formulated:

- Is the *hydraulic conductivity* of the peat material high enough to allow reasonable horizontal flow velocities with a limited pressure gradient (at least 10^{-6} to 10^{-7} m/sec)?
- Is the *volume fraction of pores* that conducts flow in peat large enough to allow sufficient stabilization of the bulk volume?
- What is the impact of infiltration of the reactive fluid on hydraulic conductivity of peat? Do the reactive components, silica and biopolymer, attach and precipitate preferably on the peat fibres, and not in the pore space where precipitation could lead complete clogging?

Experimental Methods

The feasibility of the proposed stabilization technique was determined based on laboratory research. To answer the specific research questions, three laboratory experiments were performed. A batch experiment was performed to research the design of the injection fluid (Retardation of silica…). A batch experiment in the presence of peat was performed to research attachment of silica to peat (Attachment of silica…). At last, an infiltration experiment was performed to investigate the transport of the reactive components and to evaluate the effect of injection on the porosity of a peat column (Infiltration of injection fluid…). Peat material as used in the Attachment and Infiltration experiments originated from Bellingwedde. The infiltration test an extra type of peat was tested that originated from location close to Zegveld. Peat from Bellingwedde was a reed-sedge bog peat. Peat from Zegveld was a fen peat classified as sedge type of peat. The materials and methods used to answer the research questions, as formulated for the three separate research parts, are shortly described in this section.

Retardation of silica polymerization and silica particle growth

The polymerization and aggregation of silica was monitored in the presence of the biopolymer Celquat L200. Flasks were prepared with an initial silica concentration of 100, 300, 600 or 1250 ppm SiO_2 using sodium metasilicate as the source of silicon. These flasks contained a biopolymer to silica weight ratio of 1 to 1, 0.5 to 1 or 0.1 to 1.

The polymerization reactions were induced by neutralizing the super saturated alkaline silica solution (from pH >12 to 7.5) and monitored by the time-dependent depletion of dissolved silica and time-dependent particle formation and growth. The experiment was completed 113 hours after pH adjustment.

Attachment of silica to peat fibre surface

The attachment efficiency of silica to peat solids was determined at initial concentrations of 60, 100, 300, 600 and 1250 ppm as SiO_2; and a biopolymer to silicate wt. ratio of 1. The distribution of silica and biopolymer between the liquid and the solid phase in presence of peat was the subject of research. The amount of silicate and biopolymer in the solid phase was calculated from the difference between the initial dissolved concentration before adjustment of pH and the final dissolved concentration after exposure to peat. The starting point of the attachment test was the moment the pH was adjusted to 7.5. The dissolved concentration of silica and biopolymer were measured after 65 hours and 113 hours of incubation.

Infiltration of injection fluid in peat

To derive the horizontal hydraulic conductivity of Bellingwedde and Zegveld peat a constant head test was performed. By in line electrical conductivity measurements and analyses of effluent composition at specific time intervals breakthrough curves of tracer infiltration and elution were constructed. Five peat columns were treated. Injection and elution of sodium chloride solution (0.09 and 0.07 M) was performed. Injection and elution of saturated silica solution (217.5 and 199.5 ppm SiO_2) was performed; followed by the injection and partial elution of reactive colloidal suspensions (1247 ppm and 705 ppm SiO_2/ ppm L200). And the fifth column was infiltrated with a biopolymer solution of 1962 ppm L200.

Conclusions

The conclusions drawn per research part are described below. These conclusions are directly related to the results of the experimental tests. In the next section the implication of these conclusions for the feasibility of in-situ stabilization of peat soil by infiltration of reactants, is given.

Retardation of silica polymerization and silica particle growth

The biopolymer Celquat L200 does effectively retard the polymerization process of silica. Dissolved silica concentrations of 300 to 400 ppm SiO_2 were achieved. The efficiency in which the biopolymer retards the polymerization of silica does not depend on initial silica concentration and biopolymer dosage. The biopolymer Celquat L200 does effectively retard the growth of silica particles and this does depend on initial silica concentration and biopolymer dosage. Colloidal suspensions were formed during the 113 hours of incubation. Optimum composition of the injection fluid is obtained at initial silica concentration of 600 ppm SiO_2 and the 600 ppm biopolymer Celquat L200.

Attachment of silica to peat fibre surface

The biopolymer Celquat L200 effectively adsorbs to peat in the presence and absence of silica; 90% to 99% of the biopolymer initially added was removed from solution. Attachment of silica to peat solids in the presence of the biopolymer Celquat L200 is effective; 79% to 90% of silica was removed from solution in the presence of the biopolymer Celquat L200.

Infiltration of injection fluid in peat

It appeared not to be possible to obtain sufficient infiltration of the injection fluid in the peat columns (with permeabilities of 10^{-6} and 10^{-7} m/s). A hard transparent gel was observed at the inlet on the interface between the porous disc and the peat. Penetration of the gel was in the order of millimeters. It appeared that the attachment was too fast to get sufficient infiltration. This has to be researched further before the method can be used in the field.

Implications for the Application

Solely based on present results in-situ stabilization of peat is not feasible, though the performed research is far from complete. If significant transport distances of the reactants can be obtained in-situ stabilization of peat might be feasible. And significant transport distances might be achieved if the attachment of silica is delayed.

It should however be noted, that the intrinsic hydrologic properties of a peat soil complicates infiltration of reactants – irrespective of the properties of the reactants. Given the relatively low hydraulic conductivity of peat, the small pore volume that actually conducts flow and the heterogeneity of the aspects on small and bulk scale, the question arises if the method could be efficient and under which conditions. That is, efficient in the period of infiltration needed and the bulk strength obtained within this period.

In-situ stabilization would provide a solution for a niche of the construction-market on soft soils. The focus is at applications where time is not a constrain. Treatment could then be applied as long-term method; with the advantage of preservation of water storage capacity of the peat layer, and low burden to the surroundings, as opposed to the common applied long term method of preloading.

A better assessment could be made if in-situ stabilization or even mixed in place stabilization technique is the method of choice for a specific type of peat; or if they are at all efficient methods to apply; in the case chemical and botanic characteristics of peat are known. This aspect should be acknowledged when aiming for optimization of the mechanical properties of peat – and therefore included in geotechnical research on behavior and stabilization of peat soils.

1 Introduction

Construction on peat soils has proven to be a challenging task to civil engineers as this soil type is highly compressible. Moreover, peat retains neither its form nor its strength after oxidation and is therefore highly sensitive to fluctuating water tables and therefore dryness. Layers of peat in the subsoil lead to irregular subsiding of roads, railways and foundations. Especially in densely populated delta area's as the Rijn or the Maas delta in the western of the Netherlands infrastructure needs to be constructed on soft non-bearing soil layers. Construction on soft soils like peat is frequently accompanied by high geotechnical risks and costs. In conclusion, a peat layer is unsuitable to use as a founding material. The material has the following properties, which result in high risks for geotechnical engineering: anisotropy in stiffness as strength, compressibility and a relatively low resistance to chemical or biological induced oxidation.

Conventional stabilization techniques, applied in soft soils are consolidation, mixed in place and prefab construction techniques. These techniques have several disadvantages: consolidations takes time, mixed in place techniques may create deformations and/or strengthening may not be achieved. Moreover, the water storage capacity of the soil layer is not preserved using these techniques. A novel stabilization method is proposed, which takes infiltration and reactive transport of silicon as the starting point.

Mixed in place is a placement technique based on chemical stabilization of the soft soil. Chemical stabilization techniques use the element calcium as the 'building block'. In current research it is proposed to use silicon as the main element to create an amorphous mineral which enhances bulk soil properties. The goal of the treatment is to strengthen the soil matrix *without a significant loss of porosity*. The aim is to create a silicate coating which encloses or at least connects the peat fibres, hereafter referred to as *fibre encapsulation*. It is proposed that encapsulation of the fibre alters the mechanical and chemical bulk properties of a peat layer. The proposed stabilization technique concerns an *in-situ* process. That is, stabilization should be achieved by infiltration and transport of the reactive components, including the component silica. If the process does not impose a significant loss of porosity, extended transport distances could be obtained and injection pressures could be lowered. Transport distances well over 1 meter and low injection pressures increase the efficiency of the stabilization technique and thereby its applicability.

The starting point for this research project is the patent "Soil Strengthening Composition" (Zon, 2007). This modification method of peat soils comprises strengthening *of the highly compressible solid matrix*. It is shown (Zon, 2007) that the peat properties can be modified in order to enhance its suitability for foundation. The technique proposed by Van der Zon has been developed on a laboratory scale and under mixing, batch conditions. However, several proceedings in the patented technique are likely to be unfeasible to apply in the field. Furthermore, the technique was only tested under batch conditions. *Hence, optimization of the patented treatment method and evaluation of its feasibility under continuous flow conditions is necessary*. The most critical aspects of the patented method, which are the subjects of optimization, are enumerated below.

First of all, a highly concentrated source of silica is required that could function as injection fluid in a peat soil. However, a distinctive characteristic of highly organic soils, like peat, is an acidic to neutral pH (Killops, 2005). The presence of monomeric silica i.e. silicic acid ($H_4SiO_4^o$) in solution is restricted to concentration less than 120 mg Si per liter in the pH range of 2 to 9.5 and at ambient temperature (Iler, 1979). The load of silica in solution per unit volume of injection fluid is therefore relatively low upon injection. From a practical point of view, applying a silica solution as injection fluid implicates a non realistic stabilization method. Accordingly, there is the need to increase the load of silica in the injection fluid at acidic to neutral pH conditions. The use of additives is one possibility addressed by literature to achieve this, either in the form of a true solvent or in the form of dispersed colloids. The use of a highly alkaline solution is proposed in the patent. However, care should be taken with the application of this approach in the field. Naturally, the approach should not include the addition of a toxic or hazardous substance.

Secondly, the reactive components i.e. silica and the additive, need to be transported within the porous matrix. During transport the reactive components interact with the surface of peat particles and solutes present in the pore water.

The aimed reaction should occur at the interface of pore fluid and receiving template, the peat fibre, instead of a reaction in the pores space itself. Using mixing techniques directly in the soil[1] the pore space is filled up with solid material. The porosity is thereby severely reduced. If one could solely encapsulate the fibre, trigger a reaction solely at the interface, the open structure of the soil matrix could be maintained. The aimed interaction with the peat layer is attachment of silica. 'Attachment' is considered to be the transformation of dissolved silica in the pore water to solidified silica at the surface of a peat fibre. Infiltration is then the method of choice to transport and place the reactive components.

Efficiency of the treatment is dictated by transport distances that can be reached and the obtained strengthening of the porous matrix over this distance. Both transport distance and interaction between silica and peat solids sets demands to the physical and chemical properties of the silica present in the injection fluid. The composition of the injection fluid in batch and continuous flow conditions, and in the presence and absence of peat is therefore subject to research.

To summarize, the general objective of present research was: *Stabilization of peat by formation of a silica based coating supplied by infiltration of the reactants.*

The requirements that should be met to achieve the general objective are:

a. Restricted amount of flushes to obtain stabilization.
b. Pore filling precipitation should be avoided as it reduces the water storage capacity of peat layer and feasible transport distances.
c. Transport distance well over one meter.

Based on literature survey three laboratory experiments were performed to optimize the stabilization method as proposed by Zon (2007) and to test its feasibility under flowing conditions. The requirements as named above are met as follows:

a. Retardation of silica polymerization and silica particle growth

The injection fluid has to be a highly concentrated source of silicon at neutral to acid pH conditions. This can be achieved by the addition of an additive and subsequent retardation of the phase transition of silica. The polymerization process of silica needs to be delayed and the production of large particles that block peat pore throats needs to be avoided.

b. Creating the attachment of silica to peat fibre surface

Attachment of silica to the peat surface needs to be obtained. That is, attachment of silica needs to be obtained at the surface or interface of pore fluid and fibre surface. This could be achieved by alternation of the surface charge of either the receiving template or the silica entity in the solution from negative to positive charge. The drive for attachment at the surface is then assumed to be electrostatic. Steric attractive forces and or precipitation at the surface could induce 'attachment' instead of pore filling precipitation as well.

c. Enhancing infiltration of silica in peat soil matrix

Colloidal or solute transport of reactive components in the peat over a distance of well over one meter is crucial to develop a promising in-situ stabilization technique. The water storage capacity and the hydraulic conductivity of the bulk peat should not significantly be reduced by the stabilization technique.

[1] referred to as 'mixed in place' techniques

It is proposed to assign various functions to the added additive in order to meet the set requirements. By using the same additive for various functions, the treatment can preferably be reduced to one or a maximum of two steps. The different functions are listed below:

a. Use of *surface active polymer* to delay the polymerization process of silica and delay the growth of silica particles.

b. Use of a *cationic polymer* to alter the surface charge of receiving template (the fibre) or silica entity dissolved or dispersed in the pore water.

* Use of *biodegradable* (biopolymer) *cationic polymer* as a non toxic additive and induce local production of fatty acids which induce further coagulation of silica gel.

The function of the biopolymer as precursor for fatty acids (Zon, 2007) and the resulting condensation of a silica gel, is disregarded in present research.

Outline Thesis

The structure of this report is as follows. The Chapter Theoretic Background provides a collection of literature and gives a short introduction to silica chemistry, the interaction between silica and surface active agents, and mechanisms that drive solute and colloidal transport in peat soils.

To reach the general objective, described above various aspects of the process as proposed by Van der Zon had to be studied separately. This resolved into three problem statements as briefly mentioned above. For clarity, each problem statement and proposed solution is evaluated in a separate chapter: 'Retardation of Silica Particle Growth', 'Attachment to Peat Surface' and the Chapter 'Infiltration Experiment'. Each chapter describes the performed laboratory research including results, discussion and conclusions. In principle these chapters could be read independent of each other. At the end of this report a synthesis of the three subjects is given. The overall feasibility of the novel stabilization technique is evaluated with prospects to future research.

2 Theoretic Background

2.1 Peat in West Holland

Peat is an accumulation of dead plants and forms in any location sustaining plant growth at rates higher than the decay like for example wetlands. The geotechnical properties of peat are related to its moisture content which can be as high as 90% of the bulk weight, and its high content in organic matter in the order of 80% to 100% (Sparks, 2003; Killops, 2005; Gonzales, 2009). The geotechnical properties of different peat soil types are presented in Table 2.1. The relation between characteristics of peat and geohydrological properties is described in more detail in 2.5.3.

Peat is found in a variety of depositional environments ranging from the back swamps of a delta to blankets on hillsides. Peat is quite common in The Netherlands, see Figure 2.1. For a long time these locations were considered marginal, not suited for cultivation or the construction of infrastructure. Nowadays estuaries and deltas - where thick peat layers can be found - have become increasingly subject to concentrated economical activities like infrastructure and building activities. The increasing demand for space calls for engineering solutions to deal with the adverse properties of these grounds: extreme compressibility, low strength and susceptibility to chemical and biological induced oxidation.

Table 2.1: Geotechnical properties of different peat soil types (Venmans, 2009).

	organic clay	low moor peat	transitional peat	raised bog peat
water content	< 100 %	100 – 500 %	500 – 1000 %	> 1000%
organic content	< 20	20 – 70 %	70 – 95 %	> 95 %
compressibility				
permeability				
strength				
anisotropy				
potential volume loss				
weight				

Figure 2.1: Peat in The Netherlands (Alterra, 2012).

2.2 Conventional stabilization methods of soft soils

Various techniques can be applied to reduce or eliminate the adverse effects of construction on peat. One of these effects is port construction settlements when constructing in or on peat. Post construction settlements can be restricted by preloading, lowering of the groundwater level or vacuum drainage. Upon installation of vertical drains subsidence of a peat layer is obtained within a shorter time period. The use of light weight fill materials can reduce settlements both during and after construction. For example, using Expanded Polystyrene (EP) foam reduces settlements allowing fast construction. Another method to reduce settlements is stiffening of the subsoil by inclusion of stiff elements e.g. piles. To place stiff elements in a soft soil various techniques exist among which mix in place techniques or placement of prefab piles. Also embankment stability benefits from application of light weight fill materials, mix-in-place (MIP) techniques (Karol, 2003) or piled embankments. These techniques allow an increase in embankment fill rate and require less space for stability of slopes. To increase the stability of levees, located in peat lands, the techniques applied are soil nailing, sheet pile walls, coffer dams and diaphragm walls (Molendijk, 1996; Nichol and Farmer 1998; Hebib and Farrell, 2003; Karol, 2003; Hamer, 2009).

Serious concerns and disadvantages of these techniques remain despite their widespread application and performed extensive research (Hebib and Farrell, 2003). This results in elevated risks for construction of infrastructures on and in peat soils. Especially, this goes for the mixed in place technique. Mixed in place technique is applied to obtain chemical stabilization of a soil (Karol, 2003). The creation of a homogeneous mixture of soil and the additive causes a permanent concern. Moreover, cement is the common additive to stabilize a soft soil. Humic substances however interfere with the hardening process of cement. Strength development, final strength and durability of the formed element are thereby frequently reduced (Sing, 2008; Sherwood, 1993; Babean and Sevc, 1997). Besides the weakening mechanism of humic substances other chemical properties of peat lead to less and or slowed hardening in comparison to clay or sandy soils. Due to the relatively high water content of a peat soil, in the order of 90%, more solids are required to form a solid matrix (Hobbs, 1986; Ahnberg and Holm 1999). That is, more cement needs to be added. Consequently, chemical stabilization of peat by MIP technique does not always succeed. Furthermore, the lifetime expectance of a mixed in place pile can not be guaranteed beyond 10 to 30 years when construction does succeed (Karol, 2003). Equally important the pile or sheet of piles has a much lower permeability than the original soil, which might result in the undesired build up of water-pressures.

Next to mixed in place techniques several injection techniques are applied in civil engineering to improve soil stability and or reduce soil permeability. Common techniques are grout injection, which is calcium based, and the injection of waterglass, which is silicon based. Again the same applies for grouting as for mixed in place techniques performed in peat soils: interference of the hardening by humic substances. Waterglass readily precipitates when mixed with carboxylic acids, a major component in a peat soil. The resulting fast reaction rate is a disadvantage. Precipitation is so fast that stabilization is achieved relatively close to the point of injection. Another important risk of grout injection in a peat layer is the risk of a blow-out. If injection pressures are too high the grout fluid or waterglass takes the path of least resistance, i.e. straight to ground level. Therefore, chemical stabilization based on grouts or waterglass are rather not applied in peat soils.

Apart from these quality and durability issues, mix in place and other traditional soil stabilization methods cannot be applied under already existing constructions. Corrective and preventative *in-situ* applications become more and more important. Maintenance and repairs can then be performed on the construction without to much a burden to its surroundings. In conclusion, current applied methods for stabilization of peat are not always suitable. The drawbacks of these methods are expected to be less and less accepted in civil engineering practice. Therefore, a general need for the development and use of stabilization techniques, which are *in-situ* applicable, exists.

2.3 Technical requirements

Injection in peat

The aim is to inject in the peat layer and obtain treatment distances well over 1 meter. The applied injection pressure should not be more than 0.5 bar in order to prevent a blow out. The minimum hydraulic conductivity of a peat layer in the horizontal directed should be in the order of 10^{-6} to 10^{-7} m/s. This estimation is described in more detail in 3.4.2. Practical conditions state that the transport time should be max. 1 week. The reaction rate needs to be significantly lower than the velocity of the reactive components: reaction time > injection time.

2.4 Silica speciation and precipitation

The presence of neutral mono-silicic acid $H_4SiO_4^o$ in solution is restricted to a concentration of 120 mg Si per liter at ambient temperature and less than 100 mg/l at 10 °C, in a pH range of 2 -9.5 (Iler, 1979). Figure 2.2 A illustrates the relation between dissolved silica concentration controlled by amorphous silica and pH at 25°C. Amorphous silica becomes more soluble at pH above 9.5 and very soluble above pH of 11 (Iler, 1979). At pH values below 9 – 9.5 the solubility of silica becomes independent of pH. In Figure 2.2 B the speciation of silica is depicted as a function of pH. The solubility of silica is now controlled by both quartz (thick black line) and amorphous silica (dotted line) at temperature of 25°C. The y axis expresses dissolved silica in terms of the log ion activity, which is directly related to concentration in dilute solutions (Kehew, 2001). At pH conditions between 2 and 9.5 silicic acid ($H_4SiO_4^0$) is the dominant specie, as illustrated by the horizontal line that coincides with the thick black line. At pH values above 9.9 $H_3SiO_4^-$ becomes the dominant specie. At pH above 11.7 $H_3SiO_4^-$ deprotonates and $H_2SiO_4^{2-}$ becomes the dominant specie.

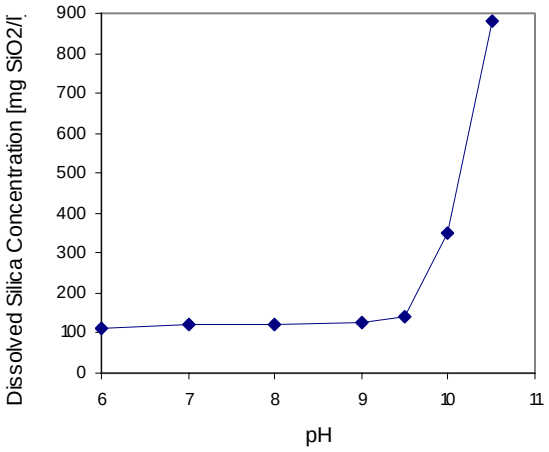

A. The solubility of amorphous silica as a function of pH, and at a temperature of 25 °C (Iler, 1979).

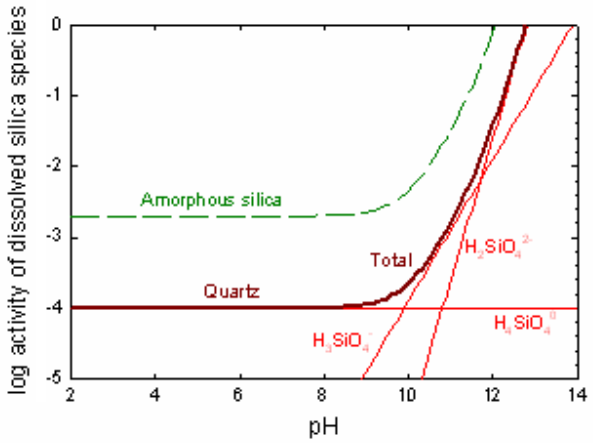

B. Activities of dissolved silica species in equilibrium with amorphous silica and quartz at a temperature of 25 °C (Kehew, 2001: Ch. 4). Red line illustrates the species of dissolved silica. The thick black line and the greed dotted line are the total of dissolved silica species, controlled by quartz and amorphous silica respectively. The dotted line representing amorphous silica is located 1.8 log activity units above quartz. This represents the fact that amorphous silica is circa 20 times as soluble as quartz.

Figure 2.2: Solubility of amorphous silica and speciation of dissolved silica as function of pH

The phase transition of silica is a very complex process. Numerous reactions model describe the transition of dissolved silicic acid to the amorphous solid form of silica (Icopini, 2005). In a simplistic version the phase transition of dissolved silicic acid to amorphous silica follows a 3- step process, at super saturation and in the absence of any additive (Perry, 1992; Perry and Keeling-Tucker, 2000; Iler, 1979; Zhang, 2011; Tobler, 2009). These steps are silica polymerization, formation of colloidal particles and aggregation of colloidal silica to sedimenting particles (Coradin, 2007; Zhang, 2011). A short description of every step is given below.

The first step in polymerization of silica is the condensation of silicic acid (monomeric silica) to polymeric silica. The polymerization of silicic acid is believed to occur through a S_N-2 mechanism (Demadis, 2009; Icopini, 2005; Gill, 1993). A deprotonated ≡Si–O^- group and a Si atom in the center of silicic acid form a siloxonate (Si-O-Si) bond with the exclusion of OH^- (condensation). The polymer chain length increases with continuous condensation of monomeric and polymeric silica. Linear dimmers, trimers, tetramers and, linear and cyclic oligomers are formed, eventually producing three dimensional highly hydrated networks. See Figure 2.4 for an illustration.

The rate of polymerization is influenced by temperature, pH, ionic strength and degree of super saturation (Perry, 1992; Gill, 1993, Icopini, 2005). Silicic acid is reported to polymerize already at concentrations exceeding 1 ppm SiO_2. A non saturated solution of silica therefore contains both monomeric as polymeric silica (Zhang, 2011). At saturation, the rate of silica polymerization is catalyzed by the presence of hydroxyls at pH values exceeding 4. At pH in the range of 6 to 8 the rate of polymerization increases dramatically. Hence nuclei formation and particle growth of silica become very rapid at neutral pH (Iler, 1979; Staffan, 1996; Bishop and Bear, 1972; Goto, 1956; Gill, 1993; Tobler, 2009). It has been reported that the reaction that yields silicic acid dimmers is kinetically slower than those reactions that give trimers, tetramers, pentamers, etc (Staffan 1996; Coradin, 2007).

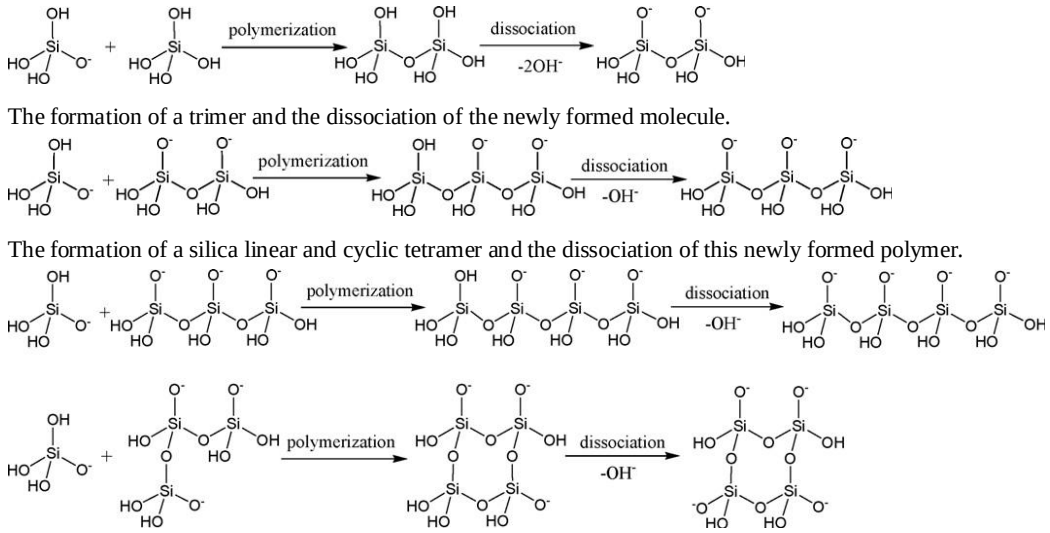

Figure 2.3: The polymerization process of silica. Figure is obtained from the work of Zhang et al. (2011).

The second step in the phase transition of silica is the transformation of silica 3-D networks to spherical particles (colloids). The highly hydrated networks condensate internally and coagulate to more dense colloidal particles. Furthermore, the colloidal particles grow by further accretion of silica oligomers and or by Oswald ripening (Iler, 1979; Perry, 1992; Perry and Keeling-Tucker, 2000; Conrad, 2007; Icopini, 2005; Tobler, 2009). Oswald ripening is the process of dissolution of silica molecules located at the surface of the particle and re precipitation on particle surface (Hiemenz, 1997).

The last step in the phase transition of silica is aggregation of colloids. Colloidal particles collide with each other to form aggregates of increasing size. Collision is driven by interparticle forces and random Brownian motion; more on interparticle forces in 2.4.1. The actual clustering of colloidal particles is thermodynamically favorable, since new surface is created. That is, the clustering of colloids results from a decrease of Gibson energy. As a result the specific surface area reduces. Furthermore, as a result of ongoing condensation of the silica network the density of the particle increases. This causes the particle to settle out under the influence of gravity. A process referred to as sedimentation. In comparison to the deposition of more crystalline forms of silica like quartz, the deposition of amorphous silica is a rapid process. The kinetics of crystal formation is slow, as opposed to the kinetics of silica polymerization and aggregation given its chaotic i.e. amorphous nature (Gallup, 2002; Iler 1979).

Surface charge

The surface charge or molecular charge of various phases of silica dictates its reactivity and interparticle behavior (Hiemenz, 1997). For example, the surface charge dictates the stability of the silica phase in the solution of suspension. This is illustrated in Figure 2.2 and Figure 2.4. The molecular charge of monomeric silica is neutral at pH conditions in the range of 2 to 9.5. The silanol groups located at the surface of the particle can be either protonated or deprotonated depending on the pH. Polymeric silica bears a neutral to negative surface charge at pH ranges of 2 to 9.5. Upon polymerization silanol groups (Si-OH) become increasingly acidic and bear a negative charge. Coradin and Livage (2007) report that the silanol groups again protonate at pH values smaller than 4 to 5. As a result the surface charge becomes neutral and the reactivity of the silica polymer reduces. Figure 2.4 shows the relation between pH and the stability of dispersed colloidal silica. The surface charge of colloidal silica is neutral to negative in the pH range of 2 to 9.5. However, as depicted in Figure 2.4, the stability of colloidal silica is the lowest at pH range of 6 to 7. Maximum stability is obtained at pH 2 to 3 (Iler 1979). At increasing pH values silanol groups located at the surface of the colloid deprotonated, the surface charge becomes more negative elevating the electrostatic forces of repulsion and dispersion stability is obtained.

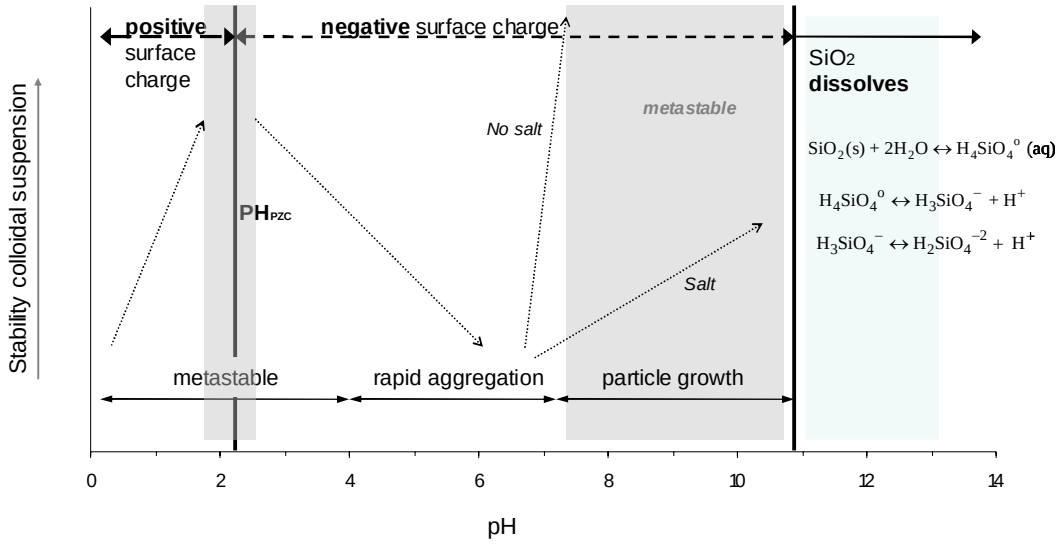

Figure 2.4: Change of surface charge of colloidal silica with pH and the implications for dispersion stability. Figure is derived from Bergna (2006: 21) and is based on experimental data from Iler (1979). The thin arrows indicate stability. At decreasing stability the aggregation rate increases. At pH values between 6 and 7 precipitates are formed immediately. If the pH approaches 8 to approximately 11 the surface charge becomes increasingly negative, and the stability of the dispersion increases (electrostatic forces of repulsion). The particles though still increase in size in this pH range.

Designation

The terminology of silicates as applied in current report is briefly introduced here. The term "silica" is a general term that refers to silicon dioxide in all of its crystalline, amorphous, hydrated, and hydroxylated forms. The silicon content in present research is given in terms of the weight of silicon dioxide (SiO_2). 'Silica' and 'Silicate' are often used interchangeably. In this research the terms are use interchangeably as well to indicate all the forms of the species $Si(OH)_4$ at various deprotonated states, and the product of silicate polymerization. The term 'dissolved or reactive silica' is the fraction of silica indicated by the silicomolybdate spectrophotometric method – an analytical method applied in present research. The deviation between silica and silicate is based on molecular of particle size. A silicon entity can be classified depending on its size, as soluble (diameter < 1 nm), polymeric (diameter of 1-10 nm), colloidal (diameter 10–1000 nm) or suspended (1–10 μm) particles (Hiemenz, 1997). Particle size distribution analyses indicate whether particulate matter is present in the continuous phase and the diameter size classes present. Shift of particle size distributions in time provides information on the stability or instability of dispersed particulate matter.

2.4.1 Treatment approaches to maximize silica load

Several methods are reported in literature to elevate the concentration of dissolved silica in an aqueous solution or suspension. Present section describes the use of acids and bases to elevate amorphous silica solubility, disruption of silica polymerization, and the prevention of colloid aggregation and sedimentation.

Acid and bases

A very simply approach is the use of acids and bases to increase the solubility of silica with respect to amorphous silica (Yates, 2006). The solubility of silicic acid depends on the pH and on the temperature, as discussed in previous paragraph. Upon pH adjustment to more than 9.5 a tremendous increase of silica solubility is obtained. Furthermore by choosing the direction of pH adjustment the surface charge and stability of colloidal silica could be controlled. If the pH is controlled in the acidic range (pH< 2-3) stability of colloidal silica is increased. Clearly, these are extreme pH ranges for natural soil systems.

Inhibition or retardation of silica polymerization process

Control of the phase transition of silica is desired for many applications and in various industrial processes. In material design controlled formation of amorphous or crystalline silica is the goal. In industrial (waste) waters inhibition of silica scale formation is desired. Super saturated concentrations of silica and saline conditions result in precipitation and scale formation. This results in a loss of equipment efficiency and premature shut down.

Inhibition or retardation of silica polymerization is defined as the disruption or delay of silicic acid polymerization (Zhang, 2011; Demadis, 2009). The addition of non-organic ligand forming metalloids or halogen acids with silica is proved to retard the polymerization of silica and increase dissolved concentrations (Meier and Dubin, 1987; Dubin, 1985). Dubin (1985) suggested that the addition of boric or fluoride acids and or its water soluble salts even inhibits silica polymerization due to the formation of more soluble borate/fluoride-silicate complexes.

Research performed by various groups in the field of desalinization, geothermal and microbial research, suggests the use of bio macromolecules to inhibit or retard the polymerization process of silica; as opposed to use of toxic and/or more expensive additives like hydrofluoric acid and boric acid. Functionalized bio macromolecules used as an additive to control the phase transition of silica are from hereon referred to as biopolymers. Although the exact retardation mechanism of silica polymerization by biopolymers and surfactants is not entirely understood, Demadis (2009) and Zhang (2011) suggest that the inhibitor 'disrupts' condensation of silicic acid at the formation of biopolymer-silica complexes.

Not every cationic biopolymer is suitable to retard the polymerization process of silica (Gill, 1993; Damadis, 2009; Coradin, 2007; Neofotistou, 2004). The retardation efficiency or even the fact that the additive is acting as a retardant and not as a catalyst to condensation and/or aggregation depends on various factors. Among these factors are the structural features of the additive itself and the characteristics of the silica suspension that should be stabilized (Demadis, 2005; Demadis, 2009; Stathoulopoulou, 2008; Coradin and Livage, 2007). Various suitable biopolymers an surfactants are reported in literature that retain silica in its dissolved state (mono- to oligomeric silica) at super saturation. From these reports it is derived that the best results are obtained using a cationic or zwitterionic biopolymer to delay the polymerization of silica. Consensus in all these research reports is that using a cationic or zwitterionic biopolymer as additive results into *retardation* of the process. A reference of complete inhibition of silica polymerization could not be found, and is according to Amjad (1999) not yet achieved.

Inhibition or retardation of colloid aggregation and sedimentation

The preferred approach to maximize the load of silica in the injection fluid is complete inhibition of silica polymerization. However, as is indicated by literature as described in previous section and form preliminary laboratory work (Appendix 1.2); it is more likely that the selected biopolymer works mainly as a dispersant for colloidal silica. Aggregation of colloidal silica and subsequent deposition are then (temporarily) avoided, maximizing the load of colloidal silica in the injection fluid. Certain polymers have shown to be capable of dispersing fine particles of amorphous silica once they have formed (Bergna, 2006; Shimabayash, 1992; Candelaria, 1996; Harrar, 1982) and some polymers have the opposite effect (Mikhailova, 2002; Ueda, 2000).

A colloidal suspension is considered to be stable if the colloids resist coagulation and aggregation e.g. if particle growth is restricted (Hiemenz, 1997). In general there are two approaches to stabilize a colloidal dispersion kinetically, namely electrostatic stabilization and steric stabilization, which can occur simultaneously (Hiemenz, 1997; Pashley, 2004). The interaction between two particles is determined by the balance of interparticle forces. Interparticle forces include the short range (within two times the radius of the particle) attractive forces like Van der Waals and London forces, and long range attractive or repulsive electrostatic and steric forces. The principle of stabilization is based on overcoming the attractive Van der Waals and London forces by creation of an energy barrier (in the energy potential field surrounding a particle) at long range distance from particle core. The energy barrier prevents the approach and thus coagulation of two colloidal particles. Electrostatic induced stabilization is the creation of equal charge and thereby repulsion. The zeta potential needs to exceed +/- 30 mV for electrostatic repulsion to result in stabilization of colloidal dispersion. Steric induced stabilization is the creation of a steric hindrance by formation of polymeric shield and or springs at the surface of the colloid (Hiemenz, 1997; Napper, 1983; Bergna, 2006). The steric stabilization method is used by Gallup, (2002), (2005), Amjad (1985) to control silica scale deposits.

Several research groups report or postulate on the mechanism(s) that drive(s) the interaction between a biopolymer and/or surfactant, and colloidal silica at super saturation. Healy (2006) created a model for a system in which coagulation of colloidal silica is controlled by surface steric barriers to polysilicates plus bonded cations. Harrar (1982) postulates that retardation of silica scale formation by biopolymers is caused by the adsorption of the biopolymer on the surface of the colloid and subsequent formation of a steric barrier. Harrar (1982) states that the interaction between biopolymer and colloidal particle could involve two mechanisms. First there is the possibility of hydrogen bond formation between oxygen (hydroxyls) or nitrogen functional groups (quaternary, tertiary, secondary amines) located at the biopolymer chain, and the silanol groups located at the surface of the colloid. This is supported by Gallup (2002) and (Demadis, 2009). However, Minones et al. (1988) states that involvement of hydrogen bonding between the silanol groups and the quaternary amine group could be ruled out based on pressure surface-area measurements. The second mechanism involves electrostatic attraction between positively charged (cationic) segments of the biopolymer and the negatively charged surface of the colloid.

The last option is supported among others by Damadis (2009), Coradin (2007), Ueda (2000) and Minones (et al, 1988). Minones (1988) indicated also that the electrostatic interaction between silica colloid and biopolymer depends on pH, despite the permanent cationic charge of the amine group. Since dissociation of the silanol group (the acidity) depends on polymerization degree, and hence on pH and concentration.

Sudden destabilization of a colloidal system can be caused by increase of the ionic strength of the suspension, charge neutralization or depletion of active biopolymer. Increasing the ionic strength compresses the diffuse double layer surrounding each particle. Van der Waals attractive forces then become effective (Hiemenz, 2007; Pashley, 2004). Another cause destabilizing a colloidal system is charge neutralization of the colloidal surface (in case electrostatic stabilization was applied) by shift in pH (Vaslin-Reimann, 1990). A third option causing destabilization concerns disruption of steric hindrance of the biopolymer. If the concentration of active biopolymer drops, the behavior of the biopolymer can shift from creating a steric barrier to cross-linking mutual colloids instead. If the latter is the case depends on structural features of the biopolymer (Demadis, 2009).

2.5 Solute and Colloidal Transport in Peat Soils

The empirical relation as formulated by Henry Darcy (Darcy's law, 1856) and conservation of mass first formulated by Lavoisier, forms the basis for transport analyzes of solutes and colloid in various soils. The hydraulic conductivity as described in present section only considers saturated conditions.

2.5.1 Solute Transport

The general flow equation for solute transport in a porous matrix defines three physical processes that change the concentration of the solute over time (Appelo and Postma, 2005). The first term is the advective term, referring to the velocity of groundwater through the connective and conducting pores. If a solute is conservative and non-reactive then the advective flux of mass in the flow direction is a function of the specific discharge and concentration of the solute. The average rate of solute migration equals the average linear velocity of the ground water if the solute is conservative. If the solute is not conservative but reactive than the velocity of the solute is smaller than the velocity of the groundwater.

The second term is the combined dispersion and diffusion term. Dispersion is the difference in flow velocity due to spatial variety in pore geometry. Tortuosity is a measure of how tortuous the typical flow path is through the medium. The toruosity is proportional to the ratio between transport distance in straight line (i.e. length of the column), and the length of the actual flow path traveled. The result of dispersion is increased variation in solute transport velocity. Diffusion is the movement of solutes due to a gradient in concentration of that solute in a certain direction. The diffusion coefficient also includes the difference in solute transport velocity due to random movement of molecules, also referred to as Brownian motion. The coefficient also includes the variances in velocity induced by differences in molecular mass and size. For example, smaller molecules diffuse faster than larger molecules. Diffusion becomes important in soil types with a low hydraulic conductivity, in the order of $<10^{-9}$ m/s (Appelo and Postma, 2005). Soil types like clay and some decomposed and compacted peat soils. Evaluating the impact of dispersion and diffusion on a breakthrough curve of a solute tracer, dispersion causes the leading and tailing edge to slope. Diffusion on the other hand smoothes away variations of velocity on micro scale and thereby sharpens the front of a breakthrough curve (Fitts, 2002; Appelo and Postma, 2005).

The third term is the reactive term. The reactive term in the general flow equation is often defined as a decay term, or a sink/ source term. In any case, the term defines the change in solute concentration over time and distance due to an exchange of mass between phases. This could be an exchange between the aqueous and solid phase or the exchange between the aqueous phase and the 'biomass phase' indicating the uptake by microbes (Fitts, 2002). Reactive processes in a porous matrix as peat soil are abundant (Sparks, 2003; Cosovic, 1990; Allen, 2004).

The reaction processes of interest in present research are sorption, precipitation and possibly ion exchange (Killops, 2005; Weng, 2002; Stumm, 1996). To this process is often referred to as tracer retardation (Appelo and Postma, 2005).
The impact of reaction processes on solute migration is that upon injection of the tracer solute, the solute mass is being transferred from the aqueous phase to the solid phase. As a consequence, the leading edge of a breakthrough curve thus sharpens. Furthermore, transport velocities of the solute decrease due to mass transfer. Arrival of the front is thereby delayed. Upon elution of the tracer, the solute concentration in the pores decreases and mass is now transferred back from the solid phase into the aqueous phase. Thereby the slope of the trailing edge decreases, long tailing sections occur and as a consequence asymmetries of the breakthrough curve (Appelo and Postma, 2005).

Mass transfer mobile to immobile zone

Sorption is a major part of the reactive processes in peat soils, and of interest to present research given the interaction between a surface active polymer, silica and peat fibre surface. Sorption of a component to peat solids, like for example a biopolymer, is a relatively fast reaction (Cumming, 2010; Fitts, 2002). The relation between dissolved and sorbed concentration of a component is expressed by the sorption coefficient. The relation can be linear, convex or concave depending on the favored state of the component (Appelo and Postma, 2005; Stumm, 1996).
However, it is not likely that equilibrium is obtained in terms of sorption in a peat soil (Blodau, 2002). A peat soil consists large pores conducting advective transport (referred to as the mobile zone), and smaller pores with less mobile pore water and even stagnant water (less mobile and immobile zones) (Holden, 2008; Quinton, 2008; Gnatowski, 2010; Rezanezhad, 2009). Molecular diffusion limits the flux of solute molecules to sorption sites located in the less mobile and especially in the immobile zones. Surface sites located at these stagnant zones therefore differ in sorbed concentration from surface sites located at the mobile zone (Fitts, 2002). In peat soils a significant fraction of the solid interface (and thus surface sites) is not in direct contact with the mobile pore water (Holden, 2008; Quinton, 2008; Gnatowski, 2010; Rezanezhad, 2009). The relation between the fraction of the flux that is conducted and pore size in peat soils, is described in more detail in section 2.5.3.
The fact that some pores are dead-ended or even pockets of pore water disconnected from mobile pore water is referred to as dual porosity (Ours et al, 1997). The degree of mass transfer between the mobile and immobile zone and the impact of this mass transfer on the actual dissolved concentration in the mobile water depends in principle on time and advective transport velocities (Haggerty, 2004; Ours et al, 1997). The term physical (non-) equilibrium expresses the difference in velocities of advective and diffusive transport. If mobile water maintains a fixed concentration long enough then the solute and sorbed concentration will become the same in the mobile as in immobile water (referred to as physical equilibrium) transport (Appelo and Postman, 2005). If the duration of tracer injection is too short, and the concentration is not fixed at a constant level long enough, then a physical non-equilibrium between the two regions exists. A diffusive flux of mass between these regions will be ongoing (Haggerty, 2004; Appelo and Postma, 2004).

Moisture content and mobile pore volume

In a peat soil, even at saturation, the volume of water present in the bulk does not represent the pore volume. Even more so, the volume of water present in the bulk does not represent the pore volume conducting flow as described in previous section. In saturated purely sand soils the total amount of water present in the bulk represents the total pore volume. In soils containing organic components this is not correct. Intergranular water is a fraction of the water volume in the bulk. Intergranular water is water present in the plant residues and humus matrix itself (Kellops, 2005). In organic fibers water is for example included in the vacuoles. Furthermore, physical water is the static water layer enclosing a particle. This layer does not contribute to advective or dispersive transport of solutes (Fitts, 2002). Any exchange is possible through diffusive transport into and out this layer (Appelo and Postma, 2005). To estimate the pore volume available for advective transport column tracer experiments are performed (Appelo and Postma, 2005).

Column Tracer experiments

To investigate solute transport trough a porous matrix like a soil, tracer experiments are commonly performed. This can be in the field or column experiments. Sodium or potassium chloride is reported to be used as tracer solution (Appelo and Postma, 2005; Day-Lewis, 2003). The use of sodium chloride and using electronically conductive measurements to trace the solute concentration is a low – cost method to obtain geohydrological data (Singha, 2011). The electrical conductivity of a fluid is the sum of the conductivity of all molecules in solution bearing an electronic charge (ions) in a dilute solution, as shown by Kohlrausch law (1897). The relation between ionic strength and electrical conductivity of the fluid is described by Singha et al. (2011). See equation 1. In present research the relation in equation 1 is assumed to be linear, which is in accordance with the report of among others Mallants et al. (1996).

$$\sigma_{fluid} = \frac{1}{2} F \sum_{j=1}^{n} u_j C_j \left| Z_j \right| \qquad \text{Equation 1}$$

Where F is Faraday's constant (96.485 C/mol), u_j is the electric mobility of ion j (m^2 V/s), C_j is the molar concentration of the ion j (mol/m^3) and Z_j is the charge of the ion j and n is the number of ions in solution.

The electrical conductivity in present column experiment is however measured at the outlet. The electrical conductivity as measured in the effluent represents the bulk electrical conductivity. Singha (2011) relates the fluid electrical conductivity, i.e. the electrical conductivity of the injection fluid, to the bulk electrical conductivity applying Archie's law (Archie, 1942). Archie's law describes that the bulk conductivity relates to the fluid conductivity by the effective porosity and the tortuosity of the pores. The concentration of dissolved species bearing a charge thus determines the fluid and bulk electrical conductivity.

Furthermore, by the deviation between bulk electrical conductivity (effluent) and fluid electrical conductivity (injected tracer fluid) dispersive transport can be derived, next to advective transport (Singha, 2011). That is, breakthrough curves of injection and flushing of a conservative i.e. salt tracer give insight in dispersive and advective transport (Appelo and Postma, 2005). In present research the premise was that any mass transfer between the mobile and immobile zone was minimal, since advective flow rate differ orders of magnitude from diffusive rates. The tracer only represents the pore volume available for advective transport.

2.5.2 Colloidal Transport

The colloidal size range is not defined by rigid boundaries, as is illustrated by the various size ranges reported in literature. Stumm (1990) and Fitts (2002) for example define colloids as particles smaller than 10 μm. However, Karaman and Pashley (2005) state that colloidal particles range in the size from 50 Å to 50 μm. The definition as given by Bergna (2006) is the most appropriate linking the size range to specific physical properties of a colloidal particle. Bergna (2006) defines a colloid as follows: "The colloidal state of subdivision comprises particles with a size sufficiently small (≤ 1 μm) not to be affected by gravitational forces, but sufficiency large (> 1 nm) to show marked deviation from properties of true solution".

Physical properties that are specific for colloidal particles are the limited effect of gravitation on a particle, and the extremely high surface volume ratio or surface mass ratio. These physical properties affect the behavior of a colloid upon infiltration in a porous matrix (Pashley, 2004). If the impact of gravity on a particle is limited, the particle tens to remain in suspension for a long time. Gravitational force is one of the fundamental forces that operate on a particle next to Brownian motion and a resistance to motion (Pashley, 2004; Heimanz, 1997). As a function of its density the particle tens to settle (referred to as sedimentation). At small particle radius the energy of random movement (Brownian motion) is predominant over the impact of gravitational force. As a result sedimentation of particles takes a very long time and the dispersion is considered to be metastable (in a kinetic sense).

Brownian motion is a dominant process in dispersion. Brownian motion however causes collision of colloidal particles. Collision could result in the formation of and growth into larger aggregates. To this process is referred as coagulation. These aggregates will settle out due to an increase in particle size, and reduced surface to volume ratio. Consequently a precipitation is formed and the dispersion is not considered to be metastable any more (Pasley, 2004; Heimenz, 1997; Bergna, 2006; Napper, 1983). More on the stability of dispersed colloidal particles is described in section 2.4.2.

Colloids are reported to be transported through porous mixtures like soils, in laboratory column tests and field studies (Harvey, 1989; Enfield and Bengtsson 1988; Reimus 1995; Becker, 1999, Fitts 2002). The transport of colloids through a porous matrix depends on the difference between pore size and particle size. If the colloid is larger than the pore throats present in the matrix a build up of particles occurs; followed by clogging of pores and of the matrix as a whole. If the colloids are larger than some pore throats in the matrix then they are excluded from transport through these smaller pores. Preferential flow paths occur if the colloids are small enough to migrate through the larger pores. Due to lower toruosity at transport through the large pores, the flow path of the colloids shortens in comparison with a solute. In a column infiltration experiment the result is early arrival of the colloids at the outlet (Fitts, 2002; Enfield and Bentsson 1988; Harvey et al. 1989; McKay et al. 1993; Vilks et al. 1997). A difference between solute and colloidal transport was observed by several research groups. Harvey and Garabedian (1991) and Toran and Palumbo (1992) point out that this difference increases with increasing physical heterogeneity of the porous matrix (Harvey and Garabedian 1991; Toran and Palumbo, 1992; Becker 1991). In that sense colloids could function as a tracer to indicate the volume of pore space available for colloidal transport in relation to pore geometry (Harvey et al 1989; Fitts, 2002).

A typical physical property of colloidal particles is their large surface area in relation to their volume and mass. This has some consequences for the behavior of colloids upon filtration into a porous matrix. Due to the large surface area colloids are very susceptible to sorption processes (Bergna, 2006; Pasley, 2004; Heimenz, 1997; Stumm, 1996; McCarthy, 1989). The surface properties of a colloid play herein a dominant role (Bergna, 2006). For example, if the colloid surface is charged, the colloid tens to attach to a surface of opposite charge, i.e. attraction by electrostatic forces (McCarthy and Zachara, 1989). If colloidal particle sorbs onto the solid surface or phase interfaces the transport velocity of the colloidal particle is retarded. Transport of the colloid through the porous matrix is thereby delayed and tailing of breakthrough curve occurs (Fitts, 2002; Wan and Wilson, 1994).

In peat soils organic colloidal particles (particular organic matter, POM) are partly mobile and migrate with groundwater through the pore spaces (McCarthy and Zachara, 1989). Research on colloidal transport through peat was only found in relation to the impact of particle organic matter on the transport of contaminants (Harthhorn and Yong 1995; Perdrial, 2010; Weng, 2002; McCarthy and Zachara, 1989). Any research on the transport of foreign colloidal particles through a peat soil was not found in literature. However, the transport of colloids subject to sorption in a peat soils shows similarities with the transport of viruses and bacteria through sand columns. Viruses and bacterial cell are in the colloidal size range and bear a surface charge (Torkbazan, 2007; Lie, 2006; RIVM, 2009). Lei (2006) and Yun (2009) describe the attachment and detachment of virus cells to sand particles and the consequences of this reaction process on the retardation of virus in sand soils.

2.5.3 Hydraulic properties of peat soils

Peat has very unique physical properties that dictate the nature of water flow through a peat layer. The hydraulic conductivity of a peat layer is determined by among other factors, the botanic composition (Weiss et al., 1998; Bloemen, 1983; Gnatowski, 2010), de degree of decomposition (Gnatowski, 2010; Quinton, 2000) and the degree of compaction (Quinton, 2008). These properties are interrelated. Present section describes how these properties affect the hydraulic conductivity of a peat layer.

Botanic composition

The botanic composition of a peat layer refers to the original plant material and interrelated conditions in which peat material was formed. Peat soils composed of non and partly decomposed plant residues and its decomposition products. Peat soil therefore consists of plant residues, humus, water and possibly a small fraction of mineral matter (Sparks, 2003). The plant residue is commonly originated from moss, sedge, reed or wood vegetation. In the Netherlands both fen and bog peats are present in the Western and Northern part of the Netherlands respectively (Bos, 2010). Fen and bog types refer to the condition in which the peat layer was formed. Fen peat refers to wetlands fed by another water sources than rainwater, for example flooding by mineral rich seawater. Bog peat are the more acidic peat fed by rainwater runoff (Gnatowski, 2010; Killops, 2005; Bos, 2010).

Dissimilarities in hydraulic properties and moisture retention properties of various peat types relates to bulk density, differences in plant residues, cell structure and pore geometry (Gnatowski, 2010). First of all highly fibrous and undecomposed peats have a typical anisotropy structure (Zwanenburg, 2005; Ponziani, 2011; Hartlén, 1996). The plants remains usually have a horizontal orientation. The permeability of the soil in the horizontal direction is relatively high and is often many times higher than in the vertical direction (Zwanenburg, 2005). Secondly, not only the fibrousness and length of the fibres varies with botanic composition, but also the bulk density, water content and pore size, size distribution and shape (Gnatowski, 2010; Kruse, 2006; Holden, 2006). For example in wooden peats water is preserved and pore size distribution is quite wide. In moss peat types, the fibres are much smaller and more abundant. The structure is more homogeneously on bulk scale than wood peat (Gnatowski, 2010). Peat based on reed or mangroves, contains long hallow fibres. Gnatowski et al. (2010) concluded in his research to the moisture retention characteristics of wooden, moss and herbaceous (reed and sedge) peat retrieved from the Biebrza River Valley that the hydraulic conductivity depends on the botanic composition and the degree of decomposition. Wood peat, with high degree of decomposition i.e. humus content, had the lowest volume of hydraulic active pore space. The moss peat had a more fibrous structure and was less decomposed (contained less humus). The hydraulic active pore space was the highest in the moss peat, though it had the lowest hydraulic conductivity. The herbaceous peat had a unsaturated hydraulic conductivity higher than the wooden and moss peat.

Decomposition degree

The hydraulic conductivity of a peat layer is related to the decomposition degree of the peat (Gnatowski, 2010; Boelter, 1969; Paivanen, 1973). Assuming constant botanic composition and hydrological regime, the degree of decomposition increases with depth. Depth of the layer and the age of the plant residues are in this case proportional (principle of super position) (Hartlén, 1996). By decomposition the organic residues of plants are broken down in humus. Eventually even the more rigid structures like lignin and cellulose are decomposed into humus substances. This process is also referred to as humification (Sparks, 2003). Humus is defined by Stevenson (1982) as the total of the organic compounds in the soil excluding the undecayed plant, their ‘partial decomposition’ products, and the soil biomass. Because of decomposition, pore spaces become smaller and the size distribution of the pores become more narrow (Quinton et al 2000; Gnatowski, 2009). Furthermore, the fibrousness of the bulk material decreases and the bulk material becomes increasingly isotropic (Ngan-Tillard, 2010). The decrease in pore space implies also a decrease in water content and thus an increase in the bulk density (Kruse, 2007; Gnatowski, 2010).

The degree of decomposition is indicated in engineering fields by the Von Post scale (Hobbs, 1986; Delft Geotechnics, 1994; Post, 1926) or the humification degree as developed by Klavins et al (2009). The Von Post classification is method judging visually the color of peat pore water and texture of the peat material. The Von Post classification is therefore quite subjective measure. A more scientific measure is the humification degree, although not often used in the geotechnical filed. The humification degree relates humic substances to the total of organic matter present (Klavins, 2009).

Compaction degree (depth)

The process of decomposition is accompanied by the process of compression. Again taking the principle of super position as the starting point, this implicates that deeper layers being older and have undergone in general longer and heavier compaction – due to the increasing weight of the overlaying soil layers. Quinton et al (2008) observed a large decrease in saturated horizontal hydraulic conductivity of peat with depth. Quinton et al. (2008) demonstrated that compaction results into an increased portion of solids per volume. The larger pores collapse with depth due to compression and increased decomposition with depth (Hayward, 1982). The hydraulic resistance of the pores, especially the larger pores is thereby increased. The effect is an increase in pore density but a decrease in pore size and thus in inter-connectivity and in the total pore volume for available for flow.

Pore geometry and hydraulic conductivity

Hydraulic conductivity is known to increase proportionally with the square of the mean pore diameter (Freeze, 1979). The theory on solute transport also recognizes that hydraulic conductivity is affected by the shape and orientation of pores (pore geometry), the total surface area of the solid-liquid interface and the tortuosity of flow paths (Berryman and Blain 1987). The characteristic on flow through different sized pores could provide an estimate of the fibre surface area that the solution can come into contact with (Allaire et al. 2002).This section describes various reports as found in literature on the subject of hydraulic radius of the pores, pore geometry and interconnectivity of pores (tortuosity).

Pore structure and configuration are highly irregular in peat soils (Rezanezhad, 2010; Gnatowski, 2009). Though, connectivity of pore space has proven to play an important role in soil hydraulic properties (Rezanezhad, 2010; Holden 2008). The interconnectivity of pores is expressed in the term tortuosity. A decrease in the connectivity in pore space (increase of tortuosity) results in an increase length of flow path and thus a lower hydraulic conductivity of the bulk material (Dullien, 1979; Vogel, 1997).

The research performed by Holden et al. (2008) on the hydraulic conductivity of a peat soils connects well to the findings of Rezanezhad et al. (2010). Several research groups report that only a small fraction of the pore volume effectively conducts flow in a peat layer. This is the pore fraction larger than 1 mm (Rezanezhad, 2010; Holden et al., 2008; and others). This large pore fraction is thereby the most important pore fraction for solute and colloidal transport in a peat soil (Ours et al., 1997; Reeve et al., 2001). The contribution of small pores can be neglected if very large pores are active.

Holden (2002) reported that 10% of the discharge in deep peat layers is contributed to flow through large pores with a diameter larger than 1 cm. Holden et al. (2001) also showed that circa 30% of the discharge is transported through pores larger than 1 mm in diameter. Carey et al (2007) reported for a sub arctic peat that only 0.01% of the total bulk volume was pores larger than 1 mm. This large pore fraction accounted for circa 65% of the discharge at saturation.

Near ground level of a peat layer Baird (1997) reported for a fen peat that 51% to 78% of the flow is transported through pores large then 1mm. Holden (2008) reports that the fraction of large pores (> 1mm) decreases with depth in a undecayed layer of moss peat (top layer). Over a depth of only 20 cm a decline was observed in number of pores from 4 to 0.1. Also the pore density declined with depth. At 5 cm depth 85% of the discharge was generated through only 0.01% of the peat volume. At 20 cm depth 78% of the flow in the peat layer occurred in pores ranging in size between 0.25 and 1 mm in diameter, the remaining 22% was conducted through pores smaller then 0.25 mm. The porosity available for advective transport and the discharge declined with two orders of magnitude at that depth compared to the top of the layer.

3 Retardation of Silica Particle Growth

In general the pH of a peat soils in the Netherlands varies within the neutral to acidic pH range (Bos, 2010; Molendijk, 1996). The treatment method should therefore be applicable in a pH condition of maximum 7.5. The solubility of amorphous silica is however relatively low at ambient temperature and in the pH range of 2 – 9.5. The presence of silica in solution is restricted to concentration less than 120 mg SiO_2 per liter at ambient temperature. At soil temperatures, estimated to be in the order of 10 to 12^0C, dissolved silica concentrations tend to be even lower, in the order of 70 – 80 mg SiO_2 per liter (Iler 1979). In present study the solubility of amorphous silica is assumed to be at 100 ppm SiO_2 at temperature of 22^0C and pH range of 2 – 9,5.

Foremost the aim of this research section is to gain a high silica load in the injection fluid. To obtain a feasible – in a practical sense – treatment method to stabilize peat soils the load of silica in the injection fluid should be well above 100 ppm SiO_2. Such a load would reduce the number of flushes needed to stabilize a certain bulk volume. However this implies that the concentration of silica in the injection fluid exceeds the solubility limit of amorphous silica – causing immediate precipitation in the injection fluid and close to the injection point. If an alkaline solution, pH more than 9.5 should be used as source of silicon than precipitation is likely to occur upon injection to an acidic environment as peat. Instant precipitation at the injection point counteracts transport of silica over longer distances. To facilitate transport of silica the *formation of silica particles* should be either *inhibited* and/or *the growth of silica particles* should be *limited*. To elevate the concentration of dissolved silica in an aqueous solvent several methods are mentioned, as described in Chapter 2.

One of the methods mentioned in literature is the use of cationic and zwitterionic surfactants and polymers. These charged additives are reported to interfere with the process of silica polymerization at silica super saturation. Dissolved silica concentrations are obtained above the solubility limit of amorphous silica. Complementary, these additives are reported to interfere with the subsequent aggregation of silica. The formation of particles and/or the growth of these particles to a size at which they tend to sediment are thereby avoided. In the current system the additive of choice should function as a *carrier* increasing the concentration of silica that can be injected into and transported through a slightly acidic soil matrix (Demadis, 2009; Coradin, 2007; Zhang, 2011).

The additive of choice should fulfill certain requirements next to its performance as a 'silica carrier'. Naturally the stabilization treatment should be applicable in an open system as it concerns injection in a (partial) saturated soil layer. The use of hazardous or toxic surfactants, like for example the use of hexadecyl trimethyl ammonium chloride as proposed in the patent (Zon, 2007), is therefore not considered an option. Preferable is the use of a so called 'green additive' as defined by the Anastas and Warner (1998). Stathoulopoulou and Demadis (2008) proposed to use this definition as selection criteria. Coradin et al. (2007), Stathoulopoulou and Demadis (2008) name some structural features determining the ability of an additive to control dissolved silica concentrations and inhibit silica particle growth. They propose to use organic macromolecules, which play a role in the natural transport and mineralization of silicon, as a template for additive design or selection. As is performed by diatoms and plants (Staal, 2008).

Preliminary experiments showed that the Polyquaternium-4 cellulose biopolymer could be suitable to elevate dissolved silica concentrations and stabilize dispersed colloidal silica in the pH range of 6 to 7.5. A short summary of this preliminary research is given in Appendix 1.2. The results showed that the biopolymer delays silica polymerization and subsequent formation of silica particles. As opposed to total inhibition of silica polymerization as initially suggested by Stathoulopoulou and Demadis (2008).

It was decided to focus on one type of biopolymer. Thereby the chemical structure of the biopolymer and the impact of specific structural features on its performance was not a subject of research in this study. Though, the relation between structure and performance of a biopolymer is very relevant to the stated objective – and is recommended to be subject of future research.

Retardation efficiency of biopolymer

The first objective is to determine the retarding effect of the cationic biopolymer Celquat L200 on the first steps of silica polymerization. More specific, the objective is to determine the effect of the biopolymer on dissolved silica concentrations: on the phase transition of dissolved silica to a solid form of silica. The effect on silica polymerization is evaluated at silica super saturation and a pH of 7.5. In the case particles are formed the objective is complemented by the question if the biopolymer effects silica particle growth as well. The growth of silica particles is a measure of the stability of any dispersed colloidal silica present in the solvent. The process of silica polymerization and phase transition in the absence and presence of additives is briefly described in section 2.

The retardation efficiency of the biopolymer is the degree in which it is capable to I) maintain dissolved silica concentrations, and II) delay the formation or at least the growth of silica particles. As mentioned before, dissolved silica concentration should exceed the solubility limit of 100 ppm SiO_2. The growth of particles should be restricted to the colloidal size range within the 113 hours timeframe. In any case the formation of sedimenting particles should be avoided within the 113 hours timeframe upon addition of the biopolymer. The retardation effect is determined as a function of time, initial added concentration of silica and biopolymer, the weight (wt.) ratio to which silica and biopolymer are added, and the presence of dissolved and particulate organic matter.

The concentration of the biopolymer can be a critical factor in setting its behavior towards dissolved silica. It is reported that cationic biopolymers can function as a flocculent, enhancing the condensation of silicates in solution as biopolymer concentrations exceed a certain threshold (Demadis, 2009; Coradin 2007; Cumming 2010). Current research evaluates the retardation effect of the biopolymer in a concentration range below the flocculent dose.

As discussed in section 2, the stabilization of dispersed silica is based on electrostatic and/or steric forces induced by the biopolymer. Changing the ratio in which the biopolymer is present could have a different effect on a steric stabilized system than on an electrostatic based system (Heimanz, 1997). This chapter evaluates the impact of biopolymer to silicate wt. ratio on the dissolved concentration of silica. Furthermore, dissolved and particulate components in peat pore water could induce phase transition of silicates and/or instability of dispersed silica upon injection of the fluid (Heimanz, 1997; Coradin, 2007). Present chapter evaluates the influence of peat pore water on dissolved silica concentration and the stability i.e. formation and growth of biopolymer-silicate colloids present. The biopolymer is produced by Akzo Nobel under the trade name L200. Some relevant structural properties are given in Table 3.1. Product information sheet is added in Appendix 1.

Table 3.1: properties of Celquat L200 biopolymer

Name	Structural features	Molecular Weight(*)	Charge density(**)	Zeta potential(***)	Organic carbon content(****)	Flocculent dose(*****)
L-200	quaternary functional groups; cellulose backbone	138 kDa	1.1×10^{-5}	+20 mV^2	42%	1400 ppm

* den Hamer 2011 using Malvern Technology and Zetasizer

** Personal communication with Akzo Nobel

*** den Hamer 2011, using ZetaSizer Malvern

**** den Hamer 2011, based on TOC analyses

***** Cumming et al (2008)

The second objective is to determine the properties of any formed particulate matter in the mixture of biopolymer and silica, in terms of particle size distribution and zeta potential. Time evolution of the particle size distribution provides an insight in particle growth. Zeta potential analyses provide information on the electric field surrounding a particle. The zeta potential can be used to evaluate electrostatic interactions between mutual particles and their surroundings.

To apply the treatment method over a significant distance, i.e. more than 1 meter, transport of dissolved silica and particular silica through the porous matrix of peat should be feasible. Practical conditions state that the transport time should be max. 1 week, ca. 113 hours, as argued in Chapter 2. The configuration and size of a silica entity could change upon time and with solvent conditions, from a dissolved complex with the biopolymer, to a polymerized or colloidal form, or even to larger sized particulate matter. Depending on the intrinsic permeability of a porous medium particulate matter can be subject to filtration, consequently clogging the porous media.

Research Questions

The research topics as introduced and argued above are formulated into the following research questions:

1. Does the biopolymer L-200 inhibit silica polymerization and/or the formation of silica particles?
    a. Is the concentration of dissolved silica constant over time as a function of biopolymer to silica wt. ratio and initial silica concentration, i.e. degree of super saturation?
2. Does the biopolymer L-200 retard the polymerization and/or growth of silica particles?
    a. How much dissolved silica is removed from solution in time as a function of the biopolymer to silica wt. ratio and initial concentration of silica i.e. degree of super saturation?
    b. Is the mixture of biopolymer and silicate a true solution or a dispersion? If it concerns a dispersed solid phase, what is then the time evolution of the particle size as a function of biopolymer to silica wt. ratio and initial silica concentration? Moreover, are precipitates formed, indicating the instability of the dispersed phase within a 113 hour timeframe?
3. What is the effect of dissolved and particulate organic matter?
    a. What is the effect of peat pore water as a solvent as opposed to demiwater in terms of dissolved silica concentration (in analogy with 1) and particle size distribution of particulate matter (in analogy with 2), over time?
4. What are the properties of the formed biopolymer-silica entities and what is the effect of time, initial concentration, and biopolymer concentration on these properties?

The process of silica polymerization and phase transition in the absence and presence of additives is briefly described in Chapter 2.

3.1 Experimental Procedure and Analytical Methods

The performed retardation rest is based on the work of Demadis (2009). Demadis (2009) and Stathoulopoulou (2008) determined the inhibition performance of various cationic and zwitterionic biopolymers and surfactants on colloidal silica particle growth. The additives where screened by Demadis using a so-called Silica Supersaturation Test (Neuofotistou, 2008; Demadis, 2009; Mavredaki, 2005). The methodology, designed by Demadis, is based on dissolved silicate measurements in over saturated solutions, i.e. 500 ppm as SiO_2 at specific time intervals (up to 72 hours). The mixtures contained different dosages and types of inhibitors. The work of Demadis is used as a template for the design of the retardation test. As suggested by Coradin (2004) and based on the work of Mikhailova (2002), and Hiemenz (1997), the experiment is complemented by photon correlation spectroscopy analyses.

The polymerization reactions were induced by neutralizing a supersaturated alkaline silica solution (from pH 12 to 7.5) and monitored by the time-dependent depletion of dissolved silica and time-dependent particle formation and growth. The experiment was completed 113 hours after pH adjustment. The set time frame is relevant for conservative transport in a peat layer over a distance of more then 1 meter as argued in Chapter 2.

3.1.1 Retardation Efficiency of the Biopolymer Celquat L200

The distribution of silicon between the solute phase and the solid phase is determined in a closed system in the *absence* of peat soil material. The solid amount of silicon (C_s) expressed in ppm SiO_2 was calculated in terms of SiO_2 from the difference between the initial, added concentration (C_i) of silica and the final solute concentration of silica (C_w) after an incubation period of 113 hours. The solid concentration of silica in the closed system, a shaking flask, is defined by Equation 2.

The retardation efficiency is defined as the final solute concentration of silica (C_w) normalized to the solubility limit of amorphous silica (Equation 2). The solubility limit of amorphous silica at current test conditions is stated to be 100 ppm SiO_2.

$$\frac{C_{w\_t113h}}{100} = \text{Retardation Efficiency} \qquad \text{Equation 2}$$

It was expected that the biopolymer delays the condensation of dissolved silica species to larger silica polymers, i.e. that it interferes with the first step in the polymerization process of silica. If the final solute concentration of silica (C_{w_t113h}) equals the initial added concentration (C_i) then the biopolymer is argued to inhibit silica polymerization. If the final solute concentration of silica is significantly more than the solubility limit of amorphous silica (i.e. the retardation efficiency > 1) then it is argued that the biopolymer retards silica polymerization. If the retardation efficiency equals one or is even lower then 1, then it is proposed that the biopolymer has no influence or even stimulates silica condensation.

Two datasets are used to obtain a measure for the phase distribution of silicon – dissolved versus solid phase - at a certain mixture composition. The first set is dissolved silicate concentration as determined by the yellow silicomolybdic acid assay which allows titration of only the solute and low polymerized species of silica. The silicomolybdic acid method returns the mass of silica truly present as a solute and thereby provides information on the polymerization process from its very beginning (Coradin, 2004; Iler, 1979). The assay is described in paragraph 3.1.2.

The second dataset was obtained from Photon Correlation Spectroscopy (PCS) analyses (described in more detail in paragraph 3.1.2 as well). PCS analyses provide information on the latter steps of the phase transition of silica: coagulation of polymers and aggregation of colloidal particles to sedimenting particles.

After 2 hours of incubation electrostatic properties of the formed particles were determined in terms of the Zeta Potential. The magnitude of the zeta potential provides an indication of the potential stability of a colloidal system. If all particles in suspension have a large negative or positive zeta potential, then they will rend to repel each other. Attractive forces like Van der Waals forces and random Brownian motion, are then counter balanced and the tendency of particles to approach, i.e. to coagulate is reduced. The threshold for stable dispersed colloidal matter is commonly set at a zeta potential more than + 30 mV or less than -30 mV (Hiemenz, 1997; and others). It was expected that the pH had a large impact on configuration and on zeta potential of the formed biopolymer-silicate entities. Therefore the impact of pH on zeta potential is also evaluated by means of a titration test.

3.1.2 Test Protocol

A summary of the performed experiment is given below. Table 3.2 gives an overview of the prepared mixtures of the biopolymer Celquat L200 and sodium silica solution. The mixtures were prepared by adding a known weight of sodium silicate solution to a known volume of demiwater or peat pore water in a polyethylene container of 50 ml volume. Thereafter a known weight of biopolymer stock solution was added. After allowing the temperature to equilibrate, the silicate-biopolymer solution was quickly adjusted to pH 7.5 ± 0.02 using dilute hydrochloric acid (HCl) and or sodium hydroxide (NaOH) solution. The solution pH was checked to be constant for two hours after the start of the Retardation Test i.e. the first addition of HCl. If needed the concentration was corrected by a final addition of the solvent (< 5% wt.), the solvent was added to make up a total weight of 40 gram.

The original electrical conductivity of the mixture `1250_1_dw` was 6.91 mS/cm and 0.919 mS/cm of the mixture `300_0.1_dw`. The ionic strength origins from counter ions added to the solution as chloride to counter the cationic charge of the biopolymer and in the form of *sodium* meta silicate and hydro*chloric* acid. The ionic strength is thereby a function of initial added concentration of silica and biopolymer (C_i). A known volume of a sodium chloride stock solution was added to equate the ionic strength of all silicate-biopolymer solutions to 7.59 ± 0.51 mS/cm. The solutions were continuously shaken during incubation at 140 rpm. Temperature of incubation was 22^0C. Period of incubation was in total 113 hours after pH adjustment.

Silica polymerization in super saturated mixtures was monitored by analyzing the mixture and by analyzing the aliquots of the filtrate from 0.45 µm glass fibre filter; for (A) dissolved silica in time using the silicomolybdic colorimetric method, (B) particle size distribution in time using the PCS method and (C) zeta potential after 2 hours of incubation.

Reagents

Analytical grade chemicals and distilled water were mainly used throughout this laboratory research. All containers used were made of polyethylene to prevent possible leaching of silicate ions from glass containers. As source for silicon a solution of sodium meta silicate nonahydrate (reagent grade) was prepared. The cationic biopolymer was delivered as dry powder by Akzo Nobel and is produced by the former National Starch Company. The polymer is manufactured under the trade name Celquat L-200. The INCI designation is 'polyquarternium-4'. For the dilute hydrochloric acid solution a 37% solution was used. For the production of the sodium hydroxide solution, pallets were dissolved. For the sodium chloride solution powder was used. All chemicals were provided by Sigma-Aldrich.

As solvent demineralized water and peat pore water were used. Peat from location Bellingwedde was used to extract peat pore water in accordance with the peat used in the attachment tests, as described in Chapter 4 and in Chapter 5. A mass of 400 gram of wet peat is diluted with 2 liter of demiwater to a total weight of 2400 gram. The suspension is shaken at 20 ^{o}C for 5 days and was filtrated through a 0.45 µm membrane filter (Whatman). The supernatant was used as solvent for the sodium silica stock solution, to dilute the biopolymer-silicate dispersion, to dilute HCl and NaOH solutions to 1 M for pH adjustment, and to create a NaCl solution of 1 Molar for ionic strength adjustment.

Preparation of reactive stock solutions

Two stock solutions of 4000 ppm SiO_2 were prepared (demiwater and peat pore water as solvent). Both stock solutions were equilibrated to ambient temperature before use. The stock solutions were prepared 12 hours in advance and stored in a plastic air tight bottle at 20 ^{0}C. Silicate stock solution based on demiwater had a pH of 12.71 and a conductivity of 20.1 mS/cm. Using peat pore water as the solvent a pH of 12.76 and EC of 19.9 mS/cm was obtained.

A viscous stock solution of 20.000 ppm biopolymer Celquat L200 was made by means of an Ultra Thorax high shear mixer (2000 rpm) at ambient temperature. Only demiwater was used as solvent in order to prevent premature biodegradation of the biopolymer. The biopolymer stock solution was stored in air tight dark bottle at 4^{o}C two months before use. The pH of the solution was 6.7 and the EC was 2.77 mS/cm.

pH and EC

The pH of solution was measured using a Schott meter equipped with a blueline 3 mol/l KCl pH electrode. The electric conductivity was measured using an electric conductivity meter equipped with temperature and EC electrodes. Both pH and EC electrodes were calibrated before the start of each experiment with standard buffers.

Soluble reactive silica determination

The yellow silicomolybdic acid assay was performed to determine the concentration of reactive silica in solution. The assay is performed in accordance to the description given by Coradin (2004). Prior to soluble silica analyses, the extracted sample was filtered with a 0.45 μm glass fibre filter (Pall Corporation, type A/E) in order to remove any interfering turbidity. The gained supernatant was diluted with demiwater when necessary prior to analyses. Dissolved silica concentrations are expressed in terms of weight, ppm SiO_2.

The detection range of the quantitative method was 5 – 50 ppm SiO_2 as measured in a volume 12,5 ml. In present research an error of 12.75 to 9.60 ppm SiO_2 was obtained in the concentration range of 60 to 640 ppm SiO_2. Coradin specifies a relative standard deviation of 2% in the measurement range of 60 to 600 ppm SiO_2 (correction for dilution factor included). Each silica determination was performed in duplo. Evaluation was based on the average of the 2 measurements and this is the value as presented in the tables and graphs.

Particle size distribution

Photon Correlation Spectrometry (PCS) was used to determine the particle size distribution of a dispersion. Note, that PCS analysis evaluates only dispersed particles in the solvent. Zetasizer Nano ZS (Malvern) was used to perform this specific measurement. The technique is based on dynamic light scattering. More detail on the precise method of measurement can be found in Appendix 2, which is a short introduction to PCS delivered by Malvern Company. All measurements were performed in two-fold: prior filtration through 0.45 μm glass fibre filter (Pall Corporation, type A/E) and analysis without filtration. The PCS covers a detection range of 0.6 nm to 6 μm.

The Zetasizer Nano ZS instrument includes software to analyze the raw measurement data. A data analysis returns various parameters, among which the Z-average particle size, the particle size distributions and the derived count rate. The research results were evaluated based on the Z-average particle size, the particle size distribution derived from scatter intensity, and the derived count rate.
The Z-Average diameter is the mean diameter of the ensemble of particles, and is derived from the slope of the linearized form of the correlation function (Cumulant method). The term and derivation of Z-average is explained in more detail in the Manual Zetasizer (Malvern Instruments, 2003). Average particle sizes were preferentially expressed in Z-average instead of mean average particle size. The analytical error is restricted upon the use of Z-average, given the fact that the Z-average is directly derived from the raw measurement data.
The scatter intensity was plotted against diameter size classes in a particle distribution graph. The scatter intensity was expressed in percentages. The intensity percentage represents the relative differences in scattered light intensity between size classes, making up a total area of 100%. The intensity percentage is thereby not an indication for particle concentration. The derived count rate (DCR) displays the number of photons per second that are scattered by the particles *in suspension*. The count rate was useful as a *relative* indication of particle concentration in the dispersion. DCR provide an additional indication of the increase of particulate matter besides the calculation of C_s (Malvern Instruments, 2003)).

The quality of the PCS measurement and subsequent data analyses was evaluated by several parameters, among which the intercept of the correlation coefficient (should be > 0.5 and < 1.0) and the cumulant and/or distribution fitting error. This is explained in more detail in the Zetasizer manual (2003). Furthermore, if the dispersion was too polydispersed (Heimenz, 1997) than care should be taken at interpretation of the results, since the presence of relatively large particles could 'mask' the presence of relatively small particles. Namely, a large particle scatters much more light than a small particle. The scatter intensity of a particle is proportional to the sixth power of its diameter (from Rayleigh's approximation (Heimenz, 1997)). If particle sizes differ more than 1000 nm, a distorted image was likely to be obtained. The polydispersity is expressed as the polydispersity index (DIN ISO 13321, 1996) and this index should be less than or equal to 0.5 - 0.6. Besides, a poor data set could also be obtained if the concentration of particulate matter was too low. The detection limit was at a DCR of about 100 kcps.

Every distribution was based on 3 or 4 measurements of each 20 runs. First, the sample was placed in the cuvette holder and rested for 120 seconds. During that period the temperature equilibrated 25^{o}C. Each run was 10 seconds, with 14 runs per measurement and 3 measurements per sample at specific time interval. The total time of total measurement was thereby in the order of 9 minutes. Evaluation was based on the average of the 3 or 4 measurements and this is the value as presented in the tables and graphs. In some cases one of the measurements deviates from the rest of the set (based on PSD, correlation fit and distribution fit), and was excluded from the average.

Zeta potential

The zeta potential of dispersed particulate matter was determined by the Zetasizer Nano ZS apparatus. This instrument uses a combination of laser doppler velocity and phase analyses light scattering to determine the zeta potential. In brief, laser doppler electrophoresis measures small frequency shifts in the scattered light that arises due to the movement of particles in an applied electric field i.e. the electrophoretic mobility[3] of a particle. Electrophoresis measurement was performed in 3 or 4 measurements of 10 to 11 minutes in total. Zeta potential is related to electrophoretic mobility by the Henry or the Smoluchowski approximation (Malvern Instruments, 2003; Heimenz, 1997). The limit of detection for zeta potential measurement is 5 nm to 10μm sized particles.

The validity of each zeta potential measurement was evaluated based on a so called phase diagram as returned by the software. Explanation on this topic can be found in Appendix 12. We will not go into further detail on the exact method of measurement and data handling to obtain the Zeta Potential. More detailed information on electrophoresis measurement and zeta potential derivation can be found in the Malvern Zetasizer Manual (2003) and various application notes provided by Malvern Company on their website.

[3] The velocity of a particle in a unit electric field is referred to as its electrophoresis mobility.

3.2 Results

Table 3.2 summarizes the initial properties (t1) at ca. 2 hours after preparation, and final properties of the mixtures at t3, after 113 hours of incubation. Figure 3.1 shows several mixtures just ca. 2 hours after pH adjustment.

Figure 3.1: Fluid as prepared for a calibration curve at pH 7.5 prior to the retardation experiment. Initial concentrations from left to right: 1981 ppm SiO_2/ ppm L200, 1238 SiO_2/ ppm L200, 945 SiO_2/ ppm L200, 546 SiO_2/ ppm L200, 297 SiO_2/ ppm L200 and 20 SiO_2/ ppm L200 ppm L200.

Table 3.2: Overview of evaluated mixtures and their initial and final properties

Reference	Dilution series	solvent	Ci_silicate	Ci_biopolymer	Biopolymer/ Silicate	Cw_silicate (final)	EC (initial)	EC (final)	pH (initial)	pH (final)	Turbidity (final)
[Name]	[code]	[dw or ppw]	[ppm SiO_2]	[ppm L-200]	Wt ratio	[ppm SiO_2]	[mS/cm]	[mS/cm]	[-]	[-]	[y/n]
ppw_stock	-	ppw	0	0	-	-	0.431		5.09		yellow
SiO_2_stock_dw	4000	dw	3999,5	0	-	-	20.1		12.71		yes (vague)
SIO_2_stock_ppw	4000	ppw	3999.5	0	-	-	19.9		12.76		yes (vague)/ yellow
SiO_2_100_dw	100	dw	100	0	-	n.d.	7.30		7.49		no
SiO_2_100_ppw	100	ppw	100	0	-	n.d.	7.45		7.53		Yellow
SiO_2_700_dw	700	dw (no salt)	700	0	-	n.d.	4.76		11.99		no
SiO_2_700_dw	700	dw (no salt)	700	0	-	119	3.78		7.48		yes white flocks (directly)
SiO_2_1250_dw	1250	dw (no salt)	1250	0	-	n.d.	6.78		12.45		No
SiO_2_1250_dw	1250	dw (no salt)	1250	0	-	116	7.59		7.45		yes white flocks (directly)
300_1_dw	300	dw_salt	301	301	1.00	364	5.27	5.57	7.49	6.96	no
600_1_dw	600	dw_salt	597	597	1.00	338	6.95	7.06	7.48	7.36	no
1250_1_dw	1250	dw (no salt)	1246	1246	1.00	321	5.54	5.90	7.51	7.97	yes (vague)
300_1_ppw	300	ppw_salt	303	303	1.00	329	7.17	7.38	7.49	7.19	no
0_L200_ppw	0	ppw_salt	0	629		25	7.30	5.08	7.48	6.97	No
100_1_ppw	100	ppw_salt	100	100	1.00	123	6.91	6.79	7.49	6.98	No
300_1_ppw	300	ppw_salt	300	300	1.00	268	9.36	6.64	7.51	7.12	No
600_1_ppw	600	ppw_salt	600	600	1.00	367	7.48	6.02	7.49	7.12	No
1250_1_ppw	1250	ppw (no salt)	1250	1250	1.00	389	7.56	6.87	7.49	7.23	Yes (vague)
100_0.5_dw	100	dw_salt	100	50	0.50	84	7.8	6.85	7.51	7.11	No
300_0.5_dw	300	dw_salt	300	150	0.50	197	7.51	6.74	7.50	7.14	No
600_0.5_dw	600	dw_salt	600	300	0.50	424	7.54	6.78	7.49	7.18	No
1250_0.5_dw	1250	dw_salt	1230	615	0.50	382	7.57	6.99	7.49	7.24	No
100_0.1_dw	100	dw_salt	101	10	0.10	98	7.40	7.00	7.50	6.84	No
300_0.1_dw	300	dw_salt	300	30	0.10	273	7.26	7.37	7.50	7.20	No
600_0.1_dw	600	dw_salt	600	60	0.10	324	7.35	7.24	7.51	7.17	No
1250_0.1_dw	1250	dw_salt	1250	125	0.10	322	7.55	6.92	7.53	7.51	Yes (vague)

3.2.1 Efficiency of Biopolymer to retard silica polymerization

The objective was to determine the retardation efficiency of the biopolymer to the process of silica polymerization, particle formation and particle growth. This paragraph describes the effect of the biopolymer on the time evolution of the dissolved silica concentration. The dependence of dissolved silica concentration (C_w) was evaluated as a function of the initial *added* concentration of silica and biopolymer (C_i). Figure 3.2 presents the results. Figure 3.2 A. B and C illustrate the time evolution of dissolved silica at C_i of 300, 600 and 1250 ppm SiO_2. The results at initial silica concentration of 100 ppm SiO_2 are presented in Appendix 6. The series displayed in Figure 3.2 A, B and C represent biopolymer to silica weight ratio's of 1 to 1 (○), 1 to 0.5 (□) and 1 to 0.1 (△).

Initial concentration of 300 ppm SiO_2

At an initial concentration of 300 ppm biopolymer and 300 ppm SiO_2 the solution transformed into a suspension upon pH adjustment. Dissolved silica concentrations of 200 ppm SiO_2 were observed after 113 hours of incubation. That is. 66 wt. % of the initial added silica remained in solution. At C_i of 300 ppm SiO_2 and initial biopolymer to silica wt. ratio of 0.1 and 0.5, C_w values were observed not to deviate more than 50 ppm SiO_2 from C_i during the 113 hours of incubation. The measurement after 113 hours of incubation even indicates an overestimation of dissolved silica concentrations as it exceeds C_i. Given the standard error of measurement and the fact that C_w slightly increases with time, the following was proposed*: at initial concentration of 300 ppm SiO_2 and 150 or 30 ppm biopolymer the mixture remains a true solution after pH adjustment and during the subsequent 113 hours of incubation.*

Initial concentration of 600 and 1250 ppm SiO_2

Final dissolved silica concentrations were significantly higher in the presence than in the absence of the biopolymer at C_i of 600 and 1250 ppm SiO_2. Dissolved silica concentrations as measured in the absence of the biopolymer are presented in Figure 3.2 by the red open dots. Final dissolved silica concentrations of 119 and 116 ppm SiO_2 were determined after 113 hours of incubation in a 700 and 1250 ppm SiO_2 solution, respectively. This are C_w levels close to the solubility limit of amorphous silica. In the presence of the biopolymer and at C_i of 600 or 1250 ppm SiO_2, pH adjustment resulted in final dissolved silica concentrations of 320 to 488 ppm SiO_2. The value at 488 was however not trusted a sudden increase compared to t2 given Final dissolved silica concentrations was elevated by the presence of the biopolymer. However, because C_w was observed to be lower than C_i as from the first measurement in time, these mixtures could not be considered true solutions.

Increasing initial biopolymer concentrations did not result in higher dissolved silica concentrations over time – rather the opposite. At C_i equaled 600 ppm SiO_2 relatively small differences in dissolved silica concentrations between different biopolymer to silica wt. ratios were observed after 72 hours of incubation. At C_i 300 and 1250 ppm SiO_2 the biopolymer to silica wt. ratio had a larger impact on C_w then at 600 ppm SiO_2. Figure 3.2 A and C indicate that with increasing biopolymer to silica wt. ratio C_w decreased. At C_i equaled 300 ppm SiO_2 this difference was observed immediately from t=4 hours. At C_i equaled 1250 ppm SiO_2 a similar trend was observed after 113 hours of incubation.

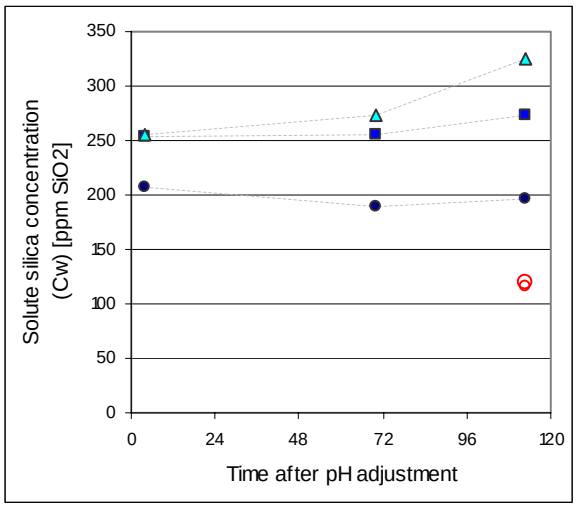

A. Initial silica concentration (C_i) of 300 ppm SiO_2

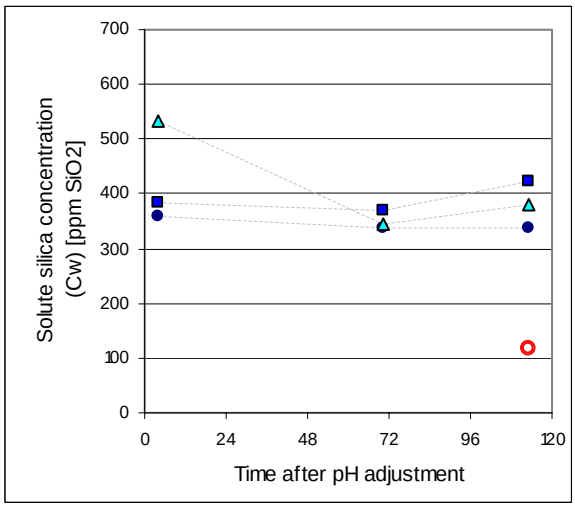

B. Initial silica concentration (C_i) of 600 ppm SiO_2

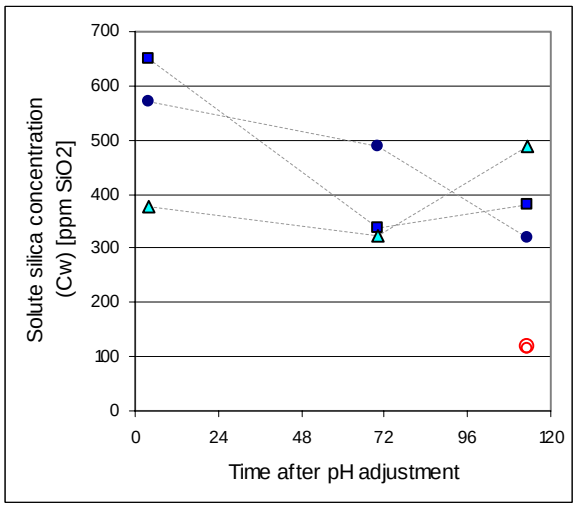

C. Initial silica concentration of 1250 ppm SiO_2

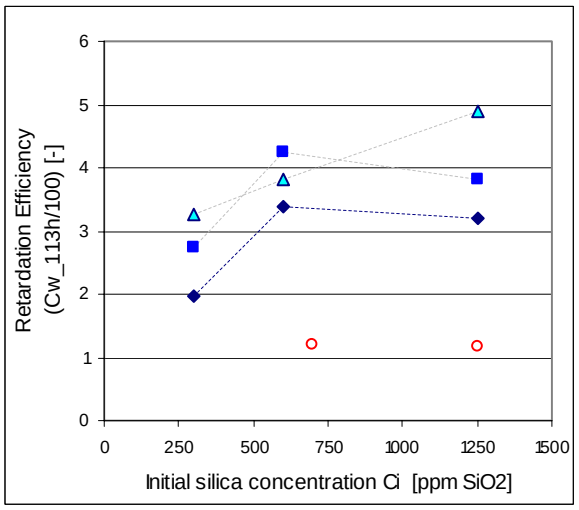

D. Retardation Efficiency in relation to C_i ppm SiO_2

Legend: The initial concentration SiO_2 is indicated by the title of graph. Initial ratio of biopolymer and silica in terms of weight:

- *1 to 0.1*
- *1 to 0.5*
- *1 to 1*
- *No L200 added. Sample codes: SiO2_700_dw and SiO2_1250_dw*

Figure 3.2: Dissolved silica concentration as a function of time and initial silica and initial biopolymer concentration. The x-axis represents the time of incubation as from the moment of pH adjustment. The y-axis represents the solute reactive concentration of silica. There is an overestimation of the solute silica concentration, especially at Ci of 300 ppm SiO_2. Details on the silicomolybdic acid assay are given in Appendix 5.

The condensation of dissolved and reactive silica into non-reactive silica species, i.e. larger oligomers and particulate matter, occurred predominantly during the first time interval (≤ 4 hours). Despite only tree measurements were conducted within the course of the experiment. the observed trends suggest *that steady state conditions were obtained within 113 hours of incubation – independent of initial biopolymer concentration*.

In general it could be stated that the biopolymer was capable to delay the condensation of reactive silica to larger polymers[4] at super saturated silica concentrations within the timeframe of 113 hours.

The retardation efficiency as defined by Equation 2 is presented in Figure 3.2 D in relation to C_i. The observed range in retardation efficiency was 3 to 5. Remarkably, the retardation efficiency did not increase with increasing initial silica or initial biopolymer concentration.

The efficiency of the biopolymer to retardate silica polymerization in a period of 113 hours was observed to be at its optimum if the mixture contains initially 1250 ppm SiO_2 and 125 ppm biopolymer.

3.2.2 Efficiency of Biopolymer to retard particle formation and particle growth

In the previous section it was concluded that the biopolymer was capable to elevate dissolved silica concentrations exceeding the solubility limit of amorphous silica. However, we also concluded that the obtained mixture was a suspension and not a true solution. Subsequent the question arises how the biopolymer influences the formation and growth of this particulate silica. Therefore the objective was to determine the retardation efficiency of the biopolymer on the process of silica particle formation and particle growth. First the stability of a formation of colloidal and sedimenting particles over time was evaluated for a super saturated silica mixture, in the absence of the biopolymer. Thereafter the stability of the dispersed silica was evaluated in the presence of the biopolymer and as a function of biopolymer dosage.

Time evaluation of particle formation (dispersion stability) was evaluation based on the time evolution of the particle size distribution, of the Z-average particle size and the derived count rate. A decrease in derived count rate with time is an indication for aggregation and/or sedimentation of particulate matter (Malvern Instruments, 2003). The total time for a measurement per sample was ca. 9 minutes. In that time interval the solvent was stripped of sedimenting particles to a certain degree depending on sedimentation velocity and amount of sedimenting particles present and formed. If two particles join together to form one aggregate this will reduce the count rate but increase the size of that ‘secondary’ particle. If the process of aggregation is significant, then derived count rates decrease and Z-average values increases over time i.e. a shift of particle size distribution to larger sized diameter will be observed.

[4] Degree of polymerization, which is non-reactive in the silicomolybdate quantification method.

Effect of biopolymer presence on time evolution of particle size distribution (PSD)

The particle size distribution in terms of Z-average particle size and derived count rate (DCR) was evaluated for a 1250 ppm SiO_2 concentrated mixture, in the *absence* and *presence* of the biopolymer L200. The results at 1250 ppm SiO_2 are discussed in this chapter. The cumulant fit for C_i 700 ppm SiO_2 reveals a poor data set. For that reason the results at C_i 700 ppm SiO_2 are presented in Appendix 7.

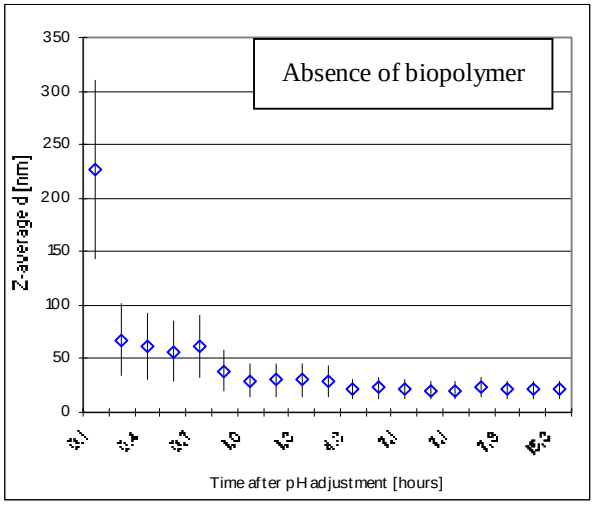

A. Z-Average in time of a 1250 ppm SiO_2 mixture. The polydispersity in nanometers is presented by the error bars.

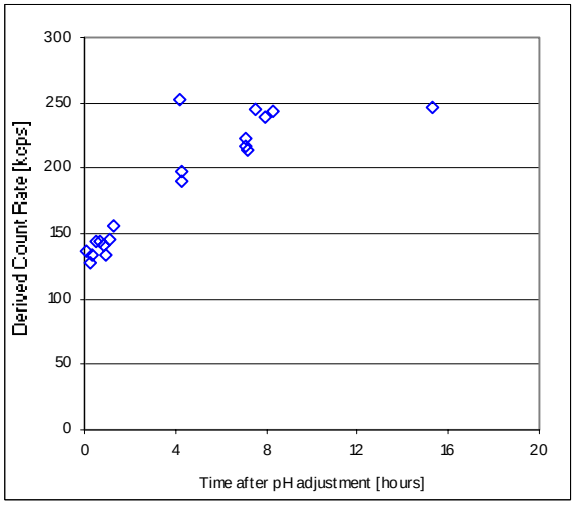

B. Derived Count Rate with time of a 1250 ppm SiO_2 mixture.

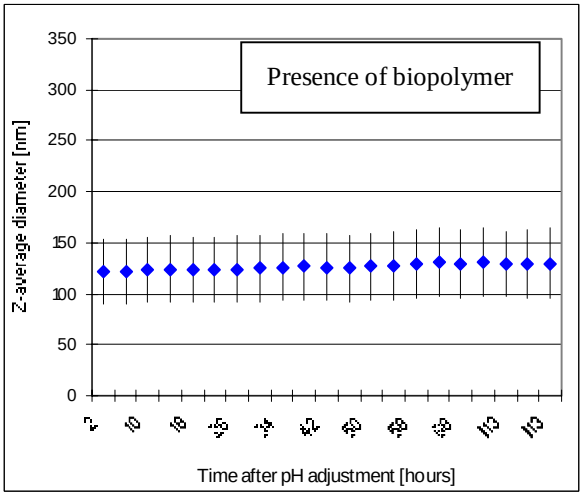

C. Z-Average in time of a 1250 ppm SiO_2 and 1250 ppm L200 concentrated mixture. The polydispersity in nanometers is presented by the error bars.

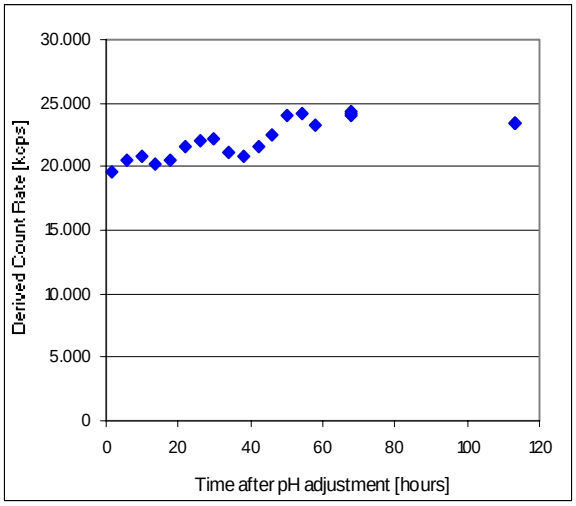

D. Derived Count Rate with time of a 1250 ppm SiO2 and 1250 ppm L200 concentrated mixture.

Legend:

- Z-average and DCR in the absence of the biopolymer
- Z-average and DCR in the presence of the biopolymer

Figure 3.3: Z-average particle size and derived count rate in the presence and absence of biopolymer at initial silica concentration of 1250 ppm SiO_2.

The results on relatively short time scale and for a silica mixture in the absence of the biopolymer, are presented in Figure 3.3 A and B. and Figure 3.5 C – sample code *SiO_2_1250_dw*. Figure 3.3 C and D. and Figure 3.5 B show the results on a longer time scale for a mixture of silica and biopolymer in a 1 to 1 wt. ratio– sample code *1250_1_dw*.

Figure 3.3 *A and B indicate that sedimentation of silica particles was significant in the absence of the biopolymer at initial silica concentration of 1250 ppm SiO_2.* If one considers the limit for detection for PCS analyses (100 kcps) it becomes clear that the amount of particulate matter dispersed in the solvent was low in the absence of the biopolymer. Especially if one compares Figure 3.3 B to D.
Moreover, the observed Z-average particle size was relatively small in the absence of the biopolymer. Z-average particle sizes decreased 24 minutes after pH adjustment from 227 nm to 60 nm. After 4.3 hours the dispersion seemed to be stable. From that moment in time, particulate matter as present in suspension had a Z-average diameter of 22 ± 1 nm as based on scatter intensity. In combination with the low derived count rates, as compared to the amount of particles dispersed in the presence of the biopolymer, these observations indicate sedimentation of particulate matter. Larger sedimenting aggregates seemed to be formed immediately upon pH adjustment. Thereby the amount of particles dispersed in the solvent reduces instantly, within a window of 4 minutes. Only the small particulate fraction was left dispersed in the solvent. Note that the error bar becomes smaller in time as well. The smaller error bars indicate that the particle size distribution becomes narrower.
These observations were confirmed by visual observation of white flocks several minutes after pH adjustment in absence of the biopolymer. Elevated dissolved silica concentrations after 113 hours of incubation in the presence of the biopolymer (320 ppm SiO_2 versus 116 ppm SiO_2) as discussed in paragraph 3.2.1 were in accordance with these observations as well.

As presented in Figure 3.3 C and D no significant sedimentation of particulate matter was observed in the presence of the biopolymer from 1.6 hours after pH adjustment (first point of measurement) to 113 hours after pH adjustment. The derived count rates in the presence of the biopolymer were 2 orders of magnitude higher then in the absence of the biopolymer. The biopolymer seemed to suppress the formation of sedimenting aggregates. The Z-average particle size was very constant in time. A Z-average of 126 ± 3 nm was observed during a time interval of 113 hours. The observed Z-average in time was significantly larger than the approximately 22 nm found in the absence of the biopolymer. Also the polydispersity in nanometers was higher than in the absence of the biopolymer. The polydispersity is indicated by the width of the distribution and is presented by the error bar in Figure 3.3.

Effect of biopolymer concentration on the time evolution of PSD

Present section evaluates the stability of dispersed colloidal silica. Time evolution of a particle size distribution (PSD) provides information on the stability of the particulate matter present. The maximum particle size present in the injection fluid sets among other factors the limit for silica transport and the potential for clogging.

The PSD for different biopolymer to silica wt ratios was evaluated after 4 and 113 hours of incubation at C_i of 300, 600 and 1250 ppm SiO_2. Figure 3.4 shows the particle size distribution at C_i of 300 ppm SiO_2 and 300 ppm biopolymer. Z-average and DCR values in relation to time of these particle size distributions are presented in Figure 3.7 A. The PSD at C_i equals 100 ppm SiO_2 and C_i equals 300 ppm SiO_2 at biopolymer to silica wt ratio of 0.1 and 0.5 are not presented in this section for reasons that will be discussed below. These results are presented in Appendix 8. Figure 3.5 A and B illustrate the obtained particle size distributions at initial silica concentration of 600 and 1250 ppm SiO_2, respectively. The different series represent the different biopolymer to silica wt. ratios tested. Z-average and DCR values in relation to time of these particle size distributions are presented in Figure 3.6 and Figure 3.7. Figure 3.5 C illustrates the shift in particle size distribution of a 1250 ppm SiO_2 mixture in the absence of biopolymer. Z-average and DCR values in relation to time of these particle size distributions are presented in Figure 3.3 A and B.

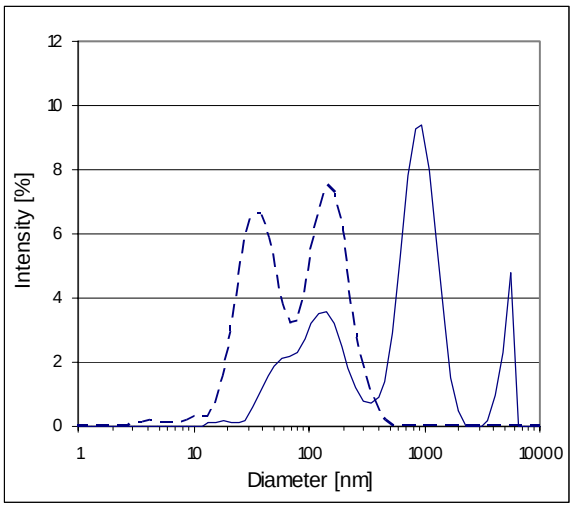

On the x-axis distribution of each size class is given. On the y-axis the relative intensity of scattered light is reported. This specific distribution is therefore known as an intensity distribution.
The size distributions of dispersions at t1 and t3 at initial concentration of 300 ppm SiO2 and 300 ppm L200 are presented here. The correlation functions at initial biopolymer concentration of 30 and 150 ppm L200 indicated a non-reliable data set. Therefore these size distributions are disregarded and not presented.

Legend biopolymer and silica mixtures:

1 to 1. at t1=4h
1 to 1. at t3=113h

Figure 3.4. Initial concentration of 300 ppm SiO_2 and 300 ppm biopolymer

Initial concentration of 300 ppm SiO_2

Figure 3.4 clearly shows that the few particles that were present at a 1 to 1 wt. ratio between biopolymer and silica, were not stable in time and aggregated to particles > 1µm. After 113 hours of incubation 95% of the distribution area, in terms of scatter intensity, was smaller than 1660 nm. This was in accordance with the lower dissolved silica concentration measured as opposed to a 0.5 or 0.1 to 1 wt ratio.

At C_i of 300 ppm SiO_2 and 30 or 150 ppm biopolymer very irregular and polydisperse distributions were obtained for all three measurements in time. The intercept of the correlation function was out of range and both cumulant as distribution analyses revealed a poor data set i.e. high fitting error. The poor fit could be explained by a combination of particulate concentrations close to zero (low DCR and relatively high C_w) and/or the presence of a few aggregates or dust particles (very high polydispersity index of 0.931). See figure in Appendix 9 for an illustration of the DCR.

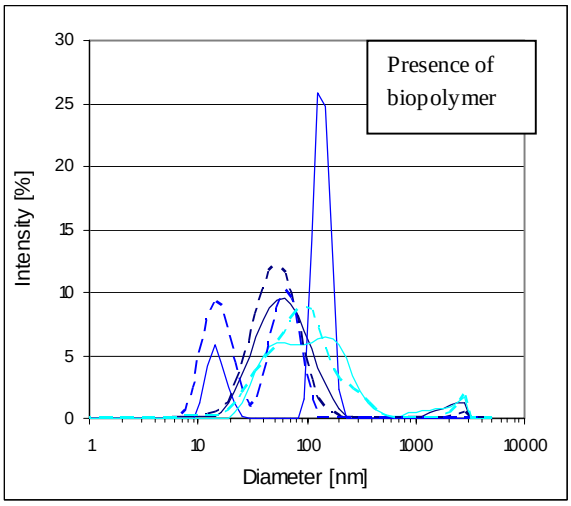

A. Initial concentration of 600 ppm SiO2 and variable biopolymer concentration.

On the x-axis distribution of each size class is given. On the y-axis the relative intensity of scattered light is reported. This specific distribution is therefore known as an intensity distribution.
The size distributions at t1 and t3 at initial concentration of 600 and 1250 ppm SiO2 and variable biopolymer concentrations are presented in figure A and B respectively. For clarity the particle size distributions at t2 are added in Appendix 10.
Figure C illustrates the shift in particle size distribution of a 1250 ppm SiO2 mixture in the absence of the biopolymer. The figure shows the shift during 8.5 hours of incubation after pH adjustment.

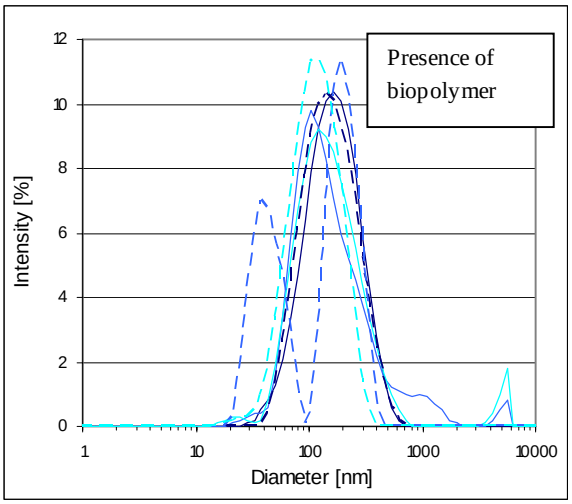

B. Initial concentration of 1250 ppm SiO_2 and variable biopolymer concentration.

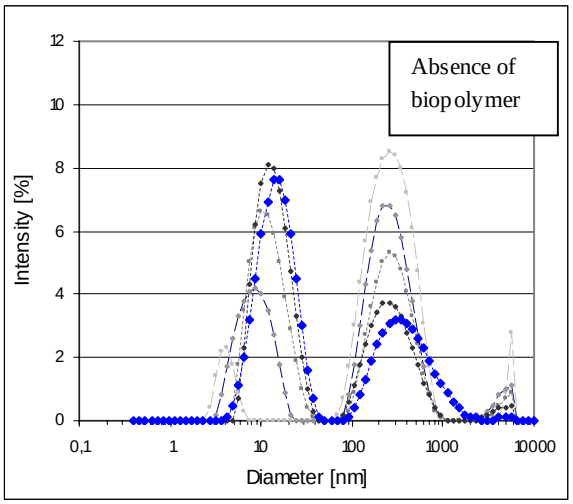

C. Initial concentration of 1250 ppm SiO_2 in the absence of biopolymer.

Legend biopolymer and silica mixtures:

Silica to biopolymer weight ratio of :

- 1 to 1. at t_1=4h
- 1 to 0.5. at t_1=4h
- 1 to 0.1. at t_1=4h
- 1 to 1. at t_3=113h
- 1 to 0.5. at t_3=113h
- 1 to 0.1. at t_3=113h

Legend silica mixture:

1250 ppm SiO_2

- t=0.07 h
- t=1.26 h
- t=4.28 h
- t=7.12 h
- t=8.27 h

Figure 3.5: Particle size distributions at various initial silica and biopolymer concentrations

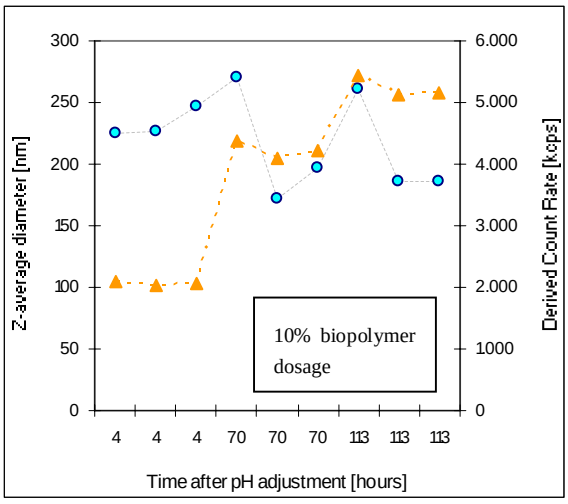

A. Initial concentration of silica is 600 ppm SiO2, initial concentration biopolymer is 60 ppm L-200.

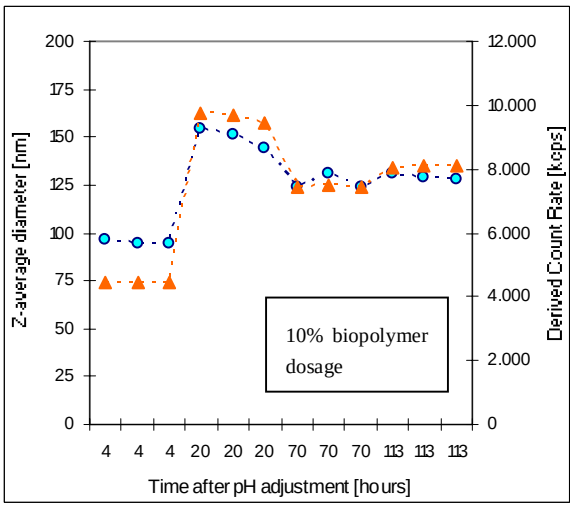

C. Initial concentration of silica is 1250 ppm SiO2, initial concentration biopolymer is 125 ppm L-200.

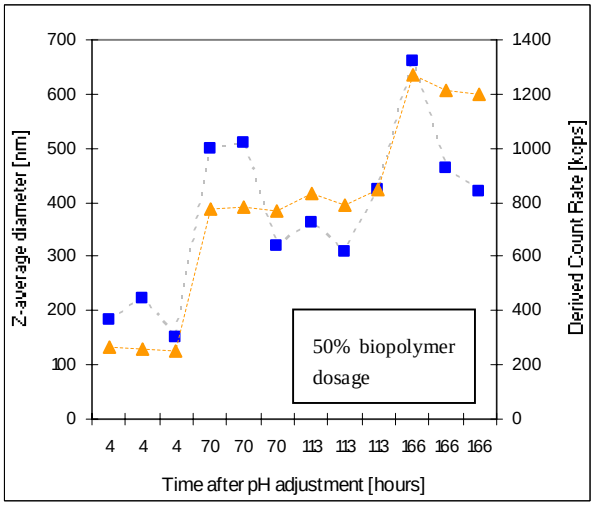

B. Initial concentration of silica is 600 ppm SiO2, initial concentration biopolymer is 300 ppm L-200.

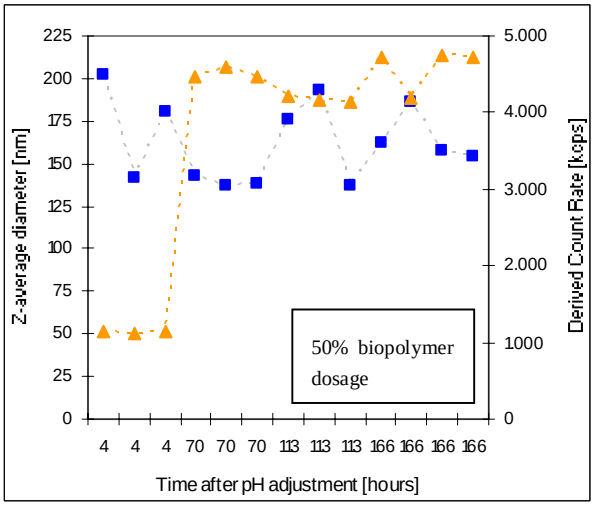

D. Initial concentration of silica is 1250 ppm SiO2, initial concentration biopolymer is 625 ppm L-200.

Legend:

Z-average particle size in terms of particle diameter [nm]. at 0.1 to 1 wt. ratio between C_i biopolymer and C_i silica

Z-average particle size in terms of particle diameter [nm]. at 0.5 to 1 wt. ratio between C_i biopolymer and C_i silica

Derived count rate [kcps]

Figure 3.6: Z-average and derived count rate of C_i 600 and 1250 ppm SiO_2 dispersions at various C_i biopolymer

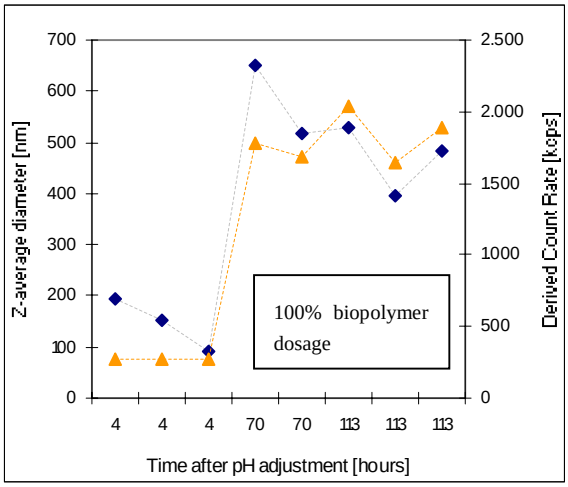

A. Initial concentration of silica is 300 ppm SiO2, initial concentration biopolymer is 300 ppm L-200.

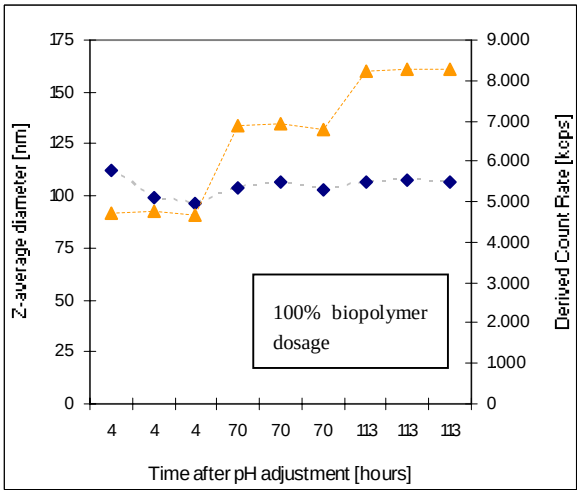

B. Initial concentration of silica is 600 ppm SiO2, initial concentration biopolymer is 600 ppm L-200.

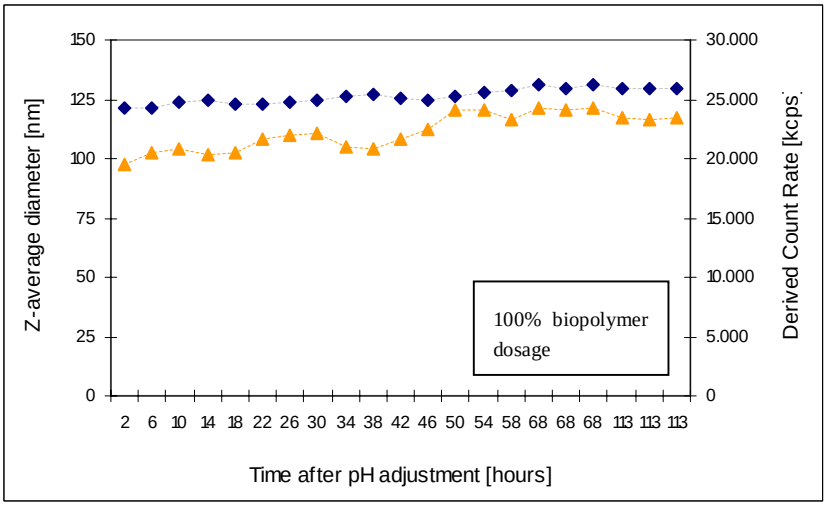

C. Initial concentration of silica is 1250 ppm SiO2, initial concentration biopolymer is 1250 ppm L-200.

Legend:

Z-average particle size in terms of particle diameter [nm]. at 1 to 1 wt. ratio between C_i biopolymer and C_i silica

Derived count rate [kcps]

Figure 3.7: Z-average and derived count rate of C_i 300, 600 and 1250 ppm SiO_2 dispersions, at 1 to 1 wt. ratio between silica and biopolymer.

Initial concentration of 600 ppm SiO_2

Figure 3.5 A shows the intensity size distribution collected after 4 and 113 hours. The series represent the initial weight ratio between biopolymer and silica. Wt. ratios of 0.1 to 1, a 0.5 to 1 and a 1 to 1 wt. ratio were tested.

The results indicate that when the biopolymer was added in a 0.1 to 1 wt. ratio, the particulate matter formed within 4 hours had a monomodal distribution, i.e. one population. With time aggregation to 'secondary' larger particles occurred and the formation of two populations became visible (two overlapping peaks). Figure 3.6 A presents the time evolution of Z-average and DCR of the formed particulate matter. Z-average particle size observed after 113 hours was 186 nm. However, the Z-average results were not conclusive given the high variance in values for the triple measurements at each time interval. The DCR increased with time from ca. 2000 kcps to ca. 5000 kcps. After 4 hours of incubation 95% of the intensity distribution area (D95%) had a particle size smaller than 164 nm. After 113 hours D95% shifted to 213 nm. The increase in DCR, D95% and the increase in polydispersity indicated a continuous process of particle growth. That is, an increased instability of dispersed particles.

When the biopolymer was added in a 0.5 to 1 wt. ratio, particulate matter aggregated in two distinct and relatively narrow populations over 113 hours time. The formation of secondary particles occurred before completion of the test. Figure 3.6 B presents the time evolution of Z-average and DCR of the formed particulate matter. The Z-average particle size increased in time and was 364 nm after 113 hours of incubation. The distribution shifted to larger size classes over time. After 4 hours D95% was smaller than 183 nm. After 113 hours D95% shifted to 367 nm. The increase in D95% over time was an indication for the formation of secondary particles, i.e. particle growth. DCR values, especially after 4 hours, were relatively low indicating low particle concentrations. Thereafter DCR increased from 200 to 1200 kcps in time. This was an indication for the formation of 'primary' particles i.e. a continuous process of dissolved silica polymerization.

When the biopolymer was added in a 1 to 1 wt. ratio, particulate matter aggregated in one relatively wide population. Subsequent growth of particles in time was not observed. The average particle size showed to be quite constant in time: Z-average particle size of 105 ± 5 nm (see Figure 3.7 B). The average particle size was smaller than at a 0.5 to 1 wt. ratio. Width and overall size range of the distribution remained quite stable over time as well. The particle size at D95% was 103 nm after 4 hours and 122 nm after 113 hours. DCR increased from ca 5000 kcps to 8000 kcps in time. Increasing DCR values are an indication for formation of 'primary' particles i.e. polymerization of dissolved silica. The DCR were higher than observed at a 0.5 to 1 wt. ratio.

Initial concentration of 1250 ppm SiO_2

At a 0.1 to 1 wt. ratio between biopolymer and silica, the results indicate a monomodal distribution of the particulate matter formed in the biopolymer silica mixture. There was an increase of polydispersity with time though a distinctive additional size population was not formed. Figure 3.6 C presents the time evolution of the Z-average particle size and DCR. The Z-average particle size was 95 ± 1 nm after 4 hours of incubation. The average particle size increased slightly during incubation. Z-average stabilized at a size of 129 ± 1 nm after 113 hours of incubation. After 4 hours of incubation 95% of the intensity distribution area (D95%) had a particle size smaller than 244 nm and 507 nm after 113 hours of incubation. A shift to the right in particle size was thus observed, i.e. particle growth was observed. Derived count rates showed a similar evolution over time as the Z-average. DCR increased within 20 hours to ca 9.500 kcps. Thereafter it gradual decreased and stabilized at a level of ca. 8.000 kcps. A decrease in DCR indicates a decrease in particulate matter. A decrease in particulate matter could be caused by aggregation and/or sedimentation of particles.

At a 0.5 to 1 wt. ratio between biopolymer and silica, the shape of the distribution was bimodal after 4 hours of incubation. The shape of the distribution after 4 hours showed the most similarities to the distribution as obtained in the absence of the biopolymer. After 113 hours of incubation the distribution transformed into a trimodal more chaotic distribution. As suggested by the shift in peak locations and size over time (Figure 3.5 B), the D95% limit shifts from 313 nm after 4 hours to 861 nm after 113 hours.

The derived count rate was relatively low 4 hours after pH adjustment. After 113 hours of incubation the DCR increased from 1000 kcps to 4500 kcps. The derived count rate stabilizes within 70 hours at 4400 kcps, indicating a relatively constant concentration of particles after 70 hours of incubation. The amount of particles dispersed after 4 hours of incubation was relatively low compared to 10% biopolymer dosage and especial to a 100% biopolymer dosage. This observation was in accordance with the dissolved silica measurements performed on the liquid fraction after 4 hours of incubation.

The polydispersity index was 0.435 and was more or less constant in time. The polydispersity Index was significantly higher than at a 10% or 100% biopolymer dosage, indicating a wider distribution. The relatively large increase of D95% of ca. 550 nm within 109 hours of incubation indicated a continuous process of aggregation and subsequent particle growth. After 113 hours of incubation particles larger than 1 μm were formed, i.e. particles exceeded the colloidal size range.

As already described on page 37, at a 1 to 1 wt. ratio between biopolymer and silica a monomodal, symmetric and more or less constant distribution in time was obtained. Z-average values after 5 hours were 121 nm and 129 nm after 113 hours. As already suggested by the minor change in Z-average and peak size, the difference in D95% over time was just 2 nm indicting a very stable particle size distribution. The obtained D95% size was 377 nm after 113 hours of incubation. The derived count rate was relatively high 19.500 kcps already after 4 hours of incubation. DCR values increased over time up to ca. 23.400 kcps after 113 hours of incubation. The width of the distribution was relatively narrow. The polydispersity index was low 0.264 after 113 hours and did not increase with time.
Relative to 0.1 and 0.5 wt. ratio, a lot of particles were formed at 1 to 1 wt. ratio already within the first 1.6 hours of incubation. The high and increasing DCR values indicate the continuous formation of new primary particles i.e. continuous polymerization of dissolved silica. These primary particles aggregated over time, resulting in the formation of secondary particles. However, the subsequent growth of these secondary particles seemed to be restricted by the presence of the biopolymer. From the moment a size of ca. 400 nm was reached growth stopped. Particles sizes larger than 1 μm were not observed.

Note that the relatively high amount of dispersed colloids did not result in a decreased ability of the biopolymer to retardate the polymerization process of silica. The dissolved silica concentrations after 113 hours of incubation were at 600 ppm C_i more or less equal to concentrations at 1250 ppm SiO_2.

In general

Each particle size distribution shows to some extent the existence of ≥ 4 μm size particles. Despite the fact that the peak decrease when the PCS data set was translated to a volume based particle size distribution, it suggests the presence of dust and/or larger aggregates. A relatively small increase of peak area with time at > 4 μm size classes was observed at all mixture compositions, suggesting particle growth or increase in contamination. The peak area remains however small and less than or equal to 5% intensity area during the period of 113 hours.

Summarizing

To summarize, a continued process of particle formation and growth despite the addition of the biopolymer was observed. The following was observed regarding the relation between initial silica concentration, particle formation and particle growth, at 1 to 1 wt. ratio. At initial concentration of 300 ppm SiO_2 only few particles were formed. The particles that were formed were not stable over time and partly sedimented. .At initial concentration of 600 ppm SiO_2, more particles were formed and particle concentrations increased with time.

The growth of particles was more than observed at 1250 ppm SiO_2 but sizes remained below 1 μm. The formation of sedimenting particles was not observed. At initial concentration of 1250 ppm SiO_2 relative many particles were formed. The particles present had a constant particle size in time, and were therefore considered stable. In general one could state that increasing the initial added concentration of silica at 100% biopolymer dosage increased the stability of the formed particulate matter.

At initial concentration of 600 and 1250 ppm SiO_2 and 100% biopolymer dosage, more particles were formed than at 10 or 50% biopolymer dosage. The dispersed material was observed to be stable over 113 hours of incubation at biopolymer dosage of 100%. At biopolymer dosage of 10% or 50% this was not observed. Furthermore, at 100% biopolymer dosage the particle sizes remain colloidal during the 113 hours of incubation. The biopolymer prevents (temporarily?) the formation of sedimenting particles. Therefore it was proposed that the biopolymer did efficiently delay the growth of silica colloidal particles.

In conclusion, the biopolymer improves the stability of dispersed colloidal silica within a timeframe of 113 hours, and this ability depends on biopolymer dosage. This observation opposes the results from section 3.2.1. The ability of the biopolymer to elevate dissolved silica concentrations during the timeframe of 113 hours did not depend on the biopolymer dosage.

The capability of the biopolymer to delay the growth of colloidal silica was the most efficient at an addition of 1 to 1 wt. ratio at initial silica concentration of 600 or 1250 ppm SiO_2.

3.2.3 Effect of dissolved and particulate organic matter on retardation efficiency

In section 3.2.1 and section 0 the capability of the biopolymer to retard silica polymerization and to stabilize colloidal silica was evaluated using demiwater as the solvent. In present section the efficiency of the biopolymer to retardate silica polymerization and to stabilize colloidal silica, was evaluated using peat pore water (ppw) as the solvent. The impact of particulate and dissolved organic matter originating from peat on the retardation efficiency of the biopolymer was determined. The impact of ppw was only determined for a 1 to 1 wt. ratio between initial biopolymer and silica concentration.

Effect of peat pore water on time evolution of dissolved silica concentration

Figure 3.8 A shows the dissolved silica concentrations after 4, 72 and 113 hours of incubation at initial concentration of 300, 600 and 1250 ppm SiO_2/ ppm L200. The derived count rate as measured is presented in Figure 3.8 B. The red open dots in Figure 3.8 B indicate the observed derived count rates for peat pore water (ppw) in the absence of silica and or biopolymer.

Initial concentration of 300 ppm SiO_2

At initial concentration of 300 ppm SiO_2 the dissolved silica concentration changed only little over the first 4 hours of incubation and showed a gradual decline over the 113 hours of incubation – if one considers the error of measurement of 9 to 12 ppm SiO_2. The relatively low derived count rates confirmed this observation of low solid silica concentrations. Because the difference between ppw including silica and biopolymer (green triangle) and ppw not containing silica and biopolymer (open dots) was small and increases only little during the initial 72 hours of incubation.

Both Figure A and B indicate a small decline in dissolved silica over time; though the retardation efficiency (Equation 2) after 113 hours of incubation was 2.68. Using demiwater as the solvent, the retardation efficiency of the biopolymer was 1.97. The presence of dissolved and particulate organic matter had therefore no negative impact on the biopolymer to retard silica polymerization at C_i of 300 ppm SiO_2, rather the opposite.

Initial concentration of 600 and 1250 ppm SiO_2

During incubation dissolved silica concentrations varied in the range of 277 up to 446 ppm SiO_2. The observed dip 72 hours after pH adjustment could not be explained. Final dissolved silica concentrations were 370 and 390 ppm SiO_2 irrespective of C_i , as determined in the range of 600 to 1250 ppm SiO_2.

The retardation efficiency (Equation 2) of the biopolymer at C_i of 600 ppm SiO_2 equaled the efficiency at 1250 ppm SiO_2, i.e. 3.4 ± 0.6. The retardation efficiency of the biopolymer in the presence of particulate and dissolved organic matter was comparable to retardation efficiency observed in the absence peat pore water (as discussed in paragraph 0 and illustrated in Figure 3.5). Hence, the presence of particulate and dissolved organic matter did not influence the efficiency of the biopolymer to retardate the polymerization process of silica – at least not significantly within a time frame of 113 hours.

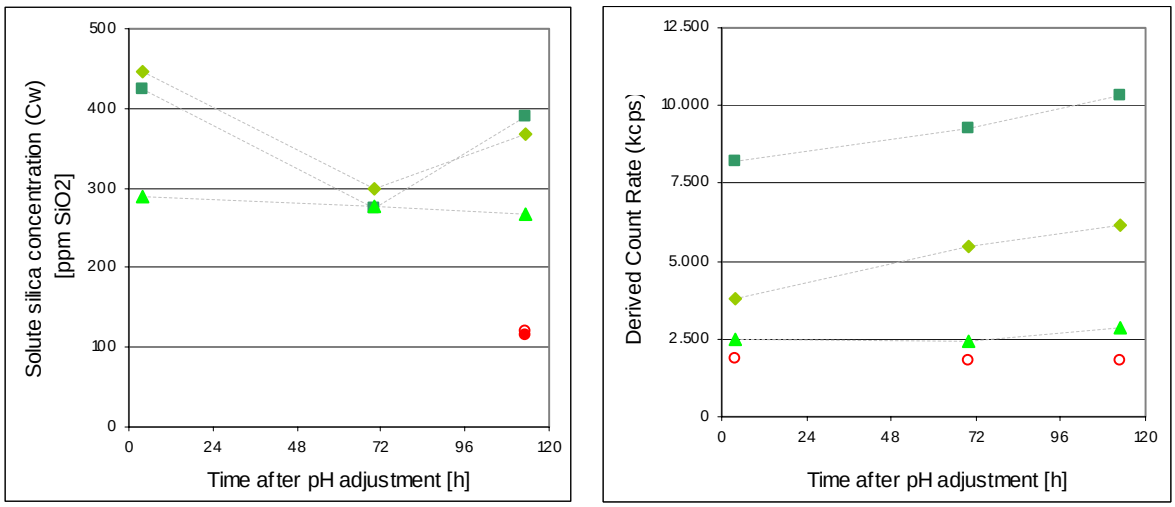

A. Solute silica concentration using peat pore water as solvent as a function of time.

B. Derived Count Rate (DCR) in time based on PCS analyses.

Legend:

C_i of 300 ppm SiO_2 at 1 to 1 wt. ratio biopolymer to silica; peat pore water as solvent

C_i of 600 ppm SiO_2 at 1 to 1 wt. ratio biopolymer to silica; peat pore water as solvent

C_i of 1250 ppm SiO_2 at 1 to 1 wt. ratio biopolymer to silica; peat pore water as solvent

Peat pore water. including particulate and dissolved organic material

C_i of 1250 ppm SiO_2 in the absence of biopolymer. demiwater as solvent

Figure 3.8: Time evolution of dissolved silica concentration and derived count rate as function initial silica concentration

Figure 3.8 A and B were performed on the same sample fluid. The x-axis represents the time elapsed after pH adjustment from >12.5 to 7.5. The concentration of dissolved silica is plotted on the y-axis. The series return the measured values at an initial added concentration of 300. 600 or 1250 ppm SiO_2 mixed with equal amounts of biopolymer (1 to 1 wt. ratio). Values in Figure 3.8 A are corrected for 'Blanco' values of solely the peat pore water solution. Note that the red closed dots represent a suspension of silica in the absence of biopolymer ánd demiwater as solvent. This is thus not a true Blanco of the performed test. To give an indication of the fluid properties in the absence of biopolymer these observations are included.

Effect of peat pore water on the time evolution of PSD

Figure 3.9 presents the time evolution of the particle size distribution at C_i of 600 and 1250 ppm in the presence and absence of particulate and dissolved organic matter.

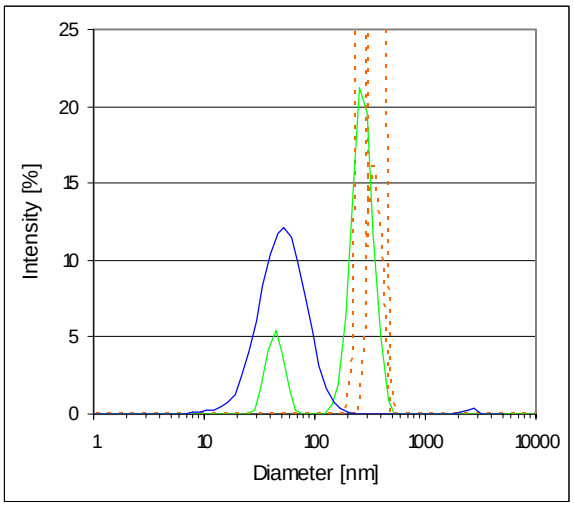

A. Initial silica concentration of 600 ppm SiO2 after 4 hours of incubation.

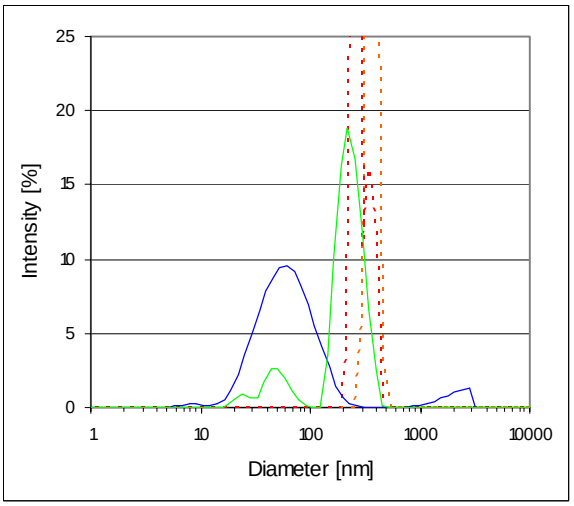

B. Initial silica concentration of 600 ppm SiO2 after 113 hours of incubation.

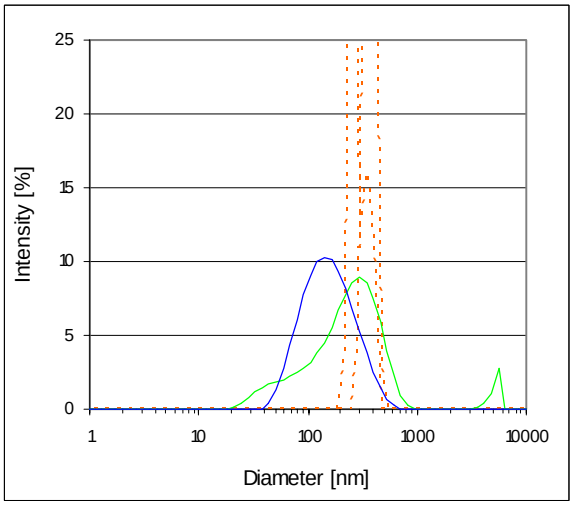

C. Initial silica concentration of 1250 ppm SiO2 after 4 hours of incubation.

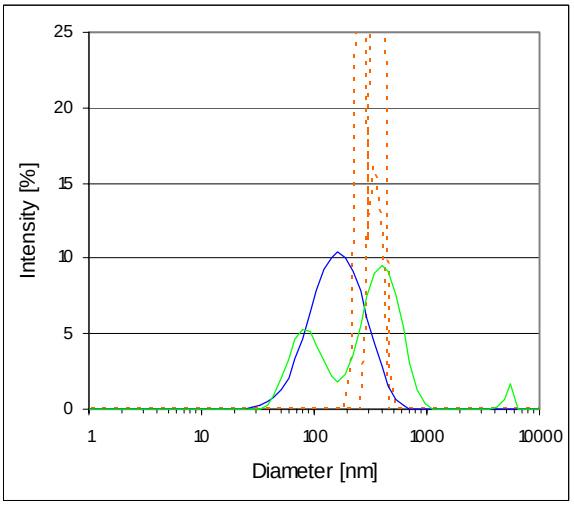

D. Initial silica concentration of 1250 ppm SiO2 after 113 hours of incubation.

Legend:

- peat pore water in the absence of biopolymer and/or silica (two PSD analyses displayed)
- mixture of biopolymer and silica in a 1 to 1 wt. ratio; peat pore water as solvent
- mixture of biopolymer and silica in a 1 to 1 wt .ratio; demiwater as solvent

Figure 3.9: Time evolution of PSD at initial concentration of 600 or 1250 ppm SiO2 and biopolymer using peat pore water as solvent. On the x-axis distribution of each size class is given. On the y-axis the relative intensity of scattered light is reported. This specific distribution is therefore known as an intensity distribution.

Peat pore water contains dissolved organic molecules (DOM) and particulate organic matter (POM). These colloidal-sized particles are operationally defined as particles with a diameter smaller than 0.45 μm diameter in the performed Retardation Test. Peat pore water is given in Figure 3.9 as the red interrupted line, indicating the presence of particulate matter in the size range of 190 to 531 nm. There was thus a small deviation between filter size and the max particle size as obtained from PCS measurement.

Again, the measure for dispersion stability was the time evolution of the particle size distribution. Figure 3.9 A and B display PSD in a mixture of 600 ppm SiO_2 and 600 ppm biopolymer after respectively 4 and 113 hours of incubation. Figure 3.9 C and D display the size distribution in a mixture of 1250 ppm SiO_2 and 1250 ppm biopolymer after respectively 4 and 113 hours of incubation. As reference the PSD of biopolymer silica mixtures in the absence of peat pore water was added. The results at C_i of 300 ppm SiO_2 did not deviate from the results as obtained in the absence of peat pore water. These results are therefore not presented here but can be found in Appendix 11.

PSD at initial silica concentration of 600 ppm SiO_2

During incubation the distribution transforms from a bimodal into a trimodal distribution. After 4 hours of incubation two distinctive peaks were observed at a mean average of 274 and 45 nm. After 113 hours of incubation three peaks were observed at mean average of 236, 49 and 24 nm. The presence of a distinctive peak at 236-274 nm was expected given the additional organic particulate matter. This peak flattened during incubation gaining more width. The presence of the smaller sized population, mean average peak size at about 45 - 49 nm, coincided with the location of the monomodal peak of the mixture in absence of particle or dissolved organic matter (blue line). The smaller populations represent most likely silica-biopolymer based particles, since their size was smaller than POM and the location coincided with the blue line. It is proposed that a part of the silica-biopolymer particles was scavenged by POM and/or DOM. The intensity area of the 49-45 nm population was smaller in the presence, than in the absence of POM and DOM. The larger sized population was therefore likely to concern POM and biopolymer-silica associated with POM particles.

Width and overall size range of the PSD remained quite stable over time. Particle size at D95% was after 4 hours 386 nm and 353 nm after 113 hours. These D95% sizes were comparable to the values observed for solely peat pore water. Moreover, these D95% sizes were significantly lower than the values obtained at an initial concentration of 1250 ppm SiO_2. The D95% size was comparable to the size as observed in the absence of POM and DOM (377 nm after 113 hours).

The time evolution i.e. stability of dispersed colloidal silica was not reduced by the presence of particulate or dissolved organic matter at C_i of 600 ppm SiO_2. The size distribution of particulate matter formed in the presence of peat components was however different from the distribution in the absence of these components.

PSD at initial silica concentration of 1250 ppm SiO_2

Figure 3.9 shows that the particle size distribution had a bimodal shape 113 hours after pH adjustment. The bimodal shape became more prominent over time. A hint of the bimodal shape was already observed after 4 hours given the negative skew of the peak at t_1. After 4 hours of incubation the distinctive peak was observed at mean average of 252 nm. After 113 hours two distinctive but overlapping peaks were observed at a mean average of 411 nm (65% area) and at 91 nm (32.6% area). Thus both the smaller and larger sized population shifted to the right over time.

The population with a small size coincided with the location of the monomodal peak of the mixture in absence of particle or dissolved organic matter (blue line). Therefore, this population seemed to represent predominantly silica-biopolymer based particles. The presence of a distinctive peak at 252 nm was expected given the additional organic particulate matter. The population with a larger particle size was therefore likely to concern POM particles and biopolymer-silica particles associated with POM. Aggregation and formation of secondary particles was observed during the hours of incubation that followed as indicated by the shift of the smaller and larger sized population.

As opposed to an initial concentration of 600 ppm SiO_2, the distribution at t_3 exceeded the size range of solely particulate organic matter (red line) and the size range of dispersed silicate and biopolymer using demiwater as solvent (blue line). The obtained D95% at 4 hours was already 712 nm. After 113 hours of incubation D95% increased to 750 nm. This was significantly higher than the D95% observed in the absence of POM and DOM (i.e. 379 nm). Furthermore, the particulate matter was more polydispersed at 1250 ppm SiO_2 than at 600 ppm SiO_2 initial concentration. These observations indicate that the presence of DOM and POM enhances aggregation at an initial concentration of 1250 ppm SiO_2. The time evolution of particle size i.e. stability of dispersed colloidal silica was reduced by the presence of particulate and dissolved organic matter at C_i of 1250 ppm SiO_2. The size distribution of particulate matter formed in the presence of peat components was different from the distribution in the absence of these components.

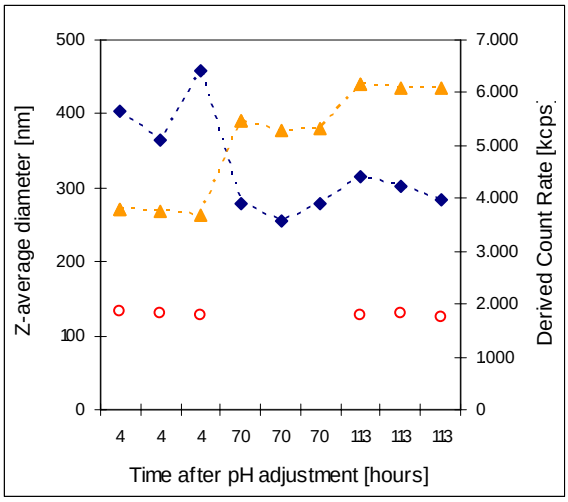

A: Z-average and DCR at C_i of 600 ppm SiO_2

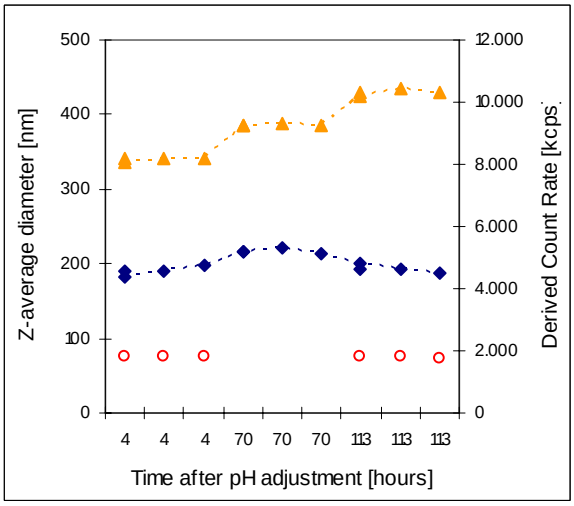

B: Z-average and DCR at C_i of 1250 ppm SiO_2

Legend:

Z-average particle size in terms of particle diameter [nm]. at 1 to 1 wt. ratio between C_i biopolymer and C_i silica

Derived count rate of biopolymer silicate mixture using peat pore water as the solvent [kcps]

Derived count rate of peat pore water [kcps]

Figure 3.10: Z-average and derived count rate at C_i of 600 and 1250 ppm SiO_2

Time evolution of Z-average particle size and derived count rate are presented in Figure 3.10 A and B. Only the results at initial silica concentration of 600 and 1250 ppm SiO_2 are given in this section. The particle size distributions at 300 ppm SiO_2 initial concentration are included in Appendix 8 and 9. Using peat pore water as the solvent the pore water itself contains already a particulate fraction in accordance with ~1.800 kcps.

DCR at initial silica concentration of 600 ppm SiO_2

The derived count rate at C_i of 600 ppm SiO_2 increased over time. Increase of derived count rate over time indicates an increase in the amount of particulate matter dispersed in the solvent. It is suggested that increase of DCR was caused by formation of primary particles and/or disintegration of aggregates. There was no indication for sedimentation during the 113 hours of incubation i.e. sharp decrease in DCR in time.

As expected, derived count rates were significantly higher than was observed in peat pore water in the absence of silica and biopolymer. However, DCR values were ca. 1.000 to 2000 kcps lower than was observed for a mixture prepared with demiwater (Figure 3.7 B). Hence, the presence of particulate and dissolved organic matter restricted the formation of particles and/or disintegration of aggregates to some extent.

DCR at initial silica concentration of 1250 ppm SiO_2

The derived count rate at C_i of 1250 ppm SiO_2 increased over time. It is suggested that increase of DCR was caused by formation of primary particles and/or disintegration of aggregates. There was no proof for sedimentation during the 113 hours of incubation i.e. sharp decrease in DCR in time.

As expected DCR were higher at C_i of 1250 ppm SiO_2 than at C_i of 600 SiO_2. Although, the increase of count rate over time was similar i.e. ca. 2.000 kcps over a period of 109 hours. Naturally, derived count rates were also higher than observed in peat pore water in the absence of silica and biopolymer.

However, DCR values as observed in the absence of particulate and dissolved organic matter were ca. 10.000 kcps higher than in the presence of POM and DOM (compare Figure 3.10 B to Figure 3.7 C). The values obtained in the absence of peat pore water were relatively high. The presence of particulate and dissolved organic matter restricted the formation of particles and/or disintegration of aggregates to a relatively large extent, compared to C_i of 600 ppm SiO_2.

Summarizing

Interaction between the dispersed silica biopolymer entities and particulate and dissolved organic matter was observed at initial concentration of 600 ppm SiO_2 and of 1250 ppm SiO_2, at biopolymer dosage of 100%. The presence of DOM and POM had an influence on the shape of the particle size distribution.

The presence of particulate and dissolved organic matter had no significant impact on the stability of dispersed colloids present at initial concentration of 600 ppm SiO_2 and 600 ppm biopolymer. The presence of particulate and dissolved organic matter reduces the stability of dispersed colloids present at initial concentration of 1250 ppm SiO_2 and 1250 ppm biopolymer. It could therefore be stated that the effect of dissolved and particulate organic matter on stability of dispersed colloidal silica depends on the initial concentration of silica and biopolymer. The ability of the biopolymer to prevent the formation of sedimenting particles – in significant amounts and within timeframe of 113 hours – was not effected by the presence of particulate and dissolved organic matter.

3.2.4 Effect of biopolymer on electrophoretic mobility

As explained in more detail in Chapter 2 zeta potential is the electrostatic potential near the surface of a particle. The zeta potential was derived from the electrophoretic mobility of particles dispersed in the solvent. Zeta potential was a function of particle properties and of solvent properties. The effect of the biopolymer on the electrophoretic mobility of particulate silica was determined. Based on the zeta potential of the particles present in the injection fluid the electrostatic interactions between particles (dispersion stability) and their surrounding (attachment to peat surface) could be evaluated.

Initially the zeta potential was determined at high ionic strength. Thereafter, the zeta potential was determined at lower ionic strengths, at various pH conditions and at various initial concentrations of silica and biopolymer. The aim was to determine the extent in which the electrophoretic mobility of the formed particles (i.e. surface charge characteristics) was related to initial silica and biopolymer concentration and to time.

Zeta Potential at High Ionic Strength

Zeta potential measurements were initially performed in mixtures at relatively high ionic strength (EC of 8 to 10 mS/cm) and neutral pH conditions (7.5 +/- 0.02). The zeta potential of several mixtures as presented in Table 3.2 was measured. The zeta potential of each mixture was within the range of +/- 30 mV, independent of initial silica or biopolymer concentration, solvent type or time. More specifically, zeta potentials were obtained in the range of +/- 10 mV, with peak values centered at 0 mV.

The obtained phase diagrams indicated an unreliable data set for derivation of the zeta potential. A typical phase diagram representing a reliable measurement is given in Figure 3.11 A. A typical phase diagram, as obtained for the high ionic strength silicate biopolymer mixtures. is shown in Figure 3.11 B. The abnormal fluctuations indicate that the data as obtained at relatively high ionic strengths was poor and that the derived zeta potential was therefore not reliable.

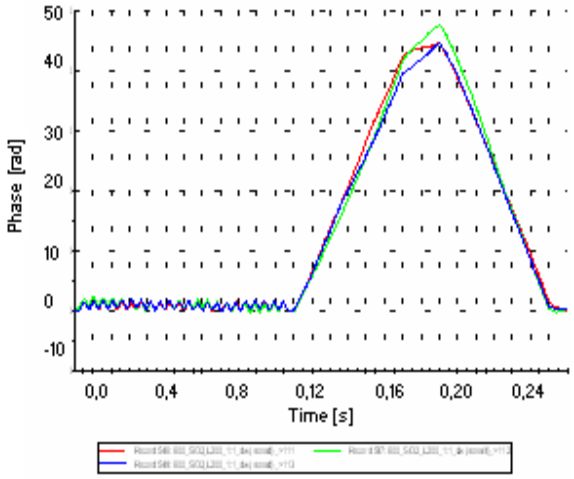

A. Phase diagram of reliable electrophoresis measurement. Phase diagram shows the results of a triplicate measurement of a 600 ppm SiO_2 and 600 ppm biopolymer suspension having a conductivity of 1.72 mS/cm.

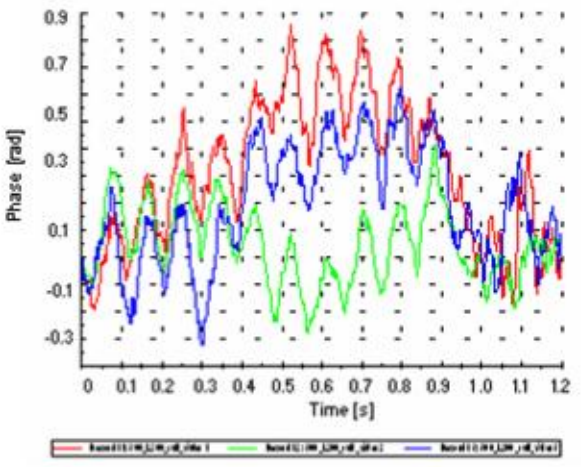

B. Phase diagram of unreliable electrophoresis measurement. Phase diagram shows the results of a triplicate measurement of a 600 ppm SiO_2 and 300 ppm biopolymer suspension having a adjusted conductivity of 8.96 mS/cm.

The zeta potential was measured in three runs. The phase difference is plotted on the x-axis in radials. The time is plotted in the x-axis in seconds.

Figure 3.11: Phase diagrams of reliable and unreliable electrophoresis measurements

Zeta Potential Relatively Low Ionic Strength

Additional mixtures, only with a 1 to 1 wt. ratio between biopolymer and silica, were created to measure the zeta potential at lower ionic strengths (Table 3.3). The mixtures as displayed in Table 3.3 were produced additionally to the mixtures as presented in Table 3.2. In exception of the Blanco's (700_0_dw series), the time evolution of dissolved silica and particle size distribution of the mixtures in Table 3.3 were not determined, due to time constrains.

Zeta potentials of mixtures were measured at 'low' ionic strength conditions and various pH values. The ionic strength was now related to the initial added concentration of silicate and biopolymer, and the adjusted pH. In other words the conductivity of the solutions was not equated to the highest measured conductivity (1250_1_dw), as opposed to the previous results. Note that conductivity varies in the range of 1 to 3 mS/cm. The conductivity still exceeds the recommended conductivity range for zeta potential measurement (Malvern Instruments, 2003).

Table 3.3: Overview of prepared samples Zeta Potential analyses

Reference	Dilution Series	L200 / SiO_2	Solvent	pH (initial[2])	EC (initial)	Phase diagram
[Name]	SiO_2 [ppm]	[wt. ratio]	[-]	[-]	[mS/cm]	[-]
700_0_dw	700	0	Demiwater	7.48	3.78	valid
700_0_dw	700	0	Demiwater	4.33	3.51	valid
700_1_dw	700	1	Demiwater	9.60	2.33	valid
700_1_dw	700	1	Demiwater	7.29	1.92	valid
700_1_dw	700	1	Demiwater	4.63	1.92	valid
700_1_dw	700	1	Demiwater	2.82	3.17	less reliable
600_1_dw	600	1	Demiwater	8.72	3.24	flat (less reliable)
600_1_dw	600	1	Demiwater	7.05	3.26	flat (less reliable)
600_1_dw	600	1	Demiwater	5.21	3.17	less reliable
600_1_dw	600	1	Demiwater	2.78	3.68	valid
300_1_dw	300	1	Demiwater	8.79	1.51	less reliable
300_1_dw	300	1	Demiwater	6.58	1.57	valid
300_1_dw	300	1	Demiwater	4.46	1.60	valid
300_1_dw	300	1	Demiwater	2.65	2.48	valid

Collective image of phase diagrams at low EC and at high EC conditions is presented in Appendix 12.

Figure 3.12 shows that there was no significant correlation between conductivity and zeta potential for the silicate-biopolymer mixtures tested. Therefore, ionic strength was not considered a dominant factor that controlled zeta potential, within the EC and initial concentration range. If ionic strength was the dominant factor setting zeta potential than Figure 3.12 should have shown a negative correlation between EC and zeta potential. This was however not the case.

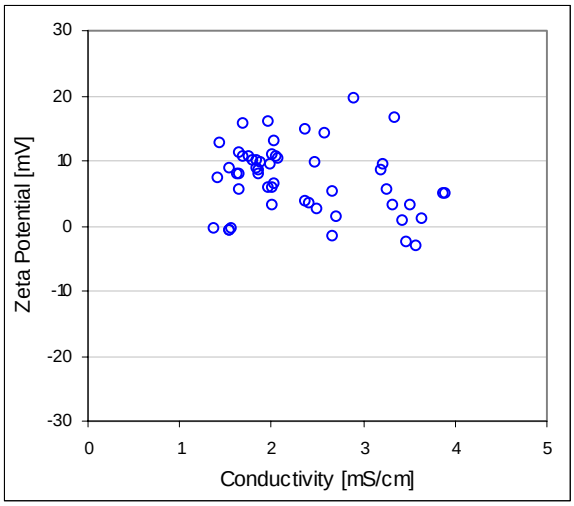

Figure 3.12: on the x-axis the conductivity in units of mS/cm is plotted, as a measure o f the ionic strength of the solution. The conductivity presented in this graph is the conductivity as obtained by PCS measurement. The y-axis shows the zeta potential in units of mV. The zeta potential is the peak value (in terms of total counts) of the zeta potential distribution.

Legend:

- *Silica-biopolymer suspensions; EC not adjusted; pH varies from 2.65 to 11.85.*

Figure 3.12: Relation between mixture conductivity and zeta potential of disperse particulate matter

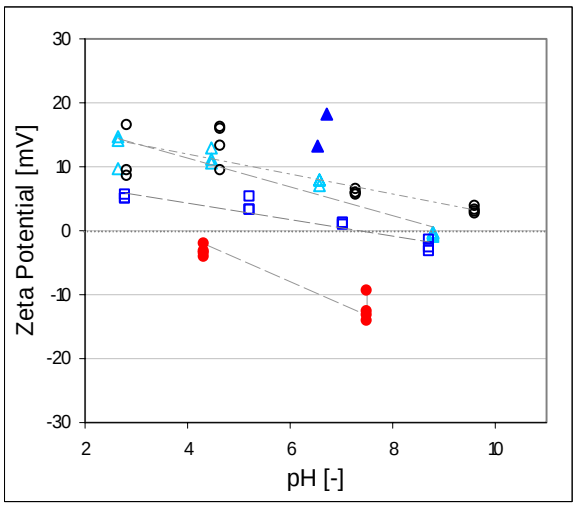

Figure 3.13: on the x-axis the pH is plotted. The pH was adjusted 2 hours before zeta potential measurement. The y-axis displays zeta potential in units of mV. Zeta potential as presented here was the peak value (in terms of total counts) of the zeta potential distribution. The reliability of the electrophoresis measurement, i.e. the quality of the phase diagram is presented in Table 3.3. The derived count rates were, independent of the pH, below or just above the advised detection limit for zeta potential measurement of 100 kcps. The result of the electrophoresis measurement and quality of the returned zeta potential was therefore less accurate.

Legend:

- 300_1_dw_no salt added; 300 ppm SiO_2 en 300 ppm L200; 2 hours after pH adjustment
- 600_1_dw_no salt added; 600 ppm SiO_2 en 600 ppm L200; 2 hours after pH adjustment
- 700_1_dw_no salt added; 700 ppm SiO_2 en 713 ppm L200; 2 hours after pH adjustment
- 700_0_dw_no salt added; 700 ppm SiO_2 en 0 ppm L200; 2 hours after pH adjustment
- 60 tot 20.000 ppm L200; no salt added. pH not adjusted

Figure 3.13: Relation between mixture pH and zeta potential of dispersed biopolymer-silica particles in 'low conductivity' solution.

Figure 3.13 shows the relation between zeta potential and pH at C_i of 300, 600 and 700 ppm SiO_2 in the presence of biopolymer. Figure 3.13 indicates that there was a negative correlation between pH and zeta potential and that this correlation was independent of C_i (within the tested range) and the presence or absence of the biopolymer.

Furthermore, Figure 3.13 shows the zeta potential at C_i of 700 ppm SiO_2 in the absence of biopolymer (blue closed triangle). The functional group of the biopolymer is a positive charged quaternary ammonium group. The charge of this group did not depend on pH – providing that aggressive conditions did not destruct the polymer chain. The zeta potential of samples consisting of solely biopolymer was 13.4 mV at EC of 0.124 mS/cm and 18.4 mV at conductivity of 2.77 mS/cm.

Zeta Potential of solely silica dispersion (low conductivity)

Silica particles had a negative zeta potential at pH of 4.3 – 7.5 in the absence of biopolymer at initial concentration of 700 ppm SiO_2. The results, as presented in Figure 3.13 were in agreement with literature. The surface charge of amorphous silica is a pH dependent charge. The silanol groups located at the surface of the particle can be either protonated or deprotonated depending on the pH. The PZC (Point of Zero Charge) of amorphous silica is commonly situated around pH 2. The surface charge of colloidal silica is reported to become more negative with increasing pH above pH 2. For this reason a gradual decrease of zeta potential in the pH range of 2 up to 9.5 and a steeper decrease exceeding pH values of 9.5 were expected, as described in section 2.4.

Zeta Potential of Silica – biopolymer dispersion (low conductivity)

Foremost the results show that the biopolymer was capable to alter the zeta potential of dispersed silica particles to a more positive potential. Figure 3.13 shows that the formed particulate matter had a neutral to positive charge in the presence of the biopolymer. As stated in the previous section and in accordance with literature, colloidal silica has a negative zeta potential in the absence of a cationic surface active agent. Thus the deprotonated silanol groups ($\equiv Si\text{-}O^-$) located at particle surface associated with the positive charge from the biopolymer; the overall net charge of the particle was thereby elevated.

Summary

Zeta potential is a measurement of the electrostatic potential at the hydrodynamic plane of a particle. Commonly applied threshold for stabilization of dispersed matter by electrostatic forces is ± 30 mV (Hiemenz, 1997). The electrostatic potential did not exceed + 30 mV over the tested pH and concentration range. Existence of additional repulsive forces (steric or hydration) should therefore be taken into account explaining the retardation efficiency of the biopolymer. Alternation to a more positive charge though may have an impact on the behavior of particulate silicate upon injection of the fluid in a peat layer. This is discussed in Chapter 3.

3.3 Discussion

The observed results are discussed in this section in terms of the efficiency of the biopolymer to retardate silica polymerization and silica particle formation and growth. The influence of initial silica concentration and biopolymer dosage on the efficiency of the biopolymer to retardate is evaluated. The results are discussed with respect to similar research found in literature.

3.3.1 Efficiency of Biopolymer to retard silica polymerization

The biopolymer retards the polymerization process of silica. The observed dissolved silica concentrations exceed the solubility limit of amorphous silica at pH of 7.5 and temperature of 22^0C. The polymerization rate of silica which is at its maximum at pH between 6 and 8 (as depicted in Figure 2.4) is reduced by addition of the biopolymer Celquat L200. The fact that the biopolymer *retards* the polymerization process of silica but does not *inhibit* silica polymerization is in accordance with literature.

G.A. Icopini (2005) discusses the removal of reactive silica from solution in the absence of an additive in more detail. Demadis (2009), Coradin (2007) and Zhang (2011) - among others - discuss the condensation of silicic acid and its subsequent removal from solution in the presence of a cationic biopolymer. A selection of their research results is presented in Table 3.4 as reference for the obtained retardation efficiency of the biopolymer Celquat L200. The selection is based on the used quantification method for dissolved silica. For all data displayed in Table 3.4 the applied method of quantification is the silicomolybdic acid method, as first suggested by Iler (1979) and described in detail by Coradin and Livage (2004).

The efficiency of the Celquat L200 biopolymer to retard the polymerization of silica is greater than the efficiency of the PALAM-1G and the PAMALAM biopolymer as determined by Demadis et al. (2009). Final dissolved silica concentrations in the presence of the biopolymer L200 are clearly higher than as observed by Demadis; see Table 3.4 for an overview. The retardation efficiency of the Celquat L200 biopolymer is comparable to the efficiency of the AA/AT/DE biopolymer as studied by Zhang et al. (2011). Zhang et al repeated the experiment as performed by Demadis (2009) with the biopolymer PALAM-1G. Although a higher final dissolved silica concentration is reported by Zhang than by Demadis, the overall final dissolved silica concentration is still comparable to the concentration as observed in the presence of L200.

Truly steady state conditions could not be confirmed by the chosen set-up. Steady state conditions are therefore apparent since the experimental testing period was restricted to 113 hours and only three points were taken in time. Apparent steady state in dissolved silica concentration is obtained in the presence of the biopolymer, at 300 to 424 ppm SiO_2. The main drop in dissolved silica concentration occurs minutes after pH adjustment in the presence and absence of the biopolymer. This is in accordance with literature (Perry et al., 2003 ; Zhang et al., 2011; Coradin and Livage, 2004).

Table 3.4: Dissolved silica concentrations in the presence of an additive as reported in literature

	Name biopolymer*	Temperature	pH	Conductivity	Biopolymer conc.	Silica conc.	Silica conc.	Time	Retardation efficiency
			Initial	Indication**	Initial	Initial	Final	Final	Final***
	[-]	[°C]	[-]	[mS/cm]	[ppm]	[ppm]	[ppm]	[h]	[-]
Demadis	PALAM-1G	20	7	0.9-1	20	500	210	72	2.10
Demadis	PAMALAM	20	7	0.9-1	20	500	165	72	1.65
Zhang	AA/AT/DE	20	7	0.9-1	20	500	295	96	2.95
Zhang	AA/AT/DE	20	7	0.9-1	40	500	350	96	3.50
Zhang	PALAM-1G	20	7	0.9-1	40	500	340	96	3.40
Hamer	L200	22	7.5	7-9	600	600	338	113	2.84
Hamer	L200	22	7.5	7-9	300	600	424	113	3.56
Hamer	L200	22	7.5	7-9	60	600	324	113	2.72
Demadis	-	20	7	0.5	-	500	160	72	-
Zhang	-	20	7	0.5	-	500	165	96	-
Hamer	-	22	7.5	3.78	-	700	119	96	-
Hamer	-	22	7.5	7.59	-	1250	116	96	-
Icopini	-	25	7.5	Low	-	1250	106	96	-
Icopini	-	25	7	Low	-	751	108	96	-
Icopini	-	25	7	Low	-	252	195	96	-
Icopini	-	25	7	High	-	1256	112	96	-
Icopini	-	25	7	High	-	751	114	96	-
Icopini	-	25	7	high	-	252	174	96	-

* All polymers named in this table are biodegradable cationic (or zwitterionic) polymers. **The electric conductivity of the tested solutions is often not mentioned in literature. Based on concentration sodium silicate solution, pH adjustment en biopolymer concentration estimation was made. ***The Retardation Efficiency was calculated by dividing the measured final silica concentration in the presence of the biopolymer by 100 ppm SiO_2. Thereby it was assumed that the test conditions in literature and present sturdy were similar, returning a solubility of amorphous silica of 100 ppm SiO_2. Clearly this was not precisely the case and retardation efficiencies have to be considered estimates.

Biopolymer dosage and retardation of silica polymerization

The efficiency of the biopolymer to retard the first steps in the polymerization process of silica *do not* depend on biopolymer dosage at an initial silica concentration of 300, 600 or 1250 ppm SiO_2. Adding higher concentrations of the biopolymer do not involve distinctive higher or lower dissolved silica concentrations within period of 113 hours. This regards biopolymer dosages of 10%, 50% and 100% of the initial silica concentration. Different statements on dosage and performance of biopolymers are reported in literature (Demadis et al 2009; Zhang et al 2011).

Both Demadis (2009) and Zhang (2011) report that the retardation efficiency of the biopolymer depend on dosage, though not to the same extent. Demadis proposes that the optimum dosage depends on the charge density of the molecule and the excess in which the biopolymer is added. Demadis concludes that colloidal silica aggregates by an excess of cationic polymer or charge present. The system is thereby depleted from active biopolymer since it is entrapped in formed amorphous silica. Consequently, this process deactivates the biopolymer and its retardation efficiency to silica polymerization diminishes.

The mechanism of biopolymer depletion by charge excess and its subsequent detrimental retardation efficiency upon excessive addition of the biopolymer – as suggested by Demadis - seems not to play a role in present research. Relatively high biopolymer dosage in present study - in relation to the research cited in Table 3.4 - do not have a noticeable stimulating effect on the polymerization process of silica.

Zhang et al. (2011) proposes that the ability of the biopolymer to retardate silica polymerization depends on its dosage up to 20 ppm biopolymer (2011). Zhang et al. (2011) reports that if the biopolymer is added in excess of 20 ppm the retardation efficiency is almost indistinguishable from the efficiency at 80 ppm. The detrimental affect of excess biopolymer as found by Demadis is thus not confirmed by Zhang et al. Compared to present research results a dosage of 20 ppm to 80 ppm biopolymer equals 4% to 16% of the total added amount of silica. In present study the lowest dosage of the biopolymer L200 equaled already 10%. Present research results are therefore in accordance with the results of Zhang et al (2011).

The retardation of silica polymerization by the presence of the biopolymer Celquat L200 does not depend on dosage for the tested range. An explanation for this phenomenon is not found in literature, though Zhang et al. reports the independency of biopolymer dosage above a certain threshold – as discussed in previous paragraph.

3.3.2 Efficiency of Biopolymer to retard particle formation and particle growth

Biopolymer dosage has a different impact on the first steps of the process of silica polymerization than on dispersion stability. The retardation of silica particle growth does depend on biopolymer dosage as opposed to retardation of silica polymerization. The phase transition of silica is a very complex process (Icopini, 2005; Gill, 1993). A very simplified description of the phase transition of silica is given in Chapter 2. How the different mechanisms of polymerization and particle formation and growth operate in the presence of a biopolymer is therefore difficult to answer. Current research results are not sufficient to propose a specific interfering mechanism that accounts for the retardation efficiency and obtained dispersion stability by presence of the biopolymer Celquat L200. We gained some insight in the effect of biopolymer on phase transition of silica in relation to its dosage. Based on this I propose the following - the steps mentioned below refer to the very simplified description silica phase transition given in Chapter 2:

Delay of step 1: Retardation of silica polymerization

The association of the biopolymer with silica monomers and oligomers at pH ~12 seems to delay the first step in the process of silica polymerization upon pH adjustment. The biopolymer blocks silanol groups located at the end of silica polymers which thereby become unavailable for the formation of a siloxonate (Si-O-Si) bond with neighboring silica polymers upon adjustment of pH to 7.5. This blocking of sites does not depend on biopolymer dosage in the tested range. The biopolymer interferes with the process of monomeric and dimeric condensation thereby maintaining a concentration of silica in its dissolved form, ca. 3 times above the solubility limit of amorphous silica.

Binding of silicic acid to biopolymer should be reflected in the dependency of residual dissolved silica on the initial biopolymer to silica wt. ratio (biopolymer dosage), which is however not the case. In terms of the retardation of silica polymerization the biopolymer is thus added in excess at biopolymer to silica wt. ratio of 0.1, 0.5 or 1.

Delay of step 2 and 3 Stabilization of colloidal silica

Addition of the biopolymer reduces aggregation rates and even prevents formation of significant amounts of sedimenting particles within a period of 113 hours. The impact of the biopolymer on dispersion stability does depend on its dosage. This observation is partly in agreement with research performed in the field of colloidal silica for industry and material sciences (Heimenz, 1997; Bergna, 2006). That is, colloidal particle interactions are reported to be controlled by the addition and dosage of a cationic additive. However, the literature cited concerns the interaction between colloidal silica and a cationic additive; and not the interaction with a cationic additive *during formation* of the colloids itself.

Nevertheless, the following can be cited on dosage of cationic additive and the obtained stabilization of colloidal silica:

- Electrostatic stabilization by increasing repulsive forces between the dispersed particles:
  - The additive is more effective at low dosage and low silica concentrations.
  - The additive needs to alter zeta potentials by ± 30 mV of the colloids by interaction at its surface.
- Polymer- induced stability by introducing steric or depletion stabilization:
  - The additive is effective at high dosage, in both low and higher concentrated fluids
  - At low concentrations of the additive it could have an opposite effect and induce flocculation

For a short introduction on the terms electrostatic and steric stabilization it is recommended to read section 2.4.1. Attachment of the biopolymer at the surface of colloidal silica or incorporation of the biopolymer into the polymeric matrix of the emerging silica colloid alters the surface properties of this particle. However, addition of the biopolymer at 10%, 50% or 100% dosage does not alter surface properties of colloidal silica to the extent that electrostatic stabilization could be obtained – as indicated by zeta potential measurements. Since the dosage is a controlling factor in dispersion stability it is proposed that steric (or hydrate?) repulsive forces are activated by biopolymer addition, obstructing the approach of mutual particles. Aggregation of colloidal silica to larger particles is thereby (temporarily?) prevented and deposition is at least avoided within timeframe of 113 hours.

Effect of dissolved and particulate organic matter on retardation efficiency

Particular and dissolved organic matter (POM and DOM) is expected to have an influence on the polymerization process of silica and stability of colloidal silica. For example, by the addition of POM the surface available for nucleation of silica is increased. Or, for example, the inactivation of the cationic segment of the biopolymer by association with DOM, which mainly has a negative surface charge. Both processes could potentially reduce the retardation efficiency of the biopolymer. The effect of POM and DOM on retardation efficiency of the biopolymer is however limited.

The phase transition of silica is researched in great detail by Perry and Yun Lu (1992) in the absence of an additive. Furthermore, they investigated the role of dissolved cellulose and particulate cellulose on silica polymerization and aggregation. This research is of interest to current research since it gives insight in the polymerization process of silicates in general and the potential influence that POM (i.e. particulate cellulose as analogy to POM) and DOM (i.e. dissolved cellulose as analogy for DOM) could have on silica polymerization and particle growth. Their research showed that the presence of particulate and or dissolved cellulose has no affect on the initial polymerization of silicic acid – in the absence of any additive. However, particulate cellulose did modify the size of the particles formed (Perry, 1992). Perry concluded that the addition of particulate cellulose -in the absence of an additive - resulted in a decrease of polydispersity and narrowed the particle size ranges. The interaction between cellulose and silica is based on hydrogen bond formation as concluded by Perry (1992). The formed hydrogen bond apparently does not affect silica polymerization but partially controls the behavior of colloidal silica. The presence of cellulose seems to prevent further aggregation of silica oligomers and colloidal particles to larger sedimenting particles.

Similar results are obtained in the presence of the biopolymer L200. Our results how that dissolved and particulate organic matter, naturally present in peat pore water, are not a factor in the process of silica polymerization. Furthermore, the influence of POM and DOM on particle size range (narrowing of size distribution) holds in the presence of the biopolymer L200 at initial concentration of 600 ppm SiO_2. It is therefore proposed that the retardation efficiency of the biopolymer is not noticeable reduced by the presence of POM and DOM at initial concentration of max 600 ppm SiO_2. However, the increase of particle diameter in the presence of POM and DOM at initial concentration of 1250 ppm SiO_2 is not in agreement with literature (Perry, 1992). It is proposed that just enough biopolymer is scavenged and nucleation surface provided by the added POM and DOM to destabilize the densely concentrated suspension, as obtained at initial concentration of 1250 ppm SiO_2.

3.4 Conclusions with respect to research questions

The conclusions with respect to the research questions as described in the introduction of present chapter are presented below. The conclusions drawn are only valid under specific conditions and for specific mixture compositions, namely:

- An initial silica concentration (C_i) of 300, 600 or 1250 ppm SiO_2 using sodium metasilicate as the source of silicon.
- Biopolymer to silica weight (wt.) ratio's of 1 to 1, 0.5 to 1 and 0.1 to 1. A biopolymer to silica wt. ratio of 1 to 1 corresponds to a biopolymer dosage of 100%, likewise a wt. ratio of 0.5 to 1 corresponds to a dosage of 50% and a wt. ratio of 0.1 to 1 corresponds to a dosage of 10%.
- A time frame of 113 hours. starting from pH adjustment from >12 to 7.5
- Continuous agitation during incubation and incubation temperature of 22^0C.

Retardation of silica polymerization, particle formation and particle growth in the presence of the biopolymer Celquat L200 at silica super saturation.

I. The biopolymer Celquat L200 does effectively *retardate the polymerization process of silica*. The efficiency in which the biopolymer retardates the polymerization of silica *does not depend* on initial silica concentration and biopolymer dosage.

II. Dissolved silica concentrations of 300 to 424 ppm SiO_2 were obtained after 113 hours of incubation, irrespective of initial silica concentration or biopolymer dosage.

   a. A true solution is formed at initial silica concentration of 300 ppm SiO_2 and biopolymer dosage of 10% or 50%. The conclusions as presented below however suggest that inhibition is only obtained for a limited time period. A gradual decline of dissolved silica concentration at initial silica concentration of 300 ppm and 10% or 50% biopolymer dosage is expected on a time span exceeding 113 hours.

   b. A colloidal suspension is formed at initial concentration of 300 ppm SiO_2 and biopolymer dosage of 100%. A colloidal solution is formed at initial silica concentration of 600 ppm and 1250 ppm SiO_2, independent of biopolymer dosage.

III. The biopolymer Celquat L200 does effectively *retardate the growth of silica particles*. The efficiency in which the biopolymer interferes with silica particle growth *does depend* on initial silica concentration and biopolymer dosage.

   The time evolution of particle size i.e. the stability of dispersed colloids depends on biopolymer dosage.

   a. At 300 ppm. 600 ppm or 1250 ppm SiO_2 and 100% biopolymer dosage the particles formed remain in the colloidal size range. After 113 hours of incubation 95% of the distribution area[5] was smaller than 1660 nm at C_i of 300 ppm SiO_2. 122 nm at 600 ppm SiO_2 and 377 nm at 1250 ppm SiO_2. Apparent stability of dispersed colloidal silica is obtained at initial silica concentration of 600 or 1250 ppm SiO_2 and 100% biopolymer dosage.

   b. At biopolymer dosage of 10% or 50% the D95% values were higher than at 100% dosage. However, the D95% values did not exceed the colloidal size range at initial concentration of 600 or 1250 ppm SiO_2. Colloidal stability was not obtained.

[5] D95%.is based in terms of scatter intensity. Not in terms of number or particle volume.

The time evolution of number of particles dispersed in the solvent at 100% biopolymer dosage.

a. The derived count rate was used as a relative measure for particle numbers dispersed in the solvent. Derived count rates over time at C_i of 300, 600 and 1250 ppm SiO_2 indicate that higher initial silica concentration results in more particles dispersed in the solvent.

The biopolymer Celquat L200 *does prevent the formation of sedimenting particles* at a biopolymer dosage of 10%, 50% at initial concentration of 300 ppm; and at a biopolymer dosage of 100% at an initial concentration of 600 or 1250 ppm SiO_2.

Effect of dissolved and particulate organic matter on retardation efficiency of the biopolymer Celquat L200.

IV. Particulate and dissolved organic matter *does not* influence the efficiency of the biopolymer Celquat L200 to *retardate the polymerization process of silica*.
   a. At 300, 600 and 1250 ppm and 100% biopolymer dosage dissolved silica concentrations after 113 hours of 268. 367 and 389 ppm SiO_2 were obtained, respectively.

V. Particle and dissolved organic matter does influence the efficiency of the biopolymer Celquat L200 to *retardate the growth of silica particles*, depending on initial silica concentration.
   a. At 600 ppm colloidal particles were formed. D95% was 353 nm of the dispersion with POM, silica-biopolymer particles and silica-biopolymer particles associated with POM. The D95% particle size did not exceed the particle size of solely POM.
   b. At 1250 ppm particles exceeding the colloidal size range were formed after 4 hours of incubation using peat pore water as solvent opposed to using demiwater as solvent. D95% of 750 nm of dispersion with POM, silica-biopolymer particles and silica-biopolymer particles associated with POM. The D95% particle size did exceed the D95% particle size of solely POM suspension.
   c. The amount of particles dispersed in the solvent are 75% (at initial concentration of 600 ppm SiO_2) and 40% (at initial concentration of 1250 ppm SiO_2) lower in the presence of POM and DOM than using demiwater It is therefore proposed that POM and/or DOM scavenges the smaller sized population of silica-biopolymer particles from solution.

Effect of the biopolymer Celquat L200 on zeta potential of dispersed particles

Zeta potential is a measurement of the electrostatic potential at the hydrodynamic plane of a particle. Dispersed particles in a solvent are assumed to be stabilized by electrostatic forces if the zeta potential of those particles is ± 30 mV. In present research the zeta potential is measured over a pH range of 2 up to 11.5 and initial silica concentration of 300, 600 and 700 ppm SiO_2. These conclusions only consider a 100% biopolymer dosage.

VI. The biopolymer increases the zeta potential of the formed silica particulate matter over the whole pH range and at initial silica concentrations of 300, 600 and 700 ppm SiO_2.

VII. The zeta potential of particulate matter formed in the presence of the biopolymer does not exceed 30mV. Existence of additional repulsive forces (steric or hydration) should therefore be taken into account explaining the retardation efficiency of the biopolymer.

3.4.1 Optimum composition of injection fluid

The best results in terms of retardation efficiency and dispersion stability over period of 113 hours of incubation are obtained at the following fluid composition:

- initial silica concentration of 600 ppm SiO_2 (based on stock solution of sodium metasilicate);
- biopolymer Celquat L200 in dosage of 600 ppm (based on liquid stock solution) and addition of the biopolymer before pH adjustment from > 12 to 7.5.

Fluid composition as stated above provides the best properties (of the tested options) for application as injection fluid in a porous and organic soil, since:

- the initial silica load is 6 times the solubility limit of amorphous silica;
- the silica load after 113 hours of incubation is 2.84 times the solubility of amorphous silica;
- the ratio dissolved silica to colloidal silica is high (i.e. 129%) indicating a relatively low amount of particles; opposed to the ratio at C_i of 1250 ppm SiO_2 (i.e. 35%);
- the zeta potential of particulate silica is elevated by interaction with the biopolymer;
- the colloidal silica that is formed within the 113 hours of incubation is not expected to cause clogging by infiltration.

It is assumed that if particle sizes are within the colloidal size range transport through the porous matrix of peat soil will not cause clogging by infiltration. See Chapter 2 for the motivation of this assumption. Clogging by infiltration is not expected given the observation that the particles:

- are small in size: particle size at D95% is 122 nm in the absence of particulate and dissolved organic matter and 353 nm in presence of particulate and dissolved organic matter;
- have a constant particle size distribution in time: shift of 20 nm of D95% within 113 hours also in the presence of particulate and dissolved organic matter.
- do not sediment due to the presence of the biopolymer (prevent formation of sedimenting particles) also in the presence of particulate and dissolved organic matter.

Naturally, filtration of particles and subsequent clogging is also dictated by the properties of the conductive media it self. That is, the size of the pores and pore throats in a soil layer. The aspect of infiltration is evaluated and discussed in more detail in Chapter 5.

3.4.2 Implications for the application

The conclusions as presented in subsection 3.4.1 have implications for the feasibility of the proposed stabilization method. The efficiency of this method is determined by the concentration of dissolved and colloidal silica that can be injected and transported through the soil. Based on the properties of the silica-biopolymer suspensions studied, the hydraulic conductivity is calculated that a peat layer should have to obtain significant transport distances; and, hence an efficient stabilization method.

The calculation is based on rough estimations of system characteristics, and only serves to provide an overview of the restrictions per injection fluid composition. Estimations have been made on the relation between silica load and strength and transport distance or injection times. The estimations are based on literature with respect to injection of silica solutions and hardeners for the creation of hard and soft silica gels, and the patent as introduced in the introduction (Zon, 2007). A classification of the most effective injection fluids in combination with a type of soils is presented in Table 3.5 (Zon, 1998).

Table 3.5 : Classification of injection fluid by soil texture

Type soil (texture)	Injection type
Coarse sand or gravel	Suspensions (particle size 0.02 μm – 120 μm)
Medium to fine sand	Colloidal suspensions and dispersions (particle size < 1μm)
Sand containing silt. clay or silt	True solutions

The data as presented in Table 3.6 provides a *rough indication* of infiltration feasibility of silica-biopolymer injection fluids in a peat soil. The estimation is based on the starting point that 2.5 kg SiO_2 is needed to strengthen 1 m^3 peat. To maintain injection times near 5 days the permeability of the soil layer should be 10^{-5} to 10^{-6} m/sec depending initial silica concentration of the injection fluid. The horizontal hydraulic conductivity of peat is in general less than this (Chapter 2).

Table 3.6: Implication of fluid type and initial silica concentration for injection time

Initial silica concentration [ppm SiO_2]	Biopolymer dosage* [%]	Type injection fluid [-]	Indication conc. particles [-]	Vol. injection fluid** [m^3]	Hydraulic conductivity [m/day]	Injection time*** [days]
300	10. 50 or 100	Solution	very low	8	$1* 10^{-5}$	1.5
600	100	Colloidal dispersion	low – medium	4	$1* 10^{-5}$	3
1250	100	Colloidal dispersion	high	2	$1* 10^{-6}$	7

* $\text{biopolymer dosage} = \frac{\text{ppm biopolymer}}{\text{ppm } SiO_2} \cdot 100\%$

** This is the total volume of injection fluid needed to stabilize 1 m^3 of peat. It is estimated based on literature that the total amount of silica needed to strengthen 1 m^3 of peat is 2.5 kg SiO_2, assuming that the pore volume available for transport equals 85% of bulk volume (Zon, 1998; PQ corporations, personal communication).

*** The injection time is an indication. Decrease of pore volume due to clogging and/or attachment, increase of injection fluid viscosity or increase of injection pressures are not taken into account.

Between the aimed stabilization method and hard silica gels there is a difference in location where the precipitate is located in the porous matrix of the soil. Present research aims encapsulation of the fibre, rather than silica precipitation in the pore void. The latter is the case at the creation of soft or hard silica gels. Logically, this has implications for the relation between silica load in the injection fluid and the obtained increase in bearing capacity. Identification of this relation should be subject to future research.

Elaborating, if one assumes that the concentration of silica needed to achieve bearing capacity is 10% of the 2.5 kg SiO_2 needed to strengthen 1 m^3 peat, in case the fiber is encapsulated than a peat soil should have a permeability of at least 10^{-6} or 10^{-7} m/sec.

4 Attachment to Peat Surface

In the previous chapter it was investigated how an injection fluid with a high concentration of silica could be designed by means of biopolymer addition. Elevation of silica concentration above the solubility limit of amorphous silica was necessary to increase the efficiency of the stabilization method. This chapter evaluates the behavior of the designed injection fluid – composition as proposed in previous Chapter –in the presence of peat solids. The objective is to determine the degree of silica attachment to peat solids surface. Silica should attach to peat solids to improve the mechanical properties of the bulk material. Encapsulation of the fibre with a silicon based amorphous mineral is the method aimed for to improve bulk strength without a significant loss of pore volume. Encapsulation in present study refers to a reaction at the surface of a peat fibre.

However, repulsion between fibre surface and silica species in pore water is in principle likely to oppose attachment of silica to fibre surface. In neutral to acid pH conditions, the surface charge of peat is negative. The surface charge of dissolved or colloidal silica is neutral to negative at pH values lower than 9.5. Equal charged surfaces result into repulsion. Overall repulsion of silicate species at the interface is the result of electrostatic forces (equal sign of charge[6]) and or the result of steric forces. The proposed solution is the use of a cationic surface active additive to initiate attachment between peat fibre and silica. The function of the additive is to alter the surface charge of colloidal silica or dissolved silica from net negative into a net positive charge. Thereby forces of attraction are created between the silica entity in solution and functional groups, which are available for attachment, located at fibre surface.

In the former chapter the capability of the biopolymer to interact with dissolved and colloidal silica was proven. Furthermore, it was indicated that the biopolymer elevates the zeta potential of colloidal silica. The expectation is that electrostatic forces between the formed biopolymer-silicate entities in the pore water and the functional groups located at the peat surface, enable attachment of silica to the peat fibre. Moreover, if the cationic biopolymer is capable to sorb to peat solids, than the net surface properties of a peat fibre could be altered, also enabling the attachment of silica. The biopolymer then functions as a 'bridge' between silica in the pore water and the fibre surface. In conclusion, the biopolymer should initiate the phase transition of silica at the surface of peat solids. This implies that the cationic biopolymer Celquat L200, as used to stabilize dispersed colloidal silica and elevate dissolved silica concentrations, could also improve or enable attachment of silica to peat fibre surface.

First of all sorption of the biopolymer Celquat L200 in the absence of silica was evaluated. Secondly, the capability of the biopolymer to initiate silica attachment to peat solids was evaluated. Evaluation was performed based on a number of attachment tests. The distribution of silica between the liquid and the solid phase in presence of peat is subject to research in the attachment test. The silica biopolymer fluids tested had a biopolymer to silica weight ratio of 1:1.

[6] As stated before, at pH 7 monomeric silica is mainly found as silicic acid and is therefore of neutral charge. At concentrations exceeding 100 mg/l SiO_2 oligomers are formed during the polymerization process. Their silanol groups (Si-OH) become increasingly acidic so that they will bear a negative charge. This is also true for silica (nano) particles (Ilner 1979).

The surface charge of a peat particle is primary determined by the dissociation-state of carboxylic and phenolic functional groups. The charge of these functional groups is pH dependent and is in general negative in the pH range of 6 to 8 (Sparks, 2003).

Research Questions

The formulated research questions are:

1. Does the biopolymer attach to peat solids? What is the sorption isotherm of the cationic biopolymer Celquat L200 to peat?

2. What is the efficiency of attachment to peat of reactive silica (H_4SiO_4 (aq)), in the presence of the biopolymer Celquat L200? How does the biopolymer Celquat L200 influence the removal of silicic acid from solution in the presence of peat?

3. How does the distribution coefficient of silica relate to the initial concentration of silica i.e. the degree of super saturation, in the presence of peat and a 1 to 1 wt. ratio of biopolymer? What is the optimum concentration of silica in the injection fluid to obtain the attachment of silica to peat?

To gain insight in the dominant mechanism(s) that could cause a potential shift in the attachment efficiency of silica with an increase in initial solute concentration, an additional research question was formulated:

4. Is an increase in distribution coefficient related to the attachment of a biopolymer-silica entity to the peat surface – or do other mechanisms contribute to an increase as well? Other mechanisms that could contribute are for example biopolymer depletion or an alternation of peat surface properties.

4.1 Experimental Procedure and Analytical Methods

The performed attachment test is based on the work of Cumming et al. 2010. Cumming and coworkers determined the humic acid to water partition coefficient of several cationic biopolymers, including a polyquaternium-6 and -10. These biopolymers resemble some features of the polyquaternium-4 structure (Cumming et al. 2008). Humic acids contribute a relatively large fraction of the reactive carboxylic groups dictating the overall reactivity of a peaty soil (Sparks, 2003; Killops, 2005). Since the research of Cumming et al. (2010) is comparable to the conditions outlined, his work is used as an example for the attachment test.

The degree of attachment is derived from the distribution coefficient. The distribution coefficient is the ratio between the concentration in the solid phase (C_s) and the concentration of the component of interest (C_w) in dissolved state in a closed system. The amount of silicate and biopolymer in the solid phase (C_s) was calculated from the difference between the initial dissolved concentration (C_i) before adjustment of pH and the final dissolved concentration (C_w) after exposure to peat. The distribution coefficient is defined in Equation 3, which is based on mass balance principles (Means et al., 1980).

$$D = \frac{C_i - C_w}{C_w} \cdot \frac{L}{S}$$ Equation 3

In this expression, C_i is the initial concentration of silicate or biopolymer in the liquid phase (mg kg^{-1} water). C_w is the final concentration in the liquid phase after exposure to peat solids (mg kg^{-1} water). The L represents total volume of liquid present in a shake flask (liter). This is the volume of the reactive solution or demiwater and the volume of the pore water added upon addition of the peat solids. The symbol S is the sum of all the solids added to the flask. i.e. the dry solid content of the added wet peat mass (kg). The unit of the distribution coefficient D is thereby l kg^{-1} dry peat solids. Significant attachment is proposed if the distribution coefficient (D) in the presence of peat solids is higher than as determined in the absence of peat.

The sorption isotherm of solely the biopolymer to peat solids is calculated in accordance to Equation 3 and the work of Cumming et al. (2010) on the sorption of polyquaternium polymers to humic acid. The dissolved concentration of the biopolymer C_w is corrected for the L/S ratio in order to gain the sorption coefficient in units comparable to the work of Cumming et al.

Elaborating on the conclusions and discussion of Chapter 3 it was decided to determine the attachment efficiency of silicon to peat solids at an initial concentration range of 100, 300, 600 and 1250 ppm as SiO_2 and a wt. ratio biopolymer to silicate of 1.

4.1.1 Test Protocol

An overview of the set-up of the flasks is given in Figure 4.1. To perform the experiments, as described and named in Figure 4.1 48 samples were prepared. The samples were prepared in 200 ml HD-PE dark flasks. In the experiments 100 ml of reactive solution was added. As stated before, two reactive fluids were used: a meta stable dispersion of sodium metasilicate nonahydrate and cationic polymer L-200 in a 1:1 ratio ("Silicate; biopolymer - Peat" experiments), and a solution of solely L-200 polymer ("Biopolymer-Peat" experiments). In the 'Water-Peat' experiments, the volume of 100 ml demiwater replaced the reactive solution.

Table 4.1: Attachment test flaks set-up

Liquid phase			Solid phase				Code	Reference
Reactive solution			Peat		average pH*		Flask	Experiment
presence	Composition	concentration	presence	concentration	pH initial	pH (t 113 h)	no.	Name***
yes	Silicate; L-200	60 – 1250 ppm	Yes	20 gr (wet)	5.9	6.5	1 to 10	"Silica; biopolymer-Peat"
no	Demi water	0 ppm	Yes	20 gr (wet)	5.7	6.1	11 to 12	"Water-Peat"
yes	L-200	60 – 1250 ppm	Yes	20 gr (wet)	6.1	6.7	13 to 22	"Biopolymer-Peat"
no	Demi water	0 ppm	Yes	20 gr (wet)	6.1	6.5	23 to 24	" Water-Peat"
yes	Silicate; L-200	60 – 1250 ppm	No	-	**	**	49 to 58	"Silica; biopolymer -No Peat"
no	Demi water	0 ppm	No	-	**	**	59 to 60	"Water-No Peat"
yes	L-200	60 – 1250 ppm	No	-	**	**	61 to 70	"biopolymer-No Peat"
no	Demi water	0 ppm	No	-	**	**	71 to 72	"Water-No Peat"

* The initial pH was adjusted to 7.5 prior to shaking, the EC was not adjusted.

** The original pH and the electric conductivity of the blanco samples without the addition of the peat (code 49 to 72) were determined but not recorded.

*** Reference to the flasks is formulated as: 'reactive solution -solid phase' . For example: "Silica; biopolymer-Peat" experiment as reference for flaks 1 to 10.

To the flask no. 1 to no. 24 ca. 20 ± 0.44 gram of wet peat was added. Peat material originated from location Bellingwedde, described in more detail in section 5.1.1. The peat material was carefully mixed by hand before addition in order not to tear up the fibres and create additional and fresh contact surface. The moisture content of the peat of the mixed paste was ca. 88% and the volumetric weight in mixed state was about 1.02 gram/ml. The Liquid to Solid ratio (L/S) obtained in these "-Peat" experiments was 50 l kg^{-1} dry peat solids (CV = 2%). The experiments without the addition of peat ("-No Peat") were prepared in a similar way but 20 gram of peat was then replaced by 20 gram of demiwater.

The pH was adjusted to a value of 7.5 with 1 molar HCl solution, prior to shaking. The pH was not maintained at 7.5 during the shaking period. The change in the resulting volume was about 1%, this volume change is not taken into account. The pH of the peat paste was 5.05. The initial and final pH values of each experiment are given in Table 4.1 as well. Each experiment was performed in duplicates of which the average was reported as the final result. Details on the preparation of the experiments and the reagents are given in Appendix 13. The duration of the experiment corresponds to the stated period of treatment as found to be reasonable in practice as argued in the Chapter 2. The distribution coefficient was determined based on a 113 hours contact period between the dissolved components (silica and biopolymer), and the peat. In other words the final dissolved concentration (C_i) was the dissolved concentration reached after a period of 113 hours of shaking. The starting point of the attachment test was the moment the pH was adjusted to 7.5, which was performed shortly before the peat was added to the flask. The frequency of shaking was set at 140 rotations per minute to prevent settlement of peat solids. From flask no. 1 to no. 24, two samples were extracted after 65 and 113 hours of shaking. The volume extracted for composition analyses was 50 ml. Pretreatment and composition analyses were performed as described in detail in Figure 4.2. Before composition analyses the extracted liquid was centrifuged for 10 minutes at 2800 G-force. With centrifugation of the extracted sample it was assumed that all suspending particles will precipitate. This physical definition functions as the distinction between the solid and the liquid phase. Silica concentration and dissolved organic carbon (DOC) were determined in the liquid phase of the "Silica; Biopolymer - Peat" experiments. Only DOC concentrations were determined in the "Bipolymer-No Peat" and "Biopolymer-Peat" experiments.

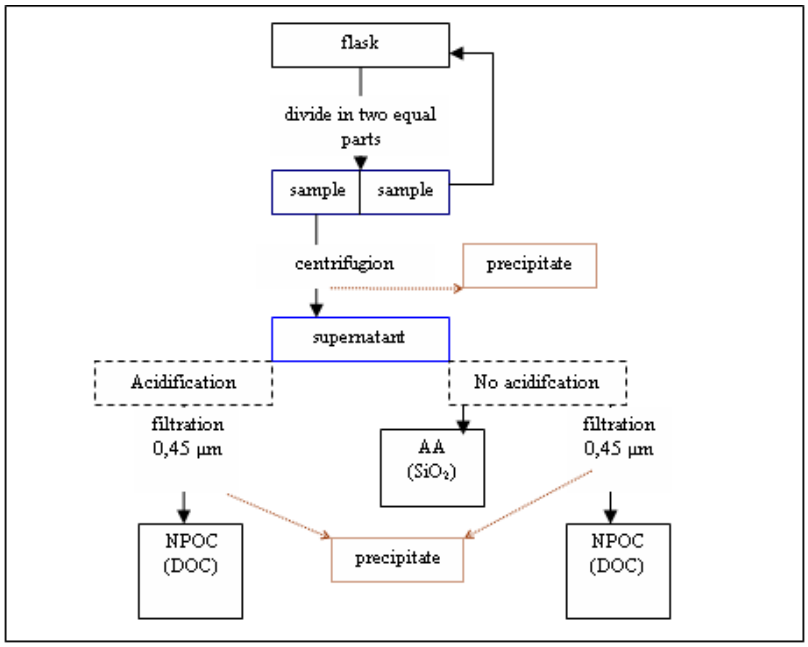

Figure 4.2: Schematic overview of pretreatment and composition analyses

Concentration dissolved (reactive) silica determination

The silicomolybdic assay as optimized by Demadis (2009) and the Deltares BGS laboratory was used in present research. We refer to Appendix 5 for a detailed description of this quantitative assay as performed by Deltares BGS laboratory. Therefore the silicomolybdic assay showed some deviation in protocol from the assay as discussed in paragraph 3.1.2.

An auto analyzer of Bran Luebbe, MultiTest MT7/8 was used to measure the absorbance. The detection range of measurement was 0 – 250 mg/l SiO_2. The gained supernatant was diluted with ultra pure water when necessary prior to analyses. The detection limit at low silica concentration (4 mg/l) was 0.008 mg/l SiO_2, at average concentration (20 mg/l) was 0.01 mg/l and in at high concentration (100 mg/l) was 1.1 mg/l.

We refer to the dissolved concentration of Si irrespective of its speciation as 'dissolved silica concentration'. The quantification used determines siliceous monomers, dimmers, tetramers and possibly the smaller oligomers. Since the boundary is not known. we use this general term. The designation of silicon based species is discussed in more detail in Chapter 2.

Concentration dissolved biopolymer determination

The quantification the biopolymer Celquat L200 employs Dissolved Organic Carbon (DOC) measurements. The concentration of dissolved organic carbon is linearly related to the concentration of L-200 in solution. The calibration curve is given in Appendix 14.1. Based on linear regression analyses the weight fraction of organic carbon in the polymer could be derived:

$$DOC = 0,4338 \cdot L200 - 1,4119 \qquad \text{Equation 4}$$

Wherein DOC is expressed in mg C/l and L-200 concentration in mg/kg. The derived weight fraction of organic carbon in L200 is thus 43.38% with an off set of 1.4 mg C/l. Note that the factor and constant. as defined in Equation 4, are not dimensionless and can therefore only be used for converting mg/kg L200 to mg C/l. The obtained squared correlation coefficient (R^2) is: 0.9985. The obtained relation is valid in the range of 10 to 1250 ppm L-200.

DOC was determined by Non-Pergeable Organic Carbon (NPOC) analyses. The purpose of purging in the NPOC method is to remove volatile carbon compounds. To this volatile fraction is referred as Purgeable Organic Carbon (POC). Using the NPOC analytical method, a small fraction of in principle volatile carbon is however not volatilized (the analytical error of this method). POC consist of compounds like benzene, toluene, cyclohexane and chloroform. These compounds were negligible in a solution of biopolymer Celquat L200. POC was therefore not of interest to evaluate L-200 concentration and thus not considered as a cause for analytical error with respect to L200 concentrations (NEN-EN 1484. 14.2).

Dissolved organic carbon originating from the peat itself was considered to interfere with quantification of L200. DOC values as measured reflect both the organic carbons originating from the L200 biopolymer and from peat pore water. To distinguish between the polymer and peat as DOC source, a set of "Water-Peat" flasks was prepared for each initial silica concentration. These experiments were prepared without the addition of biopolymer (see Table 4.1). DOC measurements in the "Silicate; Biopolymer-Peat" and "Biopolymer-Peat" experiments were corrected for these values.

Furthermore, the supernatant collected for composition analyses were acidified prior to NPOC analyses to reduce the contribution of humic acids to DOC concentration. Upon acidification to a pH < 3, the supernatant contained organic carbon solely related to a) L200 and by definition to b) fulvic acid.

4.1.2 Experimental considerations

Silicate (SiO_2): Mass Balance

From the 'Water-Peat' experiments it appeared that peat contained some silica as well. Since the peat fraction consists of a solid and a pore water fraction, the silicate could originate from both sub fractions. Hence, the total concentration of silicate *added* to the system (C_i) is not equal to the *total* concentration of silicate present in the system (C_{total}). The measured dissolved silica concentration is corrected for the value Ci_wpeat. The final solid concentration is defined by Equation 5.

$$\left[C_s\right]_{t3} = \left[C_{i\_added}\right]_{t0} + \left[C_{i\_wpeat}\right]_{t0} - \left[C_w\right]_{t3} \qquad \text{Equation 5}$$

Wherein:

$\left[C_s\right]_{t3}$: The final attached concentration of SiO_2 after exposure to peat for 113 hours (t_3)

$\left[C_w\right]_{t3}$: The final dissolved concentration of SiO_2 after exposure to peat for 113 hours (t_3)

$\left[C_{i\_added}\right]_{t0}$: The initial concentration SiO_2 of the reactive fluid added to the flask

$\left[C_{i\_wpeat}\right]_{t0}$: The initial concentration of SiO_2 present in the pore water of the peat fraction added to the flask. The total concentration of SiO_2 present in the system is the added amount of silica plus the silica initially present in the peat material. Ci_wpeat excludes the silica present in the texture of the peat solids. This silica does in principle not dissolve and therefore is not available for the attachment processes under given conditions.

Cationic polymer: Mass Balance

The biopolymer L200 a modification of a cellulosic backbone. This exact structure will therefore not exist in nature. For that reason the mass balance as presented is truly the definition of total L200 present in the system. The mass balance of the cationic biopolymer is expressed by Equation 6.

$$\left[C_w\right]_{t3} + \left[C_s\right]_{t3} = \left[C_i\right]_{t0} = C_{total} \qquad \text{Equation 6}$$

Wherein:

C_i: The initial concentration of L200 as added in the reactive fluid

C_s: The final attached concentration of L200 after exposure to peat for 113 hours (t_3)

C_w: The final dissolved concentration of L200 after exposure to peat for 113 hours (t_3)

The dissolved concentration of L200 is however calculated based on DOC analyzes. For a detailed description of the applied analytical method, see paragraph 0. The initial concentration of L200 in terms of DOC was calculated using the conversion factor as presented in Equation 4. By introducing the conversion factor (L200 consists of 43.38 wt. % organic carbon) an error is introduced as well. The error included in the calculation of the conversion factor is discussed in the Results section, paragraph 4.2.1

4.2 Results

The removal of the dissolved components silica and biopolymer from solution was considered to represent attachment of these components to peat solids. The degree of attachment of silica to peat solids was derived from the distribution coefficient in terms of the biopolymer and in terms of silica. The definition of the distribution coefficient in terms of silica or in terms of biopolymer is presented in Equation 3. However, the exact mechanism which triggers the phase transition of silica was not subject to research. Note, that attachment of silica could be either sorption or precipitation.

First, the analytical method to quantify the biopolymer in solution was evaluated. Secondly, the solubility of the biopolymer Celquat L200 in demiwater and its sorption behavior to peat solids was evaluated in the range of 0 – 1250 ppm biopolymer. Thereafter the behavior of the biopolymer L200 was evaluated in the presence of peat and silica. Likewise the behavior of silica was evaluated in the presence of peat and the biopolymer. The distribution coefficient was expressed as a function of the initial added concentration of silica in the range of 0 – 1250 ppm SiO_2 at biopolymer dosage of 100%[7].

Dissolved concentrations of the components silica and biopolymer were determined after 65 and after 113 hours of contact with peat material. The phase distribution of silica and the biopolymer after 113 hours of incubation was equal to the phase distribution as determined after 65 hours (CV 2% ± 1% for SiO_2 and 21% ± 6% for L200). This suggests that steady state conditions where reached within 65 hours of shaking. Only the final silica concentration in a mixture containing 1250 ppm SiO_2 and 1250 ppm L200 was an exception to this (CV 5%). The data presented in this chapter therefore concerns only dissolved and solid concentrations after 113 hours of shaking, leaving one exception. The data as obtained after 65 hours of contact is presented in Appendix 15.

In addition, some constrains need to be mentioned before reading this section. The classification of the mixture of silica and biopolymer Celquat L200 as a colloidal dispersion, as discussed in Chapter 3, had implications for the interpretation of the attachment test measurements. A part of the silica scavenged from solution should be attributed to dispersion instability and not to attachment to peat solids. The distribution coefficient as determined in the "-Peat" experiments could therefore not totally be assigned to attachment at peat solids. The distribution coefficient derived from the "-No Peat" experiments represents the instability of the colloidal dispersion in the absence of peat. These results were compared to the distribution coefficient as obtained in the presence of peat.

4.2.1 Quantification of the biopolymer

The concentration of biopolymer L200 was derived from dissolved organic carbon values, as explained in section 0. The calculated biopolymer concentration is an indicative number with a high factor of uncertainty.

The instrument detection limit (IDL) for biopolymer concentration analyses using NPOC was 0.9 mg l^{-1} DOC. The method detection limit (MDL) was 20.1 mg l^{-1} DOC in the absence of peat (determined at 7 degree of freedom). In the presence of peat, thus including the acidification step to eliminate DOC originating from peat, MDL increased to 58.7 mg l^{-1} DOC (determined at 7 degree of freedom). These results indicate that the analytical method to determine biopolymer concentration becomes inaccurate at biopolymer concentrations lower than 50 ppm L200 in the absence of peat.

[7] 100% biopolymer dosage is refers to a solution at time zero of for example 600 ppm SiO_2 and 600 ppm biopolymer. That is, a 1 to 1 wt. ratio between biopolymer and silica.

In the presence of peat, this limit was determined at 138 ppm L200. Therefore, DOC measurements as performed at 60 and 100 ppm initial biopolymer concentration were considered unreliable.

The standard error of estimate (SEE) of the linear regression between DOC measurements and biopolymer L200 concentration was 1.1 mg l^{-1} DOC at initial biopolymer concentrations in the range of 11.9 to 199.5 ppm L200. At initial concentration range of 60 to 1250 ppm L200 the obtained SEE was 9.0 mg l^{-1} DOC. These results indicate that changes in biopolymer concentration of less than 24 ppm L200 were not significant.

Acidification as pretreatment for biopolymer quantification – as described in paragraph 0 – had no severe impact on the actual quantification of the biopolymer. The detection limit of the NPOC instrument increased to 1.4 mg l^{-1} DOC, upon acidification. The method detection limit (MDL) increased to 29.3 mg l^{-1} DOC (determined at for solely 3 degrees of freedom).

Likewise, acidification as pretreatment had no severe impact on the accuracy of the regression line in the range of 0 to 600 ppm L200. SEE increased to 11.8 mg l^{-1} DOC – which equaled 30 ppm L200. However, at 1250 ppm L200 (541 mg l^{-1} DOC) acidification invoked a strong decline in DOC concentration, which was attributed to the pretreatment. In the range of 0 to 1250 ppm initial L200 concentration, the SEE increased to 43.4 mg l^{-1} DOC due to acidification as pretreatment. Compare the open blue dots in Figure 4.1 to the closed blue dots. All dissolved biopolymer concentrations determined at initial concentration of 1250 ppm L200 were therefore corrected.

4.2.2 Biopolymer solubility in the absence of peat

In the absence of silica ("L200- No Peat" experiments)

Figure 4.1 presents the relation between dissolved biopolymer L200 concentrations (C_w) as a function of the initial added concentration of the biopolymer L200 (C_i). The biopolymer concentration in Figure 4.1 was expressed in the unit mg DOC per liter and not in mg L200 per kg liquid, since peat DOC was not present. Thereby the error of conversion to mg L200 was not introduced. A biopolymer concentration of 60 to 1250 ppm L200 corresponded to a dissolved organic carbon concentration of 25 to 541 mg 1^{-1} DOC, respectively.

According to INCI designation the biopolymer L-200 was classified as a polyquaternium-4 polymer. Flocculation of a polymer takes place upon charge neutralization (Hiemenz, 2007) – this can occur due to interaction with negatively charged particles or dissolved organic molecules (Cumming et al. 2008; Amjad, 1999) – or if the biopolymer concentration exceeds a certain threshold (Cumming et al. 2008). In present research a decline of dissolved biopolymer concentration had to relate to attachment of the biopolymer to dissolved or particulate organic material. The possibility of flocculation and subsequent decline in dissolved biopolymer concentration had to be excluded. That is, flocks larger than 0.450 nm were considered to be part of the solid fraction, since a filter of 0.450 nm was used to separate dissolved organic carbon from particulate organic carbon.

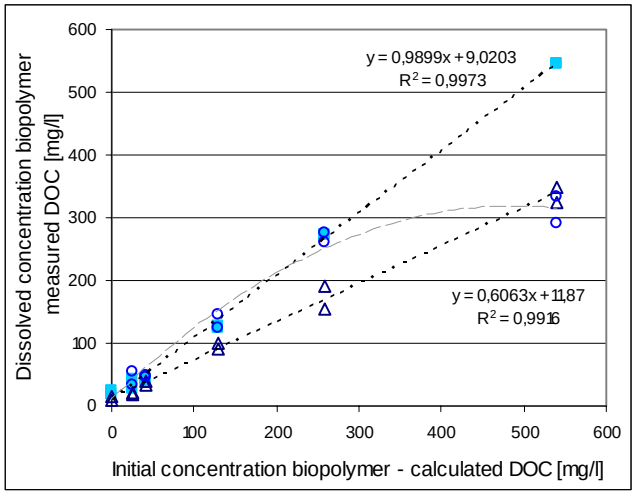

Legend:
Experiment (fluid composition):

- L200– No Peat
- L200;Silica – No Peat; 1 to 1 wt. ratio of silica to L200
- L200 – No Peat ; acidification as pretreatment

Measurements are corrected for 'Blanco' values of solely the peat pore water solution.
The values of the derived distribution coefficients were not corrected for the liquid to solid ratio as opposed to Equation 3, since the ratio is constant for all performed "-Peat" experiments. In this way clarity is maintained and the units of "-No Peat" experiments are equal to the units of "-Peat" experiments. Furthermore, the small variance in the L/S ratio was not in proportion to the heterogeneity of the peat material itself.
Note that material characteristics like total surface area, surface accessibility, number and type of surface sites, of the peat material itself will influence the efficiency of attachment. In the current research, these characteristics are not determined and the peat is considered as a template for attachment, i.e. as a non-specified sink. This causes the spreading between the duplicate values.

The x-axis gives the initial concentration of the biopolymer as based on stock concentrations and weight. The values are given in DOC mg/l. The y-axis represents the dissolved biopolymer concentration as measured by NPOC technique. expressed in measured DOC mg/l.

Figure 4.1: Biopolymer dissolved concentration in relation to the initial concentration of biopolymer in DOC units

In Figure 4.1 a linear and strong correlation between measured final dissolved concentration of the biopolymer and calculated initial biopolymer concentration is presented (symbol: blue cube). In the absence of peat the slope approaches 1. This indicates that the added amount of biopolymer was present in dissolved state after 113 hours of shaking. According to Bennett et al (2000) the optimum flocculent dose for the highly soluble cosmetic polyquaterniums (L200 belongs to this group) exceeds a concentration of 1400 mg/l. The statement of Bennett et al was confirmed by the results as presented in Figure 4.1. The concentration range of 60 to 1250 ppm biopolymer was below the concentration at which the biopolymer flocks i.e. forms particles larger than 450 nm.

In the presence of silica ("L200; Silicate- No Peat" experiments)

The dissolved concentration of the biopolymer in the presence of silica is also presented in Figure 4.1 (open triangle). A strong linear correlation between the final dissolved (C_{w_113h}) and initial concentration of the biopolymer (C_i) was observed. The slope of the relation indicates that ca. 61% of the biopolymer was present in dissolved state after 113 hours of agitation in the presence of silica; as opposed to 99% dissolved in the absence of silica. This observation indicated that part of the dissolved biopolymer associated with silica particles/ flocks larger then 450 nm. Furthermore, these observations indicate that the mass fraction of removed L200 remained constant irrespective of the initial concentration. The increase of particulate biopolymer concentration with increasing initial concentrations of the mixture coincides with observations as reported in section 0. The higher the initial concentration the more dispersed particles were present and the more biopolymer was scavenged from solution.

4.2.3 Biopolymer dissolved concentrations in the presence of peat

Sorption Isotherm biopolymer – "L200-Peat experiments"

A solution of the biopolymer L200 was considered to be a true solution in the absence of silica, as argued in the previous paragraph. The concentration range of 60 to 1250 ppm L200 was well below the flocculant dose. It was therefore proposed that a constant dissolved biopolymer concentration over time reflects equilibrium. Hence, the distribution coefficient (D) – indicating the sorption of the biopolymer to peat solids in the absence of silica – could be defined as a sorption coefficient (K_D). The sorption coefficient was derived from the sorption isotherm, in accordance with the work of Cumming et al. (2010). The sorption isotherm is presented in Figure 4.2 A. The solid to liquid ratio (S/L ratio) equaled 0.02 l kg^{-1} in current research. Cumming tested S/L ratio's in the range of 0.02 to 0.0025 l kg^{-1}.

To derive the sorption coefficient a linear correlation between C_w and $C_i - C_w$ was assumed, although the association was weak (R^2 of 0.73, Figure 4.2 A). A Langmuir relation was expected based on literature (Appelo and Postma, 2005; Cumming et al. 2010).The dispersion of the measurements was however too large to conclude a convex or concave shaped relation. Besides, the concentration range was too narrow to conclude the presence of an adsorption plateau. A linear approach was in accordance with the work of Cumming et al (2010).

To give an indication of sorption behavior and sorption efficiency of the Celquat L200 biopolymer in comparison to a reference and in relation to it's charge and structural features, the determined sorption coefficient (K_D) is presented in Table 4.3 next to the result of Cumming et al. Despite the fact that pretreated commercial humic acid is not a similar template for sorption as raw peat does, the obtained sorption coefficient was within the range of the results presented by Cumming et al. (2010).

Table 4.3: Properties of the Celquat L200 biopolymer in comparison to other polyquaterniums (Cumming, 2008)

Commercial name	INCI designation	Charge density [eq/g]	Average molecular [kDa]	K_D [l/kg]	R^2 [-]
Celquat L200	Polyquaternium-4	*1.1 x 10^{-5}	**138	503	0.72
UCare JR125	Polyquaternium-10	9 x 10^{-4}	250	470	0.94
UCare JR30M	Polyquaternium-10	1 x 10^{-3}	600	630	0.82
UCare JR400	Polyquaternium-10	1.2 x 10^{-3}	400	440	0.82
Styleze W-20	Polyquaternium-55	6 x 10^{-4}	665	500	0.91

* den Hamer 2011 using Total N-Kjeldahl as indication of charge

** den Hamer 2011 using Malvern Technology and Zetasizer

The r-square value as obtained for derivation of the L200 sorption coefficient to peat solids was relatively low. Using dissolved organic carbon as measure for the dissolved biopolymer concentration in the presence of peat solids, returns a significant analytical error. Derivation of K_D was very sensitive to analytical errors since more than 90% of the initial added biopolymer was adsorbed. This leads to uncertainly with respect to remaining concentration in solution. Moreover, solid humic particles, used as sorption template by Cumming et al (2010), was a more purified and concentrated source of sorption sites. Cumming et al (2010) proposes a relation between charge density of the biopolymer and the sorption coefficient to humic substances. Despite the observation that the K_D value was found in the range as observed by Cumming, the K_D value did not relate to the measured charge density - showing the impact of other structural features like solubility and biopolymer size. The biopolymer Celquat L200 showed the most structural similarities to UCare JR 125 product.

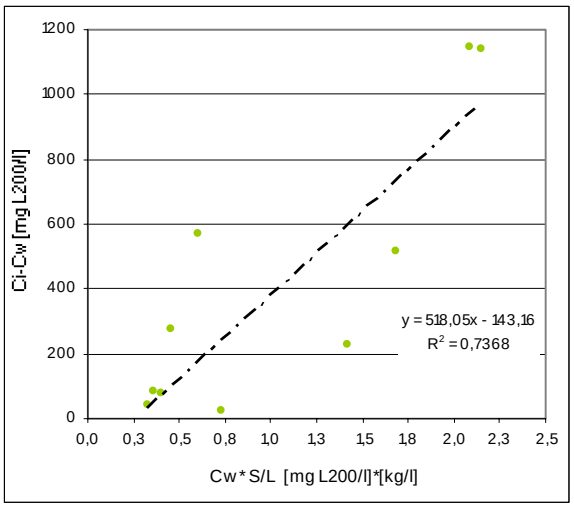

A. Sorption Isotherm L200; Attachment of biopolymer L200 to peat solids.

Legend:

Experiment:

- *L200 – Peat*
- *Trend line. assuming linear relation*

Y-axis: final solid concentration of biopolymer present at time 113 hours after pH adjustment. Calculated from DOC measurements and initial added concentration. Expressed in mg L200 per kg liquid. X-axis: dissolved concentration of biopolymer present at time 113 hours after pH adjustment. Calculated from DOC measurements and adjusted for Blanco value. Expressed in mg L200 * 0.02 (S/L).

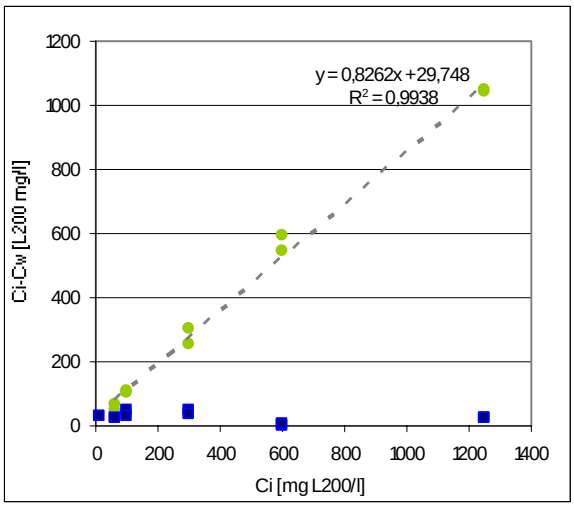

B. Biopolymer 'solid' concentration in relation to initial added concentration in the presence and absence of peat.

Legend:

Experiment:

- *L200– Peat*
- *L200 – No Peat*

Y-axis: final solid concentration of biopolymer in L200 mg/l after 113 hours of induction. Calculated from final dissolved biopolymer concentrations (C_{w_113h}) and initial added concentration (C_i). X-axis shows the initial added concentration of the biopolymer. Values are adjusted for Blanco values.

Figure 4.2: Sorption isotherm and distribution of biopolymer Celquat L200 to peat solids

Figure 4.2 B shows the efficiency of the biopolymer to attach to peat surface in the absence of silica i.e. as a dissolved component. Figure 4.2 B presents the same values as figure A. though as a function of the initial added concentration of biopolymer (C_i). The efficiency of the biopolymer to attach to peat solids was relatively high. Circa 83% of the initial added amount of biopolymer was extracted from solution over the initial concentration range of 100 to 1250 ppm L200.

In addition the results were evaluated based on total of measured dissolved organic carbon i.e. without acidification as pretreatment (results presented in Appendix 16). No distinction was made between DOC originating from peat solutes or biopolymer. The obtained results indicate that the biopolymer scavenged dissolved organic components, peat solutes, upon adsorption. The cationic biopolymer probably formed complexes with dissolved organic macromolecules naturally present in peat pore water. By this complex formation the dissolved components were scavenged from solution. Or particles were formed exceeding the threshold of 450 nm in size. Particles larger than 450 nm were filtered from the supernatant by sample pretreatment and were thereby considered as solid mass.

To summarize, the biopolymer was present as a dissolved component when no silica was added. Upon addition of peat the biopolymer adsorbs efficient to peat particles and/or forms particles with dissolved organic matter, as was expected.

4.2.4 Attachment of silica and biopolymer to peat solids

The relation between attachment of silica or biopolymer to peat solids and the initial concentration, in which these components were added, is presented in Figure 4.3, Figure Figure 4.4, Figure 4.6 and Figure 4.6. Figure 4.3 and Figure 4.4 presents the relation in terms of the component silica as ppm SiO_2. Figure 4.6 and Figure 4.6 presents the relation in terms of biopolymer Celquat L200, expressed as ppm L200. Note, that Figure 4.3 to and Figure 4.6 display values obtained from the "L200; Silica-Peat" experiment" and the "L200; Silica-No Peat" experiment. The obtained values represent composition analyses performed on the same sample. Note, that the tested mixtures had a biopolymer to silicate weight ratio of one.

"L-200; Silicate – Peat" experiment in terms of silica

Figure 4.3 expresses the 'solid' concentration of silica in terms of mass fraction of the initial added amount of silica. The figure shows that there was a significant increase in the 'solid' fraction of silica upon exposure to peat. Furthermore, the figure indicates that the solid mass fraction increases with increasing initial concentration of the injection fluid. For this reason it was proposed that the initial concentration had a synergetic effect on the attachment of silica to peat solids. The results showed that this synergetic effect diminishes at concentrations $\geq$ 300 ppm SiO_2.

Figure 4.4 A shows the relation between final solid and dissolved concentration of silica as a function of the initial concentration of silica, in the presence of peat. In the presence of peat, the final *solid* concentration of silica increased linear with an increase in initial concentration of the mixture. The final *dissolved* concentration of silica increases only slightly with increasing initial concentration. C_w remained close to 100 ppm SiO_2, which is the solubility product of amorphous silica.

Figure 4.4 B presents the dissolved and solid concentration of silica in the absence of peat. Note, the relatively high final solid concentration at initial concentration 1250 ppm SiO_2 (closed triangles). The figure illustrates the fact that a mixture of silica and biopolymer at pH of 7.5 was a colloidal suspension as discussed in Chapter 3. From this it follows that a part of C_S in the presence of peat (Figure 4.4 A) should be attributed to dispersion instability instead of attachment.

Figure 4.4 indicates that *attachment of silica to peat solids takes place*, in the presence of 100% biopolymer dosage. The solid concentration of silica was significantly higher in the presence of peat than in the absence, after 113 hours of incubation and over the initial concentration range of 100 to 1250 ppm SiO_2. Moreover, *the attachment of silica was synergetic with initial concentration*. Although, the synergetic effect seemed to diminish at initial concentration $\geq$ 300 ppm SiO_2.

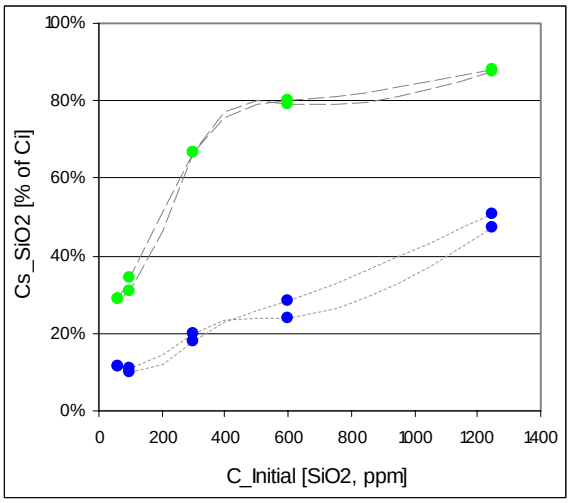

The x-axis represents the initial concentration (C_i) of the silica-biopolymer dispersion, expressed in ppm SiO_2. The y-axis represents the removed concentration of soluble silica from the dispersion at 113 hours after pH adjustment. These values were expressed as mass fraction of the initial added concentration. The data as presented was corrected for measured 'Blanco' values.

Legend:

Experiment composition:

- L200; Silica – No Peat.
- L200;Silica – Peat;

Figure 4.3: Attachment of silica to peat solids in terms of mass fraction in the presence of 100% biopolymer

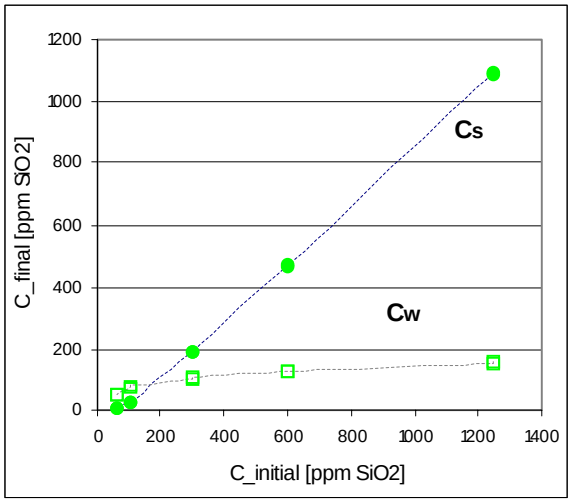

A. Final concentration of silica i.r.t. initial concentration form Silica-biopolymer dispersion in terms of mg per kg liquid – in the presence of peat.

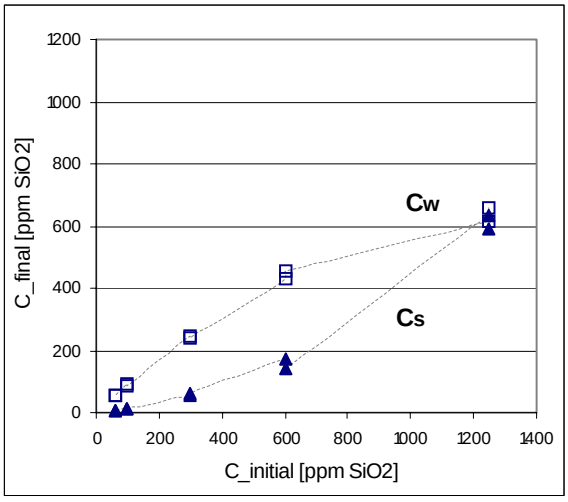

B. Final concentration of silica i.r.t. initial concentration form Silica-biopolymer dispersion in terms of mg per kg liquid – in the absence of peat.

Legend:

Experiment composition:

●	L200; Silica – No Peat.	Closed	Solid concentration($C_i - C_w$) after 113 hours of incubation
●	L200;Silica – Peat;	Open	Dissolved concentration (C_w) after 113 hours of incubation

The same measurement data is presented in present figure as in Figure 4.3, only in a different way. Figure A presents the solid and dissolved concentration of silica after 113 hours of incubation in the presence of peat. Figure B presents the solid and dissolved concentration after 113 hours in the absence of peat. The data as presented was corrected for measured 'Blanco' values.

Figure 4.4: Attachment of silica to peat solids in the presence of 100% biopolymer dosage

"L-200; Silicate – Peat" experiment In terms of biopolymer Celquat L200

Figure 4.5 expresses the 'solid' concentration of the biopolymer in terms of mass fraction of the initial added amount of biopolymer. The figure shows the relation in the presence of peat, in the absence of peat, in the presence of silica and in the absence of silica.

The biopolymer attaches *as efficient* to peat solids in dissolved form as it attaches in (partly) dispersed from, at an initial concentration range of 300 to 1250 ppm L200. The biopolymer was partly dispersed in the presence of silica, as it associates with colloidal silica. The relation between the fraction of biopolymer attached to peat solids (C_S %) in the presence of silica, and the initial concentration of biopolymer (C_i) was non-linear in the range of 60 to 600 ppm L200. At C_i of 600 ppm L200 the highest fraction of biopolymer attachment was observed i.e. 92%. The sorption of the biopolymer to peat solids in the absence of silica (dark green triangles) was comparable, 90% to 99% at initial concentration of 600 ppm L200.

The dissolved biopolymer seems to attach to peat solids *more efficient* in the absence of silica in range of 60 to 300 ppm. However, the obtained results at 60 and 100 ppm L200 were less reliable as was described in section 4.2.1. This was also illustrated by the relatively large deviation of C_S % as depicted in "Biopolymer-Peat" experiment (dark green triangle in Figure 4.5).

At initial concentration of 1250 ppm L200 the fraction of biopolymer that attaches to peat solids declines to 76% (Figure 4.5). This was observed both in the presence as in the absence of silica though in a lesser extent i.e. 83%. Despite the decline in mass fraction C_S %, a stabilization of C_S – comparable to a sorption plateau – was not reached within the tested initial concentration range; as can be seen in Figure 4.6 A. This observation suggests that at C_i of 1250 ppm L200/ ppm SiO_2 saturation of functional or nucleation sites, located at the surface of peat solids, was not yet reached.

Figure 4.6 B presents the dissolved and solid concentration of biopolymer in the presence of silica but in absence of peat. The figure illustrates the fact that the mixture of silica and biopolymer Celquat L200 at pH of 7.5 was a colloidal dispersion as discussed in Chapter 3. Biopolymer that was scavenged from solution in the absence of peat should be attributed to dispersion instability. Note, that with increasing initial concentration the contribution of C_S biopolymer increases (from 20% to 40%). This increase of C_S in the absence of peat was less than observed for the silica component, Figure 4.4 B.

In general, the results show that *attachment of biopolymer Celquat L200 to peat solids takes place, both in the presence as in the absence of silica*. The solid concentration of biopolymer was significantly higher in the presence than in the absence of peat after 113 hours of incubation, over the initial concentration range of 100 to 1250 ppm SiO_2. Furthermore, *the initial concentration had a synergetic effect on the attachment of the biopolymer to peat solids*. However, the synergetic effect seemed to diminish at initial concentration of 1250 ppm L200/ ppm SiO_2.

Comparison of dissolved silica removal from solution to the removal of dissolved biopolymer indicates *that removal of L200 from solution was more efficient than that of silica*; especially in the C_i range of 100 to 300 ppm L200/SiO_2. The biopolymer achieves 92% attachment at 600 ppm C_i. Silica reaches that level at an initial concentration of 1250 ppm. This observation is evaluated in more detail in next section.

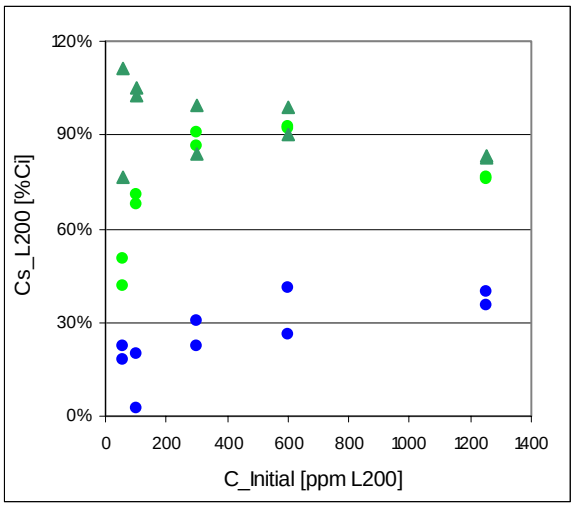

Legend
Experiment composition:
- *L200; Silica –No Peat*
- *L200;Silica – Peat*
- *L200 – Peat*

In Figure 4.5 and Figure 4.6 the x-axis represents the initial concentration (C_i) of the silica-biopolymer dispersion, expressed in ppm L200. In Figure 4.6 the y-axis represents the concentration of dissolved biopolymer removed from the dispersion after 113 hours after pH adjustment. These values represent the solid concentration of biopolymer (C_S). The solid concentration of biopolymer was derived from the difference between final dissolved and initial added concentration of biopolymer.
Figure 4.5 and Figure 4.6 present the same measurement data in a different way. In Figure 4.5 C_S is expressed as mass fraction of the initial added concentration.
Figure 4.6 A presents the solid and dissolved concentration of biopolymer after 113 hours of incubation in the presence of peat.
Figure 4.6 B presents the solid and dissolved concentration after 113 hours in the absence of peat. The obtained data as presented were corrected for the measured 'Blanco' values and for the error induced by acidification as pretreatment.

Figure 4.5: Attachment of biopolymer L200 to peat solids in terms of mass fraction in the presence of 100% biopolymer

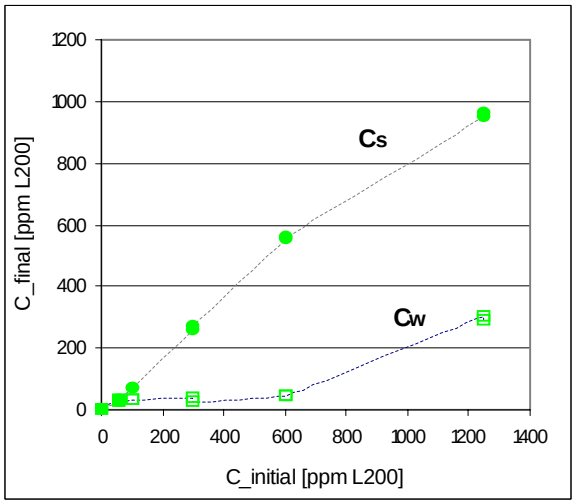

A. Attachment biopolymer i.r.t. initial concentration silica-biopolymer dispersion.

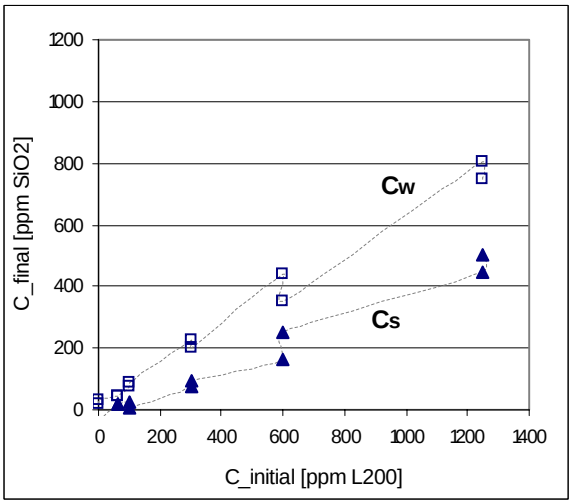

B. Attachment biopolymer i.r.t. initial concentration silica-biopolymer dispersion.

Legend Experiment composition:

L200; Silica – No Peat. Blanco	*Open*	*Solid concentration($C_i - C_w$) after 113 hours of incubation*
L200;Silica – Peat;	*Closed*	*Dissolved concentration (C_w) after 113 hours of incubation*

Figure 4.6: Attachment of biopolymer to peat solids in the presence of silica

4.2.5 Stoichiometry of attachment

In order to investigate the more efficient depletion of the biopolymer than silica from solution, the molar ratio between the two components in solution was calculated. The molar concentration of the biopolymer was calculated using the determined molecular weight of 138.5 kDa. Before pH adjustment (t_0) the molar ratio of biopolymer and silica was 2305. The molar ratio as determined experimentally after 113 hours was normalized to the initial calculated ratio of 2305. The normalized molar ratio is expressed in Equation 7. The obtained result is presented in Figure 4.7.

A molar ratio of 1 indicates that the removal of dissolved silicate and biopolymer from solution was stoichiometric, i.e. that there was no depletion of either biopolymer or silica from solution. A value of >1 indicates that the biopolymer was removed from solution more efficient than silica. When the value is < 1 then silica molecules were removed from solution more efficient than the biopolymer molecules.

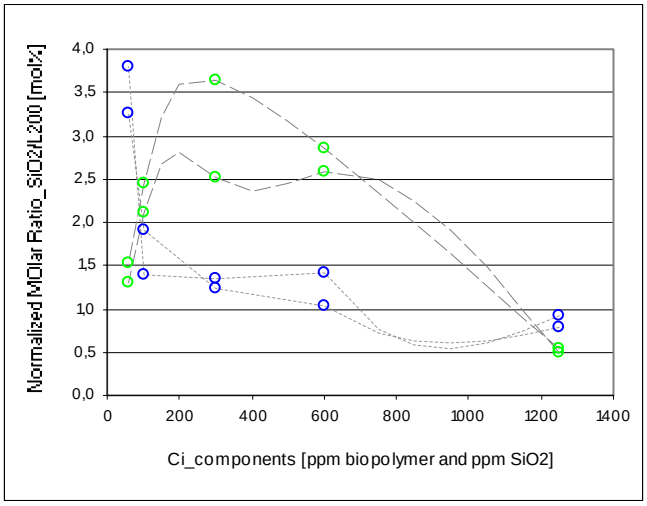

Figure 4.7: Silica to biopolymer mol ratio as a function of the initial added concentration of dispersion

The x-axis shows the dissolved silica to dissolved biopolymer mol ratio as determined after 113 hours of induction – normalized to the same ratio at t0. See Equation 7 for clarity.

$$\frac{\left[SiO_2 / L200\right]_{Cw,t3}}{\left[SiO_2 / L200\right]_{Cw,t0}} = \text{normalized Mol Ratio}$$

Equation 7

The y-axis represents the initial added concentration of the dispersion. This is the composition at t0, containing an equal amount of biopolymer as silica by weight.

Legend. Experiment composition:

- *L200; Silica – No Peat*
- *L200;Silica – Peat*

"L200; Silicate- No Peat" experiments

At C_i of 60 ppm SiO_2/ ppm L200 the ratio was > 1, suggesting a non-stoichiometric removal of the biopolymer from solution. Over the range of 60 to 100 ppm SiO_2/ ppm L200 the ratio decreased and indicated a strong decline in the removal efficiency of the biopolymer in favor of silica. Note that DOC measurements in this range were less reliable, as discussed in section 4.2.1. In the range of 100 to 1250 ppm C_i the molar ratio varied between 1.5 and 1.0. This result indicates that the removal of both biopolymer and silica from solution was stoichiometric with the ratio at which both components were present at t_0. A weak decline in the trend was observed, that could be interpreted as a preferred removal of silica with increasing initial concentrations.

"L200; Silicate-Peat" experiment

In the range of C_i 100 to 600 ppm SiO_2/ ppm L200 the molar ratio was > 1. In this range the peat had a stimulating effect on the removal of biopolymer from solution, and this affect was more prominent to the biopolymer than to silicate molecules. At C_i of 1250 ppm SiO_2/ ppm L200 the molar ratio was < 1. At initial concentration of 1250 ppm, silica was removed from solution more efficient than the biopolymer; a non-stoichiometric attachment of the components to peat solids was observed.

Thus the biopolymer was depleted from solution more efficient than silica in the presence of peat solids, and in the initial concentration range of 60 to 600 ppm SiO_2 / ppm L200. Moreover, the degree of biopolymer depletion from the solvent depended on the initial concentration of the injection fluid. At initial concentration of 100, 300 or 600 ppm SiO_2 at 100% biopolymer dosage, the biopolymer was depleted from the solvent in favor of silica.

Summarizing

In order to illustrate the observed preferred removal of biopolymer from solution in the concentration range of C_i 60 to 600 ppm SiO_2 in the presence of peat, and the preferred removal of silica from solution at C_i of 1250 ppm SiO_2, Figure 4.8 was constructed. The bar chart illustrates the relative differences between fluid composition after 113 hours of incubation in the presence and absence of peat, at increasing initial concentrations. Note, that the units in Figure 4.8 are ppm SiO_2 and ppm L200.

At initial concentration of 1250 ppm SiO_2 and in the *absence of peat* (gray), the dissolved biopolymer concentration was *higher* than the dissolved silica concentration after 113 hours of incubation. This was the opposite of a mixture at an initial concentration of 100, 300 and 600 ppm SiO_2.

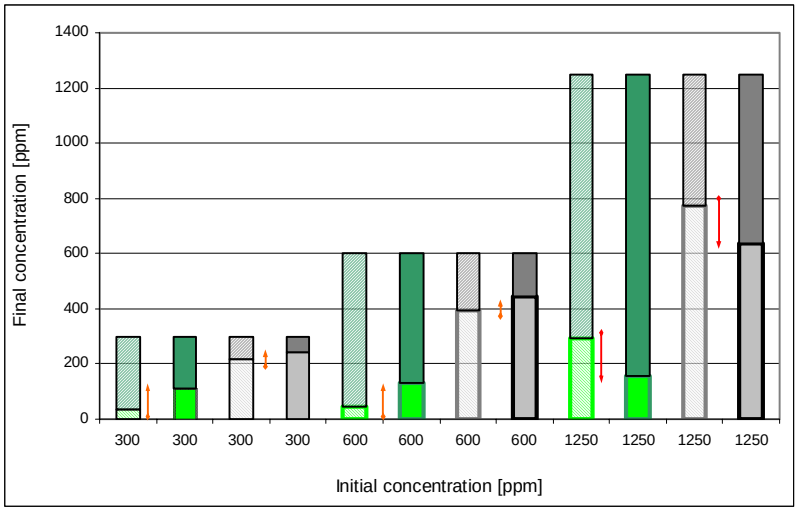

The y-axis shows the dissolved silica or dissolved biopolymer concentration as determined after 113 hours of incubation.
The initial added concentration of the dispersion is indicated on the x-axis. The initial concentration was assumed to be in dissolved state before pH adjustment from pH >12 to 7.5.
The green bars represent the result in the presence of peat. The peat was added after the adjustment of pH.
Green bars represent silica and the gray bars represent the biopolymer.

Legend:

- Solid L200 concentration. presence of peat
- Dissolved L200 concentration. presence of peat
- Solid silica concentration. presence of peat
- Dissolved silica concentration. presence of peat
- Solid L200 concentration, absence of peat.
- Dissolved L200 concentration, absence of peat.
- Solid silica concentration, absence of peat
- Dissolved silica concentration, absence of peat

Figure 4.8: Non-stoichiometric phase distribution as a function of initial concentration in presence and absence of peat.

At initial concentration of 1250 ppm SiO_2 and in *the presence of peat* (green) the total amount of dissolved biopolymer and dissolved silica decreased. However, the *difference* between the two components remained equal to the observed difference in the absence of peat; evaluated after 113 hours of incubation. This observation opposes the results at initial concentration of 100, 300 and 600 ppm SiO_2.

At initial concentration of 100, 300 or 600 ppm SiO_2 *in the absence of peat*, the dissolved biopolymer concentration was *slightly lower* than the dissolved silica concentration after 113 hours of incubation. In the *presence of peat* the concentration of both dissolved silica and dissolved biopolymer decreased and the *difference* between the dissolved components *increased*. These observations are indicated by the length and the direction of the red arrows in Figure 4.8. These observations indicate that the difference in final dissolved silica concentrations i*n the presence* of peat was related to the final dissolved concentrations *in the absence* of peat.

4.2.6 Distribution Coefficient

The aim of determining the distribution coefficient was to define the optimum composition of injection fluid in terms of silica attachment to peat. Definition of the distribution coefficient is given presented in Equation 3. The distribution coefficient as presented in this section was not corrected for the liquid to solid (L/S) ratio. In contrast to Figure 4.2 A, the distribution coefficient as displayed in Figure 4.9, was dimensionless and did not have the unit l per kg dry solids. Thereby the distribution coefficient in the absence and presence of peat could be plotted in the same figure. The contribution of dispersion instability to the removal of silica and biopolymer from solution could be distinguished from attachment to peat solids.

Distribution coefficient evaluated in terms of silica (as SiO_2)

The distribution coefficient of silica in the presence of peat was significantly higher than in the absence of peat. There is thus a transition of dissolved silica to solid silica initiated by the presence of peat. The obtained results indicate a concave relation between dissolved and solid silica, i.e. an increasing distribution coefficient with increasing dissolved concentrations. In other words attachment was synergetic. Figure A shows a second order dependency of removed silica on the dissolved concentration of the component silica. This observation illustrates the synergetic effect of C_i on the attachment of silica to peat as discussed previously.

The relation between distribution coefficient and the initial concentration of the components in the injection fluid was linear, as displayed in Figure 4.9 C. The final solid concentration of silica was up to 7 times the final dissolved concentration, at C_i of 1250 ppm SiO_2 / ppm L200. The *efficiency of silica attachment to peat solids can be increased with elevation of the SiO_2 load in the pore fluid;* as determined at a biopolymer dosage of 100%.

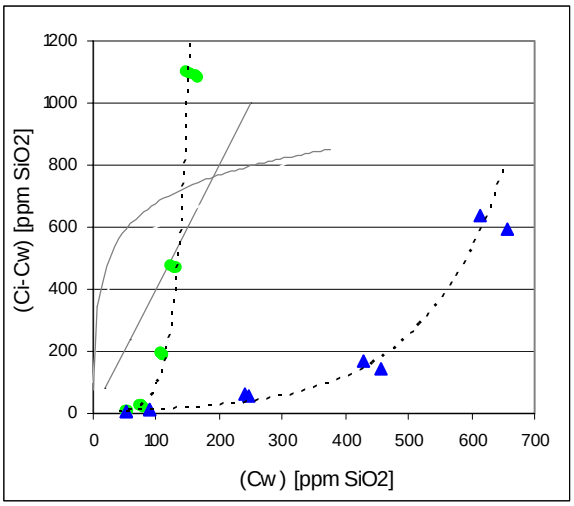

A. Relation dissolved and solid concentration for silica in presence of biopolymer Celquat L200, and in the presence and absence of peat.

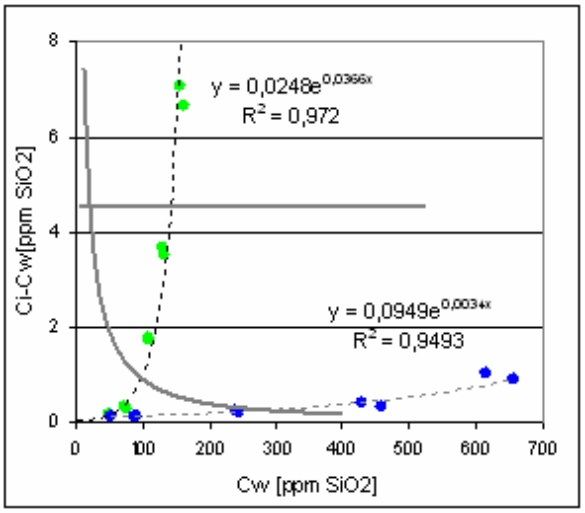

B. Distribution coefficient of silica in relation to dissolved concentration in the presence of the biopolymer and in the presence and absence of peat.

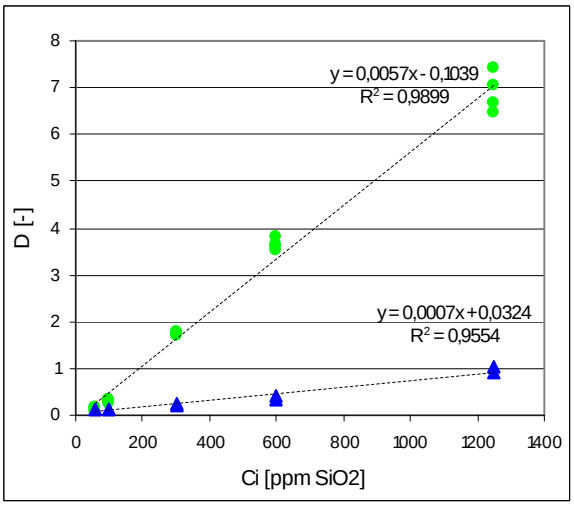

C. Distribution coefficient of silica in relation to initial added concentration of the silica-biopolymer dispersion. in the presence and absence of peat.

Legend. Experiment composition:

- *L200;Silica – Peat; after 113 hours of induction*
- *L200; Silica – No Peat; after 113 hours of induction*

The concentration of dissolved silica removed from solution in the presence of peat after 113 hours of incubation was assumed to represent attachment.

The symbol C_w represents the measured concentration of dissolved silica after 113 hours of induction. The symbol $C_i - C_w$ represents the removed concentration of silica from solution after 113 hours of incubation. The symbol D represents the distribution coefficient. D is the ratio between solid and dissolved concentration after 113 hours of incubation. i.e. the slope of the line presented in Figure (A). The symbol C_i represents the initial added concentration of the dispersion. This is the composition at t_0, containing an equal amount of biopolymer and silica by weight.

To clarity the type of relation between C_w and $C_i - C_w$ a standard linear and standard convex relation are illustrated in Figure (A) next to the measured relation.

Figure 4.9: Distribution coefficient as measure for attachment efficiency in terms of silica, as SiO_2

Distribution coefficient evaluated in terms of biopolymer as L200

The distribution coefficient of the biopolymer Celquat L200 in the presence of peat was significantly higher than in the absence of peat. Moreover, the distribution coefficient was larger than 1. A transition of dissolved to solid biopolymer was thus initiated by the presence of peat. The distribution coefficient was however not a linear function of C_i. Instead, the observed trend suggests a convex relation between dissolved and solid concentration. i.e. a decreasing distribution coefficient with increasing dissolved concentration. However, if one plots the distribution coefficient against the dissolved concentration as presented in Figure 4.10 B. a different image emerges. Figure 4.10 C confirmed the steep linear dependency of the distribution coefficient on the initial concentration – R^2 is 0.71 - in the range of C_i 60 to 600 ppm silicate-biopolymer dispersion. In the range C_w of 28 to 47 ppm L200 the solid concentration increases from 32 to 553 ppm L200. The dissolved concentration L200 was almost not effected by an increase of initial concentration. This suggests that there was a threshold, a maximum concentration of L200 to be present in solution, in the range of C_i 60 to 600 ppm L200.

At an initial concentration of 1250 ppm L200/ ppm SiO_2, the distribution coefficient was only 3 (indicated by the red circle) as opposed to 12 to 13 at an initial concentration of 600 ppm L200/ ppm SiO_2. The biopolymer seems to attach far less efficient to peat at this relative high initial concentration. The observed non-stoichiometric attachment as previously discussed in section 4.2.5 could also be derived from the difference in distribution coefficient of silica and of the biopolymer. The biopolymer attaches 3 to 4 times as efficient to peat as silica does in a C_i range of 60 to 600 ppm L200/ ppm SiO_2. The slope of the relation in terms of biopolymer in the presence of peat, as presented in Figure 4.10 C, was 3.6 times the slope of the relation in terms of silica as presented in Figure 4.9 C.

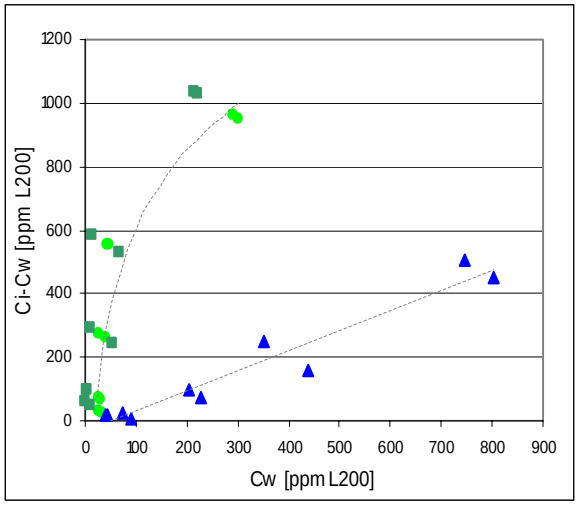

A. Relation dissolved and solid concentration for biopolymer Celquat L200 in presence of silica. and presence and absence of peat.

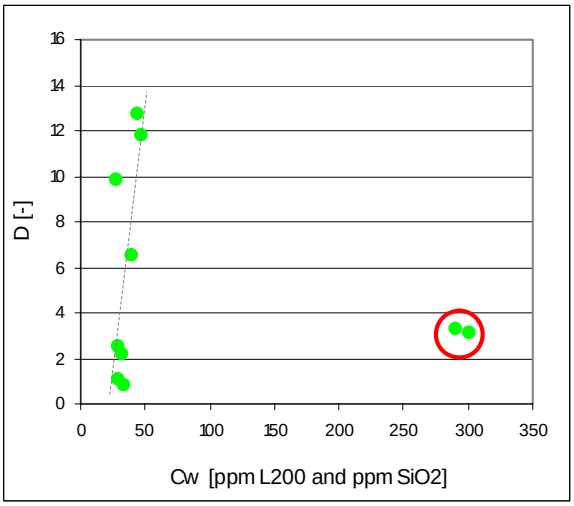

B. Distribution coefficient of biopolymer Celquat L200 in relation to dissolved concentration in the presence of silica and peat.

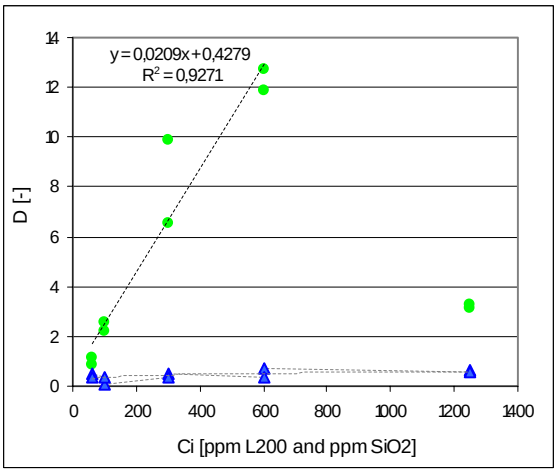

C. Distribution coefficient of biopolymer Celquat L200 in relation to initial added concentration of the silica-biopolymer dispersion. in the presence and absence of silica.

The concentration of dissolved biopolymer removed from solution in the presence of peat after 113 hours of incubation was assumed to represent attachment. The symbol C_w represents the measured concentration of dissolved biopolymer after 113 hours of induction. The value was corrected for the presence of peat. The symbol $C_i - C_w$ represents the removed concentration of biopolymer from solution after 113 hours of induction. The symbol D represents the distribution coefficient. D is the ratio between solid and dissolved concentration after 113 hours of incubation. i.e. the slope of the line presented in Figure (A). The symbol C_i represents the initial added concentration of the dispersion. This is the composition at t_0, containing an equal amount of biopolymer and silica by weight. To be complete the results of biopolymer attachment to peat in the absence of silica, as presented in section 4.2.3 were also included in Figure A.

Legend. experiment composition:

- *L200;Silica – Peat; after 113 hours of induction*
- *L200 – Peat; after 113 hours of incubation*
- *L200;Silica –No Peat; after 113 hours of incubation*

Figure 4.10: Distribution coefficient as measure for attachment efficiency in terms of biopolymer. as ppm L200

4.3 Discussion

In present section three findings of the presented attachment tests are discussed in more detail. These findings only concern the attachment of silica or biopolymer to peat solids, at biopolymer dosage of 100%. First of all, the attachment of silica and biopolymer to peat solids was non stoichiometric. The biopolymer is depleted from solution in favor of silica in the presence of peat. Secondly, the initial concentration of the injection fluid at 100% biopolymer dosage had a synergetic effect on the attachment of silica to peat solids. That is, with increasing initial concentration of the injection fluid the removal of silica and biopolymer increases. Thirdly, the degree of non-stiochiometric and synergetic attachment relate to the initial concentration of the injection fluid. Below the consequence of each finding is discussed and given in bold. In addition, the relevance of kinetics is discussed and the need this in future studies.

Possible consequences of non-Stoichiometry attachment

Non-stoichiometric removal from solution in the presence of peat indicates that silica and biopolymer are not only removed as complex from solution but also as individual components. This might imply that some of the biopolymer is released from the complex as in the aqueous phase and adsorbs individually to peat. Elaborating, if the biopolymer is depleted from the pore fluid due to preferred adhesion to peat solids, than this naturally alters the ratio of dissolved i.e. active biopolymer and dissolved plus dispersed colloidal silica in the pore fluid. The consequence of this shift could be among other options precipitation of silica. The effect of the biopolymer to retard polymerization of silica and to stabilize dispersed colloidal silica could vanish. Demadis et al (2009) proposes that extraction of dissolved biopolymer from solution could result in the re-release of silica with subsequent super saturation and precipitation, and/ or aggregation of colloidal silica as the result (Demadis. 2009). Dissolved silica concentrations then reduce to circa 100 ppm SiO_2 depending on pH and temperature. That is, the solubility limit of amorphous silica.

The consequence of preferred biopolymer adhesion to peat solids could be among other options, an alternation of surface properties of peat solids. The surface of a peat fibre could become more positively charged by sorption of the cationic biopolymer. Thereby the surface becomes more susceptible to adhesion of silica. The attachment of silica is then the result of a surface driven reaction. It is proposed that attachment of silica would have a minor impact on the pore volume available for transport if is the case. The concentration of silica occurs then at the surface of peat solids and not in the pore voids. Alternation of the surface properties of an organic template by sorption of a cationic biopolymer is described in more detail by Cumming et al. (2010), Cooper (1985) and Ayub (1987). The adhesion of silica to an altered surface, by cationic biopolymer, is discussed in more detail by (Perry, 1992). From the consequences listed above, the question raises whether the preferred removal of the biopolymer leads to silica polymerization in the pore space and not at the peat fibres. All depends however on the degree peat surface properties are altered, on the kinetics of each reaction step, and the exchange between the static double layer surrounding the peat fibre and the dynamic pore fluid. This needs to be investigated in further research.

Possible consequences of synergetic attachment

The more silica and biopolymer is added the more is removed from solution and per definition attaches to peat solids. The attainment of more and more coverage of peat solids with silica and biopolymer entities does not result into reduced attachment efficiency. The attachment of silica through the formation of multiple layers of silica and biopolymer at fibre surface is not excluded by the performed research. The following might be a consequence of synergetic attachment to consider. If the first attachment of biopolymer and silica entities to peat solid surface overcomes a threshold, and the ‘new’ surface properties are even more suitable for attachment of silica and/or biopolymer than the first attachment will initiate an accumulation of silica and biopolymer at the surface. This accumulation could potentially result in a thick layer covering the surface and clogging a pore throat, eventually reducing the effective pore volume of the soil.

The relation between properties of injection fluid and attachment

Based on the research results it is proposed that the the distribution of silica and biopolymer between solid and dissolved state in the presence of peat solids is determined by the properties of the injection fluid. This is explained as follows. The injection fluid as will be injected in a peat column resembles most likely the properties of a silica-biopolymer suspension several minutes to hours after pH adjustment from >12 to 7.5. As concluded based on present research and the retardation tests (Chapter 3) changes in dissolved silica concentration and occurrence of colloidal silica occurs mainly in the first hour after pH adjustment. Thereby it is proposed that the attachment of silica to peat solids depends on the properties of the injection fluid; and the properties of the injection fluid are set by the initial concentration of silica and biopolymer, and the time between pH adjustment and contact to peat solids. This is explained in more detail Figure 4.11.

Relevance of kinetics and the need for further studies

The rate of silica attachment to peat solids was not a subject of research in present study. However, the rate of attachment would provide an insight on the transport distances of silica that could be obtained in a peat layer. The experiments performed were not designed to answer this research question, despite its relevance. It is recommended to concentrate on the rate of attachment of silica both in the presence as in the absence of a biopolymer in future research. Measurements immediately after addition of peat should then be performed and more points in time should be obtained. Furthermore, SEM images of the fibres subject to attachment are recommended in future studies.

Component	Phase	Indication of Size	Retardation	Transport
Reactive silica (monomer – silicic acid)	Dissolved (aq)	Small molecule	no interaction with organic surface expected	Conservative transport – velocity of water – dispersion
Biopolymer	Dissolved (aq)	Small polymer (138 kDa)	Sorption to organic surface	Retardation: delay of breakthrough in case of linear sorption; delay and self sharpening of front in case of convex sorption
Biopolymer-silica complex	Dissolved (aq)	Complex > silicic acid (aq) and biopolymer (aq)	Attachment to organic surface	Lower velocities due to increased size. Delay of breakthrough due to interaction with organic surface.
Silica colloidal particle	Solid (s)	Depending on time and initial concentration, < 1um	No interaction with organic surface expected, beside providing a nucleation point for precipitation	Immediate precipitation in supersaturated conditions, facilitating no transport. In case of under saturation: advective transport and dissolution
Silica colloidal particle associated with biopolymer	Solid (s)	Depending on time and initial concentration, < 1um	Attachment to organic surface	Slow transport velocities due to relatively large particle size and interaction of with organic surface.

Figure 4.12: Illustration of assumed relation between initial concentration, fluid properties and interaction to peat solids.

4.4 Conclusions

The batch experiments to investigate the attachment of silica to peat solids in the presence of the biopolymer Celquat L200 have led tot the following conclusions:

Sorption of the cationic biopolymer Celquat L200 to peat material in the presence and absence of silica.

Sorption of the biopolymer Celquat L200 to peat material in the range of 60 to 600 ppm L200 does not depend on initial concentration. 90 to 99% of the biopolymer initially added sorbs to peat solids. The sorption coefficient is 503 mg L200 per kg d.s. peat - R^2 of 0.7. At initial concentration of 1250 ppm L200 the biopolymer sorbs less efficient, 83% of the biopolymer initially added.

Attachment of the biopolymer Celquat L200 to peat material in the presence of silica does depend on the initial concentration. In the range of 60 to 300 ppm L200 the attachment of the biopolymer is less efficient in the presence of silica than in the absence of silica. At initial concentration of 600 or 1250 ppm L200 the biopolymer attaches as efficient to peat solids in the presence as in the absence of silica.

Removal of dissolved silica from solution in the presence of 100% biopolymer Celquat L200 dosage and upon addition of peat material.

At initial concentration of 600 ppm SiO_2 92 % of silica is removed from solution within 113 hours of contact with peat material. The removal of dissolved silica increases with increasing initial concentration of the injection fluid. This synergetic effect of the initial concentration is strong in the range of 100 to 600 ppm SiO_2 but diminishes at 1250 ppm SiO_2.

The relation between distribution coefficient of silica and initial concentration of injection fluid

In terms of maximizing the load of silica in the injection fluid, attachment of silica is at its optimum at an initial concentration of 1250 ppm SiO_2 and 1250 ppm L200, as determined in the range of 60 to 1250 ppm initial concentration. Based on this observation it would be worthwhile to investigate attachment of silica at initial concentrations exceeding 1250 ppm SiO_2 at 1 to 1 wt. ratio between biopolymer and silica. However, with increasing initial concentration the instability of the silica-biopolymer suspension decreases and the concentration of colloidal particles increases, which opposes transport; as is concluded in research part Chapter 3. In conclusion, preservation of pore volume at 600 ppm will be easier to achieve than at 1250 ppm. From this it follows that the optimal composition of the injection fluid, to enable attachment of silica to peat solids, is 600 ppm SiO_2 and 600 ppm biopolymer Celquat L200.

5 Infiltration Experiment

Van der Zon et al (2007) state that reactive agents for peat stabilization can be supplied by infiltration. The dissolved and dispersed colloidal silica attaches preferably to the peat fibers and creates a layer of silica that encapsulates the fibers, which leads to strengthening of the peat fibers by the amorphous silica and a limited reduction in hydraulic conductivity. These statements are based on three conditions:

1. The hydraulic conductivity of the peat material should be high enough to allow reasonable flow velocities with a limited pressure gradient. High flow velocities are required (at least $2*10^{-6}$ m/s) to obtain significant transport distance within limited time. High pressure gradients need to be avoided as they can cause cracks and instability of a peat layer. The horizontal hydraulic conductivity of peat can be a factor ten higher than its vertical conductivity, given the mostly horizontal orientation of fibers in a peat soil (Zwanenburg. 2005).
2. The mobile pore volume - i.e. the fraction of pores that conducts flow - should be large enough to allow sufficient stabilization of the bulk volume.
3. The reactive components (silica and biopolymer) need to precipitate at the interface of pore fluid and fiber surface or attach to the fiber surface. Precipitation directly in the pore space should be avoided to prevent clogging and maintain permeability.

To evaluate to what extent these conditions are met, several infiltration experiments have been performed and are described in this chapter. It must be stated that a standard peat soil does not exist, neither in chemical properties as in mechanical properties; as opposed to sandy soils or clay. Therefore, generalization of research results should be done with care.

Research Questions

The infiltration experiments should answer the following questions:

1. What is the (horizontal) hydraulic conductivity of untreated peat?
2. What is the mobile pore volume of untreated peat?
3. How to describe the transport (advection, Dispersion, reaction) of the reactive fluid through peat in comparison with a conservative tracer? The reactive fluid was the colloidal suspension of biopolymer Celquat L200 and sodium meta silicate. A salt solution as electrical conductive tracer was assumed to be conservative.
4. To what extent is the hydraulic conductivity or the peat affected by infiltration of the reactive fluid?

5.1 Experimental procedure

The selected peat material was subject to flow in order to answer the formulated research questions. To derive the horizontal hydraulic conductivity a constant hydraulic head was imposed to a peat column. The volume of fluid passing through the column was determined by registration of effluent weight in time. By analyses of effluent composition at specific time intervals, breakthrough curves of tracer infiltration and elution were constructed. Breakthrough curves allow evaluation of advective, dispersive and reactive transport of conservative and reactive tracers (Appelo and Postma, 2005). The experimental procedure involved several steps, namely:

1. Selection and preparation of peat columns.
2. Installation of peat column in laboratory set-up.
3. Consolidation of peat column and confirmation of steady state flow.
4. Experimental Testing:
    - Determination of hydraulic conductivity before treatment.
    - Determination of effective porosity through infiltration and elution, using a salt tracer.
    - Determination of hydraulic conductivity during infiltration of the salt tracer.
    - Evaluation transport reactive tracer: infiltration and flushing of reactive tracer.
    - Determination of hydraulic conductivity during infiltration of the reactive tracer.
5. Dissection and visual inspection of peat material.

Each step is briefly described in present section. The analytical methods used to perform the different composition analyses on the solid peat material are presented in Appendix 19 and on the effluent are presented in Appendix 5 and 14.

5.1.1 Selection and preparation of peat column

Peat material originated from two different locations in the Netherlands: Zegveld and Bellingwedde. In the western part of the Netherlands, close to Zegveld, three Begemann drillings and one large core were taken (ca. 30 cm ø). The selected location corresponds to the reported location in previous research performed by GeoDelft (Venmans, 1989). One drilling was classified according to NEN 5104. The classification is added in Appendix 17. The second location was located close to Bellingwedde in the north of the Netherlands. Large size peat cores (50 cm ø) were taken for a Deltares project (Koelewijn, 2008). Classification of a drilling from location Bellingwedde is added in Appendix 17.

Sample preparation and material characterization

Peat characteristics from location Bellingwedde and Zegveld can be found in table 5.1 and 5.2. The humification degree and botanic composition are based on reports of Hamer (2010) and Grognet (2011). Additionally, the bulk density, dry solid content, loss on ignition (LOI) and pore water pH were determined of every peat column retrieved.

The peat from Bellingwedde is a bog peat and was classified as detrital, reed-sedge peat with some residues of wood (Bos, 2010). The peat from Zegveld is a fen peat and was classified as detrital sedge peat with some residues of reed. Figure 5.1 shows an image of the material structure of the different peat (A: Zegveld, B: Bellingwedde).

A. Peat material from location Zegveld B. Peat material from location Bellingwedde

Figure 5.1: Structure peat material from location Bellingwedde and location Zegveld

From the core sampled from location Zegveld a 15 cm column was retrieved. Cutting residues and material collected 5 cm below and above the core was used for dry solid content and LOI analyses. Cubic blocks of 30 cm were cut from the large peat core as sampled from the location Bellingwedde. A block from the middle of the core was selected as source material for the infiltration columns. Six columns of 20 cm length were taken from this block. Four samples were used for the infiltration experiment. For dry solid and LOI analyses and backup storage the other two samples were cut in half, length wise. For backup storage the peat was collected in an airtight vessel, flushed with N_2 and stored at 4 ^{o}C.

The five peat columns were cut by pushing a sharp-edged sample tube (6.8 cm ø) in the larger cylindrical and cubic peat blocks. The column was pushed parallel to the orientation of the fibers to ensure a relatively high permeability. Some disturbance might occurred, though no raptures were observed. The sample method did impose some smearing at column walls. The columns were weighted and the dimensions were measured. See

Table 5.2 for an overview of initial column properties. After treatment, the set-up was disabled and the dimensions and weight of each column were measured again. See for Table 5.7 an overview of column dimensions and properties at closure of the test.

Table 5.1: Material properties columns

Column no.	Location	Botanic composition	Sample Depth	Dry solids	Loss on ignition	Von Post Humification degree	Soil pH
		[-]	[m – NAP]	wt. %	wt.% ds		[-]
1,2,4,5	Bellingwedde	Detrital, reed-sedge peat; minor wood remains	-5.26	15.0 ± 1.4	74 ± 6	H3 – H4	5.3
3	Zegveld	Detrital, sedge-reed- peat	-6.05	8.4	87.5	H5 – H6	6.2

Table 5.2: Initial peat column properties

	Location	Bellingwedde		Zegveld	Bellingwedde	
	Code	1	2	3	4	5
L_{t_0}	[cm]	10.22	18.31	6.42	18.96	9.88
A_{t_0}	[cm^2]	35.26	35.26	32.80	35.26	35.26
V_{t_0}	[cm^3]	360.23	645.64	210.58	588.17	348.16
$M_{wet\_t_0}$	[gram]	342.92	629.06	224.73	592.45	319.16
γ_{wet_t0}	[-]	0.952	0.974	1.067	1.007	0.917

5.1.2 Experimental set-up

Installation of column

Peat columns were installed in a set-up for permeability testing of soils. Figure 5.2 shows a schematic overview of the experimental set-up. Pictures of the experimental set-up are added in Appendix 18. Also the details on the materials used can be found in this Appendix. The set-up was placed in a climate room, controlled at 10 ^{o}C ± 1 ^{o}C. The method of sample installation was derived from NEN 5117 and CEN 17892-11:2004. Some modifications were necessary given the available test set-up. The operation of column installation consisted of the following steps:

- Saturation of tubes in the system, ensuring no air was present.
- Placement and saturation of the bottom plate.
- Placement of a saturated porous filter plate
- Location of specimen on saturated filter plate
- Enclosing column with latex membrane (proceeding described in section 4.1.9.2 CEN 17891-11:2004).
- Placement of O-rings at bottom plate to ensure latex membrane.
- Placement of the top plate. Before fixation of the O-rings at the top plate, some water was carefully let in to remove air between the wall of the sample and the membrane.
- Connection of the top plate to the system.
- Placement and filling of the cell. Check for leakages at the bottom and top of the cell was performed.

The hydraulic conductivity of the system, excluding the peat column but including porous disc and electrical conductivity (EC) flow through cell, was in the order of 10^{-2} to 10^{-3} m/s.

Constant Hydraulic Head

A vessel with overflow was used to impose a constant hydraulic head over the length of the column. To the vessel more water was fed than passed through the column. The elevated water vessel was in turn fed by a head difference from a vacuum container containing degassed tap water, located outside the climate room. In the case of salt tracer infiltration the elevated vessel was fed by a pump connected to a storage vessel placed in the climate room. It was made sure no air was introduced during pumping.

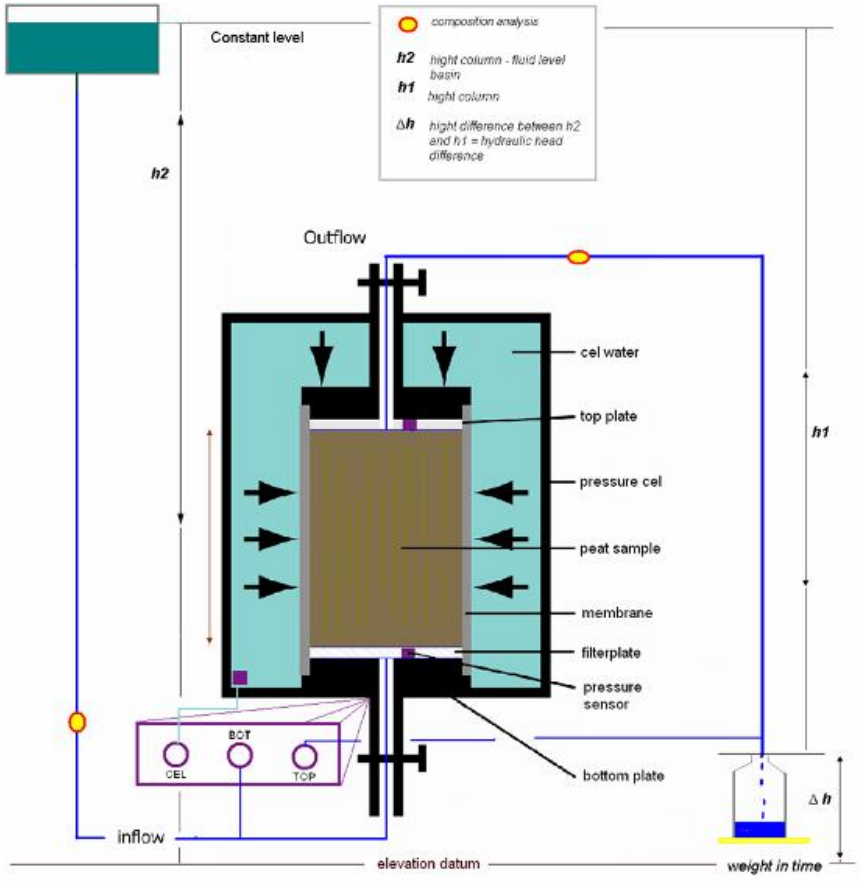

Figure 5.2: Schematic overview experimental set-up

The elevated vessel was replaced by a smaller elevated flask during infiltration of the reactive tracer fluids. The volume of fluid needed to obtain an overflow could thereby be reduced. To limit the intrusion of air and movement of the fluid, the flask was fed by a natural gradient from the moment the fluid dropped below a certain level. This set-up is presented in Appendix 18. Using a pump just enough air and movement was introduced into the system to foam the biopolymer and initiate flocculation. This was avoided applying a natural gradient instead of a pump.

Pressure gradient

In Figure 5.2 the location of the pressure sensors is indicated with the label CEL, BOT and TOP. A pressure drop of about two meters was imposed to the sample. The water head was limited by the height of the climate room. The water column was connected to the inlet of the column, i.e. the bottom. The imposed pressure at the inlet of the column was registered by the BOT sensor. The pressure at the outlet of the column, i.e. the top, was registered by the TOP sensor. The pressure at the outlet equaled atmospheric pressure in the case the tap was opened and effluent could drain freely. A confining pressure (CEL) was imposed *onto* the sample to prevent seepage along the wall of the specimen and the membrane. The radial pressure was controlled by a bladder and a pressure valve. The imposed relative pressures to each column are listed in Table 5.5.

The sensors were produced by SensorTechnics under product number RPO005D6A. Prior to installation of the peat column, the pressure sensors were calibrated and tared at atmospheric conditions. Scattering of the pressure readings was related to small fluctuations in the water column and 'background noise' fluctuations of the pressure sensors. This resulted into an inaccuracy of 5 kPa, which equaled ca. 20% of the applied bottom pressure. The sensors were connected to a data logger and values were recorded every 60 seconds. Additionally, the CELL pressure was continuously measured by means of a digital pressure device. This device was calibrated before use with a 0.01 bar accuracy. It was not possible to connect the device to the data logger and pressures were thus not recorded. Despite the calibration and resetting, the sensors were sometimes instable and showed an off-set. For this reason the sensor readings were only used as an indication for trends and moments of opening and closing taps.

The pressure drop over the length column was calculated based on the difference between the bottom pressure and the top pressure. The actual pore pressure at different column lengths was not registered. The radial cell pressure created an effective radial stress onto the column walls. This effective stress was the lowest at the entry point of the column (at the location where the pore pressure was the highest) and the highest at the outlet point of the column (at the top of the column). The minimum radial effective stress imposed to the bottom of the column was equal to the radial pressure minus the imposed bottom pore pressure (constant water head). The maximum radial effective stress imposed to the top of the column was thereby equal to the cell pressure if the top pressure equaled atmospheric pressure. The top of the column was therefore more compressed than the bottom of the column the moment the tap was opened. Upon closing of the tap the radial effective stress imposed at the top of the column reduced and swelling could take place.

Discharge of effluent (Q)

Fluid passed through the column and was collected at the outlet of the system. A bottle was placed on a digital balance (Mettler Toledo, calibrated before use), which was connected to the data logger. Every 60 seconds the weight was recorded. The opening of the bottle was partly covered in order to minimize water loss by evaporation.

In case of composition analyses of the effluent the outflow of the system was connected to an auto sampler. Thereby tubes of 15 ml were filled during a set time window. Collected effluent samples were analyzed for dissolved organic carbon content, as measure for biopolymer concentration, and or pH and dissolved silica content. The analytical methods are described in more detail in Appendix 5, 14 and 19.

The electrical conductivity was measured with in-line electrode sensor (Consort SK10T epoxy conductivity electrode including automatic temperature control), which was connected to a data logger (Consort C864). Readings were made every 60 seconds. The electrode flow-through cell was placed in between the outflow tube directly at the cell and the sample point at the outflow. The composition analyses at the conductivity cell and at the outlet were corrected for the volume difference, see Table 5.3. The total volume of the system – 93 to 98 ml - did not include the tube connecting the elevated vessel to the system-taps. If a reactive fluid was connected to the system instead of tap water, this tube was flushed before start of the experiment.

Table 5.3: Volume properties of the system

		1	2	3	4	5
Volume system total	[cm^3]	92.97	94.54	94.54	94.54	97.55
Volume tubes before column	[cm^3]	39.22	39.22	39.22	39.22	39.22
Volume tubes after column	[cm^3]	53.75	55.33	55.33	55.33	63.83
Volume tubes after EC cell	[cm^3]	15.21	15.21	21.12	15.21	39.11

5.1.3 Consolidation Phase

Consolidation of the specimen was performed in accordance with NEN 5117 and CEN 17892-11:2004, with some adjustments. Consolidation was performed at a confining pressure of 9.8 kPa. No bottom pressure was applied. The expelled water was weighed. Upon opening of the tap two events were observed. First, the membrane closed around the specimen. Second, the peat material started to consolidate. After installation there was an overpressure in the pores of the column, due to careful rising of tap water to remove entrapped air. This was first released by opening the tap. Water was expelled rapidly during membrane enclosure and slowly during the actual consolidation phase. The radial effective stress during consolidation phase was 9.8 kPa over the whole length of the column.

Given the characteristics of peat material primary consolidation stops, but secondary consolidation continues infinitely in time; a process referred to as creep. In the standard NEN 5117 the end of the consolidation phase is defined as the moment when the discharge becomes less than or equal to 2 mg effluent per hour. The total pore volume expelled during consolidation (V_{w_consol}) of the peat column was calculated by subtracting the volume expelled during membrane enclosure from the total effluent volume collected from the moment the tap was opened (Table 5.4). In principle, column dimensions after consolidation could be calculated based on V_{w_consol} and assuming isotropic consolidation; and used to calculate the hydraulic conductivity. This was however not the approach chosen, given continuous creep of peat material and an additional consolidation step as is explained in 5.1.2.

Table 5.4: Volume of water expelled during consolidation phase (excluding closure of membrane)

		1	2	3	4	5
Vw_consol	[cm^3]	17.2	79.9	0.88	43.7	14.0

Table 5.5: Properties of experimental set-up: imposed relative pressures

Relative pressures:			measured	derived	measured	assumption	calculation	calculation
Column	Phase	fluid	hydraulic head	back pressure	radial pressure	top pressure	pressure gradient (BOT-TOP)t0	Min. effective pressure
No.	[-]	[-]	[m]	[kPa]	[kPa]	[kPa]	[kPa]	[kPa]
1	Consol	-	-	n/a	9.81	n/a	n/a	9.81
	K_{hor}	tapw	2.524	24.76	25.9	0	24.76	1.14
	Tracer	salt	2.531	24.83	25.9	0	24.83	1.07
2	Consol	-	-	n/a	9.81	0	n/a	9.81
	K_{hor}	tapw	2.485	24.38	25.8	0	24.38	1.42
	K_{hor}	tapw	2.487	24.40	25.9	0	24.40	1.50
	Tracer	salt	2.487	24.40	25.9	0	24.40	1.50
3	Consol	-	-	n/a	9.81	0	n/a	9.81
	K_{hor}	tapw	2.17	21.30	25.21	0	21.30	3.91
	Tracer in	salt	2.12	20.84	25.21	0	20.84	4.37
	Tracer out	salt	2.09	20.47	25.21	0	20.47	4.74
	Tracer in	L200	1.75	17.20	25.21	0	17.20	8.01
	Tracer out	L200	2.07	20.27	25.21	0	20.27	4.94
4	Consol	-	-	n/a	9.81	0	n/a	9.81
	K_{hor}	tapw	2.489	24.42	25.9	0	24.42	1.48
	K_{hor}	tapw	2.489	24.42	25.9	0	24.42	1.48
	Tracer	SiO_2	1.881	18.45	25.9	0	18.45	7.45
	Tracer	SiO_2 L200	1.742	17.09	25.9	0	17.09	8.81
5	Consol	-	-	n/a	9.81	0	n/a	9.81
	K_{hor}	tapw	2.497	24.50	25.9	0	24.50	1.40
	K_{hor}	tapw	2.489	24.42	25.9	0	24.42	1.48
	Tracer	SiO_2	1.843	18.08	25.9	0	18.08	7.82
	Tracer	SiO_2 L200	1.917	18.81	25.9	0	18.81	7.09

5.2 Tests performed

Three tests were performed in order to answer the research questions: a constant head test, an electrical conductive and silica tracer test and a reactive tracer test. All tests were performed at a constant head. Each test is briefly described in this section.

5.2.1 Constant Head Test – Horizontal Hydraulic Conductivity

To start the constant head test, the hydraulic head had to be applied to the system, without exceeding the pressure at which the peat material was consolidated i.e. 9.8 kPa. To do so, the bottom pressure was connected to a second bladder instead of the water column. Subsequently the radial and bottom pressure were increased in turns in steps of 5 kPa. The radial pressure was set at ca. 25 - 26 kPa. The bottom pressure was set at ca. 20 kPa. Thereafter the inlet of the column was again connected to the water column.

The bottom pressure as obtained at infiltration of salt or tap water was 24 kPa. The bottom pressure as obtained during infiltration of the reactive fluids was 17 kPa. The initial applied bottom and radial pressures and the calculated gradient in effective radial stress, are presented in Table 5.5.

The hydraulic conductivity was calculated assuming saturated conditions. The degassed water was allowed to pass trough the column for about two days, before starting the experimental test. Small quantities of gas and particles were removed from the column in this period. Gas was entrapped in the column by installation and is naturally present in a highly decomposable soil like peat. After two days of flushing it was still inevitable that gas was present in the column. However, the experimental set-up did not allow determination of the saturation degree. The validity of assuming saturation could therefore not be determined.

Opening and closing of the taps invoked an additional consolidation of the top layer of the column and in principle some swelling; as already mentioned in section 5.1.2. The moment the tap was opened the effective radial stress at the top of the column increased, exceeding the stress as occurred during the consolidation phase. The moment the tap was closed again the effective radial stress at the top decreased and became equal to stress at the bottom of the column. An accurate determination of the volume expelled by this additional process of consolidation was not performed. The hydraulic conductivity was calculated based on: the measured discharge, the derived hydraulic head, and column length and area as measured after dissection.

5.2.2 Electrical Conductive and Silica Tracer Test - Mobile Pore Volume

Injection and elution of a non-reactive tracer through a soil column provides insight in advective and dispersive transport. A solution of sodium chloride and a saturated solution of silica were infiltrated and eluted from peat columns. The sodium chloride solution and the saturated silica solution were assumed to be non-reactive and hence conservative tracers. The salt and silica solutions were considered electrical conductive tracers. In other words, it was assumed that tracer concentration directly and linear related to the electrical conductivity (EC) of the pore fluid, and thus of the effluent (see section 2.5.1).

A sodium chloride solution was infiltrated in two peat columns in order to determine the pore volume available for advective transport. This fraction of the pore volume is referred to as the mobile pore volume. Injection of the sodium chloride solution started after a constant and relatively low electrical conductivity in the effluent was observed; in the order of 0.2 to 0.5 mS/cm.

The experiments were not modeled and parameters like dispersion coefficient could therefore not be derived. Nevertheless, from the general picture of a breakthrough curve some information of the system could be derived, among which the mobile pore volume.

To obtain a breakthrough curve the relative concentration of the tracer, in present case the EC, was plotted against the effluent volume collected. The tracer concentration was scaled from 0 to 1 by dividing the concentration measured at the outlet by the conductivity measured at the input, in accordance with Equation 8. The concentration at the injection point is indicated by C_0. The symbol C indicates the concentration at the outlet of the column.

$$\frac{C}{C_o} = \frac{C_{outlet} - C_{background}}{C_{inlet} - C_{background}} \qquad \text{Equation 8}$$

From the effluent volume at midpoint breakthrough ($V_{e\_C/C0=0.5}$) of the non-reactive tracers, the mobile pore volume (V_{pv_mobile}) could be derived. If the tracer was conservative V_{pv_mobile} corresponds to the effluent volume at the moment $\frac{C}{C_o}$ was equal to 0.5.

The measured dry solids content and bulk volume after closure of the experiment, result into a water volume at tend (V_{w_tend}). It was assumed that the moisture content of a column equaled the total pore volume of that column. The contributions of intergranular moisture to the total moisture content, and the contribution of gas to the total pore volume of a peat column, were thereby neglected (section 2.5.1). From the difference in V_{w_tend} and V_{pv_mobile} the immobile pore volume ($V_{pv\_immobile}$) was calculated. The mobile pore fraction equaled the ratio between V_{pv_mobile} and V_{w_tend}. Likewise, the immobile pore fraction equaled the ratio between $V_{pv\_immobile}$ and V_{w_tend}.

The volume of effluent expelled was normalized to the volume of water present at conclusion of the experiment, in order to express breakthrough in number of pore volumes replaced (Equation 9). In this way, different breakthrough curves from different columns could be compared. Additionally, the elution curves were manipulated to evaluate any deviation between infiltration and elution of a tracer.

$$(V_{effluent} - V_{tubes}) / (V_{w\_tend} - V_{tubes}) \qquad \text{Equation 9}$$

Wherein:

$V_{effluent}$: The volume of effluent expelled

V_{tubes}: The volume of tubes in the system as presented in Table 5.3.

The volume at first appearance of the tracer (V_arrival) was also derived from the EC breakthrough curve. V_arrival was defined as the effluent volume at the moment $C_{outlet} > 110\% \cdot C_{background}$. The V_arrival provides insight in the degree of preferential flow.

5.2.3 Reactive Tracer Test – Transport of Reactive Components (L200 and Silica)

In principle, the Reactive Tracer Test was performed in the same way as the Conservative Tracer Test with some adjustments. In order to determine the concentration of silicate and biopolymer, effluent samples were collected in time by means of an auto sampler. The volume of the collected sample depended on the hydraulic conductivity of a column. The discharge was based on the cumulative weight of all sample tubes collected. This approach was less accurate than using a continuously recording balance. However, it gave an indication of the impact of reactive fluid on the intrinsic permeability.

The attachment and detachment of silica and surfactant was evaluated based on the volume of first appearance and the shape of the breakthrough curve at infiltration and elution of the reactive tracer. The curve was obtained by plotting the relative concentration of the component to the effluent volume or to the normalized effluent volume (Equation 7). The relative concentration (C/C_o) of the biopolymer was determined based on dissolved organic carbon (DOC) values (C/C_o = DOC of effluent/DOC of influent) of the effluent. The relative concentration of dissolved silica was determined based on ICP-element analyses of the influent and effluent samples.

In general

Note that the location of tracer concentration measurement was not at the top of the specimen (x=L) but in between the top of the sample and the TOP pressure sensor. Porous disc, head and bottom grid plates and tubes induce some dispersion. The bulk electrical conductivity as measured in-line thereby includes dispersion imposed by this part of the system. It was assumed that this dispersion was insignificant to the dispersion induced by the porous matrix of a peat column.

In order to compare effluent concentrations of silica in time to electrical conductivity variations in time, the effluent volume discharged at time t_x is corrected for the tube volume separating location of EC measurement from outflow sampling. The induced dispersion by transport over this distance was thereby considered to be of minor influence compared to the impact of porous matrix of a peat column.

5.2.4 Treatment Schedule

Five different experiments are performed, namely:

1. Injection and elution of salt solution 0.09 M NaCl.
2. Injection and elution of salt solution 0.07 M NaCl.
3. Injection and elution of biopolymer salt solution 1962 ppm.
4. Injection and elution of saturated silica solution of 217.5 ppm SiO2, followed by injection and flush of a reactive fluid: a supersaturated silica dispersion of 1247 ppm SiO2 at biopolymer dosage of 100%.
5. Injection and elution of saturated silica solution of 199.5 ppm SiO2, followed by injection and elution of a reactive fluid: a supersaturated silica dispersion of 705 ppm SiO2 at a biopolymer dosage of 100%.

The numbers in the summation above, refer also to the label of each column. Column 1 and 2 were in principle duplicate experiments apart from a small difference in sodium chloride concentration at the inlet, and column length. Likewise, the infiltration experiment through column 4 and 5 was in principle a duplicate experiment, apart from a small difference in silica concentration at the inlet and column length. The length of column 2 and 4 were similar and results of electrical conductive tracer tests of these columns were compared. The length of column 1 and column 5 was also similar and circa twice the length of column 2 and 4. To column 2 and 4 is occasionally referred to as ‘short columns’. To column 1 and 5 is occasionally referred as ‘long columns’.

It was decided to use sodium chloride for the salt solution, as both chloride and sodium function as counter ions for the cationic charge of the biopolymer and the meta silicate, respectively. The saturated solution of silica contained a concentration of sodium equal to 7 mM and a concentration of chloride equal to 17 mM. Adjustment of pH to ca. 7.5 by adding 0.1M and 1M concentrated HCl solution caused the chloride concentration to be higher than the sodium concentration. The electrical conductivity of the silica solution was circa one order of magnitude lower than the electrical conductivity of the salt solution. The exact properties of the tracer fluids are presented in Table 5.6.

The saturated silica solution was considered non-reactive. Silicic acid is in principle not an active exchanger or sorbent as it bears a neutral charge under the given conditions. Based on the results of Chapter 3 it was assumed that only dissolved silica and no colloid silica was present in the tracer fluid.

As reactive tracer a mixture of silica and biopolymer was used as infiltration fluid. The fluids contained a dissolved fraction of both the biopolymer and silica and a colloidal fraction as was discussed in Chapter 2 and 3. Viscosity of fluids was assumed to be equal to water. This assumption was however not entirely correct for the reactive fluids, though of minor impact on the hydraulic conductivity relative to the process of clogging.

Table 5.6: Properties of the injection fluids

		Salt solution	Salt solution	Biopolymer solution + salt	Silica solution	Silica + Biopolymer	Silica solution	Silica + biopolymer
component	Unit	1	2	3	4	4	5	5
SiO_2	[ppm]	0	0	0	217.5	1247.4	199.5	705.4
L200	[ppm]	0	0	1962	0	1247.2	0	7004.7
Na^+	[mmol/l]	86	67	81	7	43	7	23.6
Cl^-	[mmol/l]	86	67	81	17	11	17	25.3
EC	[mS/cm]	9.32	7.33	8.2	0.702	5.82	0.689	3.25
pH	[-]	7.52	7.48	7.35	7.53	7.81	7.46	7.69
density	[gr/ml]	1.003	1.002	1.005	1.001	1.040	1.001	1.003

5.2.5 Dissection of the columns

After treatment the set-up was disabled and the dimensions and weight of each column and porous disc were measured. An overview of column properties at conclusion of the experiment is presented in Table 5.7. The radius of each column as measured at different column lengths is presented in Table 5.8. Thereafter, each specimen was divided into sub samples for composition analyses. Samples at various column lengths of ca. 50 ml were analyzed for dry solids content and silicon content. The structure and elemental composition of relatively small samples, ca. 1 ml, was evaluated by SEM imaging and EDAX analyses. A description of the imaging method SEM and the element analyses method EDAX can be found in Appendix 14.1

Table 5.7: Column properties at closure of the experiment

		1	2	3	4	5
V_tend	[cm^3]	320.29	591.18	213.86	571.90	307.00
A_tend*	[cm^2]	32.30	33.05	32.85	32.13	32.21
L_tend	[cm]	9.92	17.89	6.51	17.8	9.53
V_water_tend	[cm^3]	283.1	509.5	182.7	463.9	259.2
M_wet_tend	[gr]	333.3	595.21	227.28	558.29	303.5
ds_tend	[%wt.]	15.06	14.4	19.6	16.9	14.6
γ _wet_tend	[gr/cm^3]	1.041	1.007	1.063	0.976	0.989

* A_tend was calculated on radius measurements over the length of the column. The area as presented in the table is derived from the relation between length and radius is presented in Table 5.8.

Table 5.8: Column radius as a function of column length at conclusion of the experiment.

column 1		column 2		column 3		column 4		column 5	
L	A	L	A	L	A	L	A	L	A
[% of L_end]	[cm^2]	[% of L_end]	[cm^2]	[% of L_end]	[cm^2]	[% of L_end]	[cm^2]	[% of L_end]	[cm^2]
98%	32,8	100%	33,3	100%	33,2	91%	28,3	100%	32,8
77%	32,2	89%	33,3	75%	33,1	82%	31,2	75%	32,2
73%	31,2	79%	33,4	51%	33,4	71%	31,2	51%	31,2
68%	32,4	68%	33,4	37%	32,6	60%	31,8	37%	32,4
51%	32,3	56%	31,8	17%	32,2	49%	31,8	17%	32,3
0%	33,6	44%	31,8	0%	33,1	37%	32,1	0%	33,6
		32%	32,9			26%	33,0		
		21%	32,9			15%	33,0		
		10%	34,2			0%	35,0		
		0%	34,2						

5.3 Results

In the first paragraph a description of the horizontal hydraulic conductivity is given. The effect of salt, silica and reactive tracer solutions on the horizontal hydraulic conductivity was evaluated in the first section. Thereafter the results with respect to the mobile pore volume are presented and the method for mobile pore volume determination is evaluated. In the third and last section infiltration of the reactive components, silica and biopolymer, through a peat column is described.

5.3.1 Horizontal Hydraulic Conductivity

The measured discharge and the calculated horizontal hydraulic conductivities as observed before treatment are presented in

Table 5.9 and in Table 5.10.

The horizontal hydraulic conductivity of peat retrieved from the location Bellingwedde was $1.3 \cdot 10^{-7}$ m/s ± 34%. This value was calculated based on the measured discharge in column 1, 2, 4 and 5 before treatment. The horizontal hydraulic conductivity as calculated for column 1 deviated was lower than the values obtained for column 2, 4 and 5; explaining the observed deviation. The horizontal hydraulic conductivity of peat retrieved from location Zegveld was $8.0*10^{-7}$ m/s, as determined before treatment. The latter was derived from discharge measurements in only one column, namely number 3. The degree in which the hydraulic conductivity was representative for peat retrieved from Zegveld could therefore not be determined. Nevertheless, the results indicated that peat from Zegveld was more conductive to flow as peat from Bellingwedde.

The horizontal hydraulic conductivities measured for peat retrieved from both Bellingwedde as Zegveld was lower than expected. A hydraulic conductivity of $8*10^{-7}$ and $1*10^{-7}$ m/s was relatively low, given the condition that transport distances of more than one meter should be reached within one week. At the moment of laboratory testing no alternative peat types were available. It was chosen to use the selected peat types for non-reactive and reactive transport testing despite the relatively low hydraulic conductivities.

A gradual decrease in discharge was observed with every step of the experimental program, except for column 1. This increase in resistance to flow was related to a decrease in pore volume. Over the course of the experiment pore volume was lost upon consolidation and creep. An additional volume loss, besides consolation and creep was confirmed by column radius measurements at the start and at conclusion of the test. From Table 5.8 it becomes clear that the shape of the column was altered over the course of the experiment from a cylinder to a more hourglass shape. Opening and closing of the taps invoked an additional consolidation of the top layer of the column.

Figure 5.3 was included to show the variation in discharge with effluent volume from the moment the taps were opened – the pressure gradient was applied - to the moment the taps were closed. Initially, a sharp decline in discharge was observed followed by a more gradual decline and stabilization. Similar trends were observed for column 2 to 5. Accurate determination of the volume expelled by this additional process of consolidation was not performed. Therefore, the hydraulic conductivity and total pore volume as derived from the moisture content were calculated based on column length and area as measured after dissection.

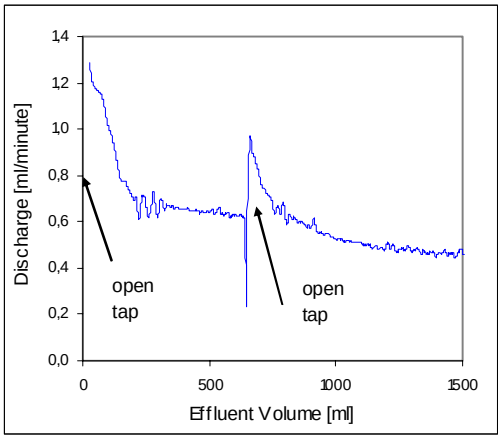

Figure 5.3: Discharge before treatment in terms of effluent volume. Opening and closing of the tap changes the effective radial stress over the length of the column, and especially at the top of the column. The moment the tap was opened the effective radial stress at the top of the column increased, exceeding the stress as existed during the consolidation phase. As a result pore volume at the top of the column decreased and effluent was expelled rapidly. The moment the tap was closed again the effective radial stress at the top decreased and became equal to stress at the bottom of the column. Now some swelling at the top of the column occurred and pore volumes again increased. The volume change at the top of the column due to this cycle of consolidation and swelling, became smaller the more often the taps were opened and closed. Compare the peak in discharge at zero effluent volume to the peak at ca. 650 ml effluent.

The discharge as presented in

Table 5.9 and Table 5.10 and the hydraulic head as derived from the measured water column, were used for hydraulic conductivity calculation. Stabilization of discharge was not reached in the columns within the period prior to tracer injection. A decline in discharge of 0.02 ml per minute with 1 liter of effluent was observed in column 1 and 2. A decline in discharge of 0.04 and 0.06 ml per minute with 1 liter of effluent was observed in column 4 and 5, respectively. A decline in discharge of 0.34 with 1 liter of effluent was observed in column 3.

Salt Tracer 0.07 and 0.09M NaCl

The measured discharge and the calculated horizontal hydraulic conductivity as observed during infiltration and elution of the salt tracer are presented in

Table 5.9 and in Table 5.10. The discharge during infiltration and elution of the salt tracer dropped to 0.30 ± 0.03 gram per minute in column 1 and 2. This was 73% ± 7% of the discharge as observed before injection of the tracer solution. In column 3 the discharge during infiltration and elution of the salt tracer dropped to 4.47 gram per minute. This was 85% of the discharge before injection of the tracer solution. During elution of the salt tracer the discharge declined. However, the observed decrease in discharge was in the same range as the observed decrease before injection of the tracer (as described in previous paragraph). Decline of discharge could be related to a decrease in pore volume and or be caused by the salt tracer. Clearly, the injection of the salt solution did not resolve into clogging of the peat column. Therefore, it is proposed that the salt tracer solution had no severe impact on the discharge and thus on the hydraulic conductivity of the peat.

Table 5.9: Discharge and hydraulic conductivity of peat column 1 and 2

parameter	phase	unit	1	2
Discharge	Before	[ml/min]	0,35	0,49
Discharge	During injection salt	[ml/min]	0,47	0,47
Discharge	During flush salt	[ml/min]	0,28	0,32
Hydraulic conductivity	Before	[m/s]	7,2E-08	1,8E-07
Hydraulic conductivity	During injection salt	[m/s]	9,4E-08	1,7E-07
Hydraulic conductivity	During flush salt	[m/s]	5,7E-08	1,2E-07

Silica Tracer 199.5 and 217.5 ppm SiO_2

The measured discharge and the calculated horizontal hydraulic conductivity as observed during infiltration and elution of the silica tracer are presented in Table 5.10. During injection of the saturated silica solution a decline of discharge was observed. The discharge dropped to 0.31 ± 0.08 gram per minute during infiltration and flushing of silica tracer in column 4 and 5. This was 60% ± 5% of the observed discharge before injection of the silica tracer solution. However, this decline was restricted to 0.02 to 0.04 ml per minute with 1 liter of effluent volume. Again the decline in discharge could be related to both pore volume reductions as interaction of the silica tracer with peat surface. Clearly the injection and elution of the saturated silica solutions in the peat columns did not result into clogging. Therefore, it is proposed that the saturated silica solution had no severe impact on the discharge and thus on the hydraulic conductivity of the peat.

Table 5.10: Discharge and hydraulic conductivity as observed in peat column 3, 4 and 5

parameter	phase	unit	3	4	5
Discharge	Before	[ml/min]	5,27	0,35	0,72
Discharge	During injection non-reactive	[ml/min]	4,81	0,28	0,41
Discharge	During flush non-reactive	[ml/min]	4,47	0,23	0,39
Discharge	During injection reactive	[ml/min]	4,11	0,0067	0,0036
Discharge	During flush reactive	[ml/min]	3,65	-	-
Hydraulic conductivity	Before	[m/s]	8,0E-07	1,3E-07	1,4E-07
Hydraulic conductivity	During injection non-reactive	[m/s]	7,5E-07	1,4E-07	1,1E-07
Hydraulic conductivity	During flush non-reactive	[m/s]	7,1E-07	1,1E-07	1,0E-07
Hydraulic conductivity	During injection reactive	[m/s]	7,7E-07	3,5E-09	1,0E-09
Hydraulic conductivity	During flush reactive	[m/s]	5,8E-07	-	-

Reactive Tracers

The measured discharge and the calculated horizontal hydraulic conductivity during infiltration of the reactive tracer are presented in Table 5.10. In column 3 the reactive tracer composed of a biopolymer solution with an elevated ionic strength. In column 4 and 5 the reactive tracer was composed of a colloidal fraction and a dissolved fraction of silica and biopolymer.

Upon infiltration of the biopolymer salt suspension the hydraulic conductivity of column 3 did not decrease or increase out of the range as determined before treatment. Upon elution of the biopolymer salt suspension with tap water the hydraulic conductivity showed a significant decrease from $7.7*10^{-7}$ to $5.8*10^{-7}$ m/s. Infiltration of tap water was still possible and complete clogging of the peat column was not observed; as opposed to infiltration of silica-biopolymer suspension in column 4 and 5.

Infiltration of silica biopolymer suspension in column 4 and 5 resulted into clogging of the peat porous matrix. Upon injection of the colloidal fluid, the discharge immediately declined to almost zero milliliter per minute. The hydraulic conductivity of the peat material declined two orders of magnitude from 10^{-7} to 10^{-9} m/s. This was observed at both 705 ppm and at 1247 ppm SiO_2 and biopolymer L200 concentrations. The decline was observed within 43 to 72 ml intrusion of the reactive fluid. The immediate decline in discharge is presented in more detail in Figure 5.4. To clearly show the impact of the reactive tracer on the discharge, both values measured during salt infiltration and during reactive fluid infiltration are shown. Figure 5.4 A and B show the increase of effluent volume in time. Figure 5.4 C and D were derived from figure A and B, and show the decrease in discharge in terms of effluent volume.

In column 5 (Figure 5.4 B and D) ca. 88 ml was expelled before the discharge started to decline. The discharge dropped to almost zero after 115 ml was expelled. Correction of system volumes returned an infiltrated volume of ca. 72 ml before the discharge started to decline. In column 4 (Figure 5.4 A and C) ca. 58 ml was expelled before the discharge started to decline. The discharge dropped to almost zero after 100 ml was expelled. Correction of system volumes returned a volume of 43 ml infiltrated after which the discharge started to decline.

Thus, the discharge started to decline shortly after reactive fluid and peat made contact. This observation suggests a chemical reaction instead of solely a filtration process causing the pores to clog. Given the volume flushed before decline of discharge, the intrusion depth of silica in a peat column could be estimated. In column 4 the estimated intrusion depth of silica was ca. 2.3 cm. In column 5 the estimated intrusion depth was ca. 7.3 cm.

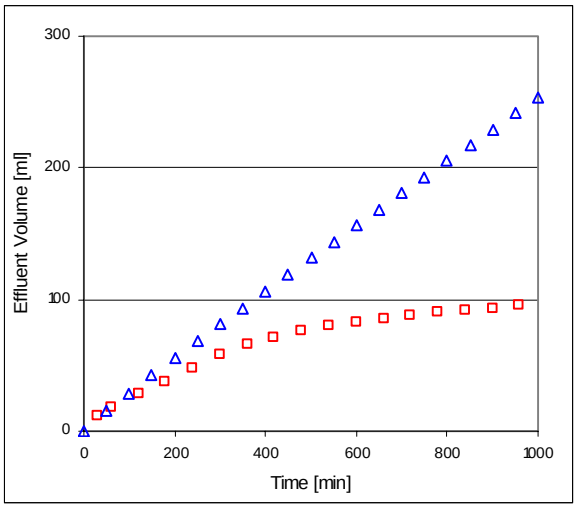

A. Decline of effluent volume expelled per time unit from the long columns. At infiltration of reactive fluid the discharge declines.

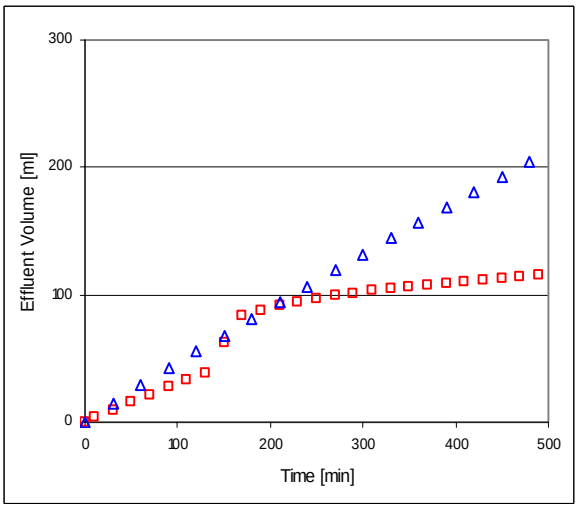

B. Decline of effluent volume expelled per time unit in the short columns. At infiltration of reactive fluid the discharge declines. The short increase is related to closing and reopen of the tap.

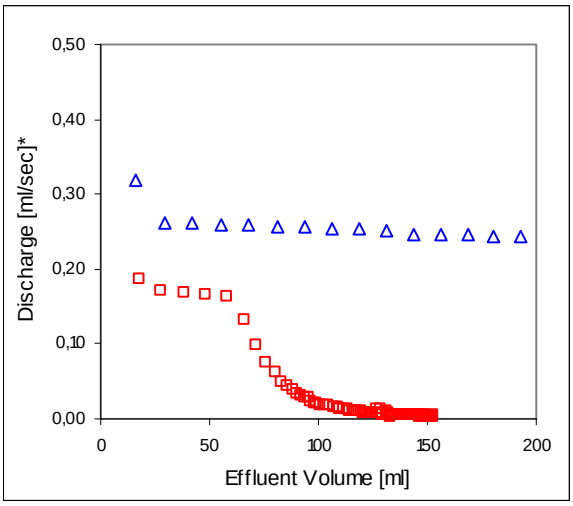

C: Decline of discharge* in the relatively long columns.

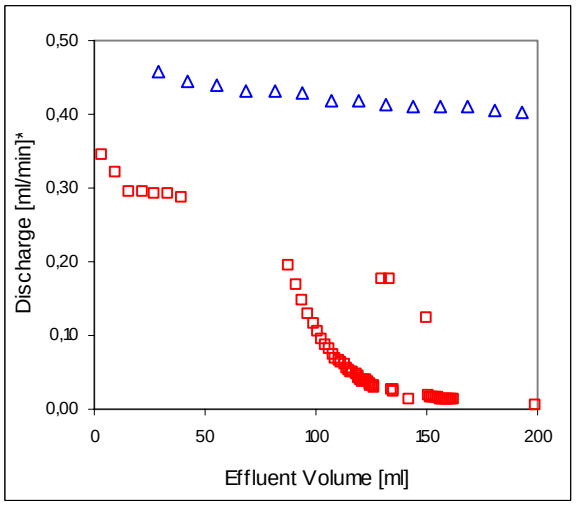

D: Decline of discharge* in the relatively long columns. Two points between 45 and 85 ml effluent were not displayed on the graph. The discharge measured was ca. 1.2 ml/min.

Legend long columns:

- Injection of reactive tracer: 1247 ppm SiO_2. ppm L200
- Flush of saturated silica solution: 217.5 ppm SiO_2

Legend short columns:

- Injection of reactive tracer: 705 ppm SiO_2. ppm L200
- Flush of saturated silica solution: 199.5 ppm SiO_2

* Discharge as measured per time interval. i.e. as measured per sample tube.

Figure 5.4: Immediate decline of discharge upon contact between reactive tracer and peat column.

5.3.2 Electrical Conductive and Silica Tracer Test – Mobile Pore Volume

The breakthrough curves of infiltration and elution from column 2 and column 4 (the long columns) are presented in Figure 5.5 A and B, respectively. The normalized electrical conductivity of the tracer was plotted on the y-axis against pore volumes replaced on the x-axis. Note that the relative breakthrough of both salt as silica tracer was based on EC measurements in the effluent.

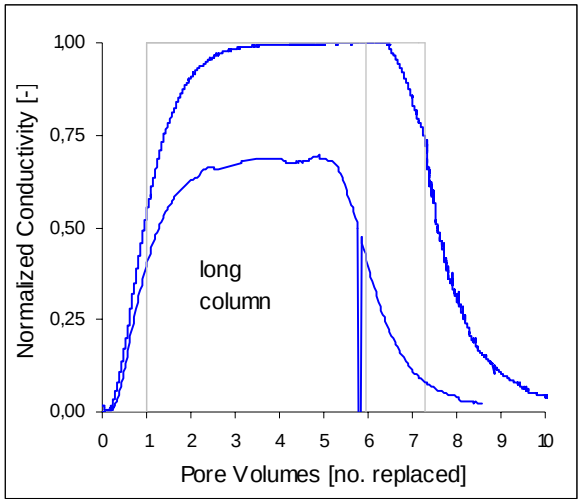

A. Breakthrough curve of salt or silica tracer from the long columns in terms of normalized electrical conductivity. The curve that does not reach C/Co=1 represents the silica tracer. The solid gray line represents plug flow.

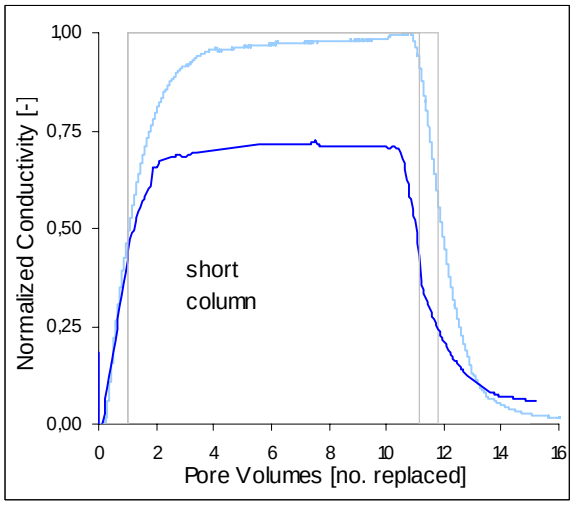

B. Breakthrough curve of salt or silica tracer from the short columns in terms of normalized electrical conductivity. The curve that does not reach C/Co=1 represents the silica tracer. The solid gray line represents plug flow.

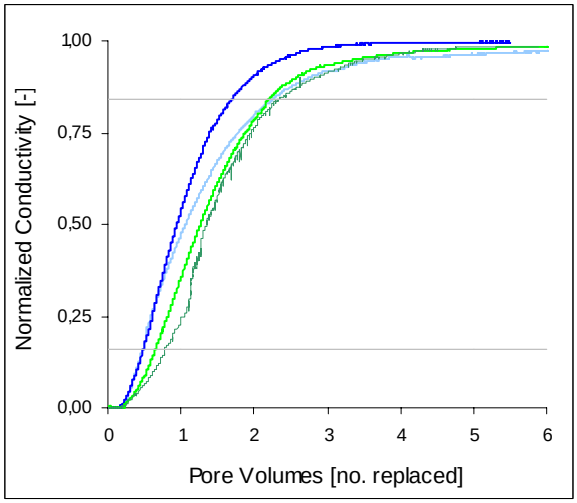

C. Symmetry of the breakthrough curves injecting salt solutions in short and long columns.
Normalized infiltration and elution curves of the salt tracer in terms of electrical conductivity are depicted. The dark blue line represents infiltration of the salt tracer in the long column and the dark green line represents elution of the salt tracer. The light blue line and the bright green line represent infiltration and elution of the silica tracer, respectively.
The solid gray lines indicate 68% around midpoint breakthrough. One line is depicted at C/Co = 0.84 and one line at C/Co = 0.16.

Figure 5.5: Breakthrough curves of salt and silica tracers through peat

It was proposed that the pore volume available for advective transport could be derived from midpoint breakthrough ($V_{e\_C/C0=0.5}$), as described in section 5.2.2. This approach to determine mobile pore volume is only valid if tracer transport is conservative, i.e. can assumed to be non-reactive to peat solids and solutes. The results in Figure 5.5 indicate that sodium chloride as electrical conductive tracer was not conservative, at least not at relatively low initial conductivity. A normalized conductivity of only 0.69 ± 3% was reached within the period of tracer infiltration. Moreover, the normalized conductivity stabilized at that value, i.e. a plateau was observed.

The reactivity of the assumed conservative tracer becomes clear if one compares the breakthrough curve of low electrical conductivity solution (0.702 mS/cm) to the relatively high electrical conductivity solution (7.33 mS/cm) as depicted in Figure 5.5 A and B. At electrical conductivity of 7.33 and 9.32 mS/cm, the plateau C/Co=1 was reached. These results indicate that the interaction between the tracer fluid and peat solids and solutes, affected the bulk electrical conductivity. The relation between the concentration of sodium and chloride in the pore fluid and effluent did thereby not correspond any longer to the electrical properties of the pore fluid and effluent. These effects seemed to be masked when using relatively high concentrated salt solutions of ca. 0.1 M NaCl. At high salt concentrations the reaction between peat and pore fluid, and the impact of these reactive processes on the electrical conductivity of the pore fluid was insignificant when evaluating the presence of a plateau and the normalized conductivity observed at the plateau.

However the impact of these reactive processes on the accuracy of the breakthrough curve of ca. 0.1 M salt tracer - how it reflects on first appearance and the slope of the breakthrough curve - was unclear. Breakthrough of electrical conductive tracers did not only reflect transport (advective and dispersive) but also reaction processes. From this it follows, that it was not correct to derive the mobile pore fraction from the obtained breakthrough curves.

Figure 5.5 C depicts the symmetry of infiltration and elution breakthrough curves. Three aspects were observed at infiltration and at elution of the highly concentrated salt tracer from the short column (no. 1) and the long column (no.2). First of all, at infiltration and elution of the tracer 0.17 to 0.21 and 0.23 to 0.22 pore volumes were replaced, respectively, until first appearance of the tracer. In relation to plug flow, the first appearance indicated an early arrival of the tracer. Early arrival of a conservative tracer can be caused, besides the effect of dispersion, by the presence of preferential flow paths. Secondly, tailing was observed both at infiltration and elution of the tracer solutions. The slopes at 0.84 C/Co were lower than at C/Co equaled 0.16. The breakthrough curves were therefore not symmetric. Thirdly, the shape of the breakthrough curve upon elution of the tracer was more dispersed and more tailing towards C/Co=1 was observed, than at infiltration of the tracer. The differences in curve shape – infiltration versus elution - suggest that the rate of release was lower than the rate of uptake of the tracer. This was especially observed in the long column, column number 2.

Column length had an impact on the shape of the breakthrough curve at both infiltration and elution of the salt tracer. At infiltration, breakthrough of the salt tracer was more dispersed on the short column (column 1) than in the long column (column 2). Upon elution, the breakthrough curves at long and short column length were more similar.

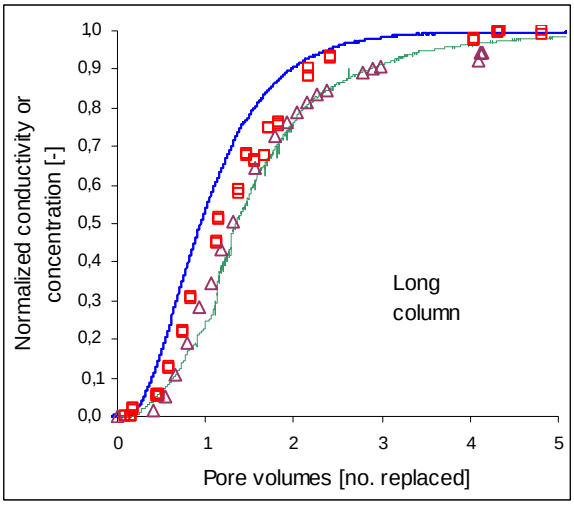

A. Injection and elution of silica and salt tracer from long columns. The red cubes indicate normalized silica concentration upon infiltration. The dark green triangles indicate normalized silica concentration upon elution. The blue and dark green line represents infiltration and elution of the salt tracer, respectively.

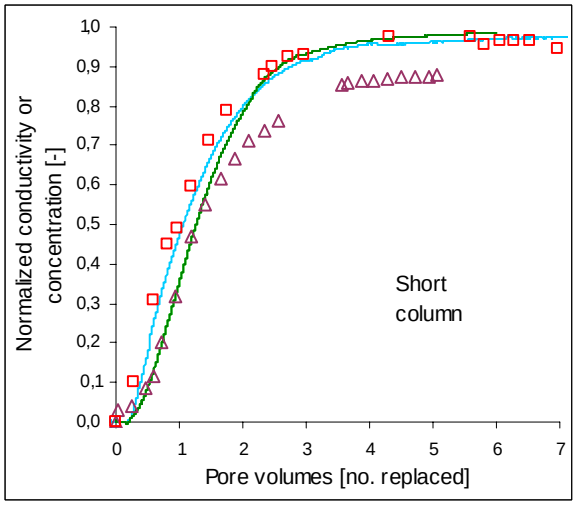

B. Injection and elution of silica and salt tracer from short columns. The red cubes indicate normalized silica concentration upon infiltration. The dark green triangles indicate normalized silica concentration upon elution. The blue and dark green line represents infiltration and elution of the salt tracer, respectively.

Figure.5.6: Breakthrough curves of infiltration and flushing of salt and silica tracers in and from peat columns

The relation between transport of silica (in terms of silica concentration) and transport of highly concentrated salt solution (in terms of EC), was evaluated based on Figure.5.6 A and B. Upon infiltration in the short columns, the first appearance of silica (column 5) was more or less equal to the first appearance of the electrical conductive tracer (column 1). Upon infiltration at the long columns, arrival of silica was delayed compared to the EC tracer. Upon elution of silica and EC tracer in the short columns, more tailing towards C/Co=1 was observed for silica than for EC. In the long columns, elution of silica solution matched breakthrough of salt very well. The curves match in first appearance, in shape and in the moment C/Co =1 was reached. Thus transport of silica through a peat column, injected as a saturated silica solution, was comparable to transport of a 0.07 to 0.09 M sodium chloride solution in terms of electrical conductivity.

5.3.3 Reactive Tracer Test – Transport of Reactive Components

Infiltration of reactive fluids in a peat column is presented in Figure 5.7 and Figure 5.8. The normalized concentration of biopolymer was derived from dissolved organic carbon concentrations.

Figure 5.7 displays the breakthrough curve of a 1962 ppm L200 biopolymer solution containing an additional amount of sodium chloride. The electrical conductivity of the fluid was thereby elevated from 0.7 mS/cm to 8.2 mS/cm**.** During elution of the biopolymer solution, the in-line EC measurement failed. For that reason, the EC during elution was only measured in the sample tubes as collected at the outlet. For comparison, electrical conductivities of the samples collected during infiltration of the biopolymer solution were also measured; though 3 days after collection and storage at 4^{o}C.

The electrical conductivity as measured in the sample tubes deviated from the in-line conductivity measurement. Infiltration of the biopolymer solution, in terms of in-line normalized electrical conductivity, showed that C/Co=1 was not reached within the period of infiltration.

The plateau was observed at a normalized conductivity of 0.90. The normalized conductivity as measured in the sample tubes stabilized at a value of 0.97. Stabilization of normalized electrical conductivity in the sample tubes was observed after ca. 2.17 pore volumes were replaced.

As opposed to normalized conductivity, the level C/Co=1 was not reached in terms of normalized organic carbon concentration during the period of infiltration. A normalized concentration of 0.40 was reached after ca. 2.71 pore volumes were replaced. The increase of normalized concentration per pore volume flushed, seemed to decline after one pore volume was replaced. During the period of infiltration, however, stabilization of normalized biopolymer concentration was not observed. That is, the biopolymer tracer was retarded relative to the electrical conductivity tracer. The fist appearance of the electrical conductivity and the biopolymer front was however similar.

Tailing was observed during elution of the tracer solution. Both the normalized biopolymer concentration as the electrical conductivity indicated tailing towards C/Co=0. However, the biopolymer solution showed less tailing than the electrical conductivity. An estimate of 49% biopolymer was recovered from the column. Note, that this percentage recovered was an inaccurate value given the method of analyses (DOC) and analyses of discrete samples. Nevertheless, the results suggest strong adsorption of biopolymer to peat solids and minor desorption of the biopolymer upon flushing the column with water, given the absence of a long tail towards C/Co=0 and the presence of a long tail towards C/Co=1.

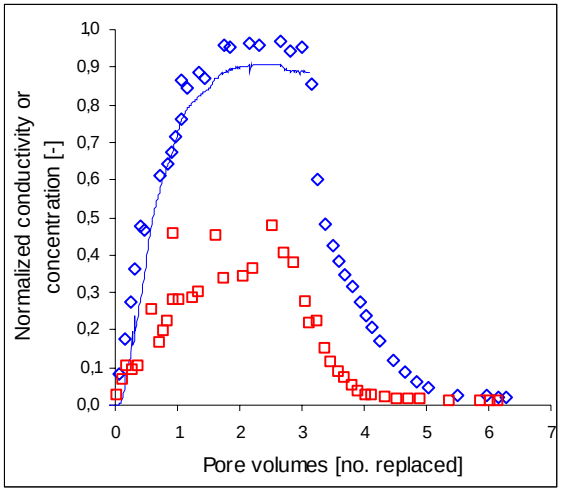

Figure 5.7: Breakthrough curve of infiltration and flushing of 1962 ppm L200 biopolymer reactive fluid with elevated electrical conductivity, through column 3. The electrical conductivity of the injected fluid was 8.2 mS/cm.

Injection of reactive tracer in terms of biopolymer Celquat L200 (mg C/l); measurement in sample tubes

Injection of reactive tracer in terms of EC; measurement in sample tubes

Infiltration reactive tracer solution in terms of EC; in-line measurement

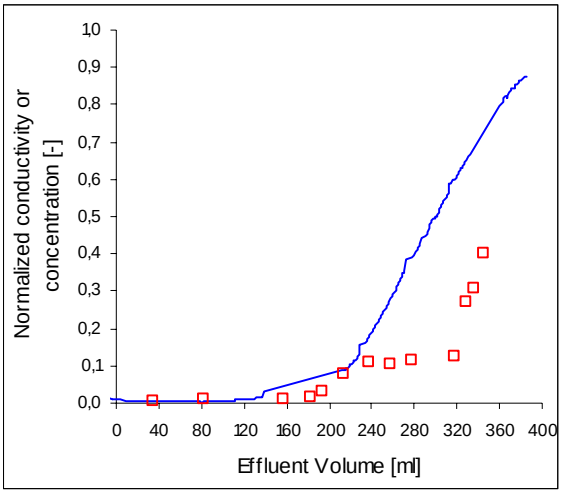

Figure 5.8: Collected data from infiltration of reactive tracer in column 5. The reactive fluid was composed of 705 ppm SiO_2 and 705 ppm biopolymer Celquat L200. Conductivity of the reactive fluid was 3.25 mS/cm.

At infiltration of a colloidal, reactive, solution of 1247 ppm SiO_2 and an equal amount of the biopolymer L200, it was not possible to collect enough effluent volume for composition analyzes (column 4). It was possible to collect enough effluent volume for composition analyzes at infiltration of colloidal reactive solution containing 705 ppm SiO_2 and equal amount of the biopolymer L200 (column 5). Clearly, infiltration of the colloidal reactive fluid resulted into clogging of the peat column; as already discussed in section 5.2.1. Therefore the breakthrough curve as displayed in Figure 5.8 is not given in terms of pore volumes replaced but in effluent volume collected.

An effluent volume of 385 ml was collected before conclusion of the infiltration test. The volume of effluent expelled at first appearance of the electrical conductivity tracer was ca. 136 ml. The first appearance of silica was observed after ca. 82 to 156 of effluent was expelled. Effluent volume expelled at first appearance of the conductive tracer was, in present case, distinctively more than observed during injection of the sodium chloride solution (column 1), as discussed in section 5.2.2. Decline of discharge was initiated before the first appearance of leading edge of either electrical conductivity or silica. Immediately upon contact between the reactive fluid and the peat material, the discharge reduced, as discussed in section 5.2.1.

The expelled volume of effluent at midpoint breakthrough of the electrical conductive tracer was 301 ml. Before conclusion of the test an elevation of normalized silica concentration was observed as well, though midpoint breakthrough was not reached. It was impossible to collect samples and construct breakthrough curves upon elution of the reactive fluids from column 4 and 5. Therefore retardation of silica could not be derived from elution of the reactive tracer solution.

5.3.4 Dissection and visual inspection of treated column material

After treatment, the set-up was disabled. The dimensions of each specimen were determined and each column was divided into sub samples for composition analyses. The final dimensions of each specimen are presented in Table 5.7 and Table 5.8. Any observations related to the final dimensions of the column are described in section 5.2.5.

Disabling the column a gel-like layer was observed between the porous disc and the peat material (Figure 5.9). Force was needed to separate the plate from the column. The plate was glued to the peat column by this layer.

The weight of the filter plate from column 4 and 5 was elevated, after correction for water content and organic material. The increase of mass was most likely related to precipitates of silica and sodium chloride within the pores and on top of the plate. Moreover, by sensory observation column 4 seemed to be dryer than column 2. In Appendix 20 several images of both columns are displayed. Final dry solid content and solid silicon concentrations are included in Table 5.11. As presented by Table 5.11 an increase of 4% to 3% in dry solid content was observed in the bottom of column 4 and column 5, relative to dry solid content measured at the top and middle of the column. The radial effective stress at the top of the column was the maximum imposed, as explained in 5.2.1. Therefore, it was expected that dry solid contents at the top of the column would be higher than at the bottom of the column in case no additional mass was added during treatment. In other words, the observed increase in mass could indicate the presence of a precipitate.

Figure 5.9: Dissection of column 4 and column 2. The figure on the right side shows filter plate of column 2 after stripping of the membrane. The figure on the left side shows the filter plate of column 4, after separation of column and filter plate. The filter plate was stuck to the peat column. By using force the filter plate could be separated from the column. A remainder of peat material was left on the filter. Between the filter and the peat material a transparent hard gel was observed.

Sample material was scraped from the filter plate. From this material and from locations at the middle and top of column 2, 4 and 5 SEM pictures were taken. Figure 5.10 displays SEM images of the material sampled from (A) untreated peat material, (B) material scraped from filter plate of column 5 and (C) at 2.5 cm column length of column 4. The rest of the SEM pictures are presented in Appendix 21.

Image (B) clearly displays the presence of a white gel like phase. The image visualizes the minor intrusion of the gel at the peat filter interface. It was confirmed by EDAX analyzes that the white gel was indeed a silicon based material. The smooth surface of the material and shrinking during visualization indicated a highly hydrated material. This, in combined with the strong connection between filter plate and peat column, suggest that the material was a highly hydrated form of solid silica, i.e. a hardened silica gel.

Moving away from the gel, penetrating into the peat material, the element silicon decreases and the elements sodium and chloride increase (image C and D). Image (D) displays the presence of small white cubes. EDAX analyses showed that the white cubes consist of the major elements Na, Cl and Si. See Appendix 21. for a presentation of the EDAX analyses performed.

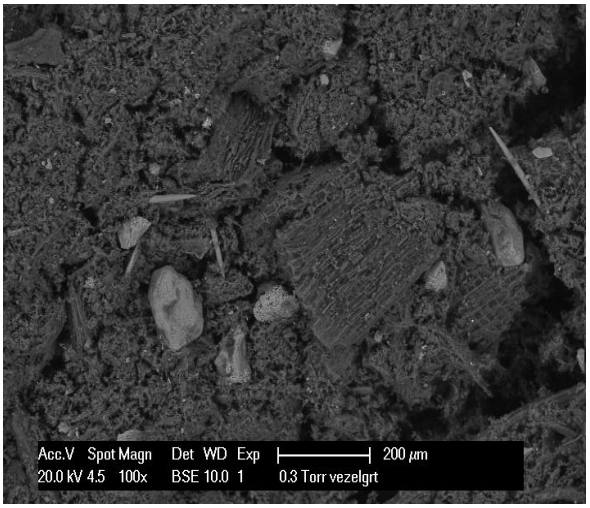

A. Untreated peat material at magnification of 100x.

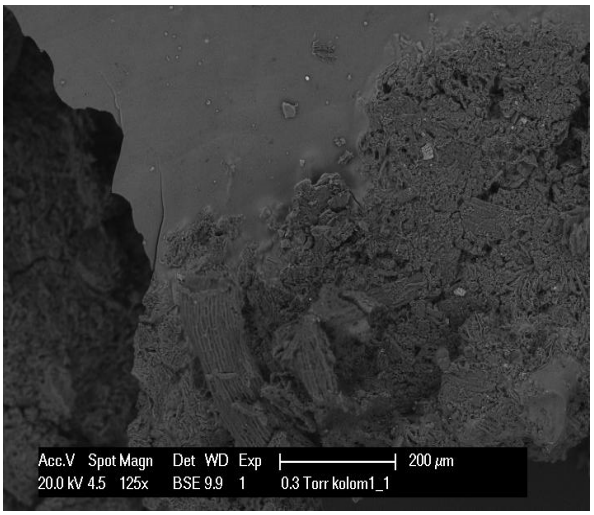

B. Scraped material from filter plate of column 5, at magnification of 125x.

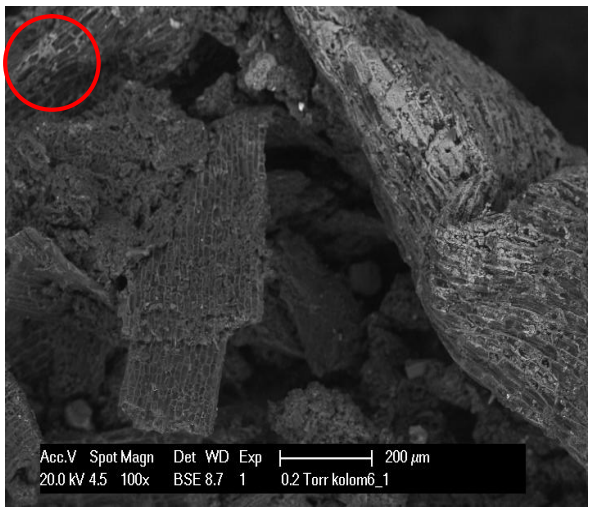

C. Material at 2.5 cm length of column 4, at magnification of 100x.

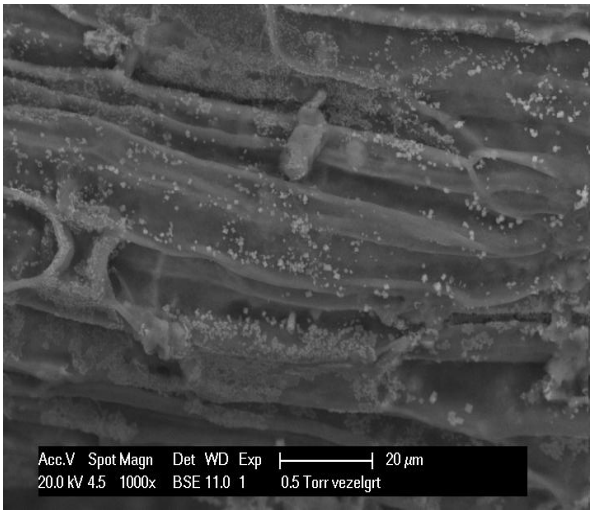

D. Zoom from image C at the red spot. Small white cubes were observed at a magnification of 1000x.

Figure 5.10: SEM images of treated and untreated peat material

Elevated concentrations of silicon at the bottom of column 4 and 5 were however not confirmed by composition analyses of peat solids. The solid silicon concentrations at increasing column length are presented in Table 5.11, with exception of column 3. The analyses were performed to create a mass balance and to obtain an impression of the silica intrusion depth. However, the results indicate that the silicon content of the Blanco columns (column 1 and 2) were in the same order of magnitude as the columns flushed with silica, i.e. column 4 and 5. The concentration of solid silicon in the centre of column 4 and 5 was slightly elevated, though not significantly higher than in the Blanco columns.

Table 5.11: dry solid content and silicon content in peat columns after treatment

Column	L	dry solids	Silicon content
[nr]	[cm]	[%]	[mg Si/kg d.s.]
1	5.38	15.6	1900
2	9.99	14.4	2100
4	16.15	16.9	1800
	14.58	16.8	2000
	12.49	16.3	2000
	10.59	16.7	1800
	2.52	17.6	1800
5	8.60	14.3	1800
	5.09	14.4	2300
	1.17	15.1	1600

5.4 Discussion

Below the important findings of the presented infiltration experiments are given in bold. The explanation of each finding is discussed.

Suitability of NaCl as conservative tracer in peat

Sodium chloride was used by as a conservative tracer but the transport of the ions might be retarded in the peat columns. Furthermore, electric conductivity as a sole method to detect the breakthrough of sodium and chloride is insufficient in peat. In addition, the mobile pore volume is a function of the flow conditions e.g. flow velocity of water through the column – irrespective of using electric conductivity or solute concentration as the method to detect sodium chloride breakthrough. These three propositions are discussed below.

Sodium chloride is not conservative

Chloride is an anion known for its low reactivity and therefore is assumed to be conservative in accordance with literature (Harvey et al. 1989; Appolo and Postma 2005). Sodium, on the other hand, is a cation more susceptible for reaction (Appolo and Postma 2005; Singha, 2011). Retardation of sodium chloride in peat can be caused by precipitation and sorption processes like for example ion exchange (described in section 2.5.1).

Electric conductivity as tracer is insufficient in peat

The total number of ions dissolved in the aqueous phase and their mobility determines the electric conductivity of a fluid (described by Kohlrausch law). Measuring the electrical conductivity of the effluent, the method is only sensitive to changes in the electrical properties of the fluid, not to changes in sodium or chloride concentration (Singha et al, 2011). Sorption or exchange of ions from solution to charged sites in the soil changes the composition of the pore fluid and could thereby alter its electrical properties (Leroy and Revil, 2004). Depending on the valence of the exchanged cation, the ionic strength and thus electrical conductivity of the pore fluid is altered. The electrical conductivity is for example altered if a bivalent calcium molecule (Ca^{2+}) at the solid surface is exchanged by monovalent sodium (Na^{+}). This example is likely to occur in a peat soil subject to sodium chloride infiltration; given the relatively high cation capacity of a peat soil and the high concentration of sodium in the pore fluid.

Peat is a soil type with a high content of organic material. Especially in soil types with a high capacity to exchange cations (CEC) and or anions (AEC), ion exchange has a significant impact on the composition of the pore fluid. Soil types with a high content in clay and or organic material have a relatively high CEC value in the order of 80 to 100 milliequivalents (meq) per 100 gram dry solids (Appelo and Postma, 2005; Sparks, 2003; Gonzales, 2009). Peat as retrieved from Bellingwedde had a CEC of 98 meq/ 100 gram dry solids (Hamer, 2011). For comparison sand only has a CEC value of 3 to 5 meq per 100 gram of solids (Sparks, 2003).

Likewise, the process of sodium complexation by dissolved organic molecules (DOC), alters the ionic strength of the pore fluid and hence the electrical conductivity of the effluent. The observed increase in dissolved organic carbons upon elution of the salt tracer could have had an impact on the electrical conductivity of the pore fluid, in two ways. First, the mobilized organic acids carry a net negative charge (Sparks, 2003). Secondly, these organic acids are capable to complexate cations like sodium present in the pore water; because of that negative charge (Appelo and Postma 2005). The overall electrical properties of the pore fluid are altered by this increase in DOC and subsequent complexation of dissolved cations. The linear relation between pore fluid electrical conductivity and concentration of chloride and sodium in the aqueous phase is not appropriate anymore.

In general, at low salt concentration the impact of reactive processes (e.g. ion exchange and complexation) on composition of the pore fluid is significant. Hence the relation between tracer concentration and electrical conductivity of pore fluid and effluent is not linear anymore. At high salt concentrations, in the order of several grams per liter, which is the case in present research, the effect of reactive processes is masked out (Singha, 2011). Nevertheless, the inaccuracy of tracer breakthrough increases by using electrical conductivity methods to trace a conductive fluid, instead of measuring the concentration of a dissolved tracer directly; especially in peat soils.

Mobile pore volume affected by flow conditions

The presence of less mobile and immobile zones can lead to an underestimation of the pore volume in tracer experiments. The tracer experiments were performed to determine the volume fraction of the bulk material which is available for transport and thus in principle accessible for silica attachment. Thereby, the mobile pore volume provides an insight in the efficiency of the stabilization method. However, the assumption that not 100% of the pore volume is available for advective transport implies the presence of mobile and immobile or less mobile zones.

In present research the occurrence of preferential flow was proposed given the early arrival of the leading edge of the electrical conductive tracers; at a specific discharge of ca. $2*10^{-6}$ m/s (Bellingwedde peat) and ca. $2*10^{-5}$ m/s (Zegveld peat). Blodau and Moore (2002) state that preferential flow in peat is insignificant at a specific discharge less than 3 mm per day, which equals ca. 10^{-8} m/s. At a specific discharge more than 10^{-8} m/s the flow is stated to be preferential. Furthermore, Blodau and Moore (2002) state that if preferential flow is significant there is disequilibrium between pore water flowing in the preferred pathways and pore water in the less mobile or non mobile zones. Thus, the retrieved pore water in present research was most likely in disequilibrium with the porous matrix of the peat. Disequilibrium is referred to as a physical non-equilibrium (Appelo and Postma, 2005), and can be explained as follows. The concentration gradient brought upon by flow in the mobile pores is in equilibrium or is not in equilibrium with the concentration within the less mobile and immobile zones. Attainment of full equilibrium by diffusion into the immobile zones is not always possible given the relation between advective flow velocity, diffusion coefficient and thickness of the less mobile region.

The electrical conductivity of the effluent is affected by both the composition of the pore fluid in the mobile as in the immobile zone. The degree in which the electrical conductivity of the effluent is affected by mass transfer between the mobile and immobile zone is dictated by the flux of mass over the interface of the zones and the duration of tracer injection (Haggerty, 2004; Singha, 2011). The mobile fraction (Φ_{mobile}) as derived from midpoint breakthrough is thereby not an intrinsic property of a peat column but depends also on the flow rate through the column.

Furthermore, in present research it was not possible to distinguish between the effect of physical non-equilibrium and reaction processes at the solid pore water interface, on the shape of the breakthrough curve. At physical non-equilibrium mass is ‘lost’ upon injection of the tracer due to migration into dead-end pores. Likewise, mass is ‘added’ upon elution of the salt tracer due to migration from dead-end pores. Physical non-equilibrium is therefore observed as tailing of the breakthrough curve. Given the probable retardation of sodium, it could not be concluded that tailing of the breakthrough curve – upon elution of the salt tracer – was caused solely by bleeding from dead-end pores.

In conclusion, a tracer experiment through a peat column asks for a different approach than commonly applied in soil tracer experiments, given the reactivity and heterogeneous structure of this soil type. Less tracer solutions are suitable to function as a conservative tracer in a peat column than, for example, in a sand column. Detection of ion concentration instead of electrical conductivity would be more appropriate for a peat column. Bromide or chloride ions are widely used tracers to study the transport of water in various soils. These components do not adsorb to any negatively charged surface sites and would therefore be useful as conservative tracers in peat. Several authors report the use of potassium bromide as a conservative tracer in peat soils (Gafni. 1986; Kettridge 2008). Bromide is reported to be more suitable than chloride given the low natural background concentration of bromide over chloride (Flury 1993). However, bromide is toxic to

humans and is therefore not preferred to work with in infiltration and flushing experiments (National Institute for Occupational Safety and Health, 1994; Flury, 1993). However, the effect of flow conditions on the obtained hydrological parameters still has to be considered using bromide or chloride concentration to detect breakthrough. Alternative methods to research soil hydrological properties are the use of heat as a tracer (Timothy, 1988; Langevin, 2010) or to determine a 3-D image by magnetic resonance imaging (MRI) (Rezanezhad, 2009).

Immediate decline of discharge upon injection of the reactive tracer

Upon injection of reactive colloidal suspension in peat some silica was transported through the column but the major part of silica injected precipitated at the entrance of the column. The silica observed in the effluent is the load of silica injected before extensive clogging was obtained of the pore volume at the inlet of the column. The phase transition of silica did not occur solely at the interface of the peat fiber but also in the pore voids of both filter plate and peat matrix.

The stability of the injection fluid in the absence of peat was tested over a period of about 5 days. However, the reactive tracer was injected in peat column for a period of 44 days. The retention time of the reactive fluid just before the inlet of the column (at the interface and in the filter plate) increased tremendously due to the reduced flow rates. The reactive fluid present at the inlet was likely to aggregate exceeding the period of 5 days. This process of dispersion instability also contributed to the formation of a solid silica gel at the interface of the filter plate and the peat column.

Consistency between batch and column experiments regarding retardation efficiency of biopolymer

The pore volume available for transport was dramatically reduced by infiltration of the colloidal silica biopolymer suspensions as indicated by the decline in hydraulic conductivity and the presence of hard silica gel several millimeters at the bottom of the column. More important, this effect was virtually instantaneous upon injection of the silica biopolymer suspensions. Based on these observations I propose that: I) the presence of the biopolymer does not result into a phase transition of silica solely located at the surface of peat solids; and II) the presence of the biopolymer does not result into a significant delay of the phase transition of silica. In other words, there is a mismatch between the results of the infiltration experiments (Chapter 5) and the attachment tests (Chapter 4).

In chapter 4 it was concluded that attachment of dissolved silica and biopolymer to peat solids occurred within a time window of 65 hours. However the degree in which the biopolymer delayed the process of attachment of silica, e.g. the rate of attachment, was not subject to research. As the results of the infiltration experiment indicates it should have been. In conclusion, the delay of the phase transition of silica upon injection in a peat column was only minor by the presence of the biopolymer Celquat L200. The delay was not substantial to initiate significant transport distances of silica.

If the reaction between silica, biopolymer and peat solids could be delayed than transport of silica through a peat layer could be a possibility. Another possibility is treatment of the peat soil with the biopolymer and subsequent infiltration of a saturated silica solution. The retardation of silica will be higher than observed in the absence of the biopolymer as tested in present research, given the interaction of biopolymer and silica observed in Chapter 3. However, the pore volume then needs to be replaced more than one time and this will require longer injection times.

5.5 Conclusions

From the experimental results the following conclusions can be drawn:

1. The peat soil collected at Beddingwedde has a horizontal hydraulic conductivity of $1*10^{-7}$ meter per seconds (after consolidation and assuming saturated conditions). The peat soil collected at Zegveld has a horizontal hydraulic conductivity of $8*10^{-7}$ meter per seconds (after consolidation and assuming saturated conditions).
2. The breakthrough curves of the salt tracer confirms that peat is a porous material with varying mobility: some pores conduct flow (mobile pore volume) and others contain stagnant water (immobile pore volume). Assuming that sodium chloride is a conservative tracer, the immobile pore volume and exchange flux between immobile and mobile zones can be estimated by transport modeling simulations. However these simulations were not performed within this thesis project due to time constraints.
3. An electrical conductive tracer, composed of sodium chloride, does not show conservative transport in a peat soil. Breakthrough curve of the silica tracer showed lower normalized electrical conductivity values than one. It is proposed that this was caused by sorption or exchange of the sodium ions at peat solids and or complexation of sodium at dissolved organic acids in the peat pore water.
4. Infiltration of the 0.07 and 0.09 M sodium chloride tracer - with an electrical conductivity one order of magnitude higher than the silica tracer - a normalized electrical conductivity of one was observed. The reactive process between tracer fluid components and peat solids is thus less significant at higher salt concentrations.
5. The transport of silica at ca. 200 ppm SiO_2 in the absence of the biopolymer through a peat soil is comparable to the transport of the 0.07 M sodium chloride tracer.
6. Encapsulation of peat fibers upon infiltration of the reactive fluid is not observed and the porosity of peat is not preserved. Infiltration of the reactive fluid resulted in immediate reduction of the hydraulic conductivity with two orders of magnitude from 10^{-7} to 10^{-9} m/s. A hard transparent gel was observed at the inlet on the interface between the filter plate and the peat. Penetration of the gel was in the order of millimeters.

6 Synergy and Future Research

Construction on peat soils has proven to be a challenging task to civil engineers as this soil type is highly compressible. Construction on soft soils like peat is frequently accompanied by high geotechnical risks and costs. There is the need for corrective and preventive applications of stabilization methods to obtain strengthening of a peat layer. In-situ stabilization of peat by infiltration of the reactants would preserve the water storage capacity of the soil layer; and thereby limit the impact of the construction on the local hydrological regime. Besides, bulk densities could be maintained close to the original density of peat, and oxidation potentials of the peat could be minimized by the treatment method. Thereby low maintenance constructions could be obtained, also on the longer term. In addition, application of an in-situ method has the advantage of a low burden to its surrounding and the possibility of use during treatment. It was therefore proposed to stabilize a peat soil by infiltration of reactants, e.g. infiltration of a colloidal suspension consisting of silica and a cationic biopolymer.

Solely based on present results in-situ stabilization of peat is not feasible, though the performed research is far from complete. Based on the research as presented, I recommend the following for future research towards a more feasible method:

- The rate of silica attachment to peat solids in the presence of the biopolymer should be the focus of any future research. Thereby more insight would be gained on the transport distances that are achievable. Transport of the reactants should be limited by the hydraulic conductivity of the peat, not by the reaction rate of silica attachment.
- As encapsulation of peat fibres is proposed to preserve porosity, the relation between the required silica load in the injection fluid and the obtained bulk strength by fibre encapsulation – as opposed to filling of the pore voids – should be subject to future research as well.
- The impact of fibre encapsulation on oxidation potential of peat should be subject to future research. Limited settlements due to fluctuating water tables could be an additional advantage of the method.

If significant transport distances of the reactants can be obtained in-situ stabilization of peat might be feasible. Thus, the in-situ method could be feasible – technically - if the attachment of silica is delayed. It should however be noted, that the intrinsic hydrologic properties of a peat soil complicates infiltration of reactants – irrespective of the properties of the reactants. Given the relatively low hydraulic conductivity of peat, the small pore volume that actually conducts flow and the heterogeneity of both aspects on small and bulk scale, the question arises if the method could be efficient and under which conditions. That is, efficient in the period of infiltration needed and the bulk strength obtained within this period.

In-situ stabilization would provide a solution for a niche of the construction-market on soft soils. The focus is at applications where time is not a constrain. Treatment could then be applied as long-term method (order of weeks to months?); with the advantage of preservation of water storage capacity of the peat layer, and low burden to the surroundings, as opposed to the common applied long term method of preloading.

The gained knowledge on chemical stabilization of peat using silicon as the major building block to create the hardened structure – is at this moment already applied in MIP admixture research and in the preparations for field experiment as performed by Deltares and Royal Haskoning.
In addition, I would like to make the following remark. The physical properties (i.e. mechanical and hydrological) and the chemical and botanic characteristics of peat are closely related. The chemical and botanical characteristics could provide an insight in the hydrological properties of a peat layer and its heterogeneity. Thereby, a better assessment could be made of in-situ stabilization or even MIP stabilization is the method of choice; or are at all efficient methods. This aspect should be acknowledged when aiming for optimization of the mechanical properties of peat – and therefore included in geotechnical research on behavior and stabilization of peat soils.

Bibliography

Ahnberg, H. and G. Holm (1999). *"Stabilization of some Swedish organic soils with different types of binder."* H. Bredenberg, G. Holm & B.B. Brons, B.B., eds., Dry mix methods for deep soil stabilization. Proceedings of the international conference on dry mix methods for deep soil stabilization: pp. 101-108.

Allaire, S. E., S. C. Gupta, et al. (2002*). "Role of macropore continuity and tortuosity on solute transport in soils: 2. Interactions with model assumptions for macropore description."* Journal of Contaminant Hydrology 58(34): 283-298.

Alterra, (2012), *Grondsoortenkaart*, in www.fruitbomen.net /Bodemkaart. Retrieved 10 februari,.2012.

Amjad, Z., J. F. Zibrida, et al. (1999). "*A new antifoulant for controlling silica fouling in Reverse Osmosis Systems*." UltraPure Water 16(2).

Anastas, P. T. and J. C. Warner (1998). *Green Chemistry. Theory and Practice.* New York, Oxford University Press.

Appelo, C. A. J. and D. Postma (2005). *Geochemistry, groundwater and pollution.* Amsterdam, the Netherlands

Archie, G. E. (1942*). "The electrical resistivity log as an aid in determining some reservoir characteristics."* Transactions of the American Institute of Mining, Metallurgical and Petroleum Engineers 146: 54-62.

Ayub, A. L., & Sheppard, H. D. (1987). "*The effect of surfactant and polymer addition to a fuel grade peat: Adsorption, Electrokinetics and Dewatering"*. Colloids and Surfaces, 26, 305-315.

Babean, J. and J. Sevc (1997). *"Calcium and Magnesium in systems with organic substances."* Acta Geologica Universitatis Comenianae 52.

Becker, M. W., P. W. Reimus, et al. (1999). *"Transport and Attenuation of Carboxylate-Modified Latex Microspheres in Fractured Rock Laboratory and Field Tracer Tests."* Ground Water 37(3): 387-395.

Bennett, D. M., Dixon, D. R., Eldridge, R. J., Le, N. P., & Rye, C. S. (2000). "*Determining the fate of flocculants by fluorescent tagging*." Paper presented at the Chemical Water and Wastewater Treatment VI, Proceedings of the Gothenburg Symposium 9th.

Bergna, H. E. and W. O. Roberts (2006). *Colloidal Silica, Fundamentals and Applications.* Wilmington, Delaware, CRC Press, Taylor & Francis, London, England.

Berryman, C. S. and Blair (1987*). "Kozeny–Carman relations and image processing methods for estimating Darcy's constant."* Journal of Applied Physics 62: 2221-2228.

Bishop, A. D. and J. L. B. T (1972). *"The thermodynamics and kinetics of the polymerization of silicic acid in dilute aqueous solution."* Thermochimica Acta 3: 339-409.

Blodau, C. and T.R.Moore (2002). *"Macroporosity affects water movement and pore water sampling in peat soils."* Soil Science 167(2): 98-109.

Bloemen, G. W. (1983). *"Calculation of hydraulic conductivities and steady state capillary rise in peat soils from bulk density and solid matter volume."* Bodemkunde 146(4): 460-473.

Boelter, D. H. (1969). *"Physical properties of peats as related to degree of decomposition."* Soil Science Society of America Journal 33: 606-609.

Bos, I. J. (2010). "*Distal delta-plain successions. Architecture and lithofacies of organics and lake fills in the Holocene Rhine-Meuse delta plain, The Netherlands."* Department of Physical Geography. Utrecht, University of Utrecht.

Conrad, C. F., G. A. Icopini, et al. (2007). *"Modeling the kinetics of silica nanocolloid formation and precipitation in geologically relevant aqueous solutions."* Geochimica et Cosmochimica Acta 71(3): 531-542.

Cooper, D. G., D. W. Pillon, et al. (1986). *"Biological additives for improved mechanical dewatering of fuel-grade peat."* Fuel 65: 255-259.

Coradin, T. and J. Livage (2007). *"Aqueous Silicates in Biological Sol Gel Applications: New Perspectives for Old Precursors."* Accounts of Chemical Research 40(9): 819-826.

Coradin, T., J. Livage, et al. (2004). *"The silicomolybdic acid spectrophotometric method and its application to silicate/biopolymer interaction studies."* Spectroscopy 18(4): 567-576.

Corapcioglu, Y. M., S. Chowdhury, et al. (1997). *"Micromodel visualization and quantification of solute transport in porous media."* Water Resources Research 33(11): 2547-2558.

Cosovic (1990). "*Adsorption kinetics of the complex mixture of organic solutes at model and natural phase boundaries." Aquatic Chemical Kinetics.* W. Stumm. New York, John Wiley & Sons: 291-311.

Cumming, J. L. (2008). *Environmental Fate, Aquatic Toxicology and Risk Assessment of Polymeric Quaternary Ammonium Salts from Cosmetic Uses.* PhD thesis, Science, Environment, Engineering and Technology Group, Australia. Brisbane, Griffith University. Doctor of Philosophy: 188.

Cumming, J. L., D. W. Hawker, et al. (2010). *"Analysis of polymeric quaternary ammonium salts as found in cosmetics by metachromatic polyelectrolyte titration."* Toxicological & Environmental Chemistry 92(9): 1595-1608.

Cumming, J. L., D. W. Hawker, et al. (2010*). "Sorption of Polymeric Quarternary Ammonium Compounds to Humic Acid."* Water, Air and Soil Pollution volume 214(1-4): 5-11.

Darcy, H. (1856). *"Les fountaines publiques de la Ville de Dijon."* Victor Dalmont, Paris.

Day-Lewis, F. D., J. W. Lane, et al. (2003). *"Time-lapse imaging of saline-tracer transport in fractured rock using difference-attenuation tomography."* Water Resources Research 39(10-11).

Demadis, K. and E. Mavredaki (2005). *"Green additives to enhance silica dissolution during water treatment."*

Environmental Chemistry Letters 3(3): 127-131.

Demadis, K. D., E. Neofotistou, et al. (2005). "*Inorganic foulants in membrane systems: chemical control strategies and the contribution of green chemistry."* Desalination 179(1-3): 281-295.

Demadis, K. D., K. Pachis, et al. (2009). *"Bioinspired control of colloidal silica in vitro by dual polymeric assemblies of zwitterionic phosphomethylated chitosan and polycations or polyanions."* Advances in Colloid and Interface Science 151(1-2): 33-48.

DIN ISO 13321 (1996). Polydispersity Index (PdI) is an indication for width of the distribution. The index is returned by Malvern software as a result. The calculation is performed according. In cumulant analyses a polynomial is fitted to the obtained results. From the 2nd and 3rd coefficient of the Taylor series the PdI can be derived: 2c/b2.

Dubin, L. (1985). "*Silica Inhibition: Prevention of Silica Deposition by Boric Acid/ Orthoborate Ion."* U.S. Patent. 4,584,104.

Dullien, F. A. (1979). *Porous media fluid transport and pore structure*. London, Academic Press

Enfield, C. and C. Bengtsson (1988). *"Macromolecular transport of hydrophobic contaminants in aqueous environments."* Ground Water 26(1): 64-70.

Fitts, C. R. (2002). *Groundwater Science*. London, Elsevier.

Flury, M., & Papritz, A. (1993). "*Bromide in the Natural Environment: Occurrence and Toxicity."* Journal of Environmental Quality, 22(4), 747-758.

Fontes, D. E., A. L. Mills, et al. (1991). *"Physical and chemical factors influencing transport of microorganisms through porous media."* Applied Environmental Microbiology 57: 2473-2481.

Freeze, R. A. and J. A. Cherry (1979). *Groundwater*. Upper Saddle River, Prentice Hall.

Gafni, A. (1986). *Field Tracing approach to determine flow velocity and hydraulic conductivity in saturated peat soils*. Unpublished PhD thesis. University of Minnesota, St. Paul.

Gallup, D. L. (2002). *"Investigations of organic inhibitors for silica scale control in geothermal brines I."* Geothermics 31(4): 415-430.

Gallup, D. L. and E. Barcelon (2005). *"Investigations of organic inhibitors for silica scale control from geothermal brines II."* Geothermics 34(6): 756-771.

Gill, J. S. (1993). *"Inhibition of silica silicate deposit in industrial waters."* Colloids and Surfaces A: Physicochemical and Engineering Aspects 74(1): 101-106.

Gnatowski, T., J. Szatylowicz, et al. (2010). "Hydraulic properties of fen peat soils in Poland." Geoderma 154: 188-195.

Gonzales, A. P. S., M. A. Firmino, et al. (2009). *"Peat as a natural solid-phase for copper preconcentration and determination in a multicommuted flow system coupled to flame atomic absorption spectrometry."* Analytica Chimica Acta 636(2): 198-204.

Haggerty, R., C. F.Harvey, et al. (2004). *"What controls the apparent timescale of solute mass transfer in aquifers and soils? A comparison of experimental results."* Water Resources Research 40.

Hamer, D. A. d. (2011). C*haracterization of Peat* - not yet published. Delft, Deltares.

Hamer, D. A. d., A. Venmans, et al. (2009). "*Stabilization of peat by silica based solidification."* 17th International Conference on Soil Mechanics & Geotechnical Engineering Alexandria, Egypt, EOS press.

Harrar, J. E., L. E. Lorensen, et al. (1982). "*Method for Inhibiting Silica Precipitation and Scaling in Geothermal Flow Systems."* U. S. Patent. 4,328,106.

Harthhorn, W. E. and D. R. Yonge (1995). "*The assessment of groundwater pollution potential resulting from stromwater infiltration BMP's."* Washington, Washington State Transportation Center Washington State University.

Hartlén, J. and W. Wolski (1996). *Embankments on organic soils.* Amsterdam, Elsevier.

Harvey, R. W. and S. P. Garabedian (1991). *"Use of colloid filtration theory in modeling movement of bacteria through a contaminated sandy aquifer."* Environmental Science and Technology 25(1): 178-185.

Harvey, R. W., L. H. George, et al. (1989). *"Transport of micro spheres and indigenous bacteria through a sandy aquifer: Results of natural- and forced-gradient tracer experiments."* Environmental Science and Technology 23(1): 51-56.

Hayward, P. and R. Clymo (1982). *"Profiles of water content and pore size in Sphagnum and peat, and their relation to peat bog ecology. Proceedings of the Royal Society of London, series B (1934-1990)."* Biological Sciences 215(1200): 299-325.

Healy, T. W. (2006). "*Stability of Aqueous Silica Sols. Colloidal Silica: Fundamentals and Applications."* H. E. Bergna and W. O. Roberts. New York, CRC Press, Taylor & Francis Group.

Hebib, S. and E. R. Farrell (2003). *"Some experiences on the stabilization of Irish peats."* Canadian Geotechnical Journal 40(1): 107.

Hiemenz, P. C. and R. Rajagopalan (1997). *Principles of Colloid and Surface Chemistry.* California State Polytechnic University, Pomona, California

Heimenz (1997). Rayleigh's approximation returns the intensity I of light scattered by a single particle from a beam of unpolarized light of wavelength λ and intensity I_0. Intensity I depends on the sixth power of particle diameter d: $I = I_0 \frac{1+\cos^2\Theta}{2R^2}\left(\frac{2\pi}{\lambda}\right)^4\left(\frac{n^2-1}{n^2+2}\right)^2\left(\frac{d}{2}\right)^6$ Where R is the distance to the particle, θ is the scattering angle, n is the refractive index of the particle.

Hiemenz (1997). A dispersion or suspension is polydisperse if a broad range of particle sizes are present.

Holden, J. (2006). Peatland Hydrology. Chapter 14: Peatlands: "*Evolution and Records of Environmental and Climate Changes."* I. P. Martini, A. M. Cortizas and W. Chesworth. New York, Elsevier: 319-346.

Holden, J. (2009). *"Flow through macropores of different size classes in blanket peat."* Journal of Hydrology 364: 342-348.

Holden, J., T.P. Burt, and N.J. Cox, "*Macroporosity and infiltration in blanket peat the implications of tension disc infiltrometer measurements*." Hydrological Processes 2001. 15: p. 289-303.

Icopini, G. A., S. L. Brantley, et al. (2005*). "Kinetics of silica oligomerization and nanocolloid formation as a function of pH and ionic strength at 25°C."* Geochimica et Cosmochimica Acta 69(2): 293-303.

Iler, R. K. (1979). *The Chemistry of Silica.* New York, NY., John Wiley and Sons.

Karol, R. H. (2003). *Chemical grouting and soil stabilization*. New York, Dekker

Kehew, A. E. (2001). *Applied chemical hydrogeology.* New Jersey, Prentice Hall.

Kettridge, N., & Binley, A. (2008). "*X-ray computed tomography of peat soils: measuring gas content and peat structure"*. Hydrological Processes, 22, 4827-4837.

Killops, S. D. and V. J. Killops (2005). *Introduction to organic geochemistry,* Malden MA. Blackwell.

Klavins, M., J. Sire, et al.(2009). *"Approaches to estimating humification indicators for peat."* Mires and Peat,3(3):1-15.

Koelewijn, A., Aantjes, H., & Zwanenburg, C. (2008*). Macrostabiliteitsdijk Ijkdijk*. Delft: Deltares.

Kohlrausch, F. (1897). "*Ueber concentrations-verschiebungen durch elecrolyse im innern von lösungen und lösungsgemischen."* Annals of Physical Chemistry 62(210-239).

Kruse, G. A. M. and E. J. d. Haan (2006). "*Characterization and Engineering properties of Dutch peats."* Proceedings of the Second International Workshop on Characterization and Engineering Properties of Natural Soils, Singapore, Taylor & Francis.

Langevin, C., Dausman, A., & Sukop, M. (2010). "*Solute and Heat Transport Model of the Henry and Hilleke Laboratory Experiment*." Ground Water, 48(5), 757-770.

Leroy, P., & Revil, A. (2004). "*A triple-layer model of the surface electrochemical properties of clay minerals."* Journal of Colloid and Interface Science, 270, 371-380.

Lie, H., J. Yan, et al. (2006). *"Virus Retention and Transport in Chemically Heterogeneous Porous Media under Saturated and Unsaturated Flow Conditions."* Environmental Science & Technology 40(5): 1547-1555.

Mallants, D. M. M., N. Vanclooster, et al. (1996). *"Comparison of three methods of calibrate TDR for monitoring solute movement in unsaturated soil."* Soil Science Society of America Journal 60: 747-754.

Malvern Instruments. (2003). Zetasizer Nano User Manual. England.

Mavredaki, E., E. Neofotistou, et al. (2005). *"Inhibition and Dissolution as Dual Mitigation Approaches for Colloidal Silica Fouling and Deposition in Process Water Systems: Functional Synergies."* Industrial & Engineering Chemistry Research 44(17): 7019-7026.

McCarthy, J. F. and J. M. Zachara (1989). *"Subsurface transport of contaminants."* Environmental Science and Technology 23(5): 496-502.

McKay, L. D., R. W. Gillham, et al. (1993). *"Field experiments in a fractured clay till. Solute and colloid transport."* Water Resources Research 29(2): 3879-3890.

Means, J. C., S. G. Wood, et al. (1980). *"Sorption of polynuclear aromatic hydrocarbons by sediments and soils."* Environmental Science & Technology 12(12): 1524-1528.

Meier, D. A. and L. Dubin (1987). *"A Nobel Approach to Silica Scale Inhibition."* Corrosion 87: 335.

Mikhailova, I. V. and I. I. Gerashchenko (2002). *"Stability and Adsorption Properties of Suspensions of Finely Dispersed Silica in the Presence of Cationic Surfactants."* Colloid Journal 64(5): 583-587.

Minones, J., & Conde, O. (1988). "*Interaction of polysilicic acid with monolayers of substances containing quaternary ammonium groups*." Colloid & Polymer Science, 266, 353-358.

Molendijk, W. O. and E. J. d. Haan (1996). *Construction on peat and organic soils.* Delft Netherlands, Rijkswaterstaat DWW and GeoDelft: 123.

Napper, D. H. (1983). *Polymeric Stabilization of Colloidal Dispersions. Ad advanced and in-depth treatment of the role of polymers in colloid stability.* London, Academic Press.

National Institute for Occupational Safety and Health (1994). *International Chemical Safety Cards, Bromine*. http://www.cdc.gov/niosh/ipcsneng/neng0107.html. Retrieved 5 January, 2012.

Neofotistou, E. and K. D. Demadis (2004). *"Silica scale inhibition by polyaminoamide STARBURST® dendrimers." Colloids and Surfaces A: Physicochemical and Engineering Aspects 242(1-3): 213-216.*

Neofotistou, E. and K. D. Demadis (2004). *"Use of antiscalants for mitigation of silica (SiO2) fouling and deposition: fundamentals and applications in desalination systems."* Desalination 167: 257-272.

Nichol, D. and I. W. Farmer (1998). *"Settlement over peat on the A5 at Pant Dedwydd near Cerrigydrudion, North Wales."* Engineering Geology 50(3-4): 299-307.

Ours, D. P., D. I. Siegel, et al. (1997). *"Chemical dilation and the dual porosity of humified bog peat."* Journal of Hydrology 196(14): 348-360.

Päivänen, J. (1973). *"Hydraulic conductivity and water retention in peat soils."* Acta Forestalia Fennica 129: 1-70.

Pashley, R. M. and M. E. Karaman (2004). *Applied Colloid and Surface Chemistry.* Department of Chemistry, The National University of Australia, Canberra, Australia, John Wiley & Sons.

Perdrial, N., J. N. Perdrial, et al. (2010). *"Temporal and spatial monitoring of mobile nanoparticles in a vineyard soil: evidence of nanoaggregate formation."* European Journal of Soil Science 61(4): 456-468.

Perry, C. C. and T. Keeling-Tucker (2000). *"Biosilicification: the role of the organic matrix in structure control."* Journal of Biological Inorganic Chemistry 5(5): 537-550.

Perry, C. C. and T. Keeling-Tucker (2003). *"Model studies of colloidal silica precipitation using biosilica extracts from Equisetum telmateia."* Colloid & Polymer Science 281(7): 652-664.

Perry, C. C. and Y. Lu (1992). *"Preparation of Silicas form Silicon Complexes: Role of Cellulose In Polymerisation and Aggregation Control."* Journal of the Chemical Society, Faraday Transactions 88(19): 2915-2921.

Ponziani, M., D. J. M. Ngan-Tillard, et al. (2011). *"A new prototype cell to study electrical and geo-mechanical properties of peaty soils."* Engineering geology 119(1-2): 74.

Post, L. v. and E. Granlund (1926). *"Södra SverigesTorvtillgångar I (Peat resources in southern Sweden I)."* Sveriges Geologiska Undersökning 335(19): 1-125.

Quinton, W. L. and G.Marsh (2000). *"Subsurface drainage from hummock-covered hillslope in the Arctic tundra."* Journal of Hydrology 237: 113-125.

Quinton, W. L., M. Hayashi, et al. (2008*). "Peat hydraulic conductivity in cold regions and its relation to pore size and geometry."* Hydrological Processes 22: 2829-2837.

Reimus, P. W. (1995). *The use of synthetic colloids in tracer transport experiments in saturated rock fractures.* New Mexico, Los Alamos National Laboratory.

Rezanezhad, F., W. L. Quinton, et al. (2009). *"Examining the effect of pore size distribution and shape on flow through unsaturated peat using 3-D computed tomography."* Hydrological and Earth System Sciences (Discussion) 6: 3835-3862.

RIVM (2009). Virus Transport. Utrecht, Summer School Course: Flow and Transport in porous media. University of Utrecht.

Sherwood, P. (1993). *Soil stabilization with cement and lime.* London, State of the Art Review. London: HMSO.

Shimabayashi, S., K. Nishino, et al. (1992). *"Aggregation/dispersion of amorphous silica particles by simultaneous adsorption of two polymers in an aqueous phase."* Colloids and Surfaces 63: 121-129.

Sing, W. L., R. Hashim, et al. (2008). "*Behavior of Stabilization Peat Soils in Unconfined Compression Tests."* American Journal of Engineering and Applied Sciences 1(4): 274.

Singha, K., Li, L., Day-Lewis, F. D., & Regberg, A. B. (2011). "*Quantifying solute transport processes: Are chemically "conservative" tracers electrically conservative*?" Geophysics, 76(1), F53-F63.

Sparks, D. L. (2003). *Environmental Soil Chemistry*, Elsevier, Academic Press.

Speelman, J. (2009). *Personal Communication*, Scientist at Akzo Nobel

Staal, M., L. A. Van Paassen, et al. (2008). "*Can biological mediated silicate binding in biofilms be used for biogrouting?"* Netherlands, Delft, BGCE Conference 2008: 5.

Staffan, S. b. (1996). *"Silica in aqueous environments."* Journal of Non-Crystalline Solids 196(0): 51-57.

Stathoulopoulou, A. and K. D. Demadis (2008). *"Enhancement of silicate solubility by use of "green" additives: linking green chemistry and chemical water treatment."* Desalination 224(1-3): 223-230.

Stathoulopoulou and Demadis, (2008): 'A green chemical should be synthesized in a safe and energy efficient manner; its toxicity should be minimal, whereas its biodegradation should be optimal. Lastly, its impact to the environment should be as low as possible'.

Stevenson, F. J. (1982). *Humus Chemistry.* New York, Wiley & Sons.

Stumm, W. (1990). *Aquatic chemical kinetics: reaction rates of processes in natural waters.* New York, Wiley.

Stumm, W. and J. J. Morgan (1996). *Aquatic Chemistry*. United States of America / Canada, John Wiley & Sons. Inc.

Timothy, L. P. (1988). *Computer studies of heat tracer experiments in fractured rock*. Msc. Thesis, University of Arizona, Arizona.

Tobler, D. J., S. Shaw, et al. (2009). *"Quantification of initial steps of nucleation and growth of silica nanoparticles: An in-situ SAXS and DLS study."* Geochimica et Cosmochimica Acta 73(18): 5377-5393.

Toran, L. and A. V. Palumbo (1992). *"Colloid transport through fractured and unfractured laboratory sand columns."* Journal of Contaminated Hydrology 9: 289-303.

Torkzaban, S. (2007). *Fate and transport of viruses and colloids in saturated and unsaturated porous media.* PhD thesis, Faculty of Geosciences Utrecht, University of Utrecht. Doctor.

Ueda, A., K. Kato, et al. (2000). *"Recovery of silica from the Sumikawa geothermal fluids by addition of cationic reagents."* Journal of Geothermal Research Society of Japan 22: 249-258.

Ueda, A., K. Kato, et al. (2003). "*Silica removal from Mokai, New Zealand, geothermal brine by treatment with lime and a cationic precipitant*." Geothermics 32(1): 47-61.

Vaslin-Reimann, S., F. Lafuma, et al. (1990). *"Reversible flocculation of silica suspensions by water-soluble polymers."* Colloid & Polymer Science 268(5): 476-483.

Venmans, A. (2009), *Summary Material Properties*, AES1630 engineering properties of soil and rock, Editor. Deltares: Delft.

Venmans, A. (1989). *Veen karakterisatie*. Delft: GeoDelft.

Vilks, P., L. H. Frost, et al. (1997). *"Field scale colloid migration experiments in a granite fracture."* Journal of Contaminated Hydrology 26: 203-214.

Wan, J. and J. L. Wilson (1994). *"Colloid transport in unsaturated porous media."* Water Resources Research 30(4): 857-864.

Weiss, R., J. Alm, et al. (1998*). "Modeling moisture retention in peat soils."* Soil Science Society of America Journal 62: 305-313.

Weng, L. P. (2002). *Interactions between Metal Ions and Biogeo-Surfaces in Soil and Water.* PhD thesis, Department of Soil Quality. Wageningen, Wageningen University.

Yates, P. C. (2006). "*Stabilization Against Particle Growth." Colloidal Silica, Fundamentals and Applications*. H. E. Bergna and W. O. Roberts. New York, CRC Press, Taylor & Francis Group.

Yun, J. (2009). *Retention and Transport of Viruses in Porous Media*. Summer School Course: Flow and Transport in porous media. Utrecht, University of Utrecht.

Zhang, B.-R., Y.-N. Chen, et al. (2011). *"Inhibitory effects of poly(adipic acid/amine-terminated polyether D230/diethylenetriamine) on colloidal silica formation."* Colloids and Surfaces A: Physicochemical and Engineering Aspects 385: 11-19.

Zon, W. J. v. d., J. J. Olie, et al. (2007). *Soil Strengthening Composition*, WO, 2008/072964. Deltares, the Netherlands.

Zon, W.J.v.d., *Grouting techniques*. 1998, GeoDelft: Delft.

Zwanenburg, C. (2005). *The influence of anistropy on the consolidation behavior of peat.* PhD thesis, Civil Engineering. Delft, Technical University of Delft. Doctor: 221.

Appendix 1 Product Information Celquat L200

Appendix 1.1 Product sheet Celquat L200

CELQUAT® L-200

Low viscosity cationic conditioner/fixative.

Table of Contents

Section 1: Sales Specifications for CELQUAT® L-200
Section 2: Technical Sales Bulletin for CELQUAT® L-200
Section 3: Regulatory Information for CELQUAT® L-200
Section 4: MSDS for CELQUAT® L-200
Links

Section 1

Sales Specifications for CELQUAT® L-200

AkzoNobel
Tomorrow's Answers Today

CELQUAT® L-200 polymer

INCI Name: Polyquaternium-4

Specification

Appearance	Tan powder, essentially free of foreign matter

Parameter	Limits
% Nitrogen (as is)	1.6 - 2.4
% Volatiles	8.0 maximum
pH (2% aqueous solution)	6.0 - 8.0
Viscosity (cps) (2% solution)	35 - 350

Measurements
Volatiles are determined on a 2 gram sample heated at 130°C for 1 hour.

RVT, 20 RPM, Spindle #1, 21°C

Issued: 2004.02

Europe: Sempach-Station, Switzerland, T: +41 (0)41-469-69-66, F: +41 (0)41-469-69-06, e: personalcare.europe@akzonobel.com
Americas: Bridgewater, New Jersey, U.S.A., T: 888 331-6212, F: 908-707-3664, e: personalcare.usa@akzonobel.com
South America: Itupeva, SP, Brazil, T: 55-11-4591-8800, F: 55-11-4591-8804, e: personalcare.southamerica@akzonobel.com
Asia/Pacific: Hong Kong, Tel: +852-2968-2938, Fax: +852-2745-7063, e-mail: personalcare.asia@akzonobel.com
www.akzonobel.com/PersonalCare

Section 2

Technical Sales Bulletin for CELQUAT® L-200

CELQUAT® L-200 Polymer

AkzoNobel
Tomorrow's Answers Today

CELQUAT® L-200 Polymer
INCI: Polyquaternium-4

Cationic Cellulosic for Hold and Conditioning

INTRODUCTION

CELQUAT® L-200 polymer is a low viscosity, highly cationic conditioner/fixative useful in a broad range of styling, cleansing, and skin care products. This water soluble modified cellulosic is highly cationic over the entire useful pH range, is substantive to hair and skin, and provides such aesthetic benefits as excellent combability, hold, gloss, and anti-static properties, and a smooth feel

CELQUAT L-200 polymer is one member of the CELQUAT family of polymers that are water soluble quaternary cellulose derivatives. Other CELQUAT polymers offered by AkzoNobel include:

Polyquaternium-4
- CELQUAT H-100 polymer

Polyquaternium-10
- CELQUAT SC-230M polymer
- CELQUAT SC-240C polymer

Polyquaternium-4/Hydroxypropyl Starch Copolymer
- CELQUAT LS-50 polymer

Polyquaternium-4 conditioning polymers are formed by grafting dimethyl diallyl ammonium chloride groups onto a cellulosic backbone. The Polyquaternium-4 polymers differ from the Polyquaternium-10 polymers in their comb-like distribution of the quaternized nitrogen charge rather than an even charge distribution. CELQUAT L-200 polymer is a low viscosity Polyquaternium-4 variant. It differs from the higher viscosity CELQUAT H-100 polymer in not only molecular weight, but also its degree of cationic substitution. CELQUAT L-200 polymer has approximately 2% nitrogen, which is double that of the CELQUAT H-100 polymer. Because of its lower molecular weight and higher cationic substitution, the CELQUAT L-200 polymer is recommended for use in low viscosity systems that require conditioning benefits, such as mousses. CELQUAT L-200 polymer can be used in both styling and cleansing application areas, although the CELQUAT L-200 polymer is the least tolerant of anionic ingredients of all the CELQUAT polymers.

Europe: Sempach-Station, Switzerland, T: +41 (0)41-469-69-66, F: +41 (0)41-469-69-06, e: personalcare.europe@akzonobel.com
Americas: Bridgewater, New Jersey, U.S.A., T: 888 331-6212, F: 908-707-3664, e: personalcare.usa@akzonobel.com
South America: Itupeva, SP, Brazil, T: 55-11-4591-8800, F: 55-11-4591-8804, e: personalcare.southamerica@akzonobel.com
Asia/Pacific: Hong Kong, Tel: +852-2968-2938, Fax: +852-2745-7063, e-mail: personalcare.asia@akzonobel.com
www.akzonobel.com/PersonalCare

CELQUAT® L-200 Polymer

APPLICATION AREAS

CELQUAT L-200 polymer is an excellent conditioning film former. Suggested applications can include styling and conditioning mousses, creams, lotions, gels, conditioners, and skin creams and lotions.

FEATURES / BENEFITS

- Substantive to hair and skin without build up
- Imparts smooth feel to hair and skin
- Forms clear, glossy and tough films
- Improves wet combability
- Provides excellent high humidity curl retention
- Forms clear aqueous solutions

SUGGESTED USE LEVELS, AS SUPPLIED

Styling Applications:	0.5% to 3.0%
Cleansing Applications:	0.1% to 0.5%

FORMULATION GUIDELINES

Solubility

CELQUAT L-200 polymer is water soluble. It is recommended that the CELQUAT L-200 polymer phase contain no more than 8% polymer by weight. For optimal results, prepare the CELQUAT polymer solution as a separate phase. Slowly sift the powder into water while stirring. Sifting slowly will avoid the formation of fisheyes and gels. Heat and moderate agitation will increase the solubility rate of the polymer. The polymer is completely hydrated when the solution is clear and there are no insolubles present. Complete hydration is important to ensure homogeneity, viscosity stability, formulation stability, and clarity.

pH Stability

Solutions of CELQUAT L-200 polymer are subject to chemical hydrolysis at extreme pH. A pH range of 4 to 8 is recommended for optimal stability.

Thickening

Certain formulations based on CELQUAT L-200 polymer may require additional thickening to improve their application or use. Commonly used cellulosic type thickeners are effective in raising the solution viscosity, including hydroxyethyl cellulose and hydroxypropyl methylcellulose. Blending with the higher viscosity CELQUAT-SC-230M polymer (Polyquaternium-10) can build viscosity. Finally, STRUCTURE® PLUS polymer (INCI Name: Acrylates/Aminoacrylates/C10-30 Alkyl PEG-20 Itaconate Copolymer) from AkzoNobel is an effective associative thickener which can raise the viscosity of solutions containing CELQUAT L-200 conditioning polymer.

Europe: Sempach-Station, Switzerland, T: +41 (0)41-469-69-66, F: +41 (0)41-469-69-06, e: personalcare.europe@akzonobel.com
Americas: Bridgewater, New Jersey, U.S.A., T: 888 331-6212, F: 908-707-3664, e: personalcare.usa@akzonobel.com
South America: Itupeva, SP, Brazil, T: 55-11-4591-8800, F: 55-11-4591-8804, e: personalcare.southamerica@akzonobel.com
Asia/Pacific: Hong Kong, Tel: +852-2968-2938, Fax: +852-2745-7063, e-mail: personalcare.asia@akzonobel.com
www.akzonobel.com/PersonalCare

CELQUAT® L-200 Polymer

Preservation

Aqueous solutions of CELQUAT polymers are subject to bacteriological growth and enzyme catalyzed degradation. Preservatives suggested for consideration are DMDM hydantoin, methyl p-hydroxybenzoate, propyl p-hydroxybenzoate, Germall® 115 and 2 nitro-2 bromo-1, 3 propanediol. The presence of alcohol will also minimize bacteriological growth.

COMPATIBILITY

Surfactant Compatibility

The CELQUAT L-200 polymer, because of its higher cationic activity, is generally less compatible with surfactants than its analog CELQUAT H-100 polymer. Since CELQUAT L-200 polymer has limited surfactant compatibility, it is not strongly recommended for use in clear systems with high amounts of anionic surfactant.

PERFORMANCE PROPERTIES

Styling Applications

CELQUAT L-200 polymer can have many applications in the hair care area, although the bulk of its use is in styling mousses. This polymer can be used in conditioning mousses, conditioning creams or lotions, and other styling aids.

Humidity Resistance

CELQUAT L-200 polymer is an excellent film former. The polymer has good holding power in high humidity curl retention tests. In one test procedure, hair swatches were treated with various fixatives and were combed out, formed into curls, dried, and conditioned at 50% relative humidity. They were then mounted, unwound into a helix configuration, measured and placed in a chamber maintained at 21°C and 90% relative humidity. Curl height was determined as a function of time.

Percent curl retention is calculated by means of the following equation:

% Curl Retention = $L\text{-}L_t/L\text{-}L_0$
Where:

L = length of hair fully extended
L_0 = length of hair before exposure
L_t = length of hair after exposure for time

Nine determinations were made with each sample.

Europe: Sempach-Station, Switzerland, T: +41 (0)41-469-69-66, F: +41 (0)41-469-69-06, e: personalcare.europe@akzonobel.com
Americas: Bridgewater, New Jersey, U.S.A., T: 888 331-6212, F: 908-707-3664, e: personalcare.usa@akzonobel.com
South America: Itupeva, SP, Brazil, T: 55-11-4591-8800, F: 55-11-4591-8804, e: personalcare.southamerica@akzonobel.com
Asia/Pacific: Hong Kong, Tel: +852-2968-2938, Fax: +852-2745-7063, e-mail: personalcare.asia@akzonobel.com
www.akzonobel.com/PersonalCare

CELQUAT® L-200 Polymer

The results of the evaluation are given below:

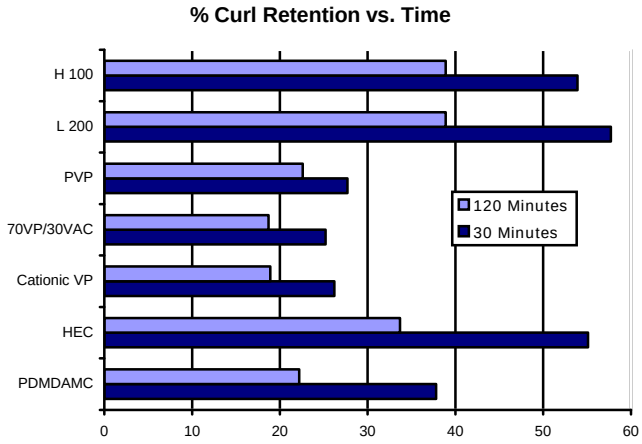

H 100:	CELQUAT H-100 polymer
L 200:	CELQUAT L-200 polymer
PVP:	Polyvinylpyrrolidone
70VP/30VAC:	70 Vinyl Pyrrolidone/ 30 Vinyl Acetate Copolymer
Cationic VP:	Cationic Vinyl Pyrrolidone Copolymer
HEC:	Commercial Cationic Hydroxyethyl Cellulose
PDMDAMC:	Polydimethyldiallyl Ammonium Chloride

This data shows that the CELQUAT L-200 polymer has superior high humidity curl retention when compared to cationic vinyl pyrrolidone copolymer, 70% vinyl pyrrolidone/30% vinyl acetate copolymer, polyvinylpyrrolidone, and poly dimethyl diallyl ammonium chloride. The polymer also has slightly higher high humidity curl retention when compared to the CELQUAT H-100 polymer and commercial hydroxyethyl cellulose after a 2 hour time period.

Subjective Evaluations

The CELQUAT L-200 polymer can deliver excellent performance in leave-in products. Subjective evaluations were run to compare the performance of the CELQUAT L-200 conditioning polymer to the Polyquaternium-10 conditioning polymers show superior comb and feel benefits for the Polyquaternium-4 polymer without sacrificing other performance attributes.

Europe: Sempach-Station, Switzerland, T: +41 (0)41-469-69-66, F: +41 (0)41-469-69-06, e: personalcare.europe@akzonobel.com
Americas: Bridgewater, New Jersey, U.S.A., T: 888 331-6212, F: 908-707-3664, e: personalcare.usa@akzonobel.com
South America: Itupeva, SP, Brazil, T: 55-11-4591-8800, F: 55-11-4591-8804, e: personalcare.southamerica@akzonobel.com
Asia/Pacific: Hong Kong, Tel: +852-2968-2938, Fax: +852-2745-7063, e-mail: personalcare.asia@akzonobel.com
www.akzonobel.com/PersonalCare

CELQUAT® L-200 Polymer

AkzoNobel
Tomorrow's Answers Today

Cleansing Systems

The physical and sensory properties of the CELQUAT L-200 polymer make it well suited for use in cleansing applications. However, the CELQUAT L-200 polymer has some formula limitations due to the nature of its cationic charge. Some incompatibilities will occur when using the polymer with anionic surfactants.

Substantivity

The cationic charge on the CELQUAT L-200 polymer makes it substantive to such keratinous substrates as hair and skin.

The substantivity of CELQUAT L-200 polymer has been defined using the Lumicrease Dye Test. In this experiment, dyeing wool swatches with an anionic polyazo sulfonate dye after they have been treated with the cationic polymer quantifies deposition of cationic conditioning polymers. Wool is similar to human hair and skin in adsorptive and charge properties and can be used as an efficient substitute substrate for hair testing. The dye is attracted to the deposited cationic polymer. A colorimeter is used to measure the degree of adsorption on each sample via intensity of the dye. The swatches are tested for deposition after 1 wash (1) and 10 washes (10). The 1 wash data is indicative of substantivity, and a significantly higher value for the 10 wash reading over the 1 wash reading is indicative of build-up.

As is shown in the following figure, the CELQUAT L-200 polymer is significantly more substantive than the two Polyquaternium-10 polymers, and is equally substantive as the CELQUAT H-100 polymer. This data also shows that this polymer does not build-up on the wool swatches during repeated washings.

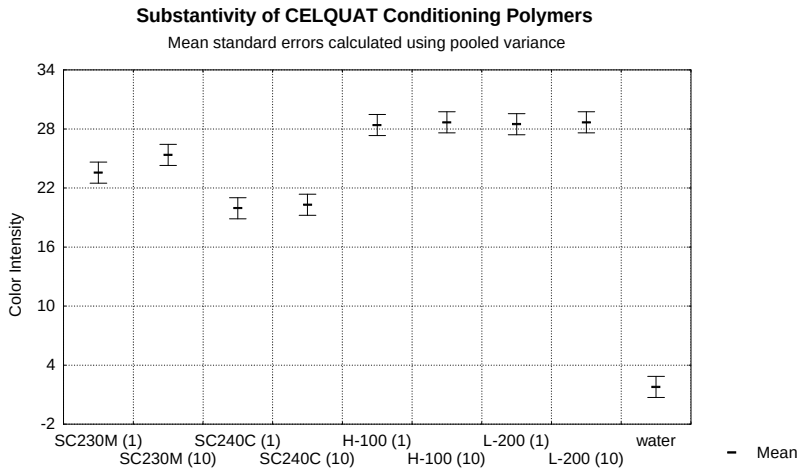

Europe: Sempach-Station, Switzerland, T: +41 (0)41-469-69-66, F: +41 (0)41-469-69-06, e: personalcare.europe@akzonobel.com
Americas: Bridgewater, New Jersey, U.S.A., T: 888 331-6212, F: 908-707-3664, e: personalcare.usa@akzonobel.com
South America: Itupeva, SP, Brazil, T: 55-11-4591-8800, F: 55-11-4591-8804, e: personalcare.southamerica@akzonobel.com
Asia/Pacific: Hong Kong, Tel: +852-2968-2938, Fax: +852-2745-7063, e-mail: personalcare.asia@akzonobel.com
www.akzonobel.com/PersonalCare

CELQUAT® L-200 Polymer

STORAGE AND HANDLING

CELQUAT L-200 polymer should be stored in a cool, dry location away from heat, sparks or fire. When not in use, the container should be kept closed to prevent moisture and dust contamination. We recommend that normal precautions be taken to avoid ingestion or contact with eyes. Respiratory protection should be used to avoid dust inhalation. Good industrial hygiene practices should be followed. Please read the MSDS before using this or any other chemical.

HEALTH AND SAFETY

A health and safety summary for CELQUAT L-200 polymer is available upon request. Information on CELQUAT L-200 polymer relating to EU Cosmetic Directive 76/768/EEC is also available upon request.

This product may be used in spray applications having a droplet particle size greater than 50 microns. The product has not been properly evaluated for safety clearance for use in pumps and/or aerosols with particle sizes less than 50 microns.

The suitability of the final formulations should be confirmed in all respect by appropriate evaluation. The marketer is advised to evaluate the final formulation with regard to performance and health safety.

9.2004, REV. 09.15.2008

Europe: Sempach-Station, Switzerland, T: +41 (0)41-469-69-66, F: +41 (0)41-469-69-06, e: personalcare.europe@akzonobel.com
Americas: Bridgewater, New Jersey, U.S.A., T: 888 331-6212, F: 908-707-3664, e: personalcare.usa@akzonobel.com
South America: Itupeva, SP, Brazil, T: 55-11-4591-8800, F: 55-11-4591-8804, e: personalcare.southamerica@akzonobel.com
Asia/Pacific: Hong Kong, Tel: +852-2968-2938, Fax: +852-2745-7063, e-mail: personalcare.asia@akzonobel.com
www.akzonobel.com/PersonalCare

Section 3

Regulatory Information for CELQUAT® L-200

AkzoNobel
Tomorrow's Answers Today

CELQUAT® L-200 polymer

Regulatory Information

Parameter	
CAS Number	111774-28-8
USA (TSCA)	Yes
Europe	Polymers of EINECS listed monomers
Canada	Yes
Australia	Yes

Issued: 2007.01

Europe: Sempach-Station, Switzerland, T: +41 (0)41-469-69-66, F: +41 (0)41-469-69-06, e: personalcare.europe@akzonobel.com
Americas: Bridgewater, New Jersey, U.S.A., T: 888 331-6212, F: 908-707-3664, e: personalcare.usa@akzonobel.com
South America: Itupeva, SP, Brazil, T: 55-11-4591-8800, F: 55-11-4591-8804, e: personalcare.southamerica@akzonobel.com
Asia/Pacific: Hong Kong, Tel: +852-2968-2938, Fax: +852-2745-7063, e-mail: personalcare.asia@akzonobel.com
www.akzonobel.com/PersonalCare

AkzoNobel
Surface Chemistry
Personal Care

10 Finderne Ave
Bridgewater, NJ
08807
United States

T+888-331-6212
F +908-707-3664
www.akzonobel.com/personalcare

AkzoNobel
Tomorrow's Answers Today

Tuesday, June 02, 2009

Re: CELQUAT® L-200 Material Origin BSE

To: Whom it may concern,

AkzoNobel Surface Chemistry Personal Care has completed a review of the ingredients used in the manufacture of our personal care products. As a result of this exercise, we are able to certify that the below product is free of any animal derived ingredients.

CELQUAT L-200 polymer

Specifically, this product is derived from plant and synthetic sources.

Sincerely,

David Bower
Regulatory, U.S.
908 707-3756

Section 4

MSDS for CELQUAT® L-200

*** MATERIAL SAFETY DATA SHEET ***

1. CHEMICAL PRODUCT AND COMPANY IDENTIFICATION

PRODUCT NUMBER	15-05169
PRODUCT NAME	CELQUAT® L-200 Conditioning polymer
Manufacturer	Akzo Nobel Surface Chemistry LLC 525 West Van Buren Street Chicago, IL 60607-3823 USA www.surfactants.akzonobel.com EMERGENCY PHONES: MEDICAL: 914-693-6946 (Health & Safety Call Center-24 hours) TRANSPORT: CHEMTREC: 800-424-9300 (24 hours) CHEMTREC International: 703-527-3887 (call collect) CANUTEC: 613-996-6666 (24 hours) MSDS Requests/Customer Service: See phone numbers in Section 16
SYNONYMS	INCI Name: Polyquaternium-4

2. COMPOSITION/INFORMATION ON INGREDIENTS

CHEMICAL FAMILY Quaternary Cellulosic Derivative

COMPONENT	CAS NUMBER	CONCENTRATION (% by weight)
None classified as hazardous under the OSHA Hazard Communication Standard (29CFR 1910.1200).		

3. HAZARDS IDENTIFICATION

EMERGENCY OVERVIEW

Possible physical irritant from dust particles. Potential for dust explosion.

Yellow Solid Slight odor

EYE	Particulates may scratch eye surfaces and cause mechanical irritation.
SKIN CONTACT	Repeated or prolonged skin contact may result in mild irritation.
INHALATION	May cause irritation to eyes and respiratory system.
INGESTION	Ingestion may cause irritation of the gastrointestinal tract. Low oral toxicity.

4. FIRST-AID MEASURES

EYE	Irrigate with eyewash solution or clean water until pain is relieved. Obtain medical attention.
SKIN CONTACT	Wash skin with soap and water. If symptoms develop, obtain medical attention.
INHALATION	Remove to fresh air. Get medical attention if irritation persists.
INGESTION	Treat symptomatically and supportively. Get medical attention. DO NOT attempt to give anything by mouth to an unconscious person.

5. FIREFIGHTING MEASURES

AUTOIGNITION	Not available
FLASH POINT	Not applicable
EXTINGUISHING MEDIA	Water Fog; Foam; Dry Chemical; CO2
SPECIAL FIREFIGHTING PROCEDURES	Fire fighters should be equipped with self-contained breathing apparatus to protect against potentially toxic and irritating fumes.
FIRE & EXPLOSION HAZARDS	Product is a finely divided combustible powder and as such constitutes a potential fire hazard. Keep workplace dust levels below the stipulated exposure limits. Prohibit smoking and open flames. Avoid sparks or other sources of static electricity.
HAZARDOUS COMBUSTION PRODUCTS	Carbon monoxide, carbon dioxide, unknown hydrocarbons.
LOWER EXPLOSION LIMIT (%)	30.0 g/m3
UPPER EXPLOSION LIMIT (%)	Not applicable
MINIMUM IGNITION ENERGY	100 - 300 mJ
Kst CLASS	1 = Weak explosion.
Kst VALUE	52.3 bar.m/s

6. ACCIDENTAL RELEASE MEASURES

SPILL AND LEAK PROCEDURES	Normal precautions for "nuisance dust" should be observed. Avoid prolonged inhalation of dust. Sweep up or vacuum up and place in suitable container for disposal.

For safety and environmental precautions, please review entire Material Safety Data Sheet for necessary information.

7. HANDLING AND STORAGE

STORAGE TEMPERATURE	Ambient.
HANDLING/STORAGE	Store in a cool, dry area away from heat, sparks or fire. Mechanical handling of the powder on inadequately grounded equipment can result in static electrical discharges.
SENSITIVITY TO STATIC ELECTRICITY	Yes
SENSITIVITY TO MECHANICAL IMPACT	No

8. EXPOSURE CONTROLS/PERSONAL PROTECTION

VENTILATION REQUIREMENTS	Provide local exhaust or general dilution ventilation to meet published exposure limits. Ventilation equipment must be explosion-proof.
EYE PROTECTION REQUIREMENTS	Wear safety glasses with side shields. Protect against dust and particulates.
GLOVE REQUIREMENTS	The use of chemically resistant gloves is recommended.
CLOTHING REQUIREMENTS	Uniforms, coveralls, or a lab coat should be worn.
CHANGE/REMOVAL OF CLOTHING	Remove contaminated clothing and launder before reuse.
WASH REQUIREMENTS	Wash before eating, drinking, or using toilet facilities.
RESPIRATOR REQUIREMENTS	None required under normal handling conditions. Use NIOSH approved dust mask if dust levels are irritating.

9. PHYSICAL AND CHEMICAL PROPERTIES

PURE SUBSTANCE OR MIXTURE	Mixture
PHYSICAL FORM	Solid
COLOR	Yellow
ODOR	Slight
ODOR THRESHOLD	Not available
PH AS IS	Not applicable
pH IN (1%) SOLUTION	6.5 - 7.5
OXIDIZING PROPERTIES	Not applicable
BOILING POINT	Not applicable
MELTING/FREEZING POINT	Not applicable
SOLUBILITY IN WATER	Soluble
PARTITION COEFFICIENT (n-octanol/water)	Not applicable
SPECIFIC GRAVITY (WATER=1)	0.48
BULK DENSITY	4 lb/gal
EVAPORATION RATE	Not applicable
VAPOR PRESSURE (mmHg)	Not applicable
VAPOR DENSITY (air = 1)	Not applicable
VOLATILES	7 %
VOLATILE ORGANIC COMPOUNDS	Not available
AUTOIGNITION	Not available
FLASH POINT	Not applicable

10. STABILITY AND REACTIVITY

STABILITY	Stable
STABILITY DETAIL	Stable under normal temperature and pressure.

11. TOXICOLOGICAL INFORMATION

ROUTE OF ENTRY Inhalation; Ingestion; Skin Contact; Eye Contact

CARCINOGEN	IARC (group)	NTP	OSHA Substance Specific Regulation

COMPONENT	
There is no evidence that this product poses a carcinogenic risk under normal conditions of handling and use.	

CHRONIC (LONG TERM) EFFECTS OF EXPOSURE

EFFECTS OF CHRONIC EXPOSURE	Prolonged or frequent breathing of excess dust may cause an adverse respiratory effect.
TARGET ORGANS	Lungs

PRODUCT TOXICOLOGY

PRODUCT INFORMATION	Unlikely to cause harmful effects under normal conditions of handling and use.

12. ECOLOGICAL INFORMATION

POTENTIAL TO BIOACCUMULATE	Unknown.
AQUATIC TOXICITY	None Established

13. DISPOSAL CONSIDERATIONS

WASTE DISPOSAL METHODS	Disposal should be in accordance with local, state or national legislation.
EMPTY CONTAINER WARNINGS	Empty containers may contain product residue; follow MSDS and label warnings even after they have been emptied.

14. TRANSPORTATION INFORMATION

This section provided for general information only.
FOR NON-BULK SHIPMENTS.
FOR MORE COMPLETE TRANSPORTATION REGULATORY INFORMATION PLEASE REFER TO THE SHIPPING DOCUMENTS ACCOMPANYING THE SHIPMENT OF THIS PRODUCT.

DOT CLASSIFICATION

PROPER SHIPPING NAME	NOT APPLICABLE

The information provided herein may not include the impact of additional regulatory requirements (eg, for materials meeting the definition of a hazardous waste under RCRA, hazardous substances under CERCLA, and/or

marine pollutants under CWA or other similar federal, state or local laws) or any associated exceptions or exemptions under regulations applicable to the transport of this material.

15. REGULATORY INFORMATION

USA

TSCA — This product is manufactured in compliance with all provisions of the Toxic Substances Control Act, 15 U.S.C. 2601 et. seq.

SARA/TITLE III	CAS NUMBER	CONCENTRATION (% by weight)
Contains no substances at or above the reporting threshold under Section 313.		

CALIFORNIA PROPOSITION 65

WARNING: This product contains the following chemicals that are known to the State of California to cause cancer, birth defects or other reproductive harm.

Unless a concentration is specified in Section 2 of the MSDS, the below chemical/s are present in trace amounts.

COMPONENT	CAS NUMBER
None reportable.	

16. OTHER INFORMATION

HMIS® Hazard Ratings

HMIS® ratings are based on a 0-4 rating scale, with 0 representing minimal hazards or risks, and 4 representing significant hazards or risks. Although HMIS® ratings are not required on MSDSs by OSHA's 29 CFR 1910.1200, we choose to provide them as a service to our customers using HMIS®. These ratings are to be used only with a fully implemented HMIS® program. To deal adequately with the safe handling of this material, all the information contained in this MSDS must be considered.

NPCA recommends that employers must determine appropriate PPE for the actual conditions under which this product is used in their workplace. For information on PPE codes, consult the HMIS® Implementation Manual.

HMIS® is a registered trademark of the National Paint and Coatings Association (NPCA).

Health	Flammability	Reactivity
1	1	0

MSDS DATE	15-December-2008
FOR INFORMATION CONTACT:	Akzo Nobel Surface Chemistry LLC Phone: 1-888-331-6212

ADDITIONAL INFORMATION: The information given and the recommendations made herein apply to our product(s) alone and are not combined with other product(s). Such are based on our research and on data from other reliable sources and are believed to be accurate. No guaranty of accuracy is made. It is the purchaser's

responsibility before using any product to verify this data under their own operating conditions and to determine whether the product is suitable for their purposes.

Links

Overview

Paper and Articles

Formulations

Presentations

Sample Order Page

Appendix 1.2 Screening Test Celquat L200

Screening Tests Biopolymer Celquat L200

This appendix summarizes the result of performed screening test. In this laboratory test the suitability of the biopolymers Celquat L200 to retardate the polymerization of silica was screened. In addition, the impact of ammonium in small quantities was evaluated on the concentration of dissolved silica over time. The screening test was performed prior to the retardation, attachment and infiltration experiments.

Set-up

Silica biopolymer mixtures were created with an initial silica concentration of 1495 ppm SiO_2 (± 63.5 ppm SiO_2) and initial biopolymer concentration of 1987, 700, 160, 54 or 0 ppm L200. After pH adjustment to 7.5 dissolved silica concentrations were monitored for period of 15 days. The tested biopolymer dosage varied thereby in the range of 133% to 0%. Biopolymer dosage equals the weight ratio between initial biopolymer to silica concentration * 100%. Silica ammonium mixtures were created containing an initial concentration of 1538 ppm SiO_2 (± 25 ppm SiO_2 and ammonium concentration of 9.9, 1.1, 0.3, 0.1 and 0 ppm NH_4^+. The start of the test is the moment of pH adjustment from >11.5 to 6.5 – 7.2. The flasks were continuously agitated at speed of 120 rotations per minute at ambient temperature (20 – 22 ^{0}C).

Methods

The dissolved silica concentration was measured after different moments in time by means of the silicomolybdate acid method (Coradin, 2004). However not filtration was performed before analyses, though the samples rested for on hour before sample collection. In addition, the transparency of the fluids was inspected visually and by microscope imaging.

Results: Biopolymer L200

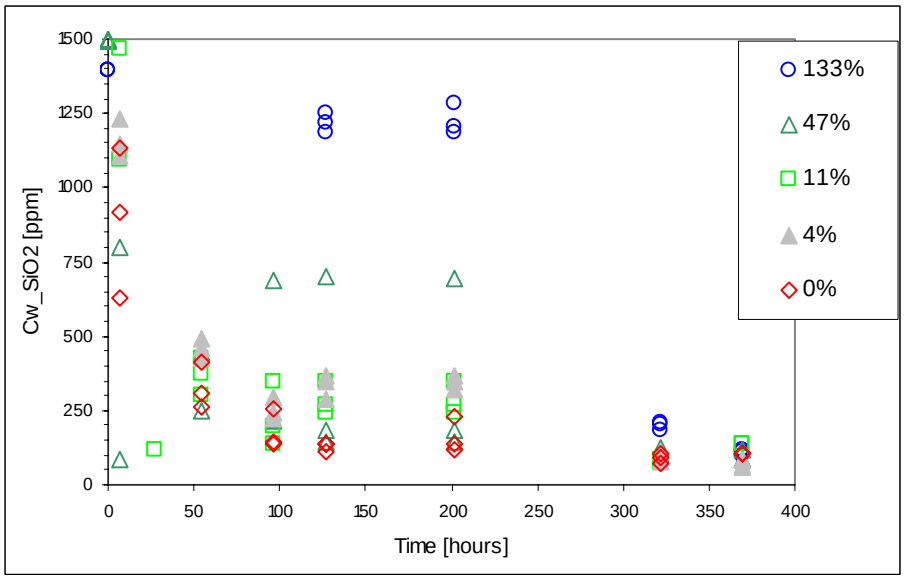

Figure A1.1: Screening test L200

The results of the screening tests indicated the following:

- Concentrations of dissolved silica exceeding the initial concentration of ca. 1500 ppm SiO2 were measured. At biopolymer dosage of 133% a dissolved concentration of ca. 4900 ppm SiO_2 was measured after 4 hours of incubation. Since no filtration was performed prior to silica quantification, the high concentration was most likely related to an increased turbidity. Thus the dissolved silica measure as performed in this test, indicated a combined value for dissolved silica and dispersed colloidal particles. The obtained values were thereby indicative and did not represent actual dissolved silica concentration.
- Nevertheless, the graph shows that the obtained values at 4% and 11% exceed the mixtures without biopolymer addition (0%). This was an indication for increased dissolved and/or colloidal silica in the suspension. The increased values at 47% biopolymer dosage for one flask did not agree with the other two flasks.
- The impact of the biopolymer ceased after 200 hours and within 322 hours.

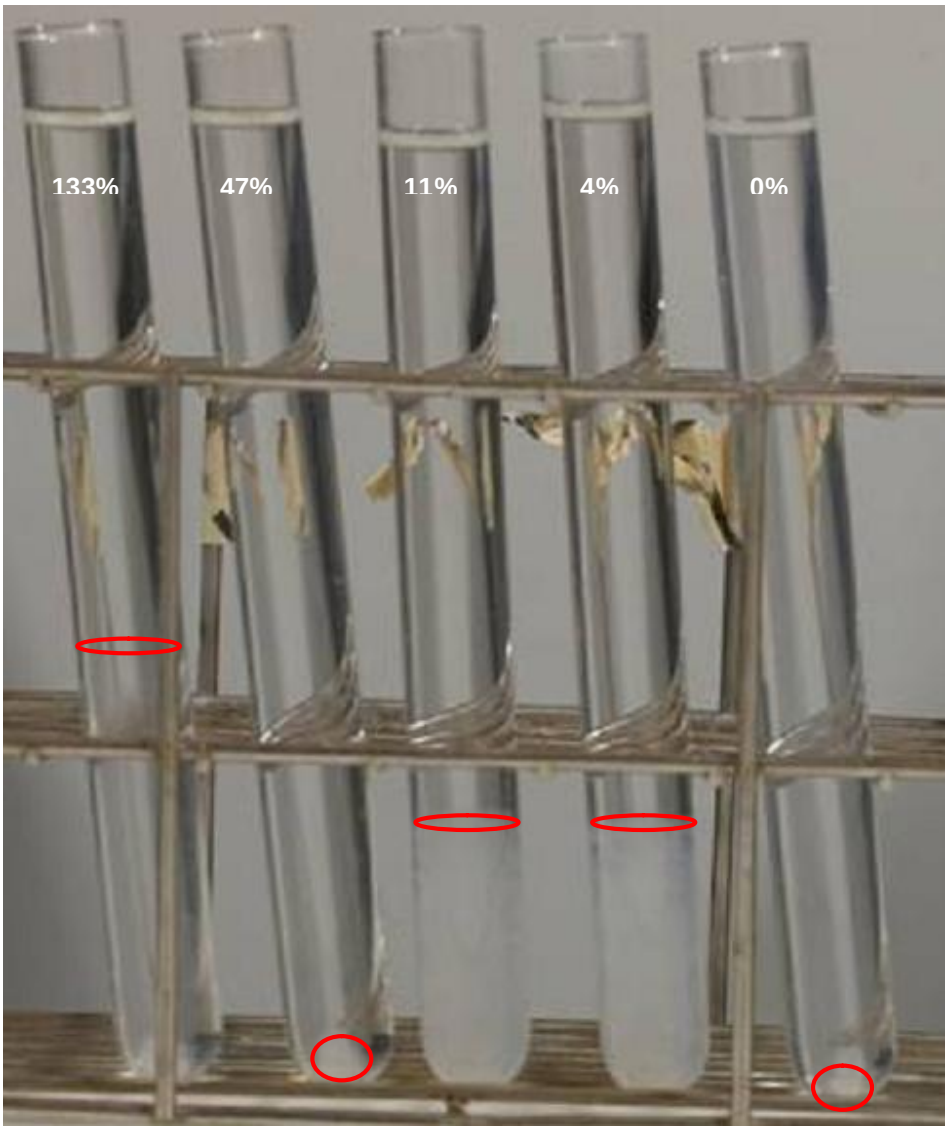

Figure A1.2: Image of silica biopolymer L200 suspensions after 15 days at pH ~7

All mixtures became turbid from the moment the pH dropped below ca. 9. Over time a precipitate became visible in some of the samples. There was a clear difference in color (white or not), turbidity and structure (gel-like network, plates or more spheroid forms) between the mutual samples. See Figure A.1.2. and for an indication of the observed differences in color, transparency and structural features of the formed precipitate after 15 days of incubation. When no biopolymer was added to the silica solution, i.e. the 'Blanco', the formation of white sedimenting flocks occurred in minutes after pH adjustment.

At 11% and 4% biopolymer dosage the presence of a white more 'fluffy' precipitate was very clear. At 133% and 47% biopolymer dosage a separation of two distinctive layers was observed after 24 hours of rest. The lower layer was a little less transparent and showed faint white glow. In addition, at 133% a denser white phase was observed at the bottom of the tubes. At 47% a separate denser flocks were visible within the lower layer. Unfortunately this is not visible in Figure A.1.2. Therefore, the liquid was placed under a microscope.

Results: Ammonium chloride addition (NH_4Cl)

NH_4^+ as a cation in solution (added as the salt NH_4Cl) could, at low concentrations, inhibit precipitation of silica at neutral pH conditions. However, we were not able to reproduce that result. Although the precipitate was not white and fluffy gel-like structure. See picture 2.

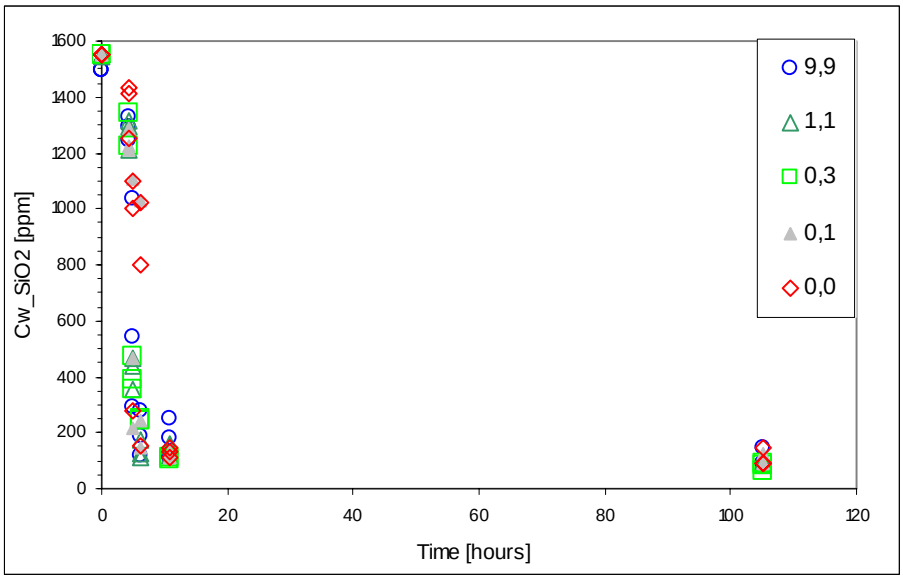

Figure A1.4: Screening test ammonium (NH_4^+)

The results of the screening tests indicated the following: ammonium did not result in a retardation of the polymerization process, at least not at ammonium concentration range of 9.9 to 0.1 ppm NH_4^+. Visually there was only a small precipitate visible after rest of 1 hour, at all ammonium dosages.

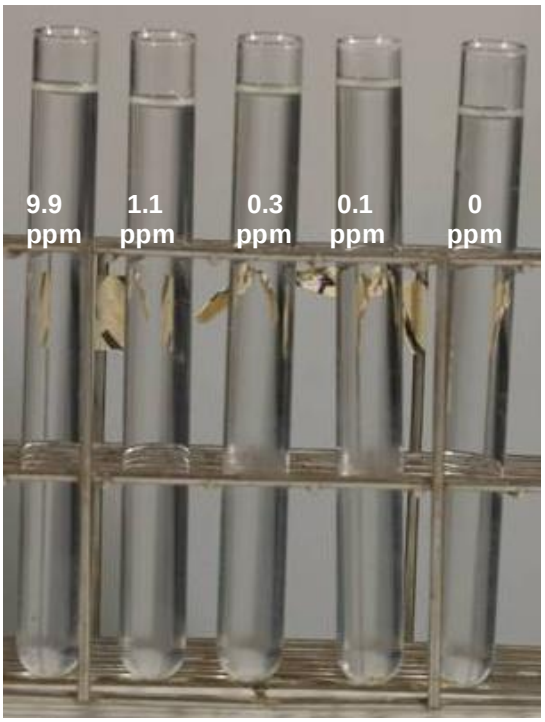

Figure A1.4: Image of silica ammonium mixtures after ca. 4 days at pH ~7

Appendix 2 Photon Correlation Spectroscopy

Dynamic Light Scattering: An Introduction in 30 Minutes

Introduction

Dynamic **L**ight **S**cattering (sometimes referred to as **P**hoton **C**orrelation **S**pectroscopy or **Q**uasi-Elastic **L**ight **S**cattering) is a technique for measuring the size of particles typically in the sub micron region.

Brownian Motion

DLS measures Brownian motion and relates this to the size of the particles. Brownian motion is the random movement of particles due to the bombardment by the solvent molecules that surround them. Normally DLS is concerned with measurement of particles suspended within a liquid.

The larger the particle, the slower the Brownian motion will be. Smaller particles are “kicked” further by the solvent molecules and move more rapidly. An accurately known temperature is necessary for DLS because knowledge of the viscosity is required (because the viscosity of a liquid is related to its temperature). The temperature also needs to be stable, otherwise convection currents in the sample will cause non-random movements that will ruin the correct interpretation of size.

The velocity of the Brownian motion is defined by a property known as the translational diffusion coefficient (usually given the symbol, D).

The Hydrodynamic Diameter

The size of a particle is calculated from the translational diffusion coefficient by using the Stokes-Einstein equation;

$$d(H) = \frac{kT}{3\pi\eta D}$$

where:-

$d(H)$ = hydrodynamic diameter

D = translational diffusion coefficient

k = Boltzmann’s constant

T = absolute temperature

η = viscosity

Note that the diameter that is measured in DLS is a value that refers to how a particle diffuses within a fluid so it is referred to as a hydrodynamic diameter. The diameter that is obtained by this technique is the diameter of a sphere that has the same translational diffusion coefficient as the particle.

The translational diffusion coefficient will depend not only on the size of the particle “core”, but also on any surface structure, as well as the concentration and type of ions in the medium. Factors that affect the diffusion speed of particles are discussed in the following sections.

Ionic Strength of Medium

The ions in the medium and the total ionic concentration can affect the particle diffusion speed by changing the thickness of the electric double layer called the Debye length (K^{-1}). Thus a low conductivity medium will produce an extended double layer of ions around the particle, reducing the diffusion speed and resulting in a larger, apparent hydrodynamic diameter. Conversely, higher conductivity media will suppress the electrical double layer and the measured hydrodynamic diameter.

The performance of a DLS instrument is normally verified by measurement of a suitable polystyrene latex standard. If the standard needs to be diluted prior to measurement, then dilution in an appropriate medium is important. The International Standard on DLS (ISO13321 Part 8 1996) says that dilution of any polystyrene standard should be made in 10mM NaCl. This concentration of salt will suppress the electrical double layer and ensure that the hydrodynamic diameter reported will be the same as the hydrodynamic diameter on the certificate or the expected diameter.

Surface Structure

Any change to the surface of a particle that affects the diffusion speed will correspondingly change the apparent size of the particle. An adsorbed polymer layer projecting out into the medium will reduce the diffusion speed more than if the polymer is lying flat on the surface. The nature of the surface and the polymer, as well as the ionic concentration of the medium can affect the polymer conformation, which in turn can change the apparent size by several nanometres.

Non-Spherical Particles

All particle-sizing techniques have an inherent problem in describing the size of non-spherical particles. The sphere is the only object whose size

can be unambiguously described by a single figure.

Different techniques are sensitive to different properties of the particle, e.g. projected area, density, scattering intensity, and in general will produce different mean sizes and size distributions for any given sample. Even the size in a microscope image will depend on parameters set such as edge contrast etc. It is important to understand that none of these results are inherently "correct".

The hydrodynamic diameter of a non-spherical particle is the diameter of a sphere that has the same translational diffusion speed as the particle.

If the shape of a particle changes in a way that affects the diffusion speed, then the hydrodynamic size will change. For example, small changes in the length of a rod-shaped particle will directly affect the size, whereas changes in the rod's diameter, which will hardly affect the diffusion speed, will be difficult to detect.

The conformation of proteins and macromolecules are usually dependent on the exact nature of the dispersing medium. As conformational changes will usually affect the diffusion speed, DLS is a very sensitive technique for detecting these changes.

Light Scattering Theories

Rayleigh Scattering

If the particles are small compared to the wavelength of the laser used (typically less than d =λ/10 or around 60nm for a He-Ne laser), then the scattering from a particle illuminated by a vertically polarised laser will be essentially isotropic, i.e. equal in all directions.

The Rayleigh approximation tells us that $I \alpha d^6$ and also that $I \alpha 1/\lambda^4$, where I = intensity of light scattered, d = particle diameter and λ = laser wavelength. The d^6 term tells us that a 50nm particle will scatter 10^6 or one million times as much light as a 5nm particle. Hence there is a danger that the light from the larger particles will swamp the scattered light from the smaller ones. This d^6 factor also means it is difficult with DLS to measure, say, a mixture of 1000nm and 10nm particles because the contribution to the total light scattered by the small particles will be extremely small. The inverse relationship to λ^4 means that a higher scattering intensity is obtained as the wavelength of the laser used decreases.

Mie Theory

When the size of the particles becomes roughly equivalent to the wavelength of the illuminating light, then a complex function of maxima and minima with respect to angle is observed.

Figure 1 shows the theoretical plot of the log of the relative scattering intensity versus particle size at angles of 173° (the detection angle of the Zetasizer Nano S and Nano ZS in aqueous media) and 90° (the detection angle of the Nano S90 and Nano ZS90) assuming a laser wavelength of 633nm, real refractive index of 1.59 and an imaginary refractive index of 0.001.Mie theory is the only theory that explains correctly the maxima and minima in the plot of intensity with angle and will give the correct answer over all wavelengths, sizes and angles. Mie theory is used in the Nano software for conversion of the intensity distribution into volume.

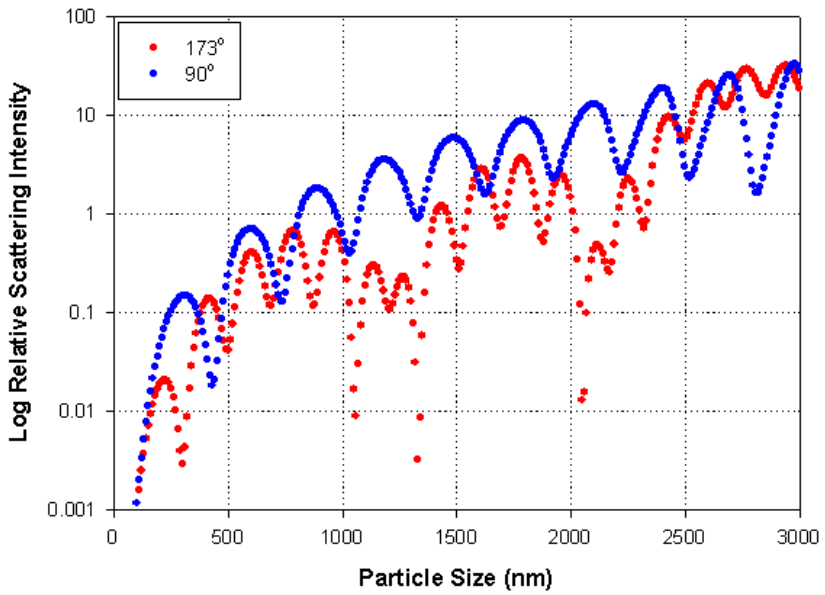

Figure 1: Theoretical plot of the log of the relative intensity of scattering versus particle size at angles of 173° (the detection angle of the Nano S, and Nano ZS in aqueous media) and 90° (the detection angle of the Nano S90 and Nano ZS90) assuming a laser beam at a wavelength of 633nm, real refractive index of 1.59 and an imaginary refractive index of 0.001

How DLS Works

In dynamic light scattering, the speed at which the particles are diffusing due to Brownian motion is measured**.** **T**his is done by measuring the rate at which the intensity of the scattered light fluctuates when detected using a suitable optical arrangement. How do these fluctuations in the intensity of scattered light arise?

Imagine if a cuvette, containing particles which are stationary, is illuminated by a laser and a frosted glass screen is used to view the sample cell. A classical speckle pattern would be seen (figure 2). The speckle pattern will be stationary both in speckle size and position because the whole system is stationary. The dark spaces are where the phase additions of the scattered light are mutually destructive and cancel each other out (figure 3A). The bright blobs of light in the speckle pattern are where the light scattered from the particles arrives with the same phase and interfere constructively to form a bright patch (figure 3B).

For a system of particles undergoing Brownian motion, a speckle pattern is observed where the position of each speckle is seen to be in constant motion. This is because the phase addition from the moving particles is constantly evolving and forming new patterns. The rate at which these intensity fluctuations occur will depend on the size of the particles. Figure 4 schematically illustrates typical intensity fluctuations arising from a dispersion of large particles and a dispersion of small particles. The small particles cause the intensity to fluctuate more rapidly than the large ones.

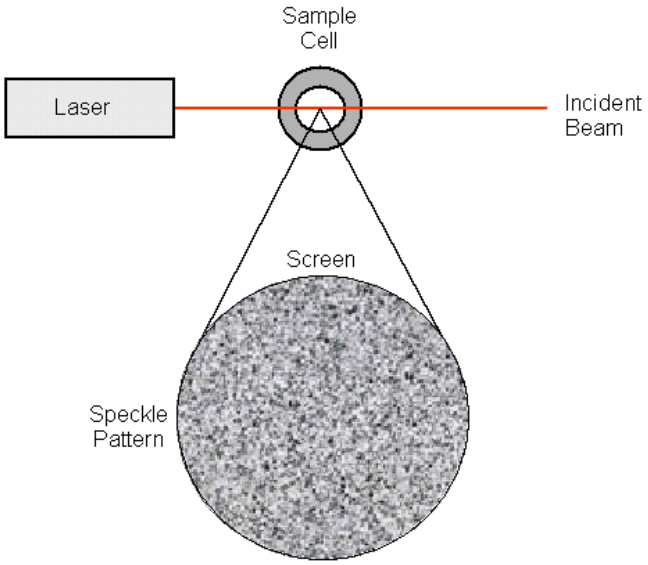

Figure 2: Schematic representation of a speckle pattern

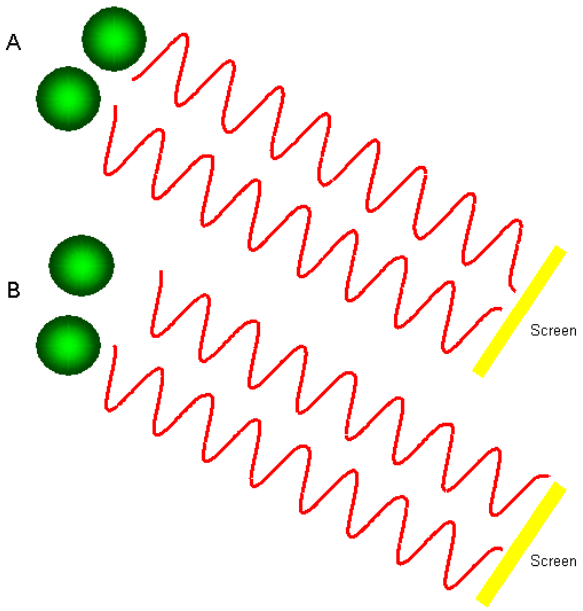

Figure 3: The observed signal depends on the phase addition of the scattered light falling on the detector. In example A, two beams interfere and 'cancel each other out' resulting in a decreased intensity detected. In example B, two beams interfere and 'enhance each other' resulting in an increased intensity detected.

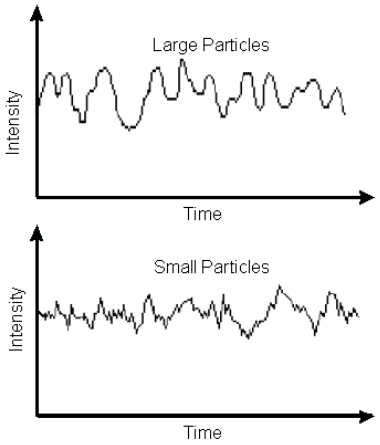

Figure 4: Typical intensity fluctuations for large and small particles

It is possible to directly measure the spectrum of frequencies contained in the intensity fluctuations arising from the Brownian motion of particles, but it is inefficient to do so. The best way is to use a device called a digital auto correlator.

How a Correlator Works

A correlator is basically a signal comparator. It is designed to measure the degree of similarity between two signals, or one signal with itself at varying time intervals.

If the intensity of a signal is compared with itself at a particular point in time and a time much later, then for a randomly fluctuating signal it is obvious that the intensities are not going to be related in any way, i.e. there will be no correlation between the two signals (figure 5). Knowledge of the initial signal intensity will not allow the signal intensity at time t = infinity to be predicted. This will be true of any random process such as diffusion.

However, if the intensity of signal at time = t is compared to the intensity a very small time later (t+δt), there will be a strong relationship or correlation between the intensities of two signals. The two signals are strongly or well correlated.

If the signal, derived from a random process such as Brownian motion, at t is compared to the signal at t+2δt, there will still be a reasonable comparison or correlation between the two signals, but it will not be as good as the comparison at t and t+δt. The correlation is reducing with time. The period of time δt is usually very small, maybe nanoseconds or microseconds and is called the sample time of the correlator. t = ∞ maybe of the order of a millisecond or tens of milliseconds.

If the signal intensity at t is compared with itself then there is perfect correlation as the signals are identical. Perfect correlation is indicated by unity (1.00) and no correlation is indicated by zero (0.00).

If the signals at t+2δt, t+3δt, t+4δt etc. are compared with the signal at t, the correlation of a signal arriving from a random source will decrease with time until at some time, effectively t = ∞, there will be no correlation.

If the particles are large the signal will be changing slowly and the correlation will persist for a long time (figure 6). If the particles are small and moving rapidly then correlation will reduce more quickly (figure 7).

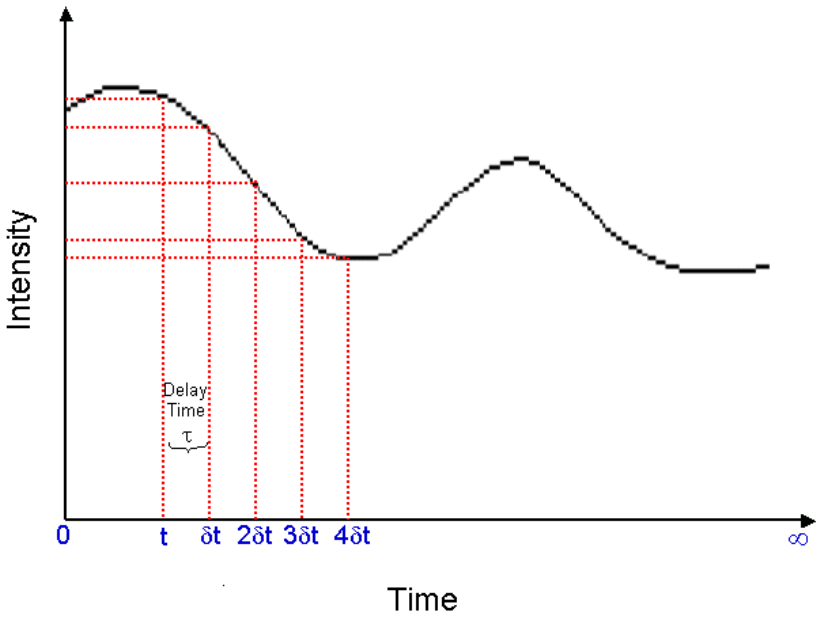

Figure 5: Schematic showing the fluctuation in the intensity of scattered light as a function of time

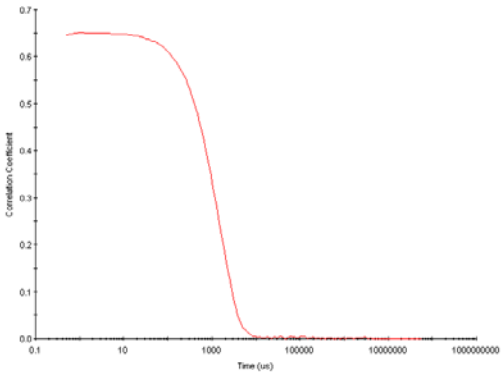

Figure 6: Typical correlogram from a sample containing large particles in which the correlation of the signal takes a long time to decay

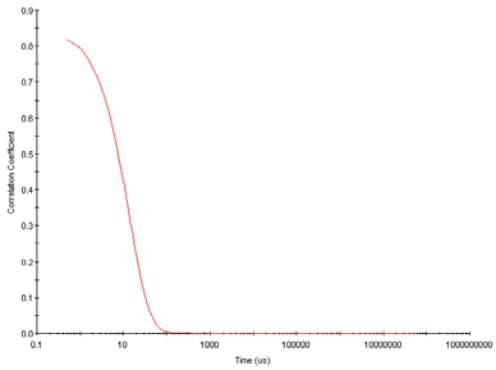

Figure 7: Typical correlogram from a sample containing small particles in which the correlation of the signal decays more rapidly

Viewing the correlogram from a measurement can give a lot of information about the sample. The time at which the correlation starts to significantly decay is an indication of the mean size of the sample. The steeper the line, the more monodisperse the sample is. Conversely, the more extended the decay becomes, the greater the sample polydispersity.

The Correlation Function

It has been seen that particles in a dispersion are in a constant, random Brownian motion and that this causes the intensity of scattered light to fluctuate as a function of time. The correlator used in a PCS instrument will construct the correlation function $G(\tau)$ of the scattered intensity:

$$G(\tau) = \langle I(t).I(t+\tau) \rangle$$

Where τ =the time difference (the sample time) of the correlator.

For a large number of monodisperse particles in Brownian motion, the correlation function (given the symbol [G]) is an exponential decaying function of the correlator time delay τ:

$$G(\tau) = A[1 + B \exp(-2\Gamma\tau)]$$

where A = the baseline of the correlation function, B = intercept of the correlation function.

$\Gamma = Dq^2$

where D = translational diffusion coefficient

$q = (4 \pi n / \lambda_o) \sin(\theta/2)$

where n = refractive index of dispersant, λ_o = wavelength of the laser, θ = scattering angle.

For polydisperse samples, the equation can be written as:

$$G(\tau) = A[1 + B\, g_1(\tau)^2]$$

where $g_1(\tau)$ = is the sum of all the exponential decays contained in the correlation function.

Obtaining Size Information From the Correlation Function

Size is obtained from the correlation function by using various algorithms. There are two approaches that can be taken (1) fit a single exponential to the correlation function to obtain the mean size (z-average diameter) and an estimate of the width of the distribution (polydispersity index) (this is called the Cumulants analysis and is defined in ISO13321 Part 8), or (2) fit a multiple exponential to the correlation function to obtain the distribution of particle sizes (such as Non-negative least squares (NNLS) or CONTIN.

The size distribution obtained is a plot of the relative intensity of light scattered by particles in various size classes and is therefore known as an intensity size distribution.

If the distribution by intensity is a single fairly smooth peak, then there is little point in doing the conversion to a volume distribution using the Mie theory. If the optical parameters are correct, this will just provide a slightly different shaped peak. However, if the plot shows a substantial tail, or more than one peak, then Mie theory can make use of the input parameter of sample refractive index to convert the intensity distribution to a volume distribution. This will then give a more realistic view of the importance of the tail or second peak present. In general terms it will be seen that:-

d(intensity) > d(volume) > d(number)

A very simple way of describing the difference between intensity, volume and number distributions is to consider 2 populations of spherical particles of diameter 5nm and 50nm present in equal numbers (figure 8). If a number distribution of these 2 particle populations is plotted, a plot consisting of 2 peaks (positioned at 5 and 50nm) of a 1 to 1 ratio would be obtained. If this number distribution was converted into volume, then the 2 peaks would change to a 1:1000 ratio (because the volume of a sphere is equal to $4/3\pi(d/2)^3$). If this was further converted into an intensity distribution, a 1:1000000 ratio between the 2 peaks would be obtained (because the intensity of scattering is proportional to d^6 (from Rayleighs approximation)). Remember that in DLS, the distribution obtained from a measurement is based on intensity.

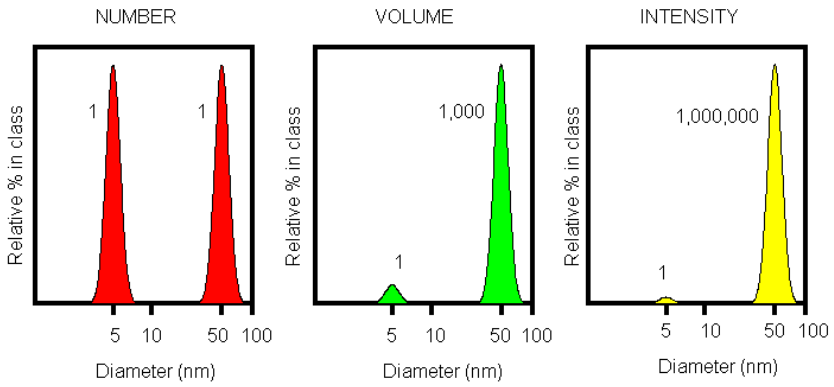

Figure 8: Number, volume and intensity distributions of a bimodal mixture of 5 and 50nm lattices present in equal numbers

Optical Configuration of a Dynamic Light Scattering Instrument

A typical dynamic light scattering system comprises of six main components. Firstly, a laser ① provides a light source to illuminate the sample contained in a cell ②. For dilute concentrations, most of the laser beam passes through the sample, but some is scattered by the particles within the sample at all angles. A detector ③ is used to measure the scattered light. In the Zetasizer Nano series, the detector position will be at either 173° or 90°, depending upon the particular model.

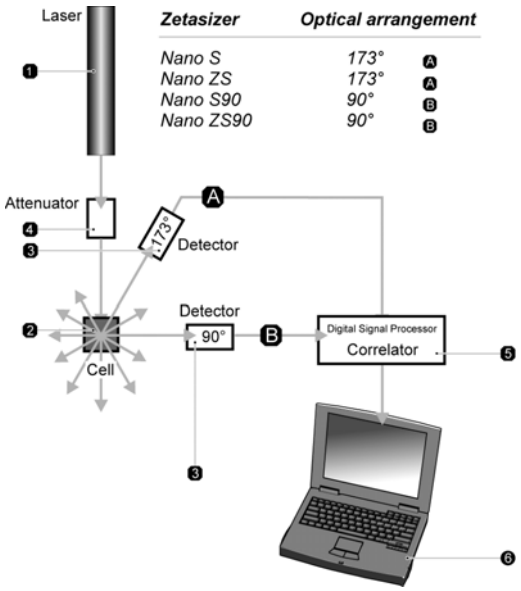

Figure 9: Optical configurations of the Zetasizer Nano series for dynamic light scattering measurements

The intensity of scattered light must be within a specific range for the detector to successfully measure it. If too much light is detected, then the detector will become saturated. To overcome this, an attenuator ④ is used to reduce the intensity of the laser source and hence reduce the intensity of scattering. For samples that do not scatter much light, such as very small particles or samples of low concentration, the amount of scattered light must be increased. In this situation, the attenuator will allow more laser light through to the sample.

For samples that scatter more light, such as large particles or samples at higher concentration, the intensity of scattered light must be decreased. The appropriate attenuator position is automatically determined by the Nano software and covers a transmission range of 100% to 0.0003%.

The scattering intensity signal from the detector is passed to a digital processing board called a correlator ⑤. The correlator compares the scattering intensity at successive time intervals to derive the rate at which the intensity is varying. This correlator information is then passed to a computer ⑥, where the Nano software will analyze the data and derive size information.

Unique Features of the Zetasizer Nano

Non-Invasive Backscatter Detection (NIBS)

The Nano S and Nano ZS instruments detect the scattering information at 173°. This is known as backscatter detection. In addition, the optics are not in contact with the sample and hence the detection optics are said to be non-invasive. There are several advantages in using non-invasive backscatter detection:

- The laser does not have to travel through the entire sample. This reduces an effect called multiple scattering, where light from one particle is itself scattered by other particles. As the light passes through a shorter path length of the sample, then higher concentrations of sample can be measured.
- Contaminants such as dust particles within the dispersant are typically large compared to the sample size. Large particles mainly scatter in the forward direction. Therefore, by using backscatter detection, the effects of dust are greatly reduced.

Variable Measurement Position For Sizing

The measurement position within the cuvette of the Nano S and Nano ZS can be changed. This measurement position is changed by moving the focusing lens and is determined automatically by the Nano software (figure 10).

For small particles, or samples at low concentrations, it is beneficial to maximise the amount of scattering from the sample. As the laser passes through the wall of the cuvette and into the dispersant, the laser will cause “flare”.

This flare may swamp the signal from the scattering particles. Moving the measurement point away from the cuvette wall towards the centre of the cuvette will remove this effect (figure 10a).

Large particles or samples at high concentrations scatter much more light. In this situation, measuring closer to the cuvette wall will reduce the effect of multiple scattering by minimising the path length over which the scattered light has to pass (figure 10b). The measurement position is determined automatically through a combination of the intercept of the correlation function and the intensity of the light scattered.

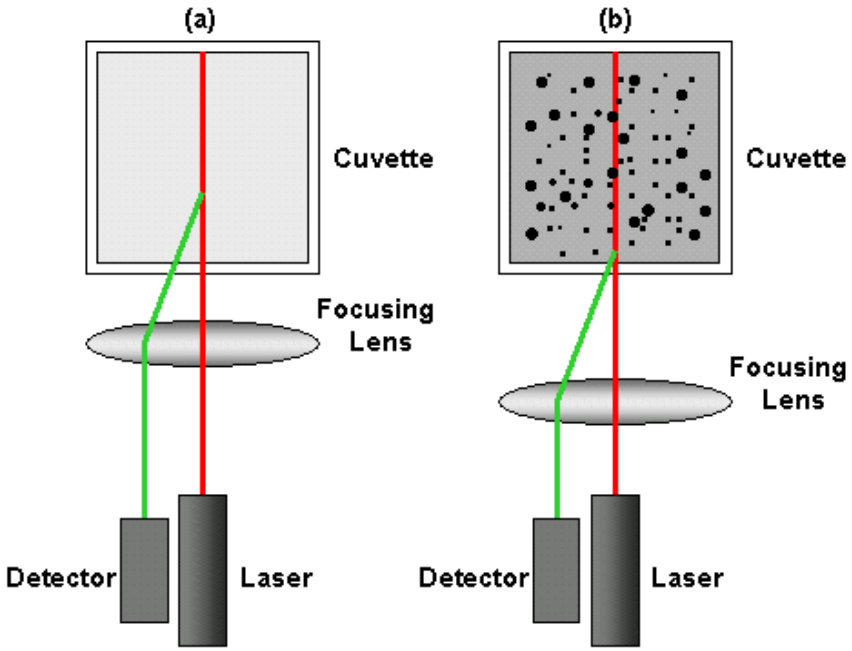

Figure 10: Schematic diagram showing the measurement position for (a) small, weakly scattering samples and for (b) concentrated, opaque samples. The change in measurement position is achieved by moving the focusing lens accordingly

Additional Reading

[1] International Standard ISO13321 Methods for Determination of Particle Size Distribution Part 8: Photon Correlation Spectroscopy, International Organisation for Standardisation (ISO) 1996.

[2] Dahneke, B.E. (ed) Measurement of Suspended Particles by Quasi-elastic Light Scattering, Wiley, 1983.

[3] Pecora, R. Dynamic Light Scattering: Applications of Photon Correlation Spectroscopy, Plenum Press, 1985.

[4] Washington, C. Particle Size Analysis In Pharmaceutics And Other Industries: Theory And Practice, Ellis Horwood, England, 1992.

[5] Johnson, C.S. Jr. and Gabriel, D.A. Laser Light Scattering, Dover Publications, Inc., New York 1981

Malvern Instruments Ltd

Enigma Business Park • Grovewood Road • Malvern • Worcestershire • UK • WR14 1XZ
Tel: +44 (0)1684 892456 • Fax: +44 (0)1684 892789

Malvern Instruments Worldwide

Sales and service centers in over 50 countries for details visit www.malvern.co.uk/contact

Appendix 3 Zeta Potential

Zeta Potential
An Introduction in 30 Minutes

Introduction

Zeta potential is a physical property which is exhibited by any particle in suspension. It can be used to optimize the formulations of suspensions and emulsions. Knowledge of the zeta potential can reduce the time needed to produce trial formulations. It is also an aid in predicting long-term stability.

Colloid Science

Three of the fundamental states of matter are solids, liquids and gases. If one of these states is finely dispersed in another then we have a 'colloidal system'. These materials have special properties that are of great practical importance.

There are various examples of colloidal systems that include aerosols, emulsions, colloidal suspensions and association colloids.

In certain circumstances, the particles in a dispersion may adhere to one another and form aggregates of successively increasing size, which may settle out under the influence of gravity. An initially formed aggregate is called a floc and the process of its formation flocculation. The floc may or may not sediment or phase separate. If the aggregate changes to a much denser form, it is said to undergo coagulation. An aggregate usually separates out either by sedimentation (if it is more dense than the medium) or by creaming (if it less dense than the medium). The terms flocculation and coagulation have often been used interchangeably. Usually coagulation is irreversible whereas flocculation can be reversed by the process of deflocculation. Figure 1 schematically represents some of these processes.

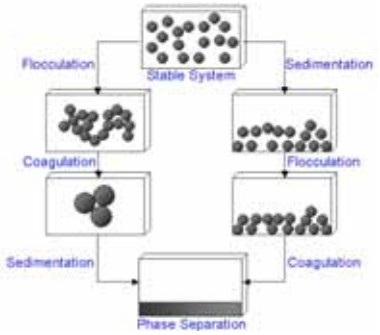

Figure 1: Schematic diagram showing various mechanisms where stability may be lost in a colloidal dispersion

Colloidal Stability and DVLO Theory

The scientists Derjaguin, Verwey, Landau and Overbeek developed a theory in the 1940s which dealt with the stability of colloidal systems. DVLO theory suggests that the stability of a particle in solution is dependent upon its total potential energy function V_T. This theory recognizes that V_T is the balance of several competing contributions:

$$V_T = V_A + V_R + V_S$$

V_S is the potential energy due to the solvent, it usually only makes a marginal contribution to the total potential energy over the last few nanometers of separation. Much more important is the balance between V_A and V_R, these are the attractive and repulsive contributions. They potentially are much larger and operate over a much larger distance

$$V_A = -A/(12\,\pi\,D^2)$$

where A is the Hamaker constant and D is the particle separation. The repulsive potential V_R is a far more complex function.

$$V_R = 2\,\pi\,\varepsilon\,a\,\zeta^2\,\exp(-\kappa D)$$

where a is the particle radius, π is the solvent permeability, κ is a function of the ionic composition and ζ is the zeta potential.

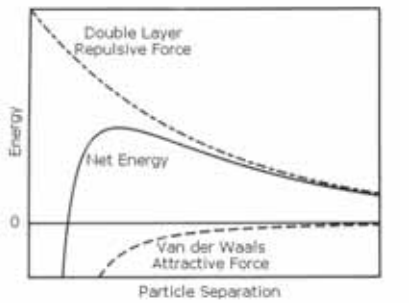

Figure 2(a): Schematic diagram of the variation of free energy with particle separation according to DVLO theory.

DVLO theory suggests that the stability of a colloidal system is determined by the sum of these van der Waals attractive (V_A) and electrical double layer repulsive (V_R) forces that exist between particles as they approach each other due to the Brownian motion they are undergoing. This theory proposes that an energy barrier resulting from the repulsive force prevents two particles approaching one another and adhering together (figure 2 (a)). But if the particles collide with sufficient energy to overcome that barrier, the

attractive force will pull them into contact where they adhere strongly and irreversibly together.

Therefore if the particles have a sufficiently high repulsion, the dispersion will resist flocculation and the colloidal system will be stable. However if a repulsion mechanism does not exist then flocculation or coagulation will eventually take place.

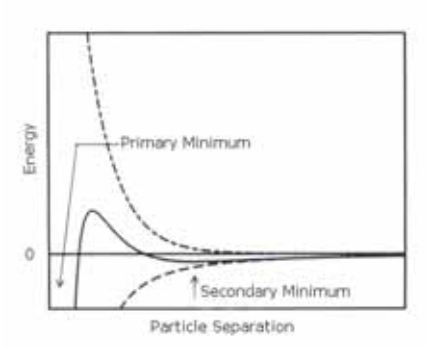

Figure 2(b): Schematic diagram of the variation of free energy with particle separation at higher salt concentrations showing the possibility of a secondary minimum.

If the zeta potential is reduced (e.g. in high salt concentrations), there is a possibility of a "secondary minimum" being created, where a much weaker and potentially reversible adhesion between particles exists (figure 2 (b)). These weak flocs are sufficiently stable not to be broken up by Brownian motion, but may disperse under an externally applied force such as vigorous agitation.

Therefore to maintain the stability of the colloidal system, the repulsive forces must be dominant. How can colloidal stability be achieved? There are two fundamental mechanisms that affect dispersion stability (figure 3):

- Steric repulsion - this involves polymers added to the system adsorbing onto the particle surface and preventing the particle surfaces coming into close contact. If enough polymer adsorbs, the thickness of the coating is sufficient to keep particles separated by steric repulsions between the polymer layers, and at those separations the van der Waals forces are too weak to cause the particles to adhere.
- Electrostatic or charge stabilization - this is the effect on particle interaction due to the distribution of charged species in the system.

Each mechanism has its benefits for particular systems. Steric stabilization is simple, requiring just the addition of a suitable polymer. However it can be difficult to subsequently flocculate the system if this is required, the polymer can be expensive and in some cases the polymer is undesirable e.g. when

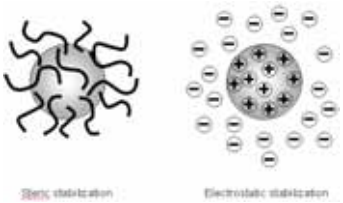

Figure 3: Steric and electrostatic stabilization mechanisms of colloidal dispersions

a ceramic slip is cast and sintered, the polymer has to be 'burnt out'. This causes shrinkage and can lead to defects.

Electrostatic or charge stabilization has the benefits of stabilizing or flocculating a system by simply altering the concentration of ions in the system. This is a reversible process and is potentially inexpensive.

It has long been recognised that the zeta potential is a very good index of the magnitude of the interaction between colloidal particles and measurements of zeta potential are commonly used to assess the stability of colloidal systems.

Origins of Surface Charge

Most colloidal dispersions in aqueous media carry an electric charge. There are many origins of this surface charge depending upon the nature of the particle and it's surrounding medium but we will consider the more important mechanisms.

Ionisation of Surface Groups

Dissociation of acidic groups on the surface of a particle will give rise to a negatively charged surface. Conversely, a basic surface will take on a positive charge (figure 4). In both cases, the magnitude of the surface charge depends on the acidic or basic strengths of the surface groups and on the pH of the solution. The surface charge can be reduced to zero by suppressing the surface ionisation by decreasing the pH in case of negatively charged particles (figure 4(a)) or by increasing the pH in the case of positively charged particles (figure 4(b)).

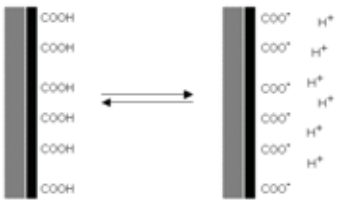

Figure 4(a): Origin of surface charge by ionisation of acidic groups to give a negatively charged surface

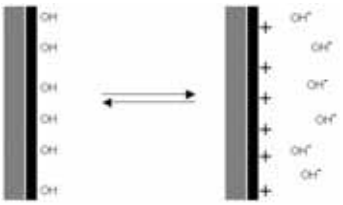

Figure 4(b): Origin of surface charge by ionisation of basic groups to give a positively charged surface

Differential loss of ions from the crystal lattice

As an example, consider a crystal of silver iodide placed in water. Solution of ions occurs. If equal amounts of Ag+ and I- ions were to dissolve, the surface would be uncharged. In fact silver ions dissolve preferentially, leaving a negatively charged surface (figure 5). If Ag+ ions are now added the charge falls to zero. Further addition leads to a positively charged surface.

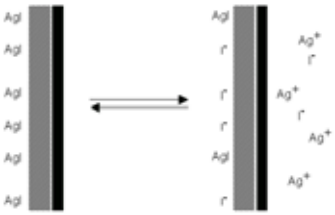

Figure 5: Origin of surface charge by differential solution of silver ions from a AgI surface

Adsorption of charged species (ions and ionic surfactants)

Surfactant ions may be specifically adsorbed on the surface of a particle, leading, in the case of cationic surfactants, to a positively charged surface (figure 6(a)) and, in the case of anionic surfactants, to a negatively charged surface (figure 6(b)).

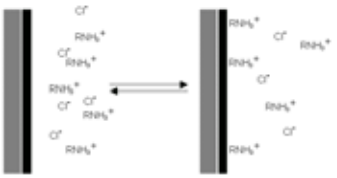

Figure 6(a): Origin of surface charge by specific adsorption of a cationic surfactant. R = hydrocarbon chain

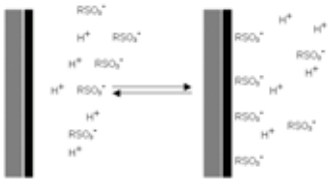

Figure 6(b): Origin of surface charge by specific adsorption of an anonic surfactant. R = hydrocarbon chain

The Electrical Double Layer

The development of a nett charge at the particle surface affects the distribution of ions in the surrounding interfacial region, resulting in an increased concentration of counter ions, ions of opposite charge to that of the particle, close to the surface. Thus an electrical double layer exists round each particle.

Zeta Potential

The liquid layer surrounding the particle exists as two parts; an inner region (Stern layer) where the ions are strongly bound and an outer (diffuse) region where they are less firmly associated. Within the diffuse layer there is a notional boundary inside which the ions and particles form a stable entity. When a particle moves (e.g. due to gravity), ions within the boundary move it. Those ions beyond the boundary stay with the bulk dispersant. The potential at this boundary (surface of hydrodynamic shear) is the zeta potential (figure 7).

The magnitude of the zeta potential gives an indication of the potential stability of the colloidal system. If all the particles in suspension have a large negative or positive zeta potential then they will tend to repel each other and there will be no tendency for the particles to come together. However, if the particles have low zeta potential values then there will be no force to prevent the particles coming together and flocculating.

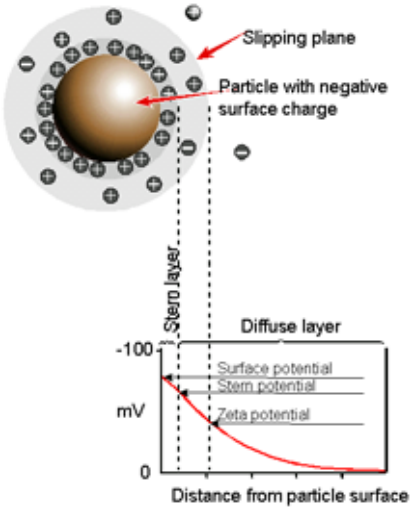

Figure 7: Schematic representation of zeta potential

The general dividing line between stable and unstable suspensions is generally taken at either +30 or -30 mV. Particles with zeta potentials more positive than +30 mV or more negative than -30 mV are normally considered stable. However, if the particles have a density different form the dispersant, they will eventually sediment forming a close packed bed (i.e. a hard cake).

Factors Affecting Zeta Potential

(1) pH

In aqueous media, the pH of the sample is one of the most important factors that affects its zeta potential. A zeta potential value on its own without defining the solution conditions is a virtually meaningless number. Imagine a particle in suspension with a negative zeta potential. If more alkali is added to this suspension then the particles tend to acquire more negative charge. If acid is added to this suspension then a point will be reached where the charge will be

neutralised. Further addition of acid will cause a build up of positive charge. Therefore a zeta potential versus pH curve will be positive at low pH and lower or negative at high pH. There may be a point where the plot passes through zero zeta potential. This point is called the isoelectric point and is very important from a practical consideration. It is normally the point where the colloidal system is least stable.

A typical plot of zeta potential versus pH is shown in figure 8. In this example, the isoelectric point of the sample is at approximately pH 5.5. In addition, the plot can be used to predict that the sample should be stable at pH values less than 4 (sufficient positive charge is present) and greater than pH 7.5 (sufficient negative charge is present). Problems with dispersion stability would be expected at pH values between 4 and 7.5 as the zeta potential values are between +30 and -30mV.

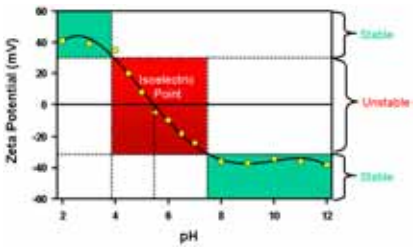

Figure 8: Typical plot of zeta potential versus pH showing the position of the isoelectric point and the pH values where the dispersion would be expected to be stable

2. Conductivity

The thickness of the double layer (κ^{-1}) depends upon the concentration of ions in solution and can be calculated from the ionic strength of the medium. The higher the ionic strength, the more compressed the double layer becomes. The valency of the ions will also influence double layer thickness.

A trivalent ion such as Al^{3+} will compress the double layer to a greater extent in comparison with a monovalent ion such as Na^{+}.

Inorganic ions can interact with charged surfaces in one of two distinct ways (i) non-specific ion adsorption where they have no effect on the isoelectric point. (ii) specific ion adsorption, which will lead to a change in the value of the isoelectric point. The specific adsorption of ions onto a particle surface, even at low concentrations, can have a dramatic effect on the zeta potential of the particle dispersion. In some cases, specific ion adsorption can lead to charge reversal of the surface.

3. Concentration of a formulation component

The effect of the concentration of a formulation component on the zeta potential can give information to assist in formulating a product to give maximum stability. The influence of known contaminants on the zeta potential of a sample can be a powerful tool in formulating the product to resist flocculation for example.

Electrokinetic Effects

An important consequence of the existence of electrical charges on the surface of particles is that they interact with an applied electric field. These effects are collectively defined as electrokinetic effects. There are four distinct effects depending on the way in which the motion is induced. These are:

Electrophoresis: the movement of a charged particle relative to the liquid it is suspended in under the influence of an applied electric field

Electroosmosis: the movement of a liquid relative to a stationary charged surface under the influence of an electric field

Streaming potential: the electric field generated when a liquid is forced to flow past a stationary charged surface

Sedimentation potential: the electric field generated when charged particles sediment

Electrophoresis

When an electric field is applied across an electrolyte, charged particles suspended in the electrolyte are attracted towards the electrode of opposite charge. Viscous forces acting on the particles tend to oppose this movement. When equilibrium is reached between these two opposing forces, the particles move with constant velocity.

The velocity is dependent on the strength of electric field or voltage gradient, the dielectric constant of the medium, the viscosity of the medium and the zeta potential.

The velocity of a particle in a unit electric field is referred to as its electrophoretic mobility. Zeta potential is related to the electrophoretic mobility by the Henry equation:-

$$U_E = \frac{2 \varepsilon z f(\kappa a)}{3\eta}$$

where U_E = electrophoretic mobility, z = zeta potential, ε = dielectric constant, η = viscosity and f(κa) = Henry's function.

The units of κ, termed the Debye length, are reciprocal length and κ^{-1} is often taken as a measure of the "thickness" of the electrical double layer. The parameter 'a' refers to the radius of the particle and therefore κa measures the ratio of the particle radius to electrical double layer thickness (figure 9). Electrophoretic determinations of zeta potential are most commonly made in aqueous media and moderate electrolyte concentration. F(κa) in this case is 1.5, and this is referred to as the Smoluchowski approximation. Therefore calculation of zeta potential

from the mobility is straightforward for systems that fit the Smoluchowski model, i.e. particles larger than about 0.2 microns dispersed in electrolytes containing more that 10^{-3} molar salt.

For small particles in low dielectric constant media (eg non-aqueous media), f(κa) becomes 1.0 and allows an equally simple calculation. This is referred to as the Huckel approximation.

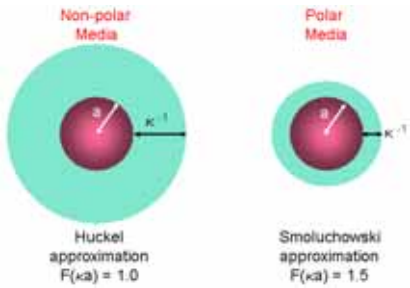

Figure 9: Schematic illustrating Huckel and Smoluchowski's approximations used for the conversion of electrophoretic mobility into zeta potential

Measuring Electrophoretic Mobility

The essence of a classical micro-electrophoresis system is a capillary cell with electrodes at either end to which a potential is applied. Particles move towards the electrode, their velocity is measured and expressed in unit field strength as their mobility.

Early methods involved the process of directly observing individual particles using ultra-microscope techniques and manually tracking their progress over a measured distance. This procedure, although still being used by many groups world wide, suffers from several disadvantages, not least that of the strenuous effort required to make a measurement, particularly with small or poorly scattering particles. The technique used in Malvern's Zetasizer Nano range of instruments is laser Doppler electrophoresis in combination with M3-PALS.

The M3-PALS Technique

The Zetasizer Nano Series uses a combination of laser Doppler velocimetry and phase analysis light scattering (PALS) in a patented technique called M3-PALS to measure particle electrophoretic mobility. Implementation of M3-PALS enables even samples of very low mobility to be analysed and their mobility distributions calculated.

PALS can give an increase in performance of greater than 100 times that associated with standard measurement techniques. This allows the measurement of high conductivity samples, plus the ability to accurately measure samples that have low particle mobilities, such as samples dispersed in non-aqueous solvents. Low applied voltages can now be used to avoid any risk of sample effects due to Joule heating.

Further information discussing the techniques of laser Doppler electrophoresis and M3-PALS can be found in various articles available on the Malvern Instruments web-site

Optical Configuration of a Zeta Potential Instrument

A zeta potential measurement system comprises of six main components (figure 10). Firstly, a laser ① is used to provides a light source to illuminate the particles within the sample. For zeta potential measurements, this light source is split to provide an incident and reference beam. The incident laser beam passes through the centre of the sample cell ②, and the scattered light at an angle of about 13° is detected ③. When an electric field is applied to the cell, any particles moving through the measurement volume will cause the intensity of light detected to fluctuate with a frequency proportional to the particle speed and this information is passed to a digital signal processor ④ and then to a computer ⑤. The Zetasizer Nano software produces a frequency spectrum from which the electrophoretic mobility and hence zeta potential is calculated. The intensity of the detected, scattered light must be within a specific range for the detector to successfully measure it. This is achieved using an attenuator ⑥, which adjusts the intensity of the light reaching the sample and hence the intensity of the scattering. To correct for any differences in the cell wall thickness and dispersant refraction, compensation optics ⑦ are installed to maintain optimum alignment.

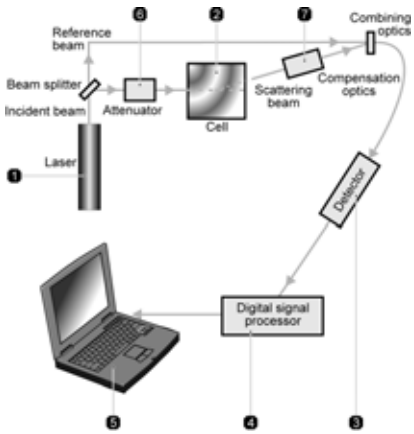

Figure 10: Optical configuration of the Zetasizer Nano series for zeta potential measurements

References

Derjaguin, B.V. and Landau, L. (1941) Acta Physiochim. URSS, 14, 633.

Verway, E.J.W. and Overbeek, J. Th. G. (1948) Theory of the Stability of Lyophobic Colloids, Elsevier, Amsterdam.

Hunter, R.J. (1988) Zeta Potential In Colloid Science: Principles And Applications, Academic Press, UK.

Shaw, D.J. (1992) Introduction To Colloid And Surface Chemistry, Butterworth Heinemann, UK.

Everett, D.H. (1994) Basic Principles Of Colloid Science, The Royal Society of Chemistry, UK.

Ross, S. and Morrison, I.D. (1988) Colloidal Systems and Interfaces, John Wiley and Sons, USA.

Lyklema, J. (2000) Fundamentals of Interface and Colloid Science: Volume 1 (Fundamentals), Academic Press, UK.

Measuring Zeta Potential: Laser Doppler Electrophoresis, Technical Note available from www.malvern.co.uk

Measuring Zeta Potential Using Phase Analysis Light Scattering (PALS), Technical Note available from www.malvern.co.uk

Measuring Zeta Potential: A New Technique, Technical Note available from www.malvern.co.uk

Simplifying the Measurement of Zeta Potential Using M3-PALS, Technical Note available from www.malvern.co.uk

Malvern Instruments Ltd

Enigma Business Park • Grovewood Road • Malvern • Worcestershire • UK • WR14 1XZ
Tel: +44 (0)1684 892456 • Fax: +44 (0)1684 892789

Malvern Instruments Worldwide

Sales and service centers in over 50 countries for details visit www.malvern.co.uk/contact

Appendix 4 Electron Scanning Microscope

Appendix 4.1 Micro structural analysis: Electron Microscopy (ESEM, SEM)

Scanning Electron Microscope (SEM) is a technique to obtain high resolution images of solid samples. The images were constructed with a Philips XL 20 scanning electron microscope, at Citg department of the Technical University of Delft. The electron microscope used is equipped with EDS (Energy Dispersed Spectroscopy) detector.

Using SEM, an image is constructed by sweeping a focused electron beam across the surface of the specimen. The specimen 'produces' signals upon the bombardment with (primary) electrons. The types of signals emitted include Auger electrons, secondary electrons, backscattered electrons, characteristic x-rays and photons of various energies. The signals are emitted from different electron penetration depths and with different emission volumes.

The signals of interest to SEM are the secondary and the backscattered electrons. The variation in secondary electron emission that takes place as the electron beam is swept across the sample surface is a measure for the difference in surface morphology. There is also a variation in the emission of backscattered electrons. The variation in backscattered electrons is directly related to the average atomic weight and thus to sample composition.

EDS analyses the radiation of the characteristic x-rays emitted by the sample. Each element has a unique atomic structure allowing X-rays that are characteristic for that specific element's atomic structure. EDS yields compositional, element specific information of a specific region at the sample surface.

When using EDS-ESEM different modes of analysis are possible, namely:

- Using SEM to visualize a soil material an image of the surface of the object is constructed. Variations in the surface morphology of a soil surface are depicted as variations in grey level of the image.
    - A photographic image depicting the distribution of elements over the surface of a sample is obtained by using SEM.SEM analysis is sensitive to variations in the average atomic weight of the solid surface. Therefore, the brightest areas in the image correspond to the highest atomic weight, i.e. to specific elements. Variations in grey level of the image are as well related to variations in elemental concentration.
    - For example, the difference in grey level wherein Calcium (Ca) and Carbon (C) show, and the similarity in shade that Carbon and Silicon (Si) show. The molecular weight ratio of Calcium with respect to Carbon is 3.3 and for Iron this is even 4.6. For Silicon this ratio is lower, namely 2.3. A region with high Iron concentration will thus show as a bright white area. A region with high Silicon concentration will not show that bright. It will show only a small difference in grey level with Carbon. Unfortunate, Silicon is the element of interest in current research and Carbon is the major component of organic material and thus abundantly present in the specimens. Therefore one expects only small distinctions in grey level when imaging.
- Classification of features according to elemental composition, size or shape. Observations of interest are differences in crystalline, the presence and location of silicon particles and the shape and roughness of the fibers present. More specifically, the objective is to depict orientation of a silicate layer (if present) at the interface of an organic fiber. Is there encapsulation of a fiber with a silicate phase (where we aim for) or is there filling of the pore space (what the break-through experiments predict)?

- Using EDS analysis, elemental analysis can be performed within regions as small as a few cubic micrometers. All the elements in the periodic table from fluorine to uranium can be detected. The sensitivity of the elemental analysis is a few tens of one percent. Objective is to indicate the presence of silicate and the abundance of this presence in various specimens.
- The result of an EDS analysis is a EDS spectra. An EDS spectra is a graphical plot of peaks identifying elements detected within the area analyzed. The peak hight, i.e. the intensity of the peak, is related to the concentration of that specific element. Besides, qualitative analysis X-ray spectrometry is specifically used to determine the chemical structure of a crystalline component. The spectrogram is then compared to a database, which should give an indication of the crystalline phases that are present.
    - One could expect that the silicate present in our system is not yet crystalline, but still in a gel-like amorphic state. Still, a spectrogram provides us with some useful information of the chemical structure. Typical for a diffractogram of an amorphous material are 'wide' peaks instead of sharp narrow peaks on the 2θ-axes.

Appendix 4.2 Sample preparation and location

The SEM operates under high vacuum. Using SEM to characterize and visualize soil material demands that it is resistant to vacuum. For samples containing volatile components (like water!) it is required that these volatile components are removed beforehand by a drying process. Both the organic material where a peat soil is constructed of and the silicate that could be present, contain a significant amount of water. Active removal of physical and partly chemically bounded water leads to a significant change in structure and composition of the internal structures. The Environmental Scanning Electron Microscope (ESEM) has been developed to overcome this problem. Unfortunately, ESEM, operating under low vacuum but high humidity, was not available to our disposal. ESEM operating at high humidity as analyses technique will therefore not be discussed in more detail. ESEM, under high vacuum was used to characterize the treated peat samples.

Several cycles of evacuating were necessary to get the internal pressure of the pressure chamber from atmospheric pressure (760 torr), to ca. 1 torr. The cycles needed to gain vacuum and the duration of this procedure is related to the concentration of volatile components (i.e. moisture) in the samples present in the chamber. The extraction of volatile components from the sample material took 40 minutes instead of 10 minutes normal for cementous and rock material. This indicates that a large fraction of water is volatilized (assuming water is the major potential volatile component in the sample material) and the expectation was that drying cracks would be visible.

The specimen volume which can be visualized and analyzed by means of EDS-ESEM techniques was very small. The maximum size of a sample has a diameter of ca.1 cm. The volume was therefore ca. 4 to 5 ml. Statistical the performed analyses therefore bear no value. Specimens were prepared by placing a collected fraction (of interest) onto a 1 cm diameter carbon sticker. The magnification varied from 100 x to 2000 x. The acceleration voltage was set at 20,0 kV for all specimens.

Sample location

Table A: Sample location and treatment of peat material

Column samples [Code]	Treatment	Location sample	Objective
4A (4_8)	Surfactant silicate solution (1250 ppm) at pH 7,5	Material at the side of the filter place (visible gel phase present)	Silicate presence: phase, orientation or peat fiber and abundance?
4B (4_8)		Material directly above the filter plate	Silicate presence: phase, orientation or peat fiber and abundance?
2 (2_1)	Silicate flush in of 214 ppm and silicate flush out with water	Material directly above the upper drainage plate	Silicate presence: phase and abundance? Impact of using a surfactant.
Blanco	Mixed sample of stored peat material (not flushed)	n.a.	Reference sample: silicate present in untreated peat material
Batch samples [Code]	**Treatment**	**Location sample**	**Objective**
3.1_dry	500 ppm Si+ surfactant solution added to mixed peat material, dried in oven at 70oC for 3 days	n.a.	Reference sample: silicate present in treated peat material. Forced condensation of the silicate phase present. Can we observe a difference in phase crystalline?
3.1_wet	500 ppm Si+ surfactant solution added to mixed peat material.	n.a.	Reference sample: silicate present in treated peat material.

Appendix 4.3 Results

Red framework: EDS analyses performed on this region

Blue framework: close-up made of this region (magnification > 100x).

Figure A

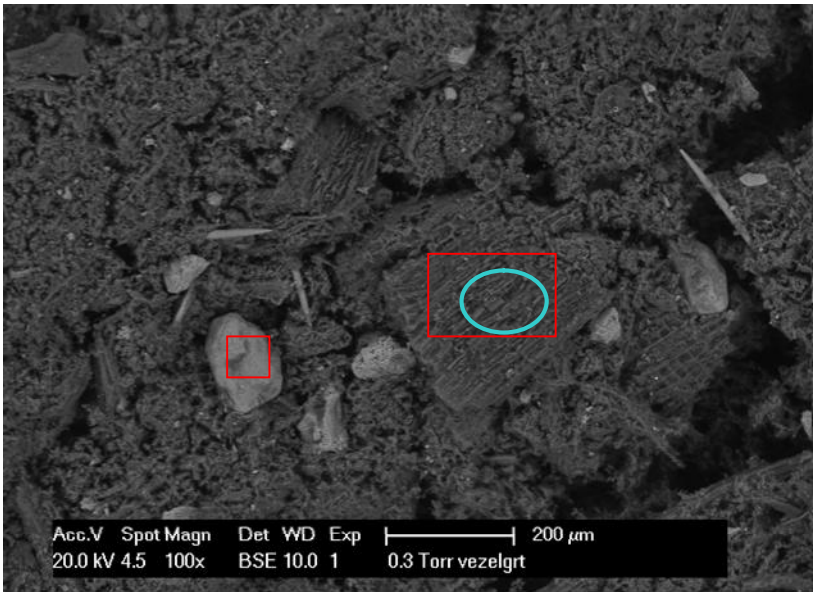

Figure B

Figure A and B.

Sample code: Blanco: mix sample of 420612_2 material (Bellingwedde peat)
Column: n.a.
Location: Table A.
Treatment: no treatment; no water flush
EDS analyses on the red spots:
Observations:
Two shades of grey present:
1. Organic matter
2. Denser inorganic crystalline material.

Structures:

- Generally two phases of organic material: structured (vesicles were clearly visible) and a more chaotic flock like material.
- Generally two phases of denser white material: needles and blocks.

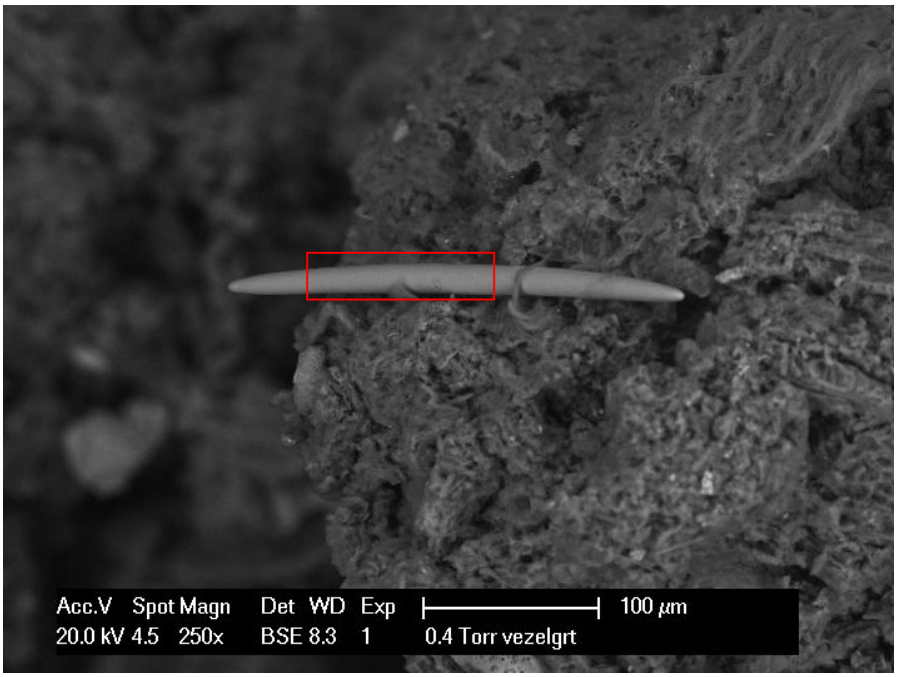

Figure C: Sample Code: 6_1A. Column: 4. Sample location: side of lower filter plate

EDS analyses on the red spot.

Observations

- Needle with a relative high silicate concentration. Likely this is a Spicula: shell of a fresh water sponge. The needle is about 300 um long and 17 um in diameter.
- This feature is found in all samples: treated and untreated peat material

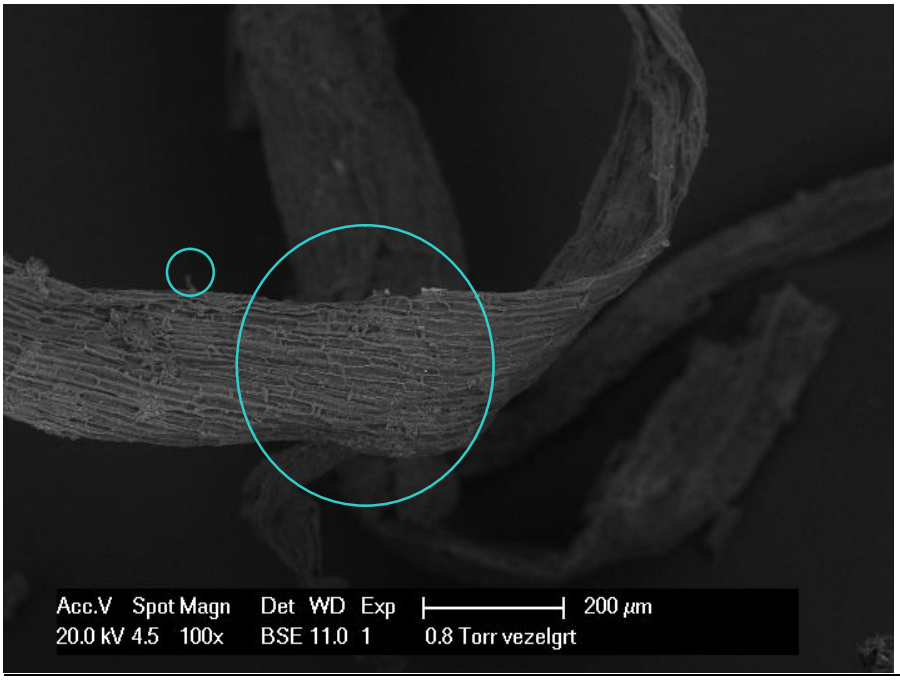

Figure D

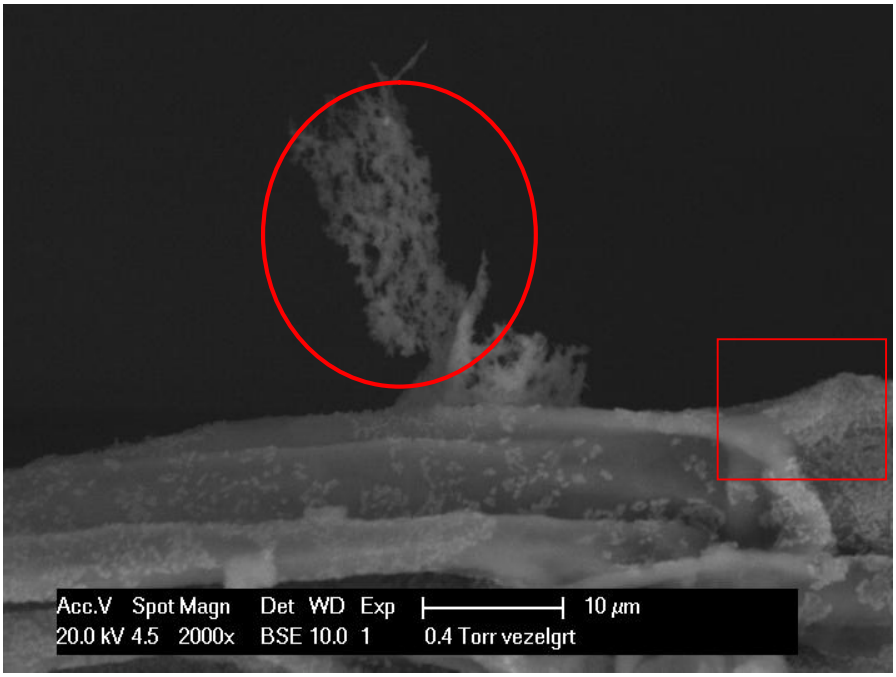

Figure E

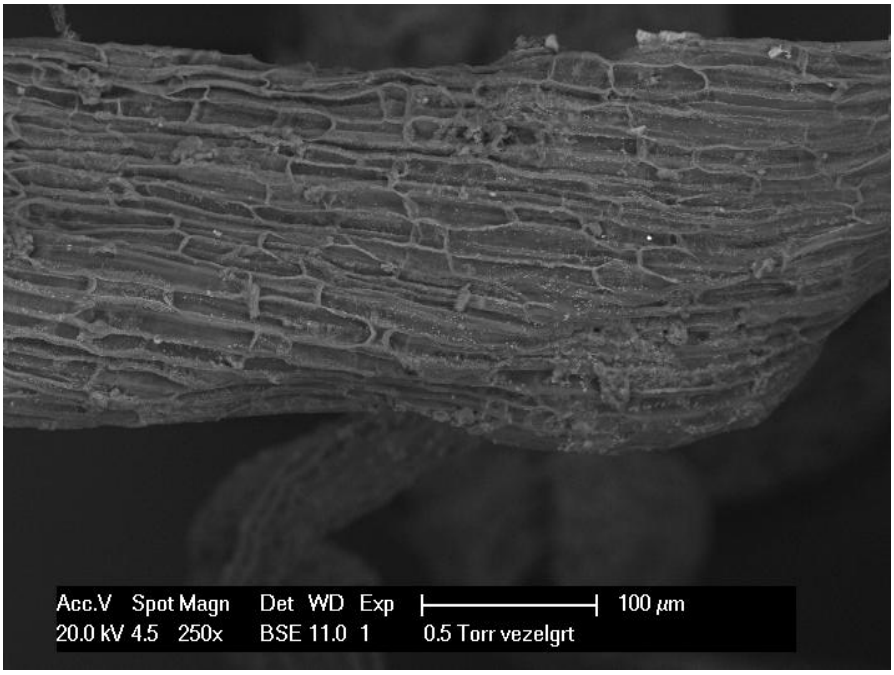

Figure F

Figure D, E en F. Sample code: 4_1A. Column: 4. Location: side of lower filter plate. EDS analyses on the red spots. Observations and structures:

Figure D:

- clearly a irregular structure, similar grayness as the organic fiber
- flock is connected to the fiber, although the connection itself is not clearly visible the white spots on the rest of the fiber are small crystalline cubes. EDS analyses shows that these are sodium chloride precipitates
- These were not present in the Blanco sample (figure b)

Figure E:

- covering of amorphous grey phase, although not very abundant
- larger bright cubes of sodium chloride

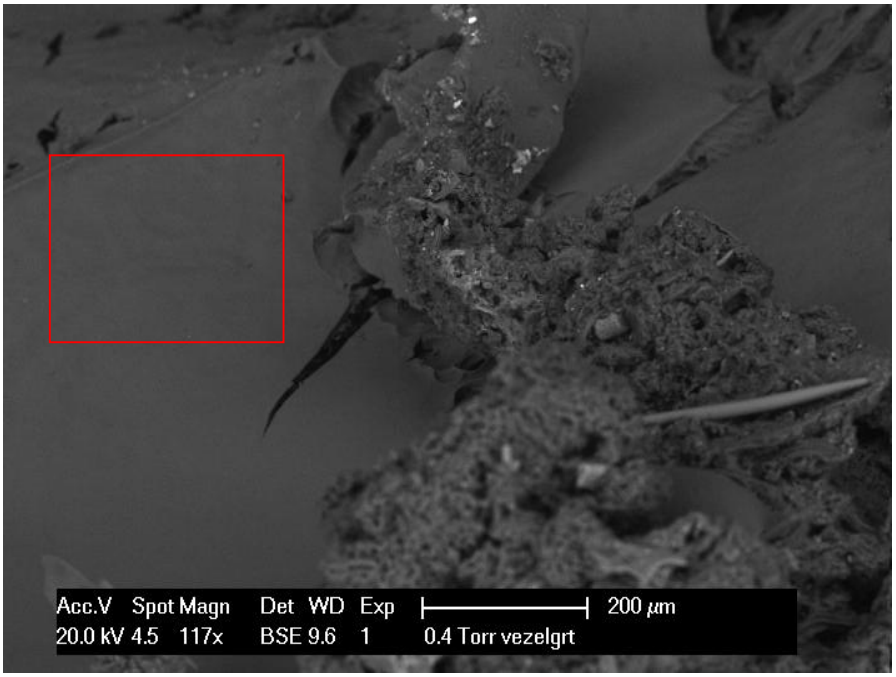

Figure G

Figure G: Sample Code: 4_1A. Column: 4. Sample location: side of lower filter plate. EDS analyses on the red spots.

Observations

- Gel phase present, which shrinks under the beam of electrodes, indicating further condensation of this silica phase.
- Crack formation visible due to dehydration of the silica gel
- Distinct difference in structure between peat unrecular phase and smooth gel phase.
- The difference is in only in structure and not in color indicating similar average molar weights in both regions.
- The bright dots are supposed to be iron and calcium based minerals.

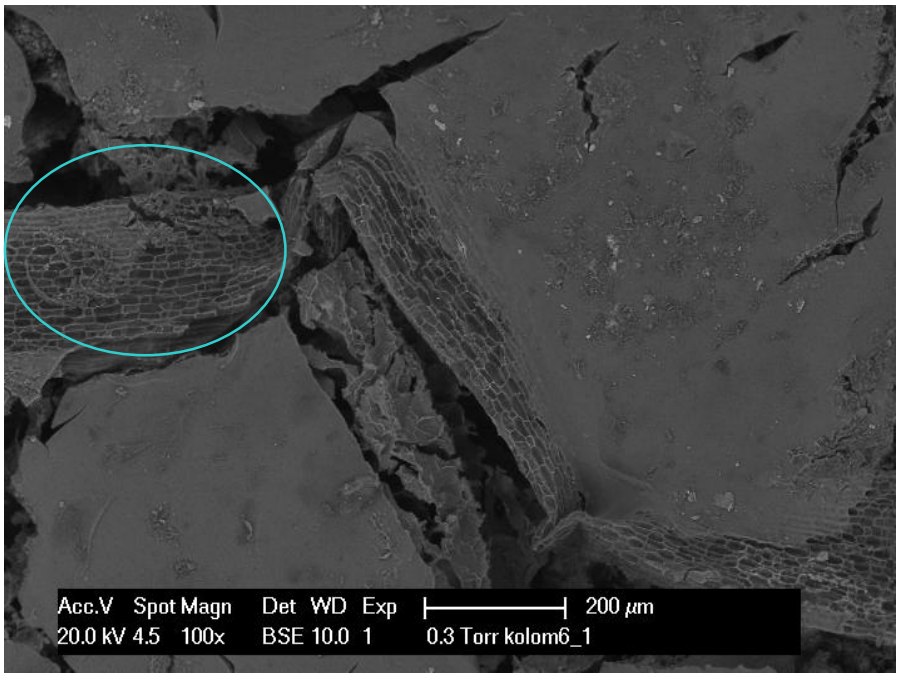

Figure H

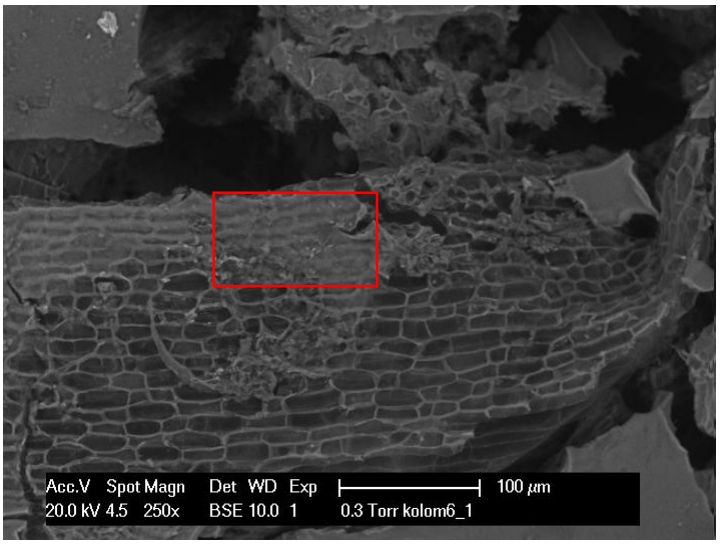

Figure I

Figure H and I: Sample Code: 4_1A. Column: 4 Sample location: directly above the lower filter plate. EDS analyses on the red spot.

Observations:

- Gel phase present
- Gel phase partly covers the peat fiber
- EDS analyses show an significant increase in silicon concentration at those locations
- Dehydration cracks visible along the fiber gel interface
- Gel phase fills up the pore space.

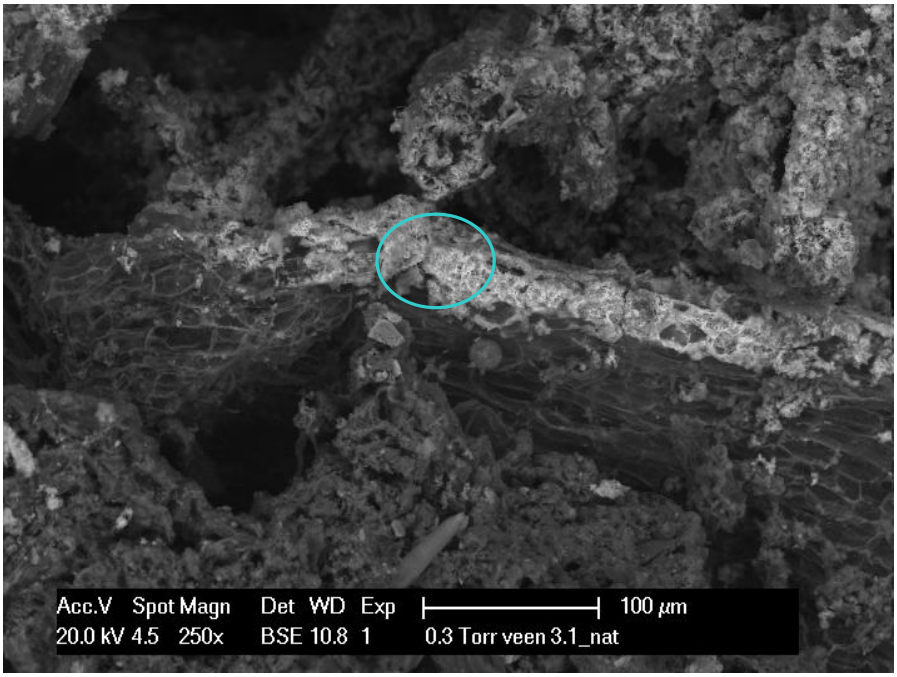

Figure J en K:

Sample Code: 2_1. Column: 2

Sample location: directly above the upper drainage plate

EDS analyses on the red spot.

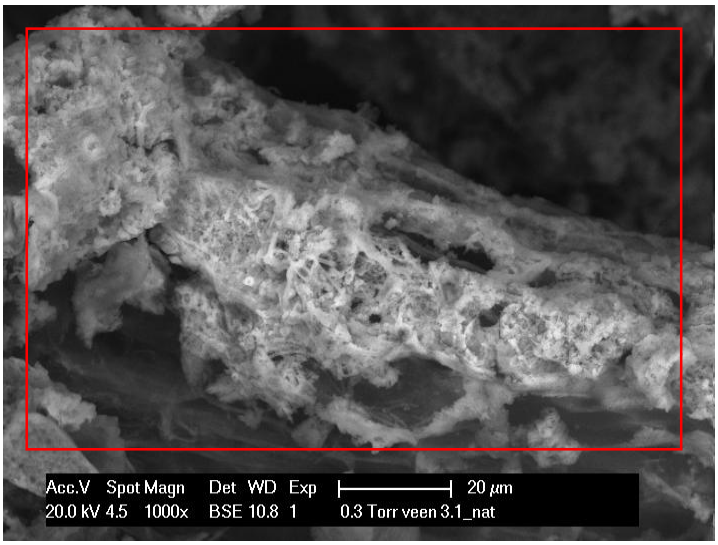

Observations:

- No gel phase present
- A bright precipitate on fiber. EDS points out that this is mainly iron precipitate. Probably the origin of the iron is the tap water used to flush the columns. Seems more abundantly present than in other samples.
- Amorphous organic material present
- Fiber organic material present

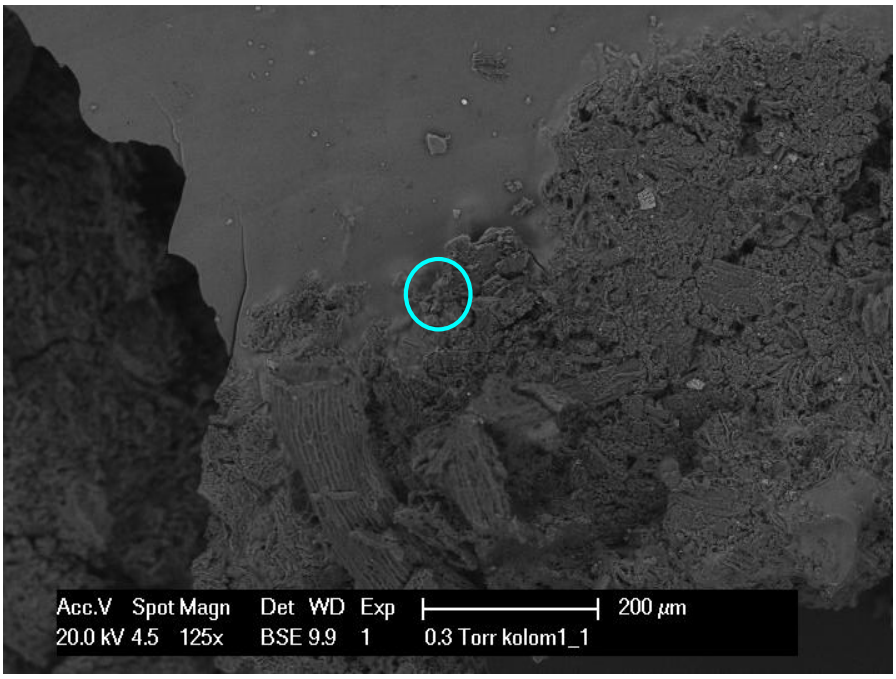

Figure L

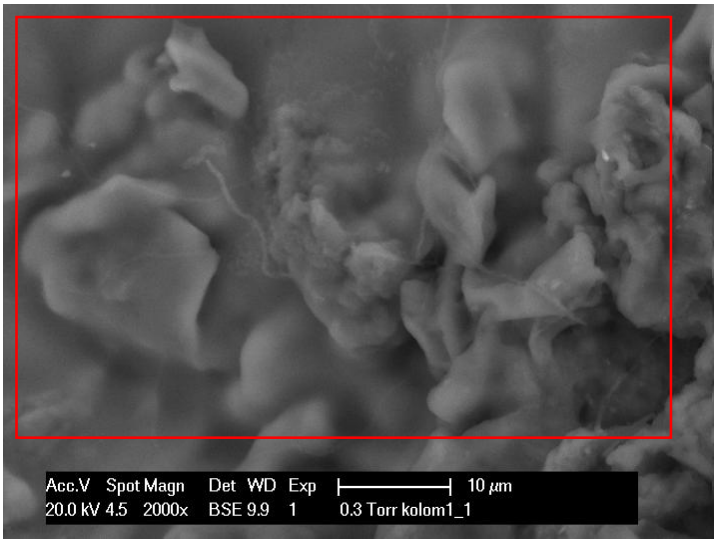

Figure M

Figure J and M: Sample Code: 1_4. Column: 4

Sample location: scrap of material at the bottom of the column, directly above the lower drainage plate. EDS analyses on the red spot.

Observations:

- Gel phase present
- Penetration depth of gel is limited, ca. 50 – 100 µm
- The initial micrometers organic particles are covered and pore spaces are filled completely

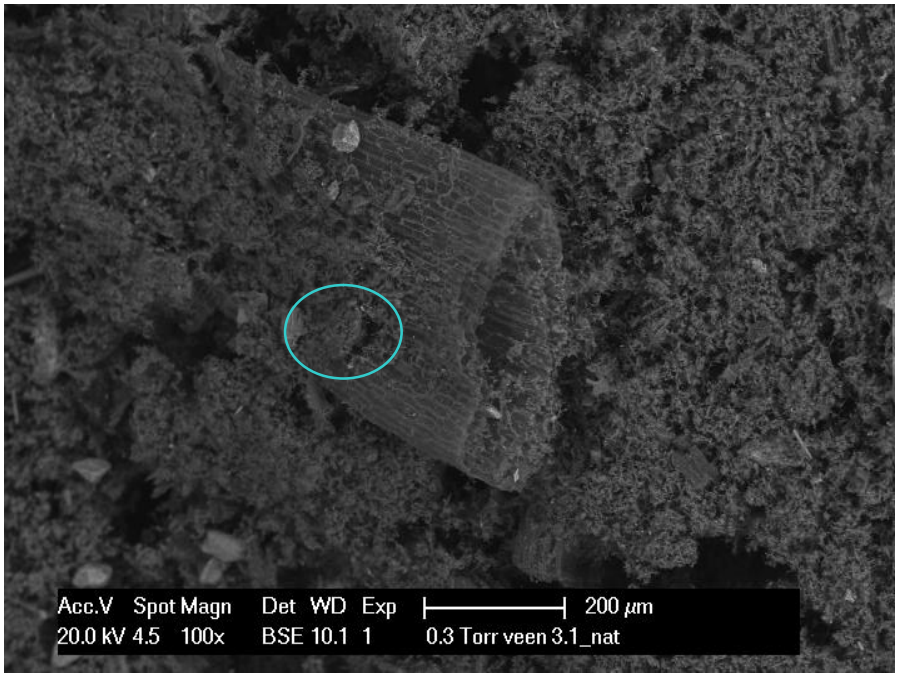

Figure N and O

Sample Code: 3.1_wet

Column: n.a.

Sample location: n.a.

EDS analyses on the red spot.

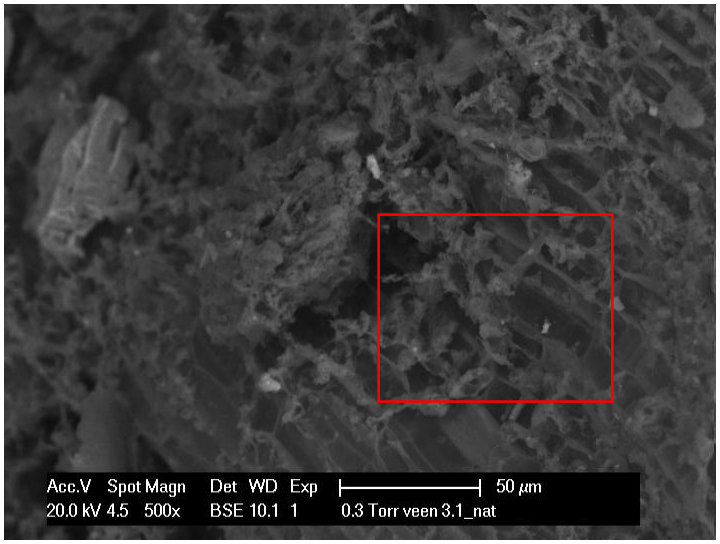

Observations:

- No smooth surface i.e. gel phase present
- EDS shows that there was only a minor amount of silica present in more condensed, amorphous phase. The structure was similar to the silicate flock shown in figure E

Figure P and Q:

Sample Code: 3.1_dry.

Column: n.a. Sample location: n.a. EDS analyses on the red spot.

Observations:

- No smooth surface i.e. gel phase present
- There was a difference in structure of the organic fibers in comparison to the wet sample (figure O). The dried peat seems to be more compacted in larger chunks.
- EDS shows that silica is present in a more condensed, amorphous phase.

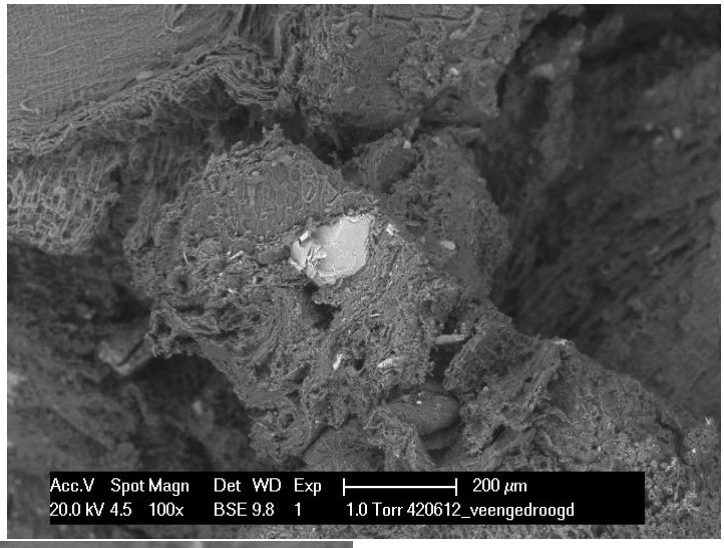

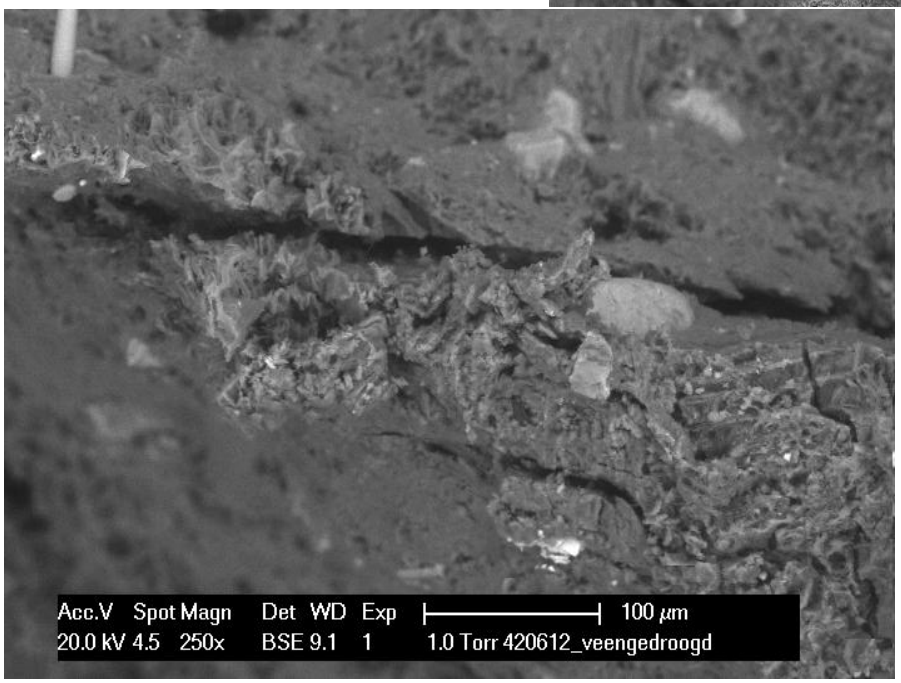

Appendix 5 Quantification Dissolved Silica

All dissolve silica concentrations in this study were expressed in ppm SiO_2. The silicomolybdate acid method is based on the principle that a reaction between monomeric and small polymeric silica, and ammonium molybdate occurs at pH of about 1.2. This reaction yields a yellow colored acid.

Interference in the silicomolybdate analyses is phosphate, which will react in a same matter with ammonium molybdate does. Phosphate thus contributes to color intensity. Therefore oxalic acid was added to destroy these interfering molybdatephosphoric acids, while leaving the silicomolybdate acid in tact.

Note that the method only measures monomeric and small polymeric silica species. In other words, oligomers were not considered to be part of the dissolved silica fraction applying this analytical method. The exact threshold to of maximum sinol-groups which can still react with ammonium molybdate is not known or could at least not be found in literature.

Appendix 5.1 Silicomolybdic acid spectrophotometric method

The silicomolybdic acid spectrophotometric method was used to determine the concentration of reactive silica in solution during the retardation test. We refer to the research of Coradin et al. (2004) on testing the dynamics of the silicate polymerization process in the presence of a biomacromolecule, and for his assay on different quantification methods including biopolymer interactions studies. Reactive silica is considered monomeric and dimeric silicic acid, although the exact number of reactive units is not known. Higher silica oligomers are not detected by this method. The assay therefore provides information on the first steps in the condensation process of silica.

The yellow silicomolybdic acid assay was performed in accordance to the description given by Coradin (2004). All soluble silica measurements are expressed in terms of ppm SiO_2. Prior to soluble silica analyses the extracted sample is filtered with a 0.45 nm glass fiber filter (Pall Corporation, type A/E) in order to remove any interfering turbidity. The gained supernatant was diluted with demiwater water when necessary prior to analyses.

According to Coradin (2004) this procedure should give a linear calibration curve in the range of 10^{-2} to 10^{-3} mol l^{-1} silicic acid (601 – 60 ppm SiO_2). Coradin (2004) provides an indicated of the relative standard deviation at 5.0×10^{-3} mol l^{-1} silicic acid (300 ppm SiO_2) of ± 2%.

According to this method the sample was filtered with a 0.45 or 0.22 um filter. The solution was diluted to 25 ml using demineralized water. The reagents, ammonium molybdate (1ml) and 18.5% HCl (0,5 ml) were added to the 25 ml sample solution. The solution was mixed well and left undisturbed for 10 minutes. After this incubation period oxalic acid (1 ml, 2 M) was added. The solution is mixed again and set aside for 2 minutes. The spectrophotometer was set at zero absorbance with demineralized water. The absorbance is measured at 452 nm as ‘reactive soluble silica’. The detectable concentrations range from 0 to 75 ppm SiO2. The dilution factor was applied to calculate the concentration in the original solution.

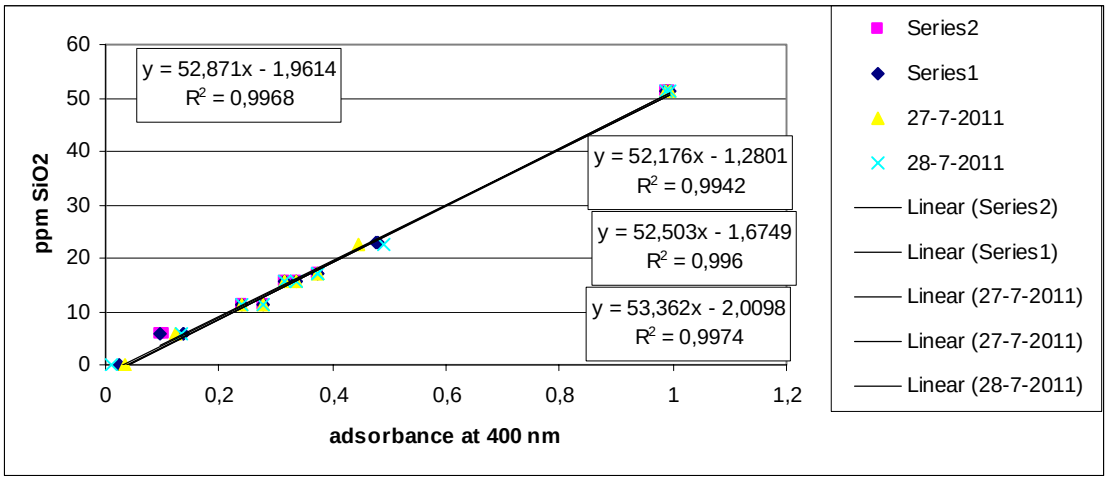

Figure A: Calibration Curve silicomolybdate measurement

The detection range of the quantitative method was 5 – 50 ppm SiO_2 as measured in a volume 12,5 ml. In present research an error of 12.75 to 9.60 ppm SiO_2 was obtained in the concentration range of 60 to 640 ppm SiO_2.

Appendix 5.2 BGS Deltares laboratory method AA3 (No.G-147-95 rev.2)

Method No. G-147-95 Rev. 2 (multitest MT7/8)

Silicate in Water and Waste Water

Ranges: **0 - 4 to 0 - 45 mg/L as SiO_2** (0 - 750 uM; 4.167 mM)

and **0 - 25 to 0 - 250 mg/L as SiO_2** (only MT7)

Description

This automated procedure for the determination of soluble silicates is based on the reduction of silico-molybdate in acidic solution to "molybdenum blue" by ascorbic acid (1). Oxalic acid is introduced to the sample stream before the addition of ascorbic acid to minimize interference from phosphates.
Tannin, large amounts of iron, colour, turbidity and sulfide interfere.

This method is a multitest with alkalinity (methyl orange), ammonia (salicylate and phenate), boron, calcium, chloride, hydrogen sulfide, iron, nitrate, nitrite, TKN, phosphate, TKP, potassium, sodium.

Hardware: 24" Dialyzer, 37°C heating bath (7.7 mL) **Pump tubes:** 7 plus 2 air plus sampler wash (AAII: +1)

Performance data using aqueous standards and AAII colorimeter

See operating notes for performance with AA3 colorimeter

Test ranges:	**20 mg/L**	**100 mg/L**
Sampling rate	50/hr	50/hr
Sample: wash ratio	5:1	3:1
Sensitivity: Extinction at 20 and 100 mg/L SiO_2	0.50	0.37
Reagent absorbance	0.01	0.01
Coefficient of variation:		
10 replicates at 50 %	0.56 %	0.51 %
Pooled Std. Dev. (5 Levels)	0.04 mg/L	0.37 mg/L
Correlation Coefficient (linear, 5 points)	0.9999	0.9991
Detection Limit (determined according EPA procedure pt. 136, app B)	0.01 mg/L	1.1 mg/L
Detection Limit in lowest range (0 - 4 mg/L SiO_2)	0.008 mg/L	

Note: the above performance specifications were developed with the exclusive use of genuine Bran+Luebbe parts and consumables.

Reference

1. Methods for the Analysis of Inorganic Substances in Water and Fluvial Sediments, U.S. Geological Survey, (I-2700-78), p. 821-825.

REAGENTS

Unless otherwise specified all chemicals should be of Analytical grade or equivalent. Chemicals used should be low in silica.

LIST OF RAW MATERIALS

	safety classification
Acetone, CH_3COCH_3	flammable
Aerosol-22*	--
Ammonium molybdate, $(NH_4)_6Mo_7O_{24}.4H_2O$	harmful
Ascorbic acid, $C_6H_8O_6$	--
Oxalic acid, $H_2C_2O_4$	harmful
Sodium dodecyl sulphate, purest grade, $C_{12}H_{25}NaO_4S$	harmful
Sodium metasilicate nonahydrate, $Na_2SiO_3.9H_2O$	--
Sulfuric acid, conc. H_2SO_4	corrosive

* Registered Trademark of American Cyanamid

REAGENT MAKE-UP

The use of plastic labware is recommended to reduce silica contamination.

DI water refers to high quality reagent water, Type 1 or Type II as defined in ASTM Standards, Part 31, D 1193-74.

SULFURIC ACID, 50%

Sulfuric acid, conc.	500 mL
DI Water,	to 1000 mL

Cautiously add 500 mL of sulfuric acid to about 400 mL of DI water and dilute to 1000 mL. Store in a plastic container.

SULFURIC ACID, 0.06N

Sulfuric acid, 50%	3.4 mL	(1.7 ml conc. H_2SO_4)
DI Water,	to 1000 mL	
Sodium dodecyl sulphate	1 g	10 ml

Add 3.4 mL of 50% sulfuric acid to about 800 mL of DI water. Add 1 g of sodium dodecyl sulphate and mix. Dilute to 1000 mL. Store in a plastic container.

AMMONIUM MOLYBDATE

Ammonium molybdate	6.82 g
Sulfuric acid, 0.06N,	to 1000 mL

Dissolve 6.82 g in about 800 mL of 0.06N H2SO4 and dilute to one liter with 0.06N H2SO4. The solution should be clear and free of precipitate upon standing. If a blue colour exists, discard the solution. Store in an amber plastic container. Stability: two weeks.

Appendix 5.3 Analytico laboratories method

The dissolved silica concentrations as measured during the infiltration test were determined by Analytico Laboratory. The reference code is : W0561 Spectrometrie Cf. NF T90-007.

Appendix 6 Retardation Silica polymerization at Ci 100 ppm SiO2

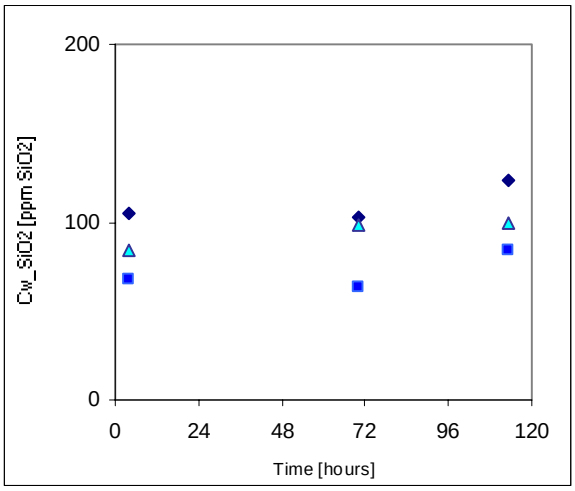

Figure A: Dissolved silica concentration at initial concentration of 100 ppm SiO_2 and 10 ppm (light blue), 50 ppm (bright bleu), or 100 ppm (dark bleu) biopolymer Celquat L200.

Appendix 7 Retardation Silica Particle Growth in Absence of Biopolymer at Ci of 700 ppm SiO2

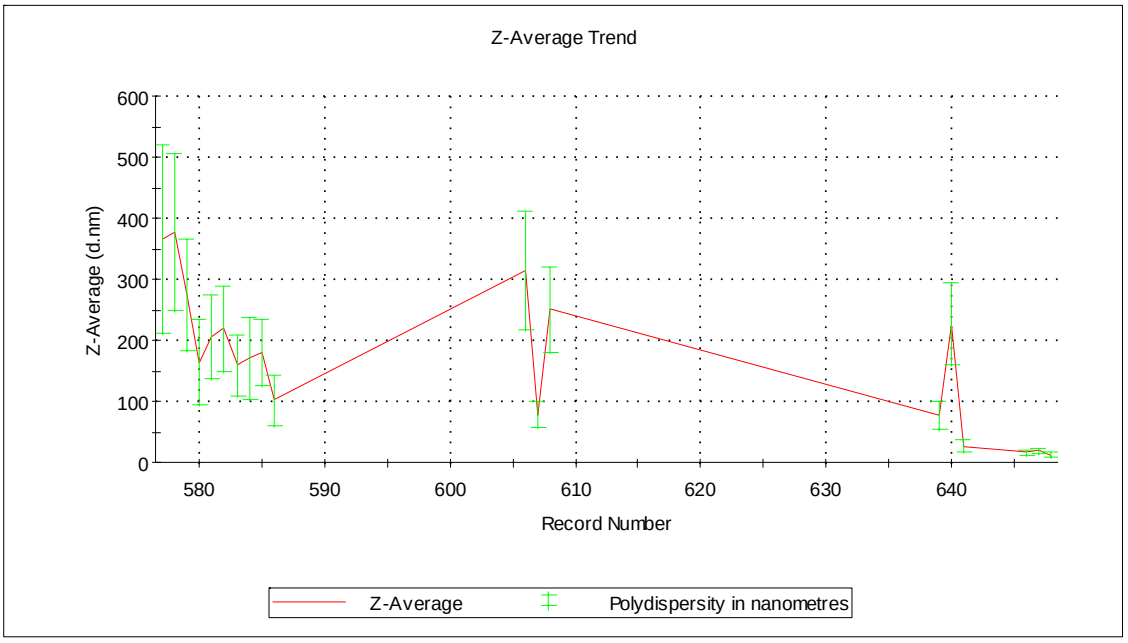

Figure A: Measurement particle diameter size at initial concentration of 700 ppm SiO_2 and no biopolymer added. The red represents Z-Average particle size. This is the particle size as directly derived from the correlation function. The green error bars represent the width of the particle size distribution i.e. the polydispersivity. Record number 577 to 586 represents measurements during the first 4-84 minutes; at +/- 610 represents 4 hours of incubation; at +/- 640 represents 7 hours of incubation; +/- 650 represents 17.5 hours of incubation.

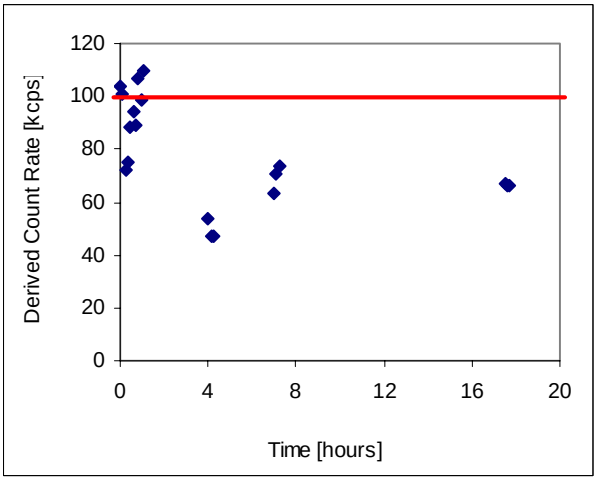

Figure B: Derived Count Rate over time. During the hour after pH adjustment the amount of particles fluctuates at 100 kcps, which is the recommended lower limit for PCS measurement.

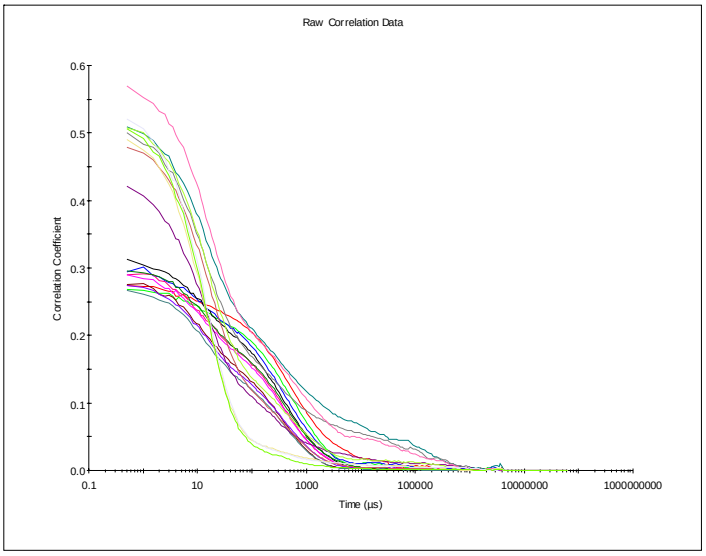

Figure C: Correlation function for PCS measurement. This figure indicates the low quality of the measurement. X-axis: time in us. Y-axis: correlation coefficient.

Appendix 8 Particle Size Distribution at 100 ppm SiO2 and biopolymer to silica wt. ratio of 0.1 and 0.5

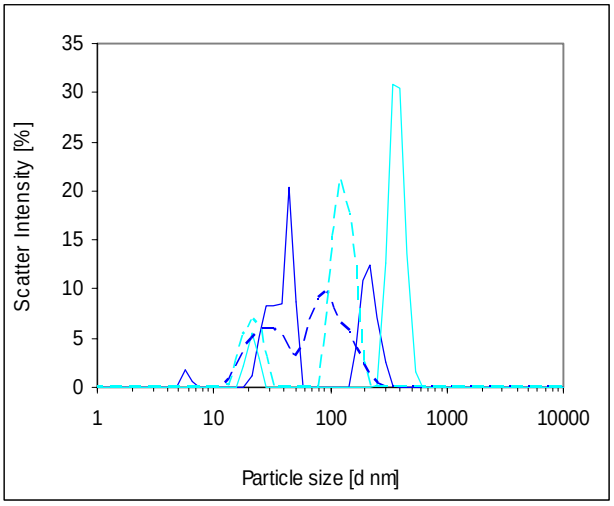

Figure A: Particle size distribution at initial concentration of 300 ppm SiO_2 and 150 ppm biopolymer (bright blue) or 30 ppm biopolymer (light blue). The particle size increases with time. The dotted line was measured at t1 and the thick line at t3 (11h).

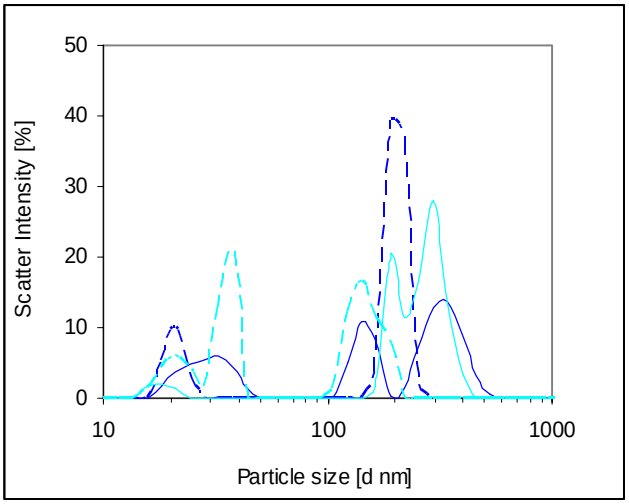

Figure B: Particle size distribution at initial concentration of 100 ppm SiO_2 and 50 ppm biopolymer (bright blue) or 10 ppm biopolymer (light blue). The particle size increases with time. The dotted line was measured at t1 and the thick line at t3 (11h).

Appendix 9 Derived Count Rate at Ci 300 ppm SiO2 and 30 or 150 ppm biopolymer

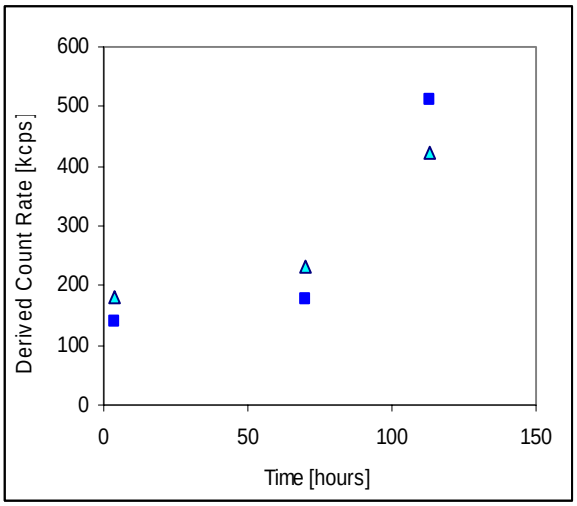

Figure A: Derived Count Rate at PCS measurement. The light blue indicates DCR at 30 ppm L200 and 300 ppm SiO_2 as initial concentration. The bright blue indicates DCR at 150 ppm L200 and 300 ppm SiO_2. The recommended lower limit for measurement is at 100 kcps.

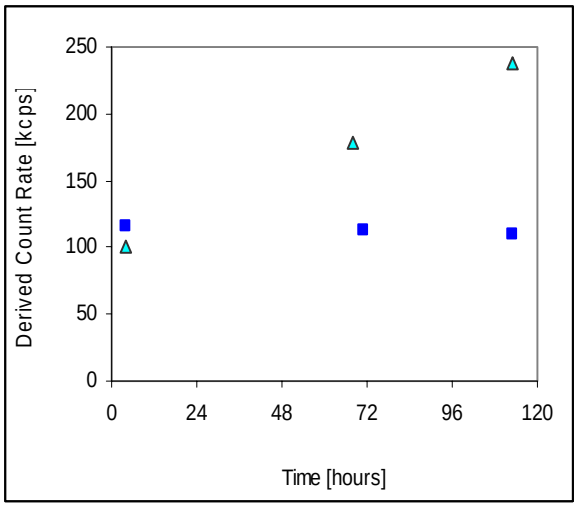

Figure B: Derived Count Rate at PCS measurement. The light blue indicates DCR at 10 ppm L200 and 100 ppm SiO_2 as initial concentration. The bright blue indicates DCR at 50 ppm L200 and 100 ppm SiO_2. The recommended lower limit for measurement is at 100 kcps.

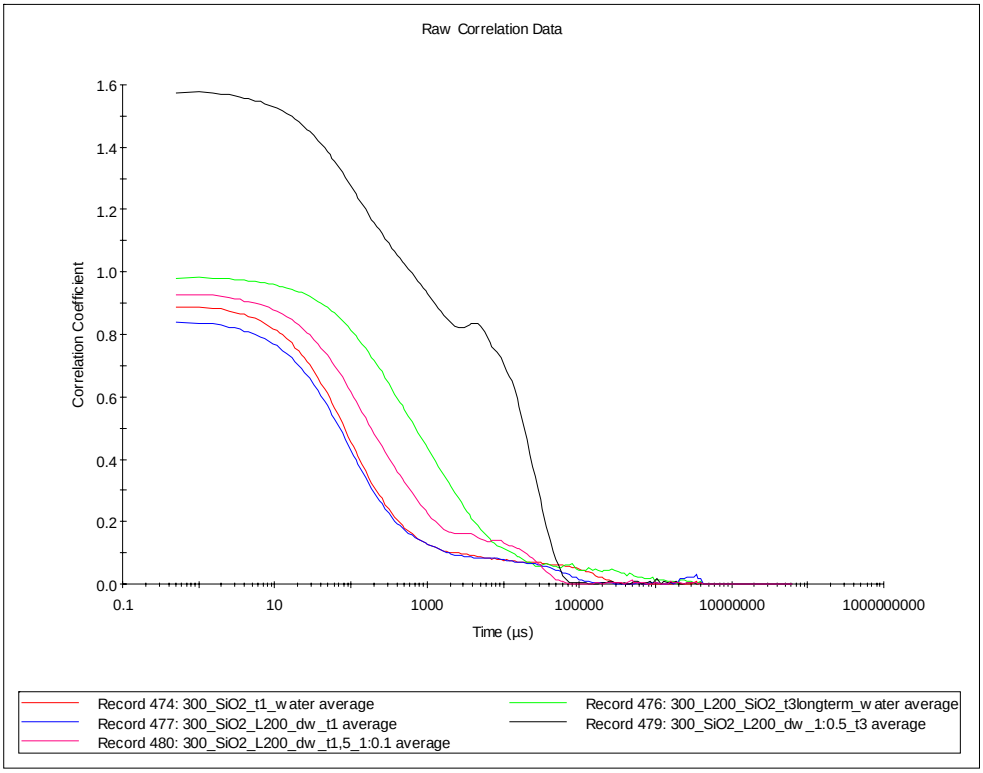

Figure C: Correlation function for PCS measurement. This figure indicates the low quality of the measurement. X-axis: time in us. Y-axis: correlation coefficient.

Appendix 10 Particle Size Distribution t2 at Ci 600 and 1250 ppm SiO2

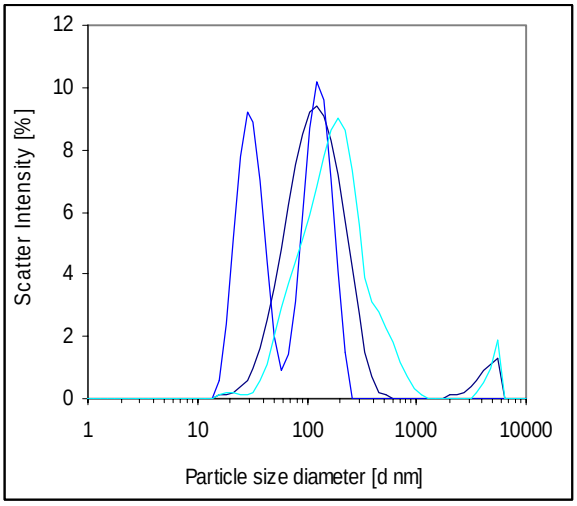

Figure A: Particle size distribution at initial concentration of 300 ppm SiO_2 and 150 ppm biopolymer (bright blue) or 30 ppm biopolymer (light blue). The particle size increases with time. The dotted line was measured at t1 and the thick line at t3 (11h).

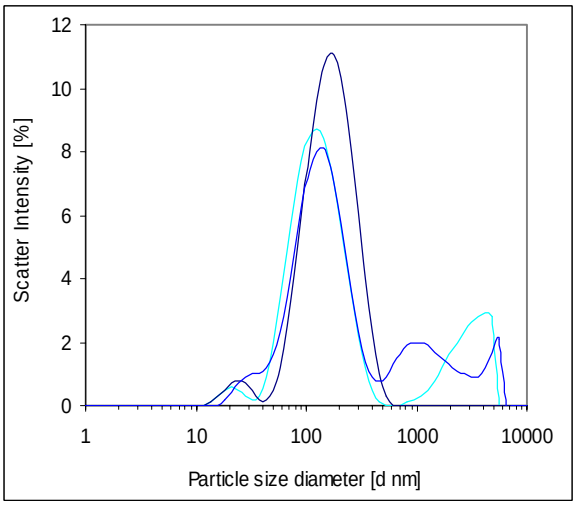

Figure A: Particle size distribution at initial concentration of 300 ppm SiO_2 and 150 ppm biopolymer (bright blue) or 30 ppm biopolymer (light blue). The particle size increases with time. The dotted line was measured at t1 and the thick line at t3 (11h).

Appendix 11 Particle Size Distribution at Ci 300 ppm SiO2 in presence and absence of peat pore water

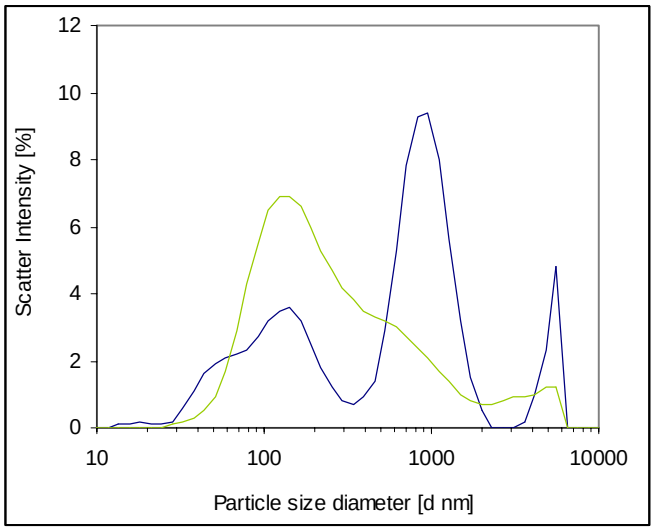

Figure A: Particle size diameter at initial concentration of 300 ppm SiO_2 and 300 ppm biopolymer. The dark green line represents the mixture created with peat pore water. That is, retardation of the biopolymer regarding silica polymerization did not decrease in the presence of particulate or dissolved organic matter. Dark blue line represents equal mixture created with demiwater and is described in Chapter 3.

Appendix 12 Zeta Potential Phase Diagrams

The phase diagram showing the phase difference in time is an index for measurement quality. A phase diagram shows the rate of change of the phase difference. On the y-axis the phase difference is plotted in terms of radicals. On the x-axis the time is given. A 'phase' can be defined as frequency x time. Phase difference is the difference between the sample and an internal reference in frequency shifts of the scattered light. The rate of change of this phase difference is related to the velocity at which particles are moving. From this data the Zeta Potential can be determined.

The applied voltage is reversed a number of times during the measurement period. To correct for electro osmosis the reversal of voltage is performed in a fast and in a slow mode i.e. Fast Field Reversal and Slow Field Reversal. In the phase diagram the FFR and SFR portion of the measurement can be distinguished, as is the case in Figure 6-1 (A). The plot shows well defined trending slopes if the phase differences with time for the FFR portion and a smooth line for the SFR portion, as opposed to the phase plot in Figure 6-1 (B).

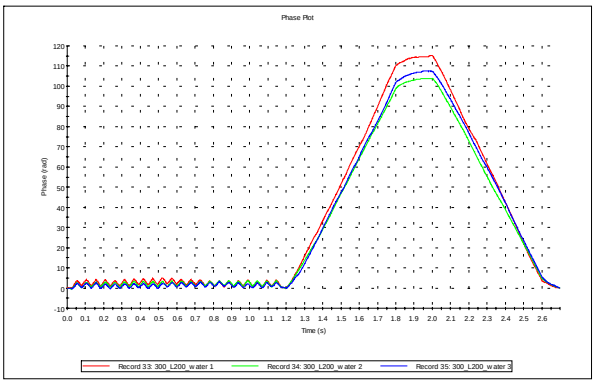

(A) Phase diagram of reliable electrophoresis measurement. Results of a 300 ppm L-200 solution having a conductivity of 50 µS/cm.

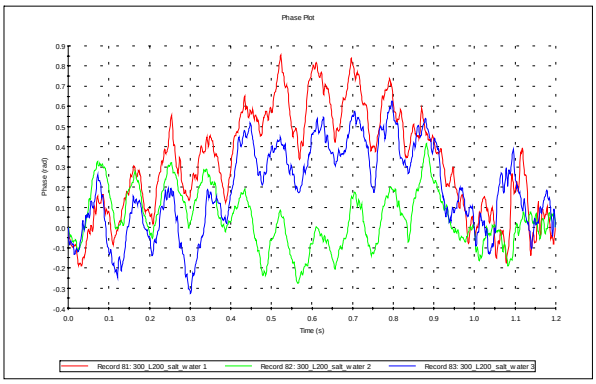

(B) Phase diagram of unreliable electrophoresis measurement. Results of a 300 ppm L-200 solution having a adjusted conductivity of 9,81 mS/cm.

.

Figure 6-1: Zeta potential is derived from a phase diagram The zeta potential is measured in three runs. The phase difference is plotted on the x-axis in radials. The time is plotted in the x-axis in seconds.

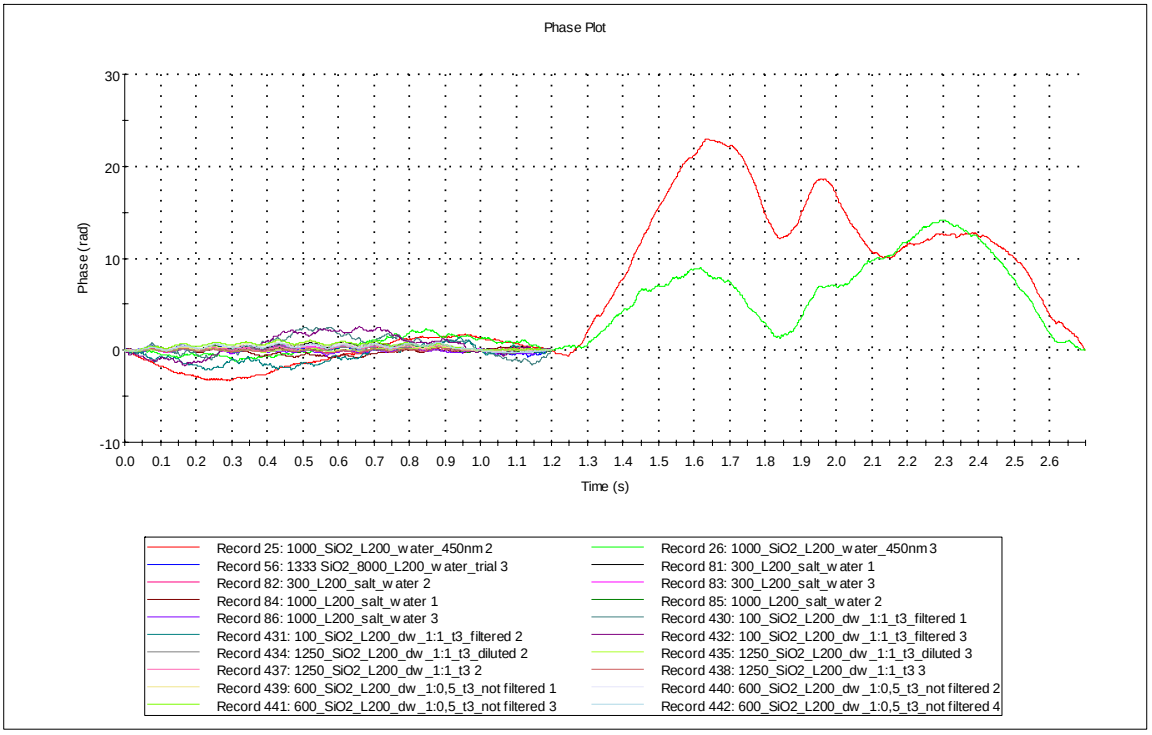

Phase diagram of silica biopolymer mixtures with an EC > 5 mS/cm

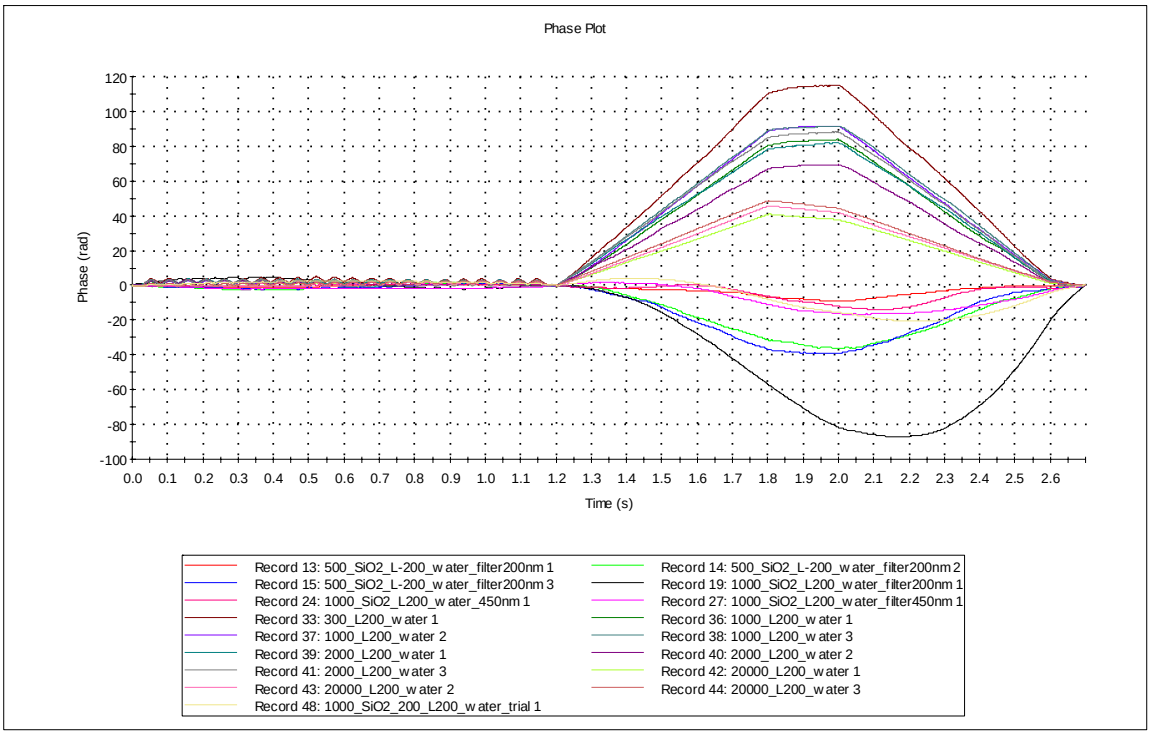

Phase plot for silica biopolymer mixtures and biopolymer mixtures with an EC < 5 mS/cm

Appendix 13 Attachment Test Experimental Protocol

Additional information Attachment Test lab protocol

The chemical analyses are performed by the geochemical laboratories of Deltares/ TNO in Utrecht. The test protocol is designed based on the article of Cumming et al. published in 2010 and in discussion with Harry Veld and Piet Peerenboom of the Deltares Lab in Utrecht.

A Equipment

The equipment used in this experiment is listed below :

Preparation of the Standard and reactive solutions
- pH (glass) electrode (Schott, blue line 3 mol/l KCl electrode)
- EC (plastic) electrode
- Magnetic stirrer and plate
- 0.001 accurate balance
- Ultra Thorax high shear mixer
- Al lab material was of plastic or metal, not of glassware.

Preparation of the flasks
- Nalgene HDPE
- Shaker
- Dark incubation room at 20^{o}C
- Al lab material was of plastic or metal, not of glassware.

B Standard Solutions and reagents

- Distilled water
- Sodium hydroxide, analytical grade
- Hydrochloric acid: 37% concentrated solution diluted to 1 M HCl, analytical grade
- Sodium chloride: dissolved to 1M NaCl, analytical grade
- Poly-quarternium 4 powder: L-200 of Akzo Nobel, commercial grade product.
- Sodium meta silicate nonahydrate (reagent grade): dissolved to 4000.37 ppm SiO_2, analytical grade.

D Preparation of stock solutions

D1 Preparation of Reactive Solutions

Reactive solution (1): 20000 ppm L200

A solution of L-200 poly-quarternium of 20000 ppm is made 2.5 months in advance of the partition test. The solution is stored in an air tight bottle at 4^{o}C. The solution is prepared as follows:

a. 3000.048 gram of demi water and 61.225 gram of L200 are weighted.
b. Demi water is weighted one day in advance and stored at ambient temperature (20 ^{o}C) to equilibrate.
c. By means of a Ultra Thorax high shear mixer the L200 is carefully added to the demiwater (mixing speed of 2000 rpm).

Reactive colloidal mixture (2): 2000 ppm SiO_2 and 1999 ppm L200

A mixture of sodium metasilicate nonahydrate and L-200 is made at a one to one ratio, one day in advance of the attachment test. During this period the mixture is stored at an air tight bottle at 20 ^{o}C.
The mixture was prepared as follows:

a. - 1000.527 gram of the 4000 ppm silicate solution is weighed
   - 200.122 gram of the 20.000 ppm L200 solution is weighed
   - 149.317 gram of the 1M HCl solution is weighed
   - 650.467 gram of demiwater is weighed
b. The silicate solution was diluted with 2/3 of the water.

c. The diluted silicate solution was placed on the magnetic stirring plate, and stirred slowly. The 20000 L200 solutions were carefully added under constant stirring and pH plus EC measurement.
d. The mixture was titrated with the 1M HCl solution pH to a pH of 7.5. At a pH of 9 a transformation in color was observed. The liquid was still transparent but gained a white glow.
e. The mixture rested for 20 minutes at 20 ^{o}C, after this period the pH is measured under slow stirring and adjusted from 7.79 to 7.5.
f. The mixture rested again for 1 hour at 20 ^{o}C, after this period the pH is measured under slow stirring and adjusted from 7.77 to 7.5.
g. The solution stood for 3 hours at 20 ^{o}C, after this period the pH is measured under slow stirring and adjusted from 7.84 to 7.5.
h. The volume of acid added is supplemented with demi-water till the appropriate concentration was reached.
i. Reactive stock suspension was used to prepare flasks with peat circa 5 hours preparation.

D2 Preparation of peat

The peat material was selected from one block of peat material (125 liter in total). 10 samples were randomly taken from this block and collected in a 1 liter air tight vial (glass). The total volume of the fabricated sample was about one liter. The used peat material originates from the same location (Peat sampled in Bellingwedde, coded 420612_2) as the peat used in the column experiments.
Pretreatment consisted of the following actions:

a. *Hhomogenization by mixing:* intensive but slow manual mixing with a spatula, this to prevent damaging and breaking of the peat fibers. Thereby creating 'fresh' and additional surface available for adsorption. The material was mixed until a smooth paste was obtained.
b. *Determination of dry solid content:* three sub samples were taken to determine the water content of the peat paste. The dry solids content was determined at 70 ^{o}C of drying and varied between 14.7% dry solids before homogenization by mixing and 11.7 % dry solids after homogenization. A dry solid content of 11.7% was used to derive the liquid solid ratio in each flask.

D3 Preparation of shaking flasks

In total 48 Nalgene HD-PE shaking flasks were prepared. They were prepared as follows:

a. The Nalgene HD-PE flasks are colored but did not retain light.
b. Ca. 20 gram of wet peat was added to flask no. 1 to 24
c. Ca. 100 ml of the reactive solution was added to all flasks except to flask 11, 12, 23, 24, 59, 60, 71 and 72. As stated before, we used two reactive solutions: a meta stable solution of sodium metasilicate nonahydrate and L-200 in a 1:1 ratio, and a solution of solely L-200. 100 ml of demiwater was added to the Blanco flasks. The Liquid to Solid ratio (L/S) obtained in flask no. 1 to no. 24 was 50 (CV = 2%).
d. Initial pH and pH adjustment:
    - The pH of the peat paste was 5,05.
    - The original pH of the Blanco flasks, containing peat and demiwater was 5.91± 0.25.
    - The original pH values of the peat with reactive fluid were in the range of 6.03 ± 0.32.

- pH adjustment: Prior to the shaking period the pH was set at 7.5 in each flask by titration with a 1M NaOH solution. This was performed immediately after addition of peat to the reactive silica biopolymer suspension.
- The original pH and the electric conductivity of the Blanco samples without the addition of the peat (code 49 to 72) were determined but not recorded. The initial pH was set at 7.5, the EC was not adjusted.

E Analytical Procedure

An overview of the set-up of the flasks is given in table x.x.

Liquid phase			Solid phase				Code	Reference
Reactive solution			Peat		average pH*		Flask	Experiment
presence	Composition	concentration	presence	concentration	pH initial	pH (t 113 h)	no.	Name***
yes	Silicate; L-200	60 – 1250 ppm	Yes	20 gr (wet)	5.9	6.5	1 to 10	“Silica; biopolymer-Peat”
no	Demi water	0 ppm	Yes	20 gr (wet)	5.7	6.1	11 to 12	“Water-Peat”
yes	L-200	60 – 1250 ppm	Yes	20 gr (wet)	6.1	6.7	13 to 22	“Biopolymer-Peat”
no	Demi water	0 ppm	Yes	20 gr (wet)	6.1	6.5	23 to 24	“ Water-Peat”
yes	Silicate; L-200	60 – 1250 ppm	No	-	**	**	49 to 58	“Silica; biopolymer -No Peat”
no	Demi water	0 ppm	No	-	**	**	59 to 60	“Water-No Peat”
yes	L-200	60 – 1250 ppm	No	-	**	**	61 to 70	“biopolymer-No Peat”
no	Demi water	0 ppm	No	-	**	**	71 to 72	“Water-No Peat”

Preparation of "Silica; biopolymer-Peat" experiment

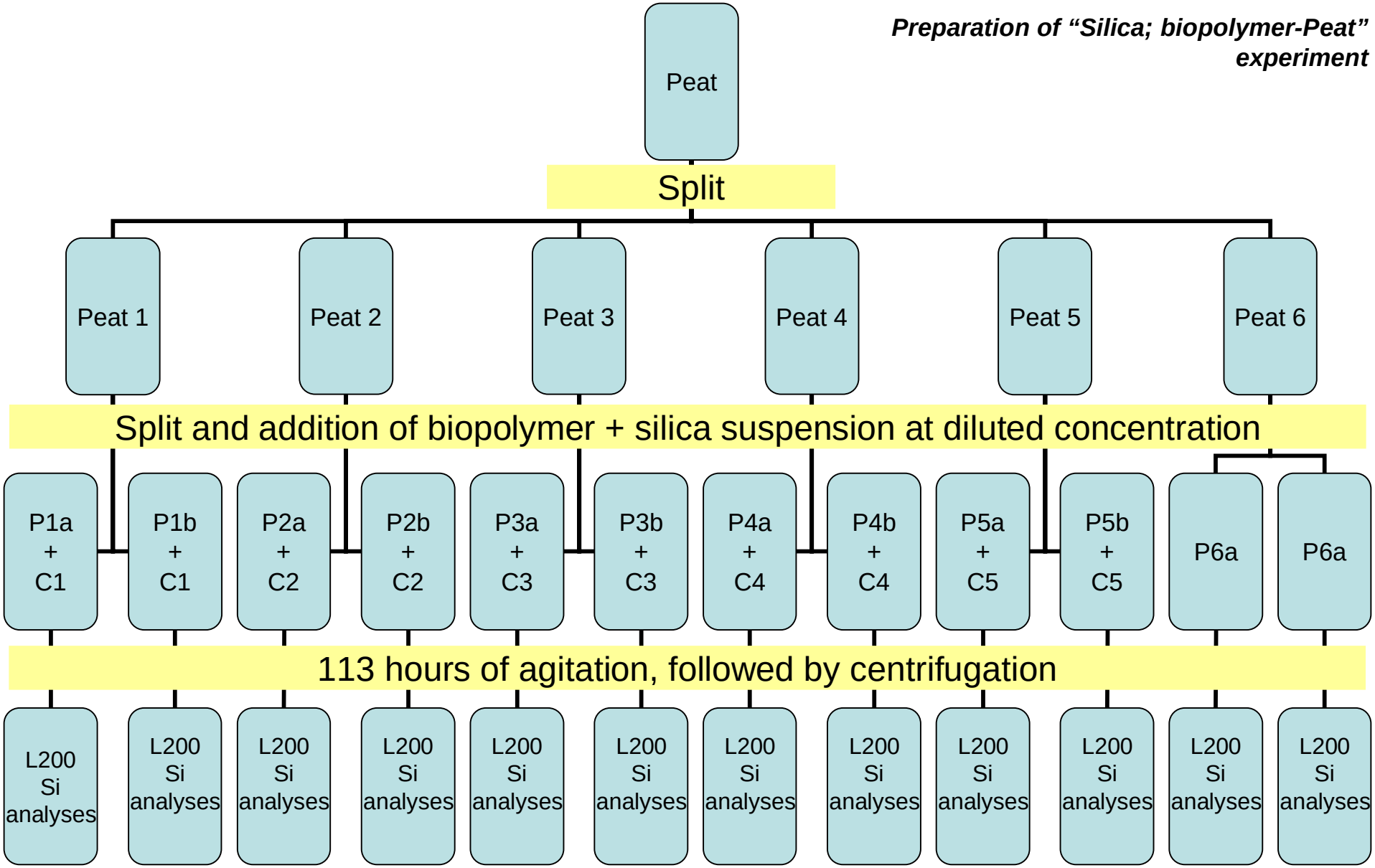

$$C_{\mathrm{i}} - C_{\mathrm{w}} = K_{\mathrm{D}}.C_{\mathrm{w}}.(m_{\mathrm{HA}}/V_{\mathrm{w}})$$

(Cumming, 2010)

Appendix 14 Quantification Biopolymer L200

Appendix 14.1 Calibration Curve – Biopolymer L200 and DOC

Correlation between DOC and L200

Calibration curve: Correlation between dissolved organic carbon NPOC measurements and L200 concentrations (calculated from weight pure biopolymer material).

Calibration line as obtained in the concentration range of ca 12-200 ppm L200. The samples were not acidified as pretreatment.

		weight	measured				Calculation	recovery
Sample Name	Analysis	mg SL-200/kg	mg C /l	SD Area	CV Area	Date / Time	mg SL-200/kg	%
A-1	NPOC	11,9	4,6	82	0,45%	29-7-2010 17:25	11,6	97
A-2	NPOC	24,6	9,8	705	1,77%	29-7-2010 17:36	24,4	99
A-3	NPOC	47,8	19,1	34	0,39%	29-7-2010 17:44	46,9	98
A-4	NPOC	99,4	40,0	251	1,35%	29-7-2010 17:53	98,1	99
A-5	NPOC	197,7	81,6	567	1,49%	29-7-2010 18:01	199,7	101
B-1	NPOC	11,9	4,5	219	1,21%	29-7-2010 18:25	11,4	95
B-2	NPOC	24,6	9,9	326	0,81%	29-7-2010 18:37	24,6	100
B-3	NPOC	48,6	19,7	40	0,44%	29-7-2010 18:45	48,5	100
B-4	NPOC	96,3	39,3	283	1,55%	29-7-2010 18:53	96,4	100
B-5	NPOC	197,9	82,3	653	1,71%	29-7-2010 19:02	201,2	102
P-1	NPOC	12,2	4,8	124	0,64%	29-7-2010 19:31	12,1	100
P-2	NPOC	24,8	10,2	561	1,35%	29-7-2010 19:42	25,4	102
P-3	NPOC	49,9	20,5	24	0,25%	29-7-2010 19:50	50,4	101
P-4	NPOC	97,2	40,4	203	1,08%	29-7-2010 19:59	98,9	102
P-5	NPOC	199,2	77,8	465	1,28%	29-7-2010 20:10	190,2	96
stA 10X verdunner	NPOC	99,0	40,0	350	1,88%	29-7-2010 20:20	98,0	99
stB 10X verdunner	NPOC	183,0	76,3	296	0,83%	29-7-2010 20:29	186,7	102
stP 10X verdunner	NPOC	100,0	41,5	124	0,65%	29-7-2010 20:37	101,6	102

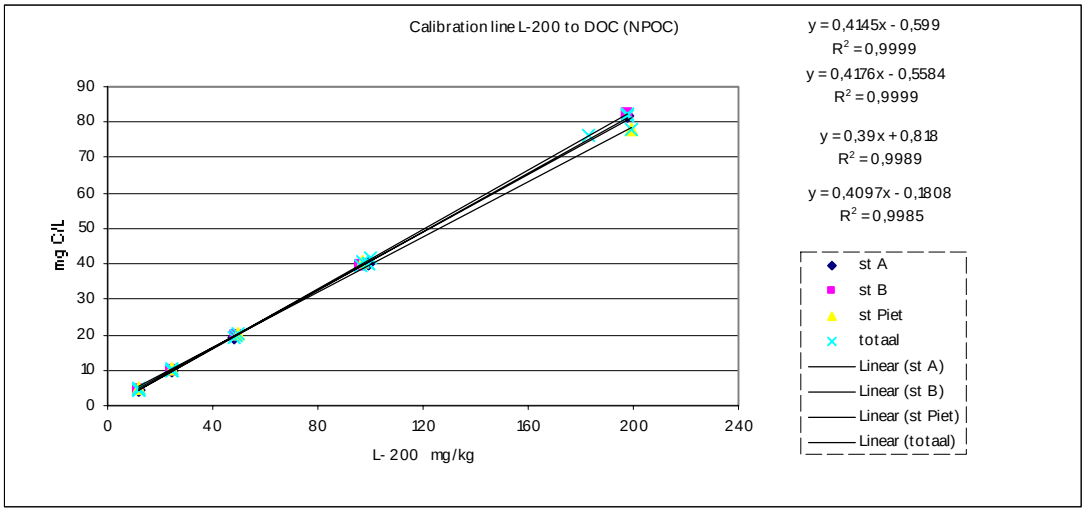

Figure A

The obtained relation in the range of 10 to 200 ppm L-200, for five different concentrations is:

$$[DOC] = 0,4097 * L200 - 0,1808$$

Wherein DOC is in mg C/l and L-200 in ppm.

The calculated Wt.% of carbon in L-200 is 40,90%. The obtained squared correlation coefficient (R^2) is: 0,9985. The Coefficient of Variances of these analyses are max. 1,88%.

Calibration line as performed in the total L-200 concentration range (12-20.000 ppm biopolymer L200).

	weight	measured
	mg SL-200/kg	mg C /l
L-200 C1	1250	544
L-200 C1	1250	544,6
L-200 C2	600	274,2
L-200 C2	600	272
L-200 C3	300	123,1
L-200 C3	300	126,96
L-200 C4	100	36,4
L-200 C4	100	42,12
L-200 C5	60	28,68
L-200 C5	60	43,08
L-200 Stock_I	20488	8793
L-200 Stock_II	20000	8593

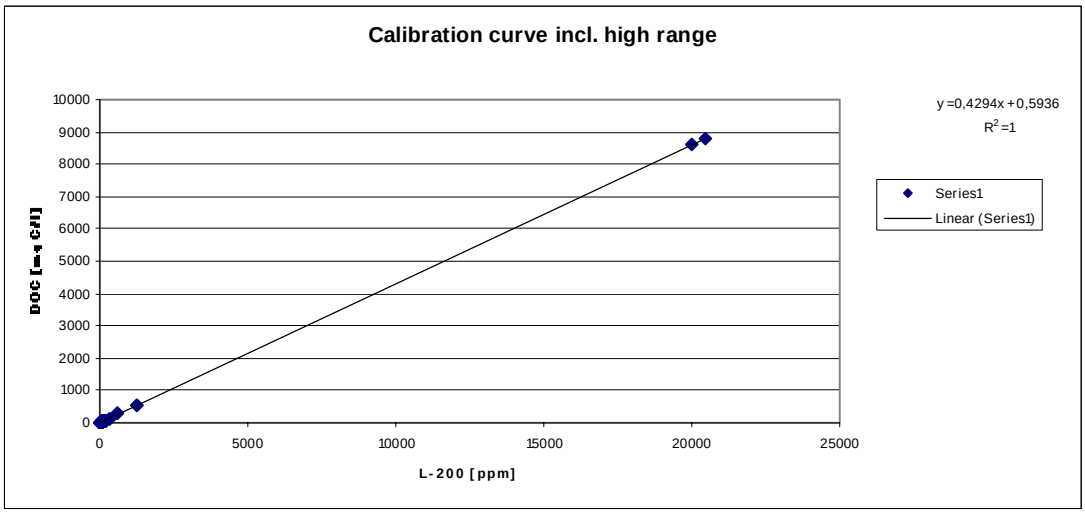

Figure B

The calibration curve shown in Figure B includes the following series measurements:

a. SL- A, SL-B, SL-Piet (in accordance with Figure A).
b. Partition coefficient Blanco L-200 analyses, flask no. 61 to 70.
c. L-200 stock-I and stock-II analyses

The obtained relation in the range of 12 to 20.000 ppm L-200, for 9 different concentrations whereof two samples in the high range, is:

$$[DOC] = 0,4294 * L200 + 0,5936$$

Wherein DOC is in mg C/l and L-200 in ppm.

The obtained squared correlation coefficient (R^2) is 0,9999918. The calculated Wt.% of carbon in L-200 is 42.94%, with a off set of 0.5936 mgC/l.

The calibration curve shown in graph C includes the series of measurements named under a and under b of the last enumeration. The curve covers the concentration range of 0 -1250 ppm L200.

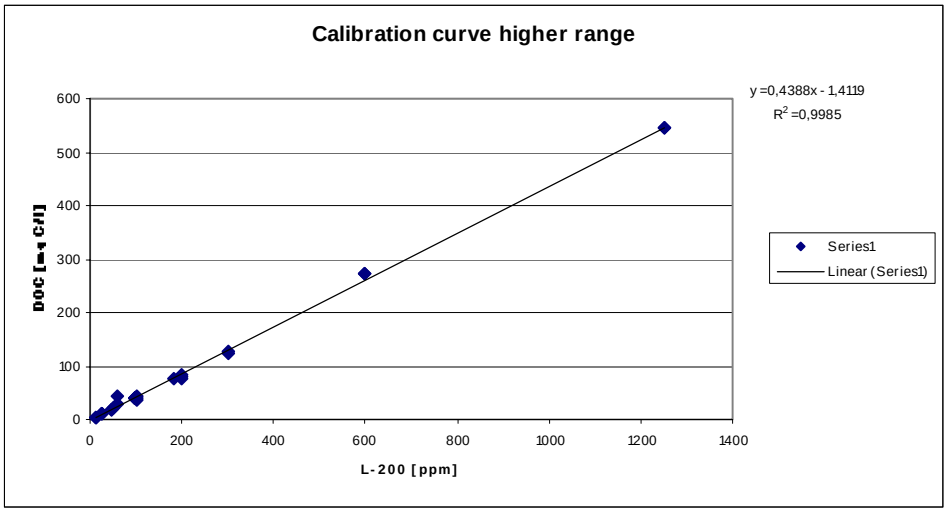

Figure C

No acidification was used as pretreatment! The obtained relation in the range of 10 to 1250 ppm L-200, for five different concentrations is:

$$DOC = 0,4338 \cdot L200 - 1,4119$$

Wherein DOC is in mg C/l and L-200 in ppm.

The calculated Wt.% of organic carbon in L-200 is 43.38% and the off set is 1.4119 mg C/l.. The obtained squared correlation coefficient (R^2) is: 0,9985

Conclusion:

The calculation factor of 43,38 Wt% and a offset of 1.4119 mgC/l is used to calculate L-200 concentration from the measured DOC concentration.

To obtain the concentration of L200 present in a sample, the DOC value is first corrected for the Blanco value and then converted to ppm L200 using this relation..

Calculation conversion mg C/l to ppm L-200:

$$\frac{[DOC]_{s\_corr} + 1.4119}{0.4338} = [L-200]_s$$

$$\frac{[DOC]_{w\_corr} + 1.4119}{0.4338} = [L-200]_w$$

$$[DOC]_{i\_calc} = [L-200]_i \cdot 0,4338 - 1.4119$$

Calculation of standard error of estimate (SEE) and limits of detection (LD) of Method and Instrument

Table A: Standard Error of estimate in samples with biopolymer dissolved in demiwater (no peat, no silica).

Ci	Ci	Cw	Cw
weight from stock	calc	NPOC geen zuur	NPOC zuur
L200	DOC	DOC	DOC
ppm	mg/l	mg/L	mg/l
1250	541	544	332
1250	541	545	292
600	259	274	276
600	259	272	261
300	129	123	125
300	129	127	146
100	42	36	45
100	42	42	48
60	25	29	35
60	25	43	53
0	0	18	23
0	0	26	31
SEE	mg/L	9,0	43,41
SEE	ppm L200	24	103

Table B: Method Detection Limit (MDL) in samples without biopolymer and no peat, thus solely demiwater.

Noise Level (no peat; no L200)			
Ci	Ci	Cw	Cw
weight from stock	calc	NPOC geen zuur	NPOC zuur
L200	DOC	DOC	DOC
ppm	mg/l	mg/L	mg/l
0	0	18	23
0	0	26	31
0	0	16	20
0	0	10	9
average	mg C/L	17,4	20,8
stdev	mg C/L	6,3	9,2
Method detection limit	mg C/L	20,1	29,3
Method detection limit	ppm L200	50	71
degrees of freedom		3	
t-distribution	confidence interval	3,182	98%

Table C: Method Detection Limit (MDL) in samples without biopolymer, including peat.

Noise Level (no L200; Peat)			
Ci	Ci	Cw	Cw
weight from stock	calc	NPOC geen zuur	NPOC zuur
L200	DOC	DOC	DOC
ppm	mg/l	mg/L	mg/l
0	0	489	70
0	0	580	28
0	0	680	54
0	0	714	77
0	0	630	28
0	0	649	29
0	0	1006	40
0	0	995	36
average	mg C/L	717,8	45,3
stdev	mg C/L	187,2	19,6
Method detection limit	mg C/L	561,3	58,7
Method detection limit	ppm L200	1297	138
degrees of freedom		7	
t-distribution		2,998	

Table D: Instrument Detection Limit (IDL) in samples without biopolymer and no peat, thus solely demiwater.

Noise Level (no peat; no L200)			
Ci	Ci	Cw	Cw
weight from stock	calc	NPOC geen zuur	NPOC zuur
L200	DOC	DOC	DOC
ppm	mg/l	mg/L	mg/l
0	0	0,79	0,99
0	0	0,52	0,45
0	0	0,89	1,17
0	0	1,28	1,55
average	mg C/L	0,9	1,0
stdev	mg C/L	0,3	0,5
instrument detection limit (IDL)	mg C/L	0,9	1,4
instrument detection limit (IDL)	ppm L200	5	6

Appendix 14.2 Analytical Method DOC (NPOC)

Werkvoorschrift:	Versie:	Datum:	Pagina:
GL-WV- 014	1.0	31-3-11	1 van 11

Water, bepaling van het gehalte aan totaal organisch koolstof (TOC) of opgelost organisch koolstof (DOC) mbv Shimadzu TOC-5050A

Dit voorschrift is opgesteld door:	Dineke van de Meent-Olieman: 2535043 Piet Peereboom, toestelnummer 2564737 Geïntegreerd laboratorium / sectie Anorganische Geochemie
Beheerder:	G.C. van de Meent-Olieman: 2535043 dr. B.J.H. van Os, toestel nummer: 2534162

Kwaliteitsfunctionaris	Dr. G. Th. Klaver
Authorisatie:	Hoofd Geïntegreerd Laboratorium
Datum: 01-09-2004	…… Dr. T.N.P. Bosma

Dit voorschrift is in gebruik met ingang van 01-09-2004
Het origineel is beschikbaar bij de kwaliteitsfunctionaris GL

Universiteit Utrecht
Faculteit Geowetenschappen, TNO-NITG, Geïntegreerd Laboratorium
Budapestlaan 4, 3584 CD, Utrecht, tel. 030 2535011 fax 030 2535030

Tabel 1 Datum uitgave versie en veranderingen tov vorige versie.

Versie	Datum	Wijzingen tov vorige versie
1.0	**0.1-09-2004**	**Niet van toepassing**

1 Onderwerp

Het meten van organisch koolstof met behulp van een Shimadzu TOC-5050A.

2 Toepasbaarheid

Deze methode is geschikt voor het meten van waterige monsters in het gebied van 0.3 mg/L tot 1000 mg/L koolstof.

3 Definities

3.1 Totaal koolstof (TC = Total Carbon): De som van organisch gebonden en anorganisch gebonden koolstof aanwezig in water, inclusief elementair koolstof.

3.2 Totaal anorganisch koolstof (TIC = Total Inorganic Carbon): De som van anorganisch koolstof in water, bestaande uit elementair koolstof totaal koolstofdioxide, koolstofmonooxide, cyanide, cyanaat en thiocyanaat. De TOC analyser registreert als TIC alleen de CO_2, die afkomstig is van waterstofcarbonaten en carbonaten.

3.3 Totaal organisch koolstof (TOC = Total Organic Carbon): De som van organisch gebonden koolstof aanwezig in water, gebonden met opgelost of gesuspendeerde stof. Cyanaat, elementair koolstof en thiocyanaat worden ook gemeten.

3.4 Opgelost organisch koolstof (DOC = Dissolved Organic Carbon): De som van organisch gebonden koolstof opgelost in water, die na filtratie over een 0.45 µm filter (8.9) in een waterig monster aanwezig is.

3.5 Niet-vluchtig organisch koolstof (NPOC = Non Purgeable Organic Carbon): De som van niet uitblaasbare organische koolstof in water.

4 Beginsel

Deze methode volgt NEN-EN 1484 (14.2). Bij 680 ^{0}C en met behulp van een catalysator wordt organisch koolstof in water tot CO2 geoxideerd. Het CO2 wordt bepaald met een infrarooddetector (non-dispersive infrared gas analyzer: NDIR). Het monster wordt voor de meting aangezuurd en de ontstane CO_2 uitgeblazen. We meten dus NPOC. Als het monster gefiltreerd wordt DOC gemeten, anders TOC.

5 Veiligheid en Milieu

Hierbij dienen de volgende UU-procedures te worden opgevolgd:

- Statuut van Toegang voor het Universiteitscentrum De Uithof, 15 november 1990.
- Algemene richtlijnen, veiligheidsvoorschriften, reglementen voor het veilig werken in laboratoria en werkplaatsen departement Aardwetenschappen: fac. Amvw.102, januari 2003.
- Centrale Inkoop, Uitgifte, Beheer chemicaliën, gassen en afvoer afval chemicaliën: fac. amv. 101, januari 2002.
- Vergunningen, regels en verplichtingen ten aanzien van Arbo-Milieuaspecten, (straling)Veiligheid en Welzijn bij aanschaf nieuwe of uitbreiding bestaande apparatuur: fac.amvw.104, april 2002
- Dispose of waste properly, instructions for the disposal of waste materials. Utrecht University FBU-afvalbeheer, june 2001 (Document nummer: II 20.3.1.A).

Bovenstaande documenten zijn op laboratorium Z111-113 aanwezig in de map Algemene Laboratorium Instructies

6 Chemicaliën

	Chemicaliën	Symbool	Conc.	Merk	Kwaliteit	Bestel nummer	Locatie	Kast nummer
6.1	Kaliumwaterstofftalaat	$C_8H_5KO_4$	Nvt.	Merck	Pro analyse		Z111	
6.2	Zoutzuur	HCl	30%	Merck	Suprapur		Z111	
6.3	Ultrapuur water	UHQ H_2O	Nvt.	Nvt.	≥18MΩ	Nvt.	Z111	Nvt.
6.4	Lucht			Airproducts	Air Zero		Gaskast bij Z115	
6.5	Fosforzuur	H_3PO_4	85%	Merck	Pro analyse		Z111	Nvt.

7 Standaarden en reagentia

Gebruik voor het maken van verdunningen altijd vers getapt UHQ H_2O (6.5).

	Reagentia	Houdbaarheid	Bewaarcondities
7.1	1500 mg C/L stock oplossing	2 maanden	Koelkast
7.2	Werkstandaarden TOC	Vers bereiden	Nvt.
7.3	HCl 2 mol/L	1 jaar	Kamertemperatuur in een kast
7.4	H_3PO_4 25 %		Zuurkast
7.5	Quality Control oplossing QC		Koelkast

7.1 1500 mg C/L stock oplossing

Voor de bereiding gedurende een uur Kaliumwaterstofftalaat (6.1) drogen tussen de 105°C en 120°C.
Weeg nauwkeurig circa 0.3 gram Kaliumwaterstofftalaat (6.1) in een goed afsluitbare glazen fles, voeg circa 100ml UHQ H_2O (6.5) toe en weeg het totaalgewicht. Los op en bereken de concentratie.

7.2 Werkstandaarden TOC

De werkstandaarden worden gemaakt uit de circa 1500 C mg/L stock oplossing (7.1). De oplossingen worden gewogen verdund.
Afhankelijk van het meetbereik worden de met UHQ H_2O (6.3) naar 30 ml uit te verdunnen hoeveelheden 1500 mgC/L stock oplossing (7.1) berekend. Bijvoorbeeld als in onderstaande tabel weergegeven.

Voorbeeld inweeg schema						
conc stock oplossing			1500	Mg C/kg		
hoeveelheid te maken oplossing			30	Ml		
gewenste concentratie Mg C/kg	toe te voegen stock opl. ml	code fles	gewicht lege fles G	gewicht stock opl g	gewicht totaal g	conc standaarden mg C/kg
0	0	1				
1.25	0.025	2				
2.5	0.050	3				
5	0.100	4				
10	0.200	5				
20	0.400	6				
40	0.800	7				
80	1.600	8				

7.3 HCl 2 mol/L

Voeg aan 100 ml UHQ H_2O (6.5), in een 250 ml fles, 30 ml 30% HCl (6.4) toe, roer en vul aan tot 250 ml met UHQ H_2O (6.5).

7.4 H_3PO_4 25%

Voeg aan 100 ml UHQ H_2O (6.5), in een 250 ml fles , 50 ml 85% H_3PO_4 (6.7) toe, roer en vul aan tot 250 ml met UHQ H_2O (6.5).

7.5 Quality Control oplossing

Weeg nauwkeurig 0.9 gram glucose af. Los op in UHQ H_2O (6.5)in een 500 mL maatkolf (8.13). Voeg 10 mg Kwikchloride toe en vul aan tot 500 mL. Bereken de concentratie (circa 720 mgC/L). Of maak de oplossing gewogen in een glazen fles(8.14). Per meetserie een verdunning in de te verwachte concentratierange maken.

8 Apparatuur en hulpmiddelen

	Apparaat en hulpmiddelen	Lab	Contact persoon	Telefoon nummer	Kast nr.	Verdere benoeming in de tekst
8.1	Total Organic Carbon Analyzer TOC-5050A	Z111	DvdM	5043	Nvt.	TOC analyzer
8.2	Autosampler AS1-5000 A	Z111	DvdM	5043	Nvt.	Monsterwisselaar
8.3	Software TOC-Control	Z111	DvdM	5043	Nvt.	Software
8.4	Schott Duran Fles 2 Liter	Z111	DvdM	5043	Nvt.	
8.5	Elgastatt UHQ water installatie	Z111	HdW	5476	Nvt.	Elga
8.6	Autosampler vial 5mL Alltech	Z111	DvdM	5043	36	5 ml Vial
8.7	Autosampler vial 50 ml Schimadzu	Z111	DvdM	5043	36	50 ml vial
8.8	Parafilm M	Z111	DvdM	5043		Parafilm
8.9	Schleicher & Schuell FP 030/0,45 CA-S filter	N103	EvV	7239		0.45 µm filter
8.10	Mettler Toledo AT400 Balans	Z111	DvdM	5043 / 5856	Nvt.	Balans
8.11	30 ml glazenflesjes	Z111	DvdM	5043	58	
8.12	250 ml fles	Z111	DvdM	5043	58	250 ml fles
8.13	Maatkolf 500 mL	Z111	DvdM	5043	58	Maatkolf 500 mL
8.14	Glazen fles 500 mL	Z111	DvdM	5043	58	500 mL glazen fles

EvV = E. van Vilsteren
HdW = H. de Waard
DvdM= D. van de Meent

9 Analysemonster

Watermonster worden aangeboden in glazen of polyetheenflessen, volledig gevuld met het monster. Het monster aanzuren tot pH 2 met HCl 2 mol/L(7.3) om neerslaan te verkomen. Opslaan in de koelkast.

10 Werkwijze

10.1 Voorbereiding

3 tot 4ml monster wordt in een vial (8.6) gebracht. Wanneer het monster niet is aangezuurd, moet dat alsnog gebeuren (30 µl HCL 2 mol/L (7.3) per 3 ml monster, pH<3). Sluit de vials met een stukje parafilm.

10.2 Calibratielijn

Er kan met maximaal 3 ijklijnen gemeten worden. Bij monstermetingen wordt, wanneer “Auto Ranging and Inj Volume” aan staat, de meest geschikte lijn genomen.

10.3 Opstarten apparaat

Start het apparaat volgens bijlage A. Bij afwijkingen altijd beheerder of handleiding (14.1) raadplegen.

Plaats per 10 tot 15 monsters controle standaarden en per serie 2 QC oplossingen(7.5).

10.4 Uitwerken data

De data in de sample table worden na controle naar Excel gekopieerd en verder uitgewerkt volgens bijlage A

11 Identificering en kwantificering

- De kwantitatieve bepaling gebeurt met een lineaire ijklijn, gemaakt met Kaliumwaterstofftalaat. Totaal anorganische koolstof wordt gerapporteerd als mgC/L en meetwaarden worden afgerond op 0.1 mgC/L
- De ijklijn wordt berekend met **y=a+bx**. We gaan er vanuit dat het UHQwater niet helemaal organisch koolstof vrij en dat asafsnede **a** mede hierdoor veroorzaakt wordt. De berekening van de onbekende monsters wordt uitgevoerd met **y=bx**.
- Bij het meten van sterk wisselende concentraties in een monsterserie moet rekening gehouden worden met een “carry over” effect. Daarom gebruiken we een bepalingsgrens die hoger ligt dan de aantoonbaarheidsgrens. Wil men onder de bepalingsgrens meten, dan zal de meetmethode aangepast moeten worden.

12 Prestatiekenmerken

Tabel 12 Prestatiekenmerken voor het bepalen van totaal anorganische koolstof in water

Prestatiekenmerk	mg C/L	%	opmerking
Aantoonbaarheidsgrens	0.2		
Bepalingsgrens	0.6		
Meetbereik	0.6-1500		Afronden op 0.1 mgC/L
Recovery grondwater	39.4	101	40 mg C/L
Recovery grondwater	4.1	110	4 mg C/L
Herhaalbaarheid	0.2	2	Voor ca 9 mgC/L
Reproduceerbaarheid	0.5	5	Voor ca 9 mgC/L

13 Verslag

De resultaten worden als Excel bestand aan het werkformulier van de monsters gehyperlinked
De standaarden en QC monsters worden toegevoegd aan de kwaliteitsdatabase.

14 Literatuur

14.1 Instruction manual total organic carbon analyzer model TOC-5050A.
14.2 TOC Control Manual.
14.3 NEN-EN 1484, Water – Leidraad voor de bepaling van het gehalte aan totaal organische koolstof (TOC) en opgelost organische koolstof (DOC)

15 Opmerkingen

Zeewatermonsters of monsters met een hoog zoutgehalte kunnen niet direkt gemeten worden.

16 Bijlagen

Bijlage A: Handleiding analyse

Bijlage A

Handleiding analyse

Het apparaat staat normaal gesproken in een Standby option. De oven is aan, de gasflow is uit. Als het apparaat helemaal uit staat, neem dan contact op met de beheerder.

Opstarten

- Dubbel klik de TOC Control software icon
- Selecteer Connect onder Measure
- Wacht tot het initialiseren voltooid is
- Open de voorkant TOC5050(8.1) Controleer:
  - gasdruk (410 kPa) en luchtvoorraad in de gaskast op de gang
  - gassnelheid lucht (150 ml/min)
  - H_3PO_4 25% (7.6) fles
  - luchtbevochtigingsfles met UHQ H_2O (6.5)
  - afvoer naar afvalvat

Maak een Sample Table.

- Open onder File het Voorbld file. We hebben nu de juiste instellingen voor Measurements Parameters en Display Settings
- Save AS onder File: jaar maand dag oA of oB ….

Meten met een bestaande methode

- Vooraf moeten een aantal UHQ metingen gedaan worden tot deze laag en stabiel zijn
- Werk vanaf **Opzet Unknown Run** zie hieronder
- Kies ipv van *New* een bestaande TOC methode
- Volg het verdere schema en start de analyse. Maar vul bij het Standby window Keep running

Maak een Standaard Run

- Ga op de eerste regel van de Sample Table staan
- Insert Standaard onder Edit
- Kies *New* in de Calibration Curve List dialog box
- Vul in onder Condition Tab
  - File Name: jaar maand dag oL, oM of oH
  - Calculation Method in: *Regression with Zero Shift*
  - Analyse Type: *NPOC*
  - Unit: mg /L
  - Sparging time: 6 min
  - Verander **niet** de Range en Injection volume
- Ga naar de Data tab en vul in voor 5 standaarden:
  - Sample naam
  - Vial

- Conc

- Ga terug naar de Conditions Tab
  - Range en Injection Volume zijn nu ingevuld.
  -.Afhankelijk van de kolomwerking moet dit volume soms aangepast worden
  - Klik *OK*
  - Save calibration: *YES*
  -*OK*
- De Sample Table komt terug met de ingevulde informatie. Ga op de volgende regel staan
- Een tweede en eventueel derde Standaard Run wordt op dezelfde manier gemaakt

Opzet Unknown Run

- Ga op de volgende vrije regel in de Sample Table staan
- Insert Sample onder Edit (voor meerdere monsters kan Auto Generate Table gebruikt worden)
- Kies *New* voor een nieuwe methode
  - Vul in onder de General tab:
    - File Name: jaar maand dag oA of oB etc
    - Sample Name
    - Sample ID
    - Analysis: *NPOC*
    - Type: Unknown
  - Onder de Tab NPOC
    - Cal Curves: Browse naar de eerste ijklijn
    - *Yes* om de calibration curve parameters te laden
    - Browse naar de tweede en eventueel derde ijklijn
    - *OK*
  - *OK*
- Plaats het monster in de Autosampler
- Vul het vial nummer in de Sample Table

- Voor de volgende monsters: Kies Insert Sample of Auto Generate Table
- Kies nu voor de zojuist gemaakte methode
- Save de Sample Table
- Plaats alle vials en **sluit** de Auto sampler

Start de analyse

- Controleer de status van het instrument
- Kies Background onder View. Alle onderdelen moeten OK zijn en de Baseline moet in range 1 ongeveer nul zijn.
- Sluit het Background Monitor window
- Druk op Start
- Het Standby window moet ingevuld worden
  - Auto restart voor Standby mode
    - Keep TC Furnace Heating
    - Auto Start Time: volgend jaar
    - *OK*

- Open het Realtime Window onder View

Verwerken van resultaten

Door op een regel in de Sample Table te gaan staan, kan de meting van die regel bekeken worden

- Bekijk de calibration curves en noteer de gegevens op het logboekblad
- Open Peak Profile
- Bekijk of alle monsters correct gemeten zijn. Noteer afwijkingen op logblad en meet monsters eventueel opnieuw
- Kopieer de Sample Table naar Excel. Het hele sheet aanklikken, Ctrl C en paste in een nieuw Excel file
- Save deze file met dezelfde naam onder Y:/TOC 500/Ruwe data
- Verwerk de metingen en save de file onder Y:/TOC 500/Resultaten
- Rapporteer de monsters
- Werk de volgende overzichtfiles bij:
  - Y:/TOC 500/QC/2004
    - *ijklijnen*
    - *QC2004.xls*
  - Y:/TOC 500/Monsterlijst/
    - *monsterlijst2004.xls*

Appendix 15 Attachment Test Measurement Data

							0 uur	0 uur	Adjustment	0 uur	0 uur
	Experimental Code	Incubation time	peat paste	Silica-biopolymer suspension	Initial conc.	Initial conc.	pH before	Ec before	vol added*	After adjust	After adjust
			solids+ ppw	reactive fluid			pH	Ec	Ec	pH	Ec
		[hour]	[gr]	[gr]	[SiO2]	[L-200]	[-]	[uS/cm]	[µL]	[-]	[uS/cm]
1	Silica L-200 C1	0	19,969	99,934	1250	1250	6,350	4470	650	~~7.50	4630
2	Silica L-200 C1	0	19,917	99,885	1250	1250	6,280	4480	650	~~7.50	4620
3	Silica L-200 C2	0	19,859	99,484	600	600	6,100	2270	550	~~7.50	2340
4	Silica L-200 C2	0	20,084	99,758	600	600	6,040	2260	550	~~7.50	2330
5	Silica L-200 C3	0	20,698	99,587	300	300	5,630	1283	450	~~7.50	1316
6	Silica L-200 C3	0	20,362	99,562	300	300	5,630	1280	450	~~7.50	1314
7	Silica L-200 C4	0	20,277	99,494	100	100	5,640	725	350	~~7.50	786
8	Silica L-200 C4	0	20,145	99,541	100	100	5,630	731	350	~~7.50	784
9	Silica L-200 C5	0	19,822	99,510	60	60	6,120	567	200	~~7.50	600
10	Silica L-200 C5	0	20,071	99,457	60	60	6,060	565	200	~~7.50	600
11	Silica L-200 C6	0	20,066	99,432	0	0	5,750	407	250	~~7.50	427
12	Silica L-200 C6	0	20,296	99,458	0	0	5,710	400	300	~~7.50	424
13	L-200 C1	0	20,096	100,000		1250	5,850	691	400	~~7.50	792
14	L-200 C1	0	20,014	100,000		1250	5,910	685	400	~~7.50	785
15	L-200 C2	0	20,053	100,000		600	6,010	485	300	~~7.50	526
16	L-200 C2	0	20,379	100,000		600	5,970	480	300	~~7.50	529
17	L-200 C3	0	18,234	100,000		300	6,180	444	400	~~7.50	491
18	L-200 C3	0	20,251	100,000		300	6,240	439	400	~~7.50	488
19	L-200 C4	0	19,564	100,000		100	6,230	370	300	~~7.50	426
20	L-200 C4	0	20,032	100,000		100	6,120	364	300	~~7.50	425
21	L-200 C5	0	19,840	100,000		60	6,350	362	300	~~7.50	413
22	L-200 C5	0	20,278	100,000		60	6,250	362	300	~~7.50	405
23	L-200 C6	0	20,070	100,000		0	6,180	351	250	~~7.50	378
24	L-200 C6	0	19,986	100,000		0	6,000	350	250	~~7.50	378

* Adjustment EC and pH flasks: 1M NaOH and 1M NaCl

Attachment Test_ Measurement Data_113h_Peat Experiment								Silica		Biopolymer L200					
										diluted	diluted	corrected	corrected	conversion	conversion
										NPOC./20	NPOC./20	NPOC	NPOC.	F=100/43	F=100/43
	Experimental Code	Incubation time	peat paste solids+ ppw	Initial conc. [SiO2]	Initial conc. [L-200]	113 uu pH	113 uu Ec	[SiO2]	Recovery [SiO2]	no acid pretreat. DOC	acid pretreat. DOC	no acid pretreat. DOC	acid pretreat. DOC	no acid pretreat. L-200	acid pretreat. L-200
		[hour]	[gr]	ppm	ppm	[-]	[uS/cm]	ppm	%	ppm	ppm	[mg C/l]	[mg C/l]	[ppm]	[ppm]
25	Silica L-200 C1	113	19,9689	1250	1250	6,31	4620	163	13	33,1	4,4	661	88	1 527	207
26	Silica L-200 C1	113	19,9167	1250	1250	6,42	2510	155	12	31,7	4,5	633	91	1 462	213
27	Silica L-200 C2	113	19,8590	600	600	6,4	2510	133	22	29,9	2,4	598	47	1 381	112
28	Silica L-200 C2	113	20,0842	600	600	6,47	1446	129	22	26,5	2,4	530	48	1 225	115
29	Silica L-200 C3	113	20,6984	300	300	6,45	1452	109	36	26,0	2,0	520	40	1 201	96
30	Silica L-200 C3	113	20,3624	300	300	6,5	811	108	36	25,8	2,3	517	45	1 194	108
31	Silica L-200 C4	113	20,2770	100	100	6,66	835	78	78	26,5	2,0	530	40	1 224	97
32	Silica L-200 C4	113	20,1445	100	100	6,68	651	74	74	33,1	2,1	662	42	1 528	99
33	Silica L-200 C5	113	19,8219	60	60	6,44	659	51	86	31,6	2,0	633	40	1 462	96
34	Silica L-200 C5	113	20,0705	60	60	5,85	404	51	86	31,9	2,1	638	42	1 474	101
35	Silica L-200 C6	113	20,0659	0	0	5,8	403	9	#DIV/0!	31,5	1,4	630	28	1 456	67
36	Silica L-200 C6	113	20,2961	0	0	6,45	708	9	#DIV/0!	32,4	1,4	649	29	1 498	69
37	L-200 C1	113	20,0959		1250	N/D	N/D			5,2	3,7	105	74	245	173
38	L-200 C1	113	20,0138		1250	6,64	523			5,2	3,8	103	75	241	176
39	L-200 C2	113	20,0531		600	N/D	N/D			5,5	2,1	111	41	259	99
40	L-200 C2	113	20,3791		600	6,56	492			5,9	3,2	117	64	274	151
41	L-200 C3	113	18,2343		300	N/D	N/D			14,9	1,9	298	39	690	93
42	L-200 C3	113	20,2508		300	6,68	458			13,7	2,9	274	59	634	139
43	L-200 C4	113	19,5639		100	N/D	N/D			32,2	1,9	644	37	1 487	89
44	L-200 C4	113	20,0319		100	6,71	455			30,9	1,8	617	36	1 426	86
45	L-200 C5	113	19,8399		60	N/D	N/D			40,4	1,8	808	35	1 865	85
46	L-200 C5	113	20,2775		60	6,75	470			40,0	2,2	799	44	1 845	105
47	L-200 C6	113	20,0697		0	N/D	N/D			50,3	2,0	1006	40	2 322	96
48	L-200 C6	113	19,9859		0	N/D	N/D			49,8	1,8	995	36	2 297	87

Attachment Test_ Measurement Data_65h_Peat Experiment								Silica		Biopolymer L200					
										diluted	diluted	corrected	corrected	conversion	conversion
										NPOC./20	NPOC./20	NPOC	NPOC.	F=100/43	F=100/43
	Experimental Code	Incubation time	peat paste solids+ ppw	Initial conc. [SiO2]	Initial conc. [L-200]	65 uur pH	65 uur Ec	[SiO2]	Recovery [SiO2]	no acid pretreat. DOC	acid pretreat. DOC	no acid pretreat. DOC	acid pretreat. DOC	no acid pretreat. L-200	acid pretreat. L-200
		[hour]	[gr]	ppm	ppm	[-]	[uS/cm]	ppm	%	ppm	ppm	[mg C/l]	[mg C/l]	[ppm]	[ppm]
1	Silica L-200 C1	65	19,9689	1250	1250	6,39	4640	149	12	6,2	4,7	124	95	290	221
2	Silica L-200 C1	65	19,9167	1250	1250	6,26	4630	167	13	30,7	5,9	614	117	1 417	274
3	Silica L-200 C2	65	19,8590	600	600	6,38	2510	124	21	17,5	2,8	350	55	810	131
4	Silica L-200 C2	65	20,0842	600	600	6,38	2530	131	22	24,0	2,4	480	47	1 110	112
5	Silica L-200 C3	65	20,6984	300	300	6,45	1443	110	37	17,3	1,9	346	37	800	89
6	Silica L-200 C3	65	20,3624	300	300	6,41	1440	110	37	22,2	3,8	443	77	1 025	180
7	Silica L-200 C4	65	20,2770	100	100	6,36	783	79	79	20,8	1,8	416	37	961	87
8	Silica L-200 C4	65	20,1445	100	100	6,56	825	76	76	24,7	1,9	493	39	1 140	92
9	Silica L-200 C5	65	19,8219	60	60	6,08	657	55	91	26,0	2,4	520	47	1 203	112
10	Silica L-200 C5	65	20,0705	60	60	6,12	661	54	90	27,1	2,2	541	43	1 251	103
11	Silica L-200 C6	65	20,0659	0	0	5,59	412	10	#DIV/0!	24,5	3,5	489	70	1 130	165
12	Silica L-200 C6	65	20,2961	0	0	5,51	406	12	#DIV/0!	29,0	1,4	580	28	1 340	68
13	L-200 C1	65	20,0959		1250	6,4	697			4,3	3,4	86	68	201	161
14	L-200 C1	65	20,0138		1250					4,4	3,4	88	68	207	160
15	L-200 C2	65	20,0531		600	5,48	476			5,6	2,2	111	44	260	104
16	L-200 C2	65	20,3791		600					5,5	2,2	111	45	259	106
17	L-200 C3	65	18,2343		300	6,05	480			10,8	3,9	216	77	502	181
18	L-200 C3	65	20,2508		300					10,3	1,9	206	38	479	91
19	L-200 C4	65	19,5639		100	6,02	456			22,6	1,8	452	37	1 045	88
20	L-200 C4	65	20,0319		100					22,3	1,8	446	37	1 032	88
21	L-200 C5	65	19,8399		60	6,42	451			28,6	3,7	572	74	1 321	175
22	L-200 C5	65	20,2775		60					28,1	2,9	562	59	1 298	138
23	L-200 C6	65	20,0697		0	6,5	457			34,0	2,7	680	54	1 570	128
24	L-200 C6	65	19,9859		0	6,4	4590			35,7	3,8	714	77	1 648	180

Attachment Test_ Measurement Data_113h_No Peat Experiment								Silica		Biopolymer L200					
										diluted	diluted	corrected	corrected	conversion	conversion
										NPOC./20	NPOC./20	NPOC	NPOC.	F=100/43	F=100/43
	Experimental Code	Incubation time	peat paste solids+ ppw	Initial conc. [SiO2]	Initial conc. [L-200]	113 uu pH	113 uu Ec	[SiO2]	Recovery [SiO2]	no acid pretreat. DOC	acid pretreat. DOC	no acid pretreat. DOC	acid pretreat. DOC	no acid pretreat. L-200	acid pretreat. L-200
		[hour]	[gr]	ppm	ppm	[-]	[uS/cm]	ppm	%	ppm	ppm	[mg C/l]	[mg C/l]	[ppm]	[ppm]
49	Silica L-200 C1	113	Blanko's	1250	1250	N/D	N/D	657	53	16,3	15,5	325	310	753	718
50	Silica L-200 C1	113	Blanko's	1250	1250	N/D	N/D	613	49	17,5	18,4	349	368	808	852
51	Silica L-200 C2	113	Blanko's	600	600	N/D	N/D	456	76	7,7	10,2	153	205	357	475
52	Silica L-200 C2	113	Blanko's	600	600	N/D	N/D	429	71	9,6	11,0	192	220	446	510
53	Silica L-200 C3	113	Blanko's	300	300	N/D	N/D	240	80	4,5	4,9	90	99	210	231
54	Silica L-200 C3	113	Blanko's	300	300	N/D	N/D	246	82	5,0	5,3	100	107	233	250
55	Silica L-200 C4	113	Blanko's	100	100	N/D	N/D	89	89	2,0	2,3	41	45	97	107
56	Silica L-200 C4	113	Blanko's	100	100	N/D	N/D	90	90	1,7	1,7	34	34	81	82
57	Silica L-200 C5	113	Blanko's	60	60	N/D	N/D	53	88	1,0	1,2	19	24	47	58
58	Silica L-200 C5	113	Blanko's	60	60	N/D	N/D	53	89	1,0	1,1	20	22	50	54
59	Silica L-200 C6	113	Blanko's	0	0	N/D	N/D	0,00	#DIV/0!	0,8	1,0	16	19,79	40	49
60	Silica L-200 C6	113	Blanko's	0	0	N/D	N/D	0,00	#DIV/0!	0,5	0,4	10	8,93	27	24
61	L-200 C1	113	Blanko's		1250	N/D	N/D			27,2	16,6	544	332	1 257	769
62	L-200 C1	113	Blanko's		1250	N/D	N/D			27,2	14,6	545	292	1 258	677
63	L-200 C2	113	Blanko's		600	N/D	N/D			13,7	13,8	274	276	635	640
64	L-200 C2	113	Blanko's		600	N/D	N/D			13,6	13,0	272	261	630	604
65	L-200 C3	113	Blanko's		300	N/D	N/D			6,2	6,3	123	125	287	291
66	L-200 C3	113	Blanko's		300	N/D	N/D			6,3	7,3	127	146	296	339
67	L-200 C4	113	Blanko's		100	N/D	N/D			1,8	2,3	36	45	87	108
68	L-200 C4	113	Blanko's		100	N/D	N/D			2,1	2,4	42	48	100	114
69	L-200 C5	113	Blanko's		60	N/D	N/D			1,4	1,7	29	35	69	83
70	L-200 C5	113	Blanko's		60	N/D	N/D			2,2	2,7	43	53	103	125
71	L-200 C6	113	Blanko's		0	N/D	N/D			0,9	1,2	18	23,5	44	57
72	L-200 C6	113	Blanko's		0	N/D	N/D			1,3	1,6	26	31,1	62	75

Preparation of reactive fluids and flasks performed by Piet Peereboom (BGS-Deltares Laboratory) and Dianne den Hamer; Composition analyses performed by Piet Peereboom. Design of test by Dianne den Hamer and Harry Veld (BGS-Deltares Laboratory).

Appendix 16 Scavenging of DOC by Biopolymer L200

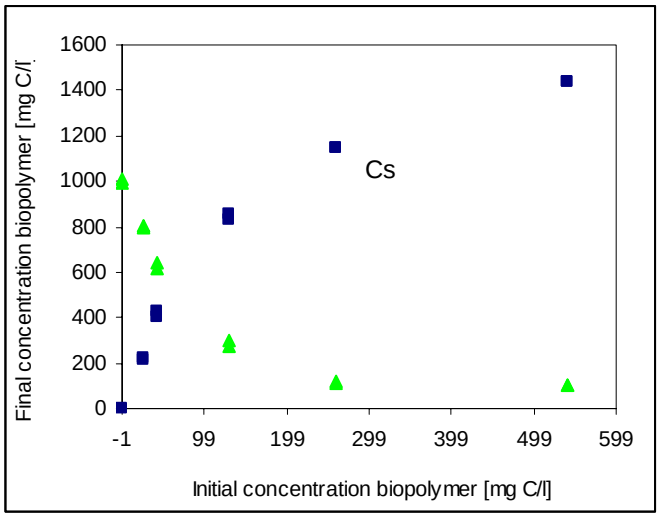

Figure A shows the relation between initial concentration and final dissolved and solid concentration of organic carbon, expressed in mgC/l. The dissolved concentration (light green) is the actual measured value. The final solid concentration was calculated based on the DOC measured in Blanco's (just water and peat) analyzed without treatment. This amount of DOC + the DOC from the biopolymer was an estimate of the total DOC present in the mixture at t 113h. In the presence of the biopolymer this value declines remarkably indicating scavenging of DOC by biopolymer.

Appendix 17 Classification Peat Types

Appendix 17.1 Bellingwedde Peat

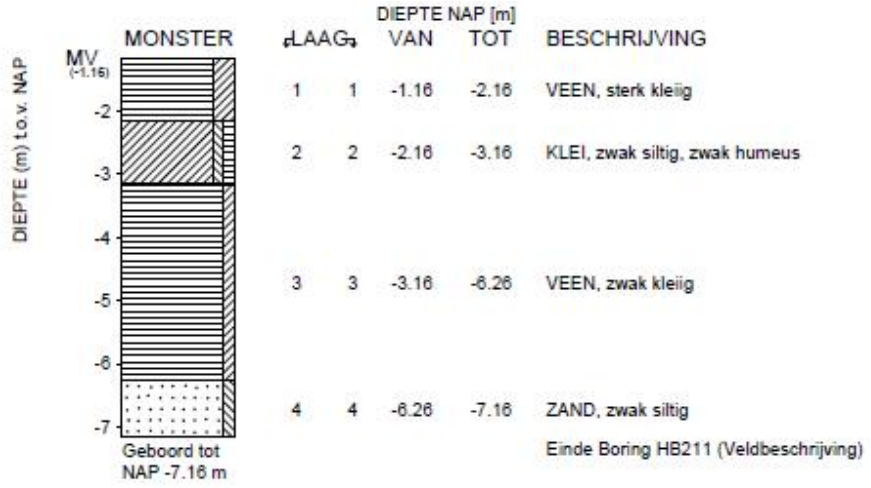

Figure A: The classification of drilling layer close to Bellingwedde.

Appendix 17.2 Zegveld Peat

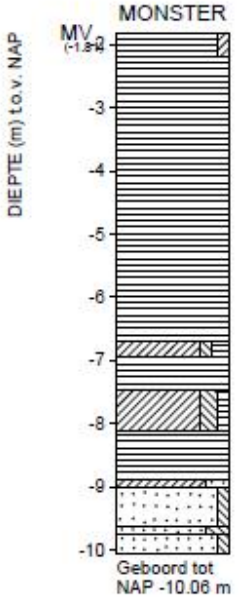

LAAG		DIEPTE NAP [m] VAN	TOT	BESCHRIJVING
1	1	-1.81	-2.21	VEEN, zwak kleiig Enkel puinstukje.
2	2	-2.21	-6.69	VEEN, mineraalarm
3 4	3	-6.69	-6.96	KLEI, zwak siltig, matig humeus Met plantenresten.
5	4	-6.96	-7.46	VEEN, mineraalarm
6 7	5	-7.46	-8.11	KLEI, matig siltig, zwak humeus Met veenstukjes.
8 9 10	6	-8.11	-8.88	VEEN, mineraalarm
	7	-8.88	-9.01	KLEI, sterk zandig Met plantenresten.
	8	-9.01	-9.63	ZAND, zwak siltig Enkele plantenrest. ZM=0.150 mm
	9	-9.63	-9.74	ZAND, sterk siltig ZM=0.150 mm
	10	-9.74	-10.06	ZAND, zwak siltig ZM=0.300 mm
				Einde Boring B5-01_TEEN (Labbeschrijving)

Appendix 18 Experimental Set-up Infiltration Test

Appendix 18.1 Pictures experimental set-up

Set-up

Bottom and top grid plates

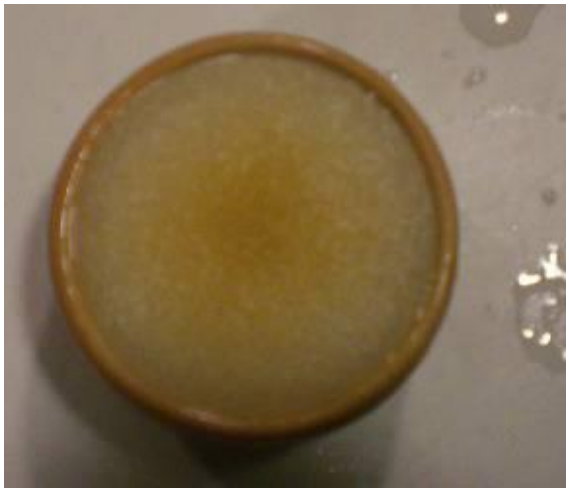

Filter plate

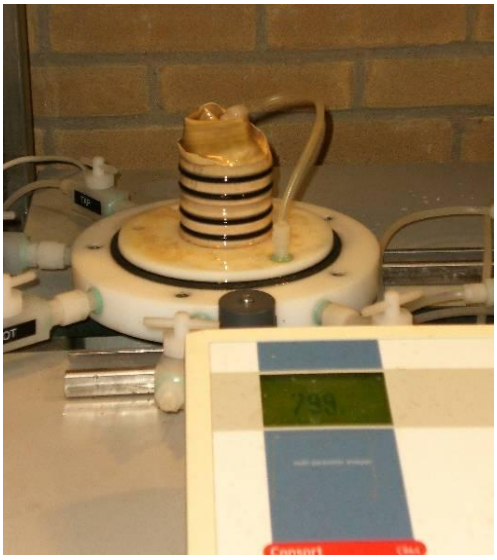

Determine resistance to flow of system

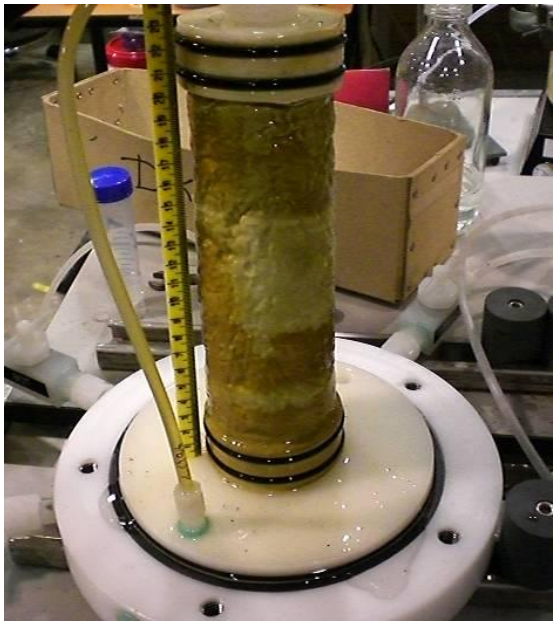

Column 2: long column; after treatment

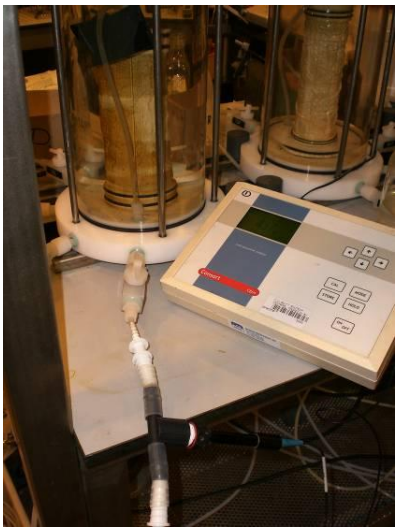

EC datalogger and in-line EC measurement

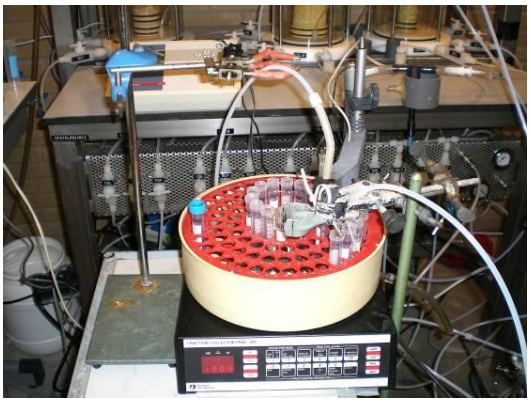

Autosampler used to take continuous effluent samples for composition analyses

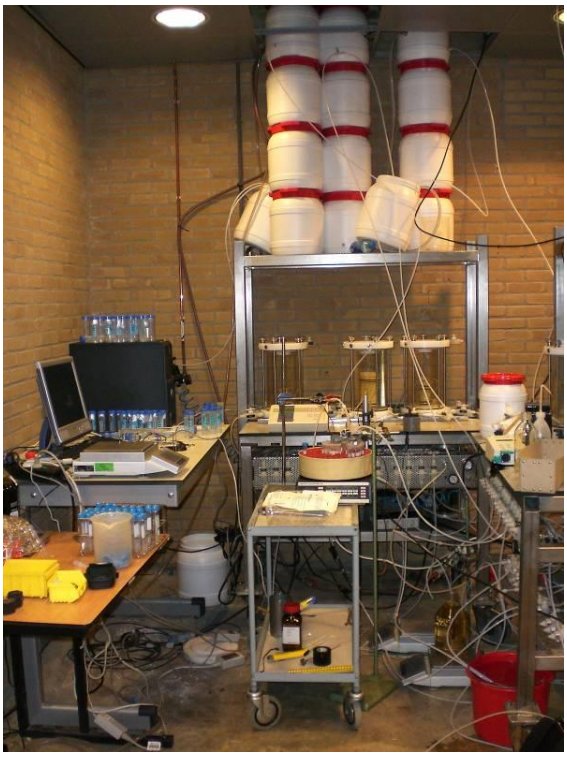

Total set-up; The barrels build up to a level of circa 2.5 meters from ground level, and 2 meters from column level.

Digital pressure devise (not connected to logger), connected to Cell or Bot pressure to check the radial pressure or hydraulic head.

Small storage flask, creating the hydraulic head during reactive tracer infiltration.

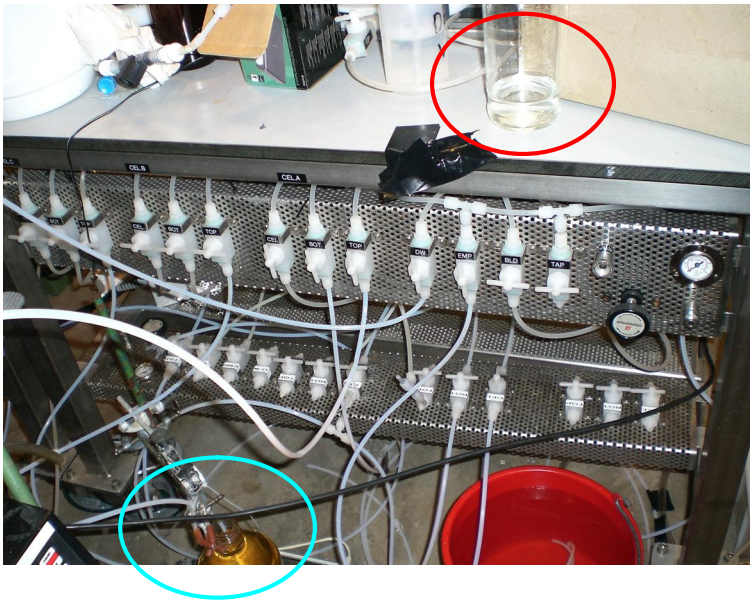

Red circle: effluent color before injection of sodium chloride solution (0.07 M NaCl).

Blue circle: effluent color during elution of sodium chloride solution from the column (using tap water – degassed).

Color of effluent indicates a increased concentration of dissolved organic carbons upon elution of the sodium chloride solution. This could be explained by the front of elevated ionic strength. This shift in ionic strength compresses the diffuse double layer surrounding each particle present in the porous matrix of the column. Thereby DOC is mobilized and colors the effluent.

Appendix 19 Analytical Methods Infiltration Test

Dry solids and Loss on Ignition

Crushed and sieved sub-samples (about 5 gram, < 10 mm) were dried in an oven at 70^{o}C for 90 hours to determine the moisture content. Subsequently, the samples were heated at 550^{o}C for 5 hours to determine LOI. Moisture content and LOI were determined gravimetrically. In addition the volumetric weight was measured and wet and dry density values were derived.

Solid silicate concentration

Composition analysis of peat material was performed by Alcontrol Laboratories. Total organic carbon content and silicon content is determined. Silicon composition analysis is performed according to a method developed by Alcontrol Laboratories. The method concerns digestion of the sample material with agua regia (ISO 15587-2) to give total silicon by ICP. The procedure applied may only partially dissolve the crystalline fraction of the silicon present in the solid matrix. Although, the amorphous fraction of silica – as the found hydrated precipitation was to be – is known to be solubilized by this method (personal communication Alcontrol). The limit of detection is 3 mg Si/ kg of dry solids.

Appendix 20 Column 4 and 2 after Experiment - Pictures

Dissection column 1

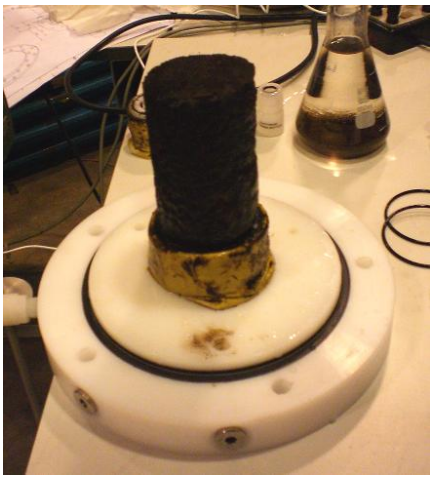

Dissection column 2

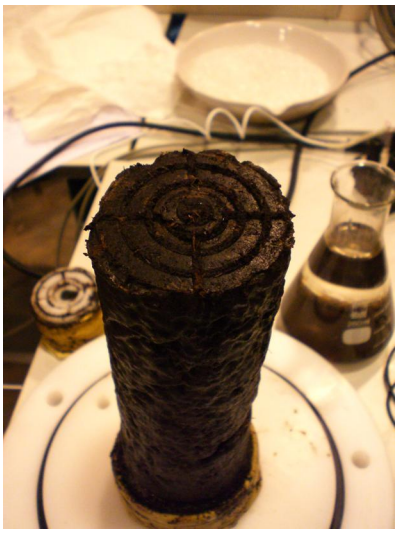

The red circles indicate some of the visible parts of the silica gel, after removal of the porous disc.

Dissection column 5

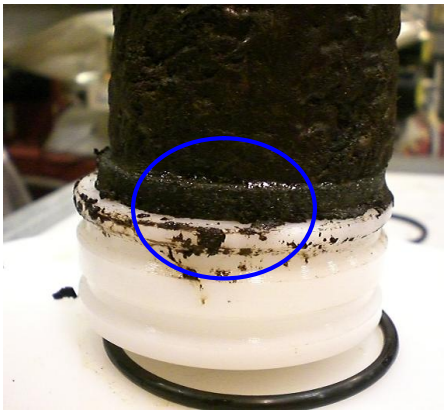

The reflection between porous disc and peat column is the silica gel.

Dissection column 3

Appendix 21 SEM images and EDAX analyses

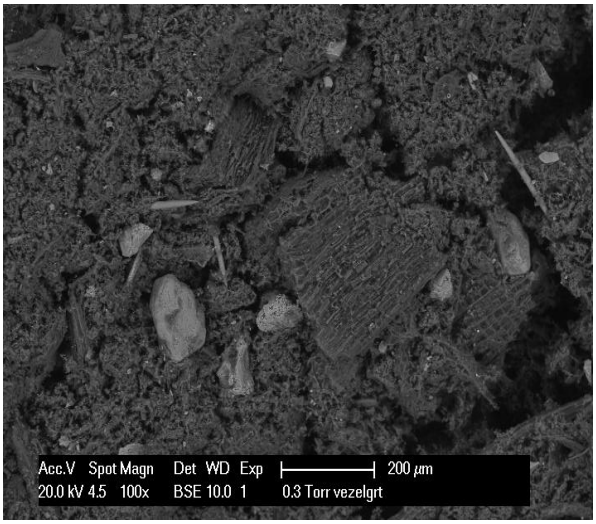

A.

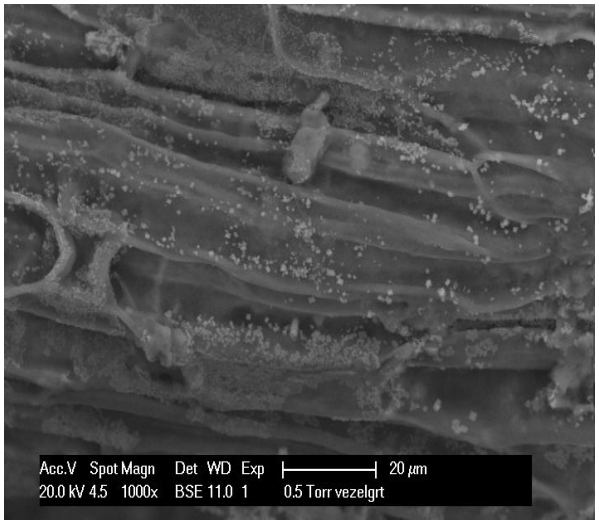

B.

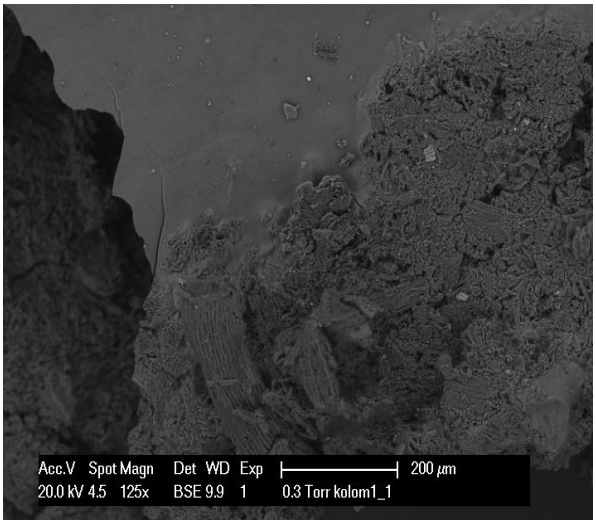

C. Scraped material from filter plate of column 5, at magnification of 125x.

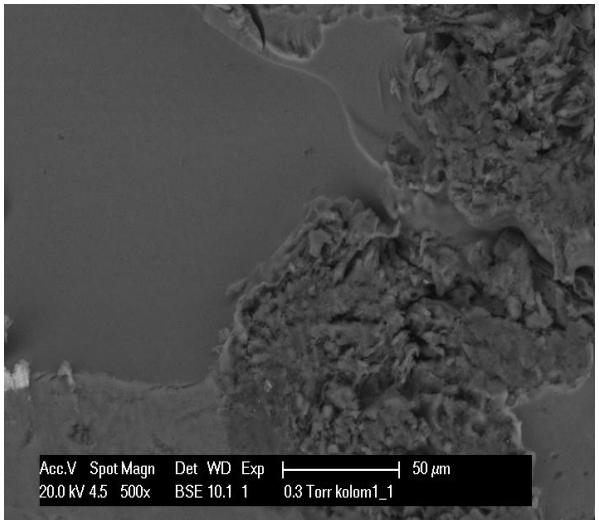

D. Zoom of figure C at magnification of 500x.

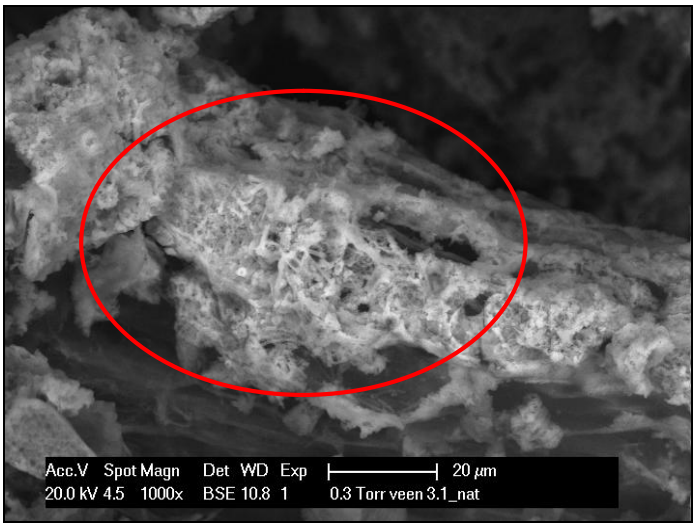

E. Column 2: only treatment with salt solution of 0.07 M NaCl

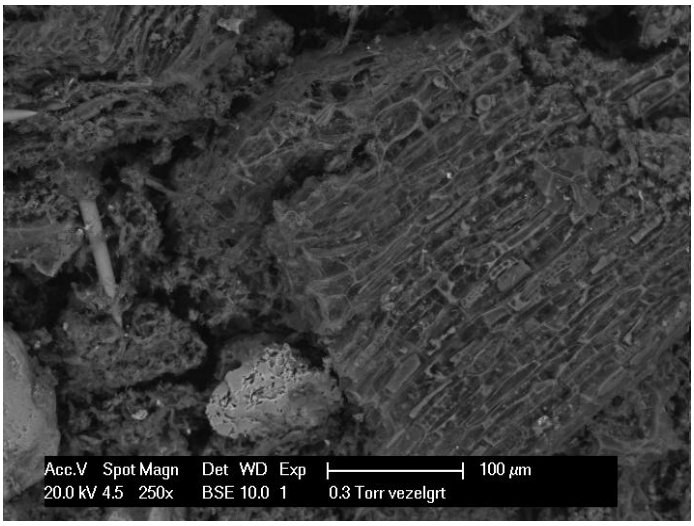

F. Peat (Bellingwedde) not treated

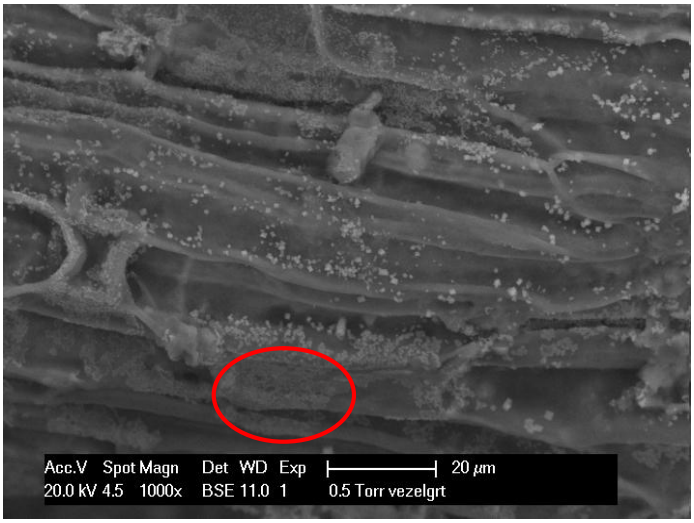

G. Column 4: the presence of white cubes was observed. EDAX analyses revealed that this were most likely sodium chloride crystals and no solid form of silica.

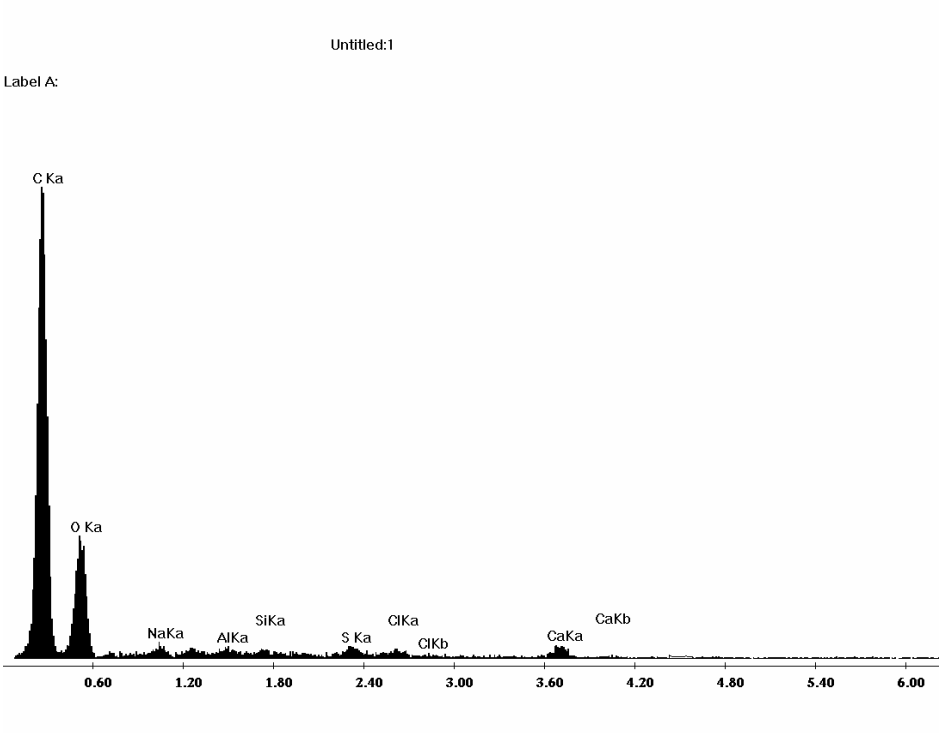

Not treated peat material from Bellingwedde.

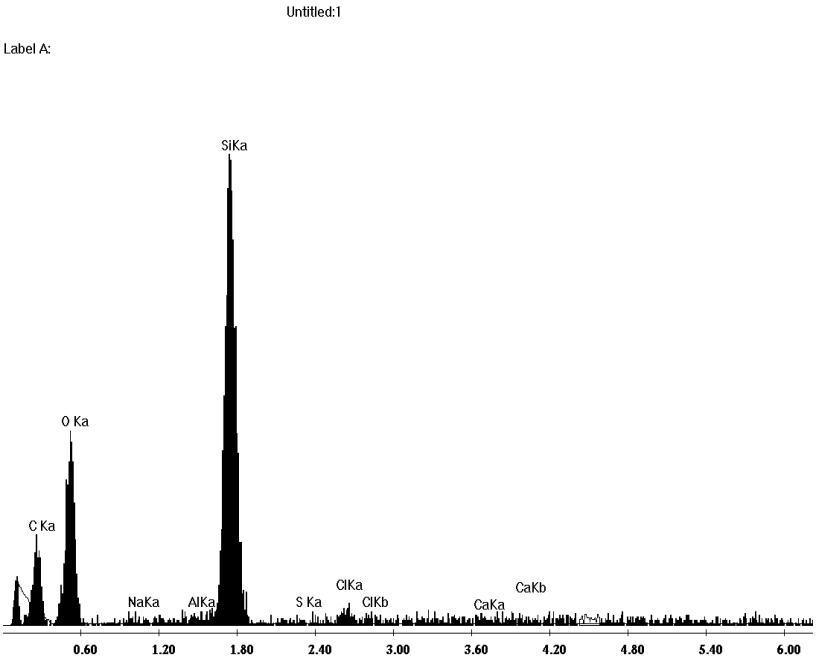

EDAX analyses column 4: gel layer between porous disc and column

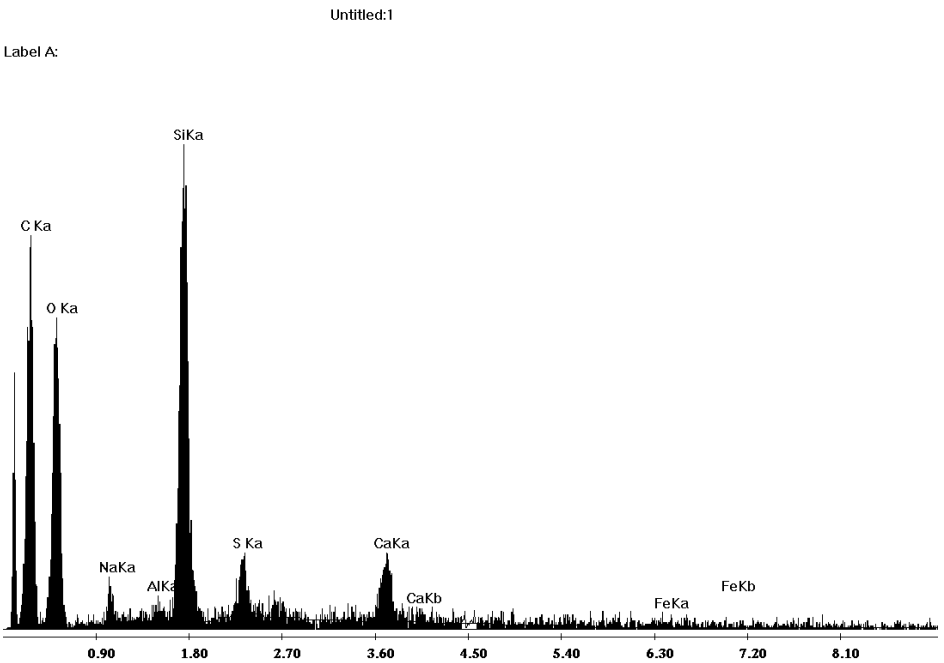

EDAX analyses column 4: Bubbles under gel layer zoom image in figure D.

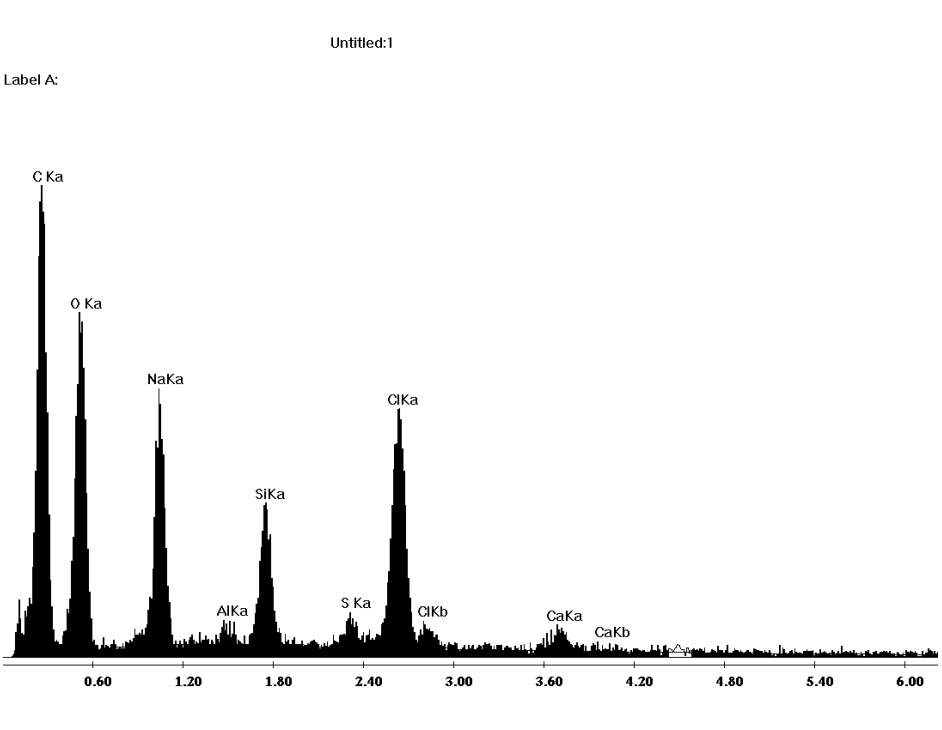

EDAX analyses column 2: Area with white cubes (red circle in figure G)

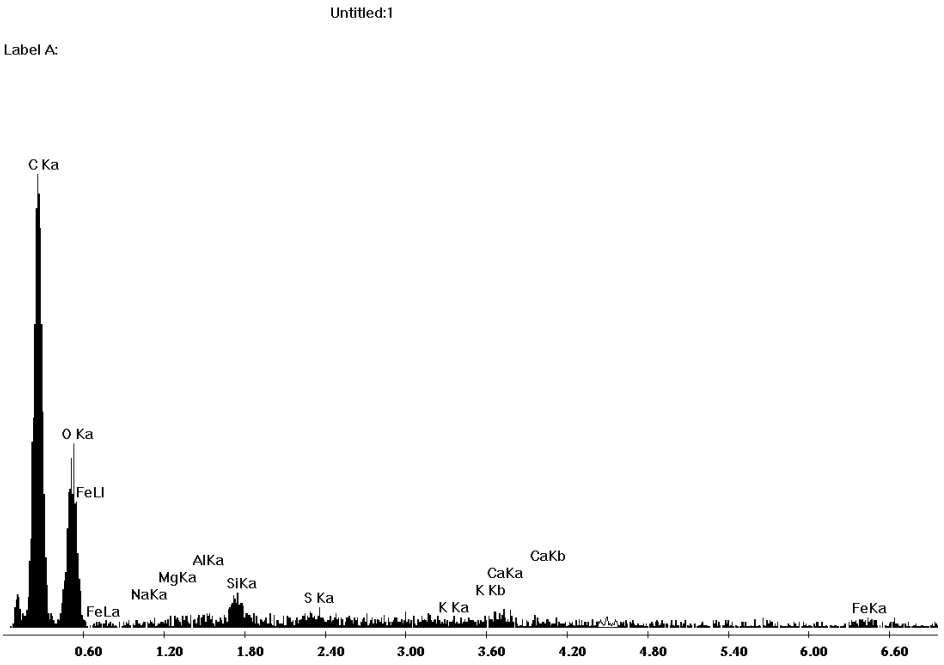

EDAX analyses column 4: Several centimeters higher in column 4 (blue circle in figure C)

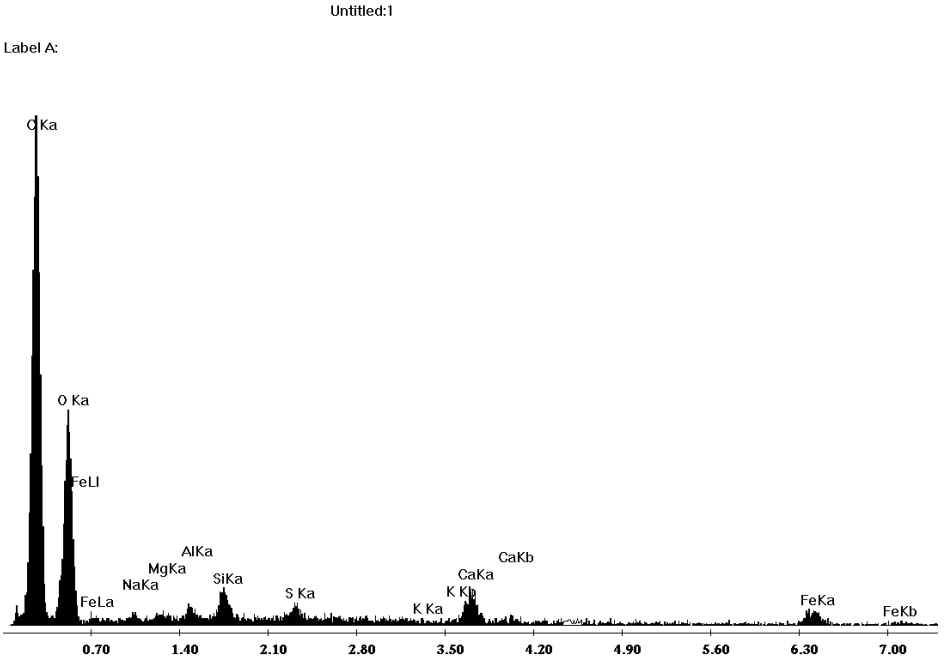

EDAX analyses column 2: White area as indicated by the red circle in figure E